IDENTIFICATION OF ABSCISIC ACID-BINDING PROTEINS USING A BIOACTIVE PHOTOAFFINITY PROBE

A Thesis Submitted to the College of
Graduate Studies and Research
in Partial Fulfillment of the Requirements
for the Degree of Philosophy Doctor
in the Department of Chemistry
University of Saskatchewan

By

Marek Michal Galka

Spring 2009

Permission to use

In presenting this thesis in partial fulfillment of the requirements for the degree of Philosophy Doctor from the University of Saskatchewan, I agree that the Libraries of this University may make it freely available for inspection. I further agree that permission for copying of this thesis in any manner, in whole or in part, for scholarly purposes may be granted by the professor who supervised my thesis work or, in their absence, by the Head of the Department of Chemistry or Dean of the College Of Graduate Studies and Research. It is understood that any copying or publication or use of this thesis or parts of thereof, for financial gain shall not be allowed without my written permission. It is also understood that due recognition shall be given to me, to the University of Saskatchewan and the National Research Council Canada in any scholarly use which be made of any material in this thesis.

Requests for permission to copy or make other use of material in this thesis in whole or part should be addressed to:

Head of the Department of Chemistry

University of Saskatchewan

Saskatoon, Saskatchewan,

S7K 5C9

Abstract

This project was expected to contribute to the understanding of abscisic acid (ABA) perception in plants through identification of new ABA-binding proteins. The novel, biotinylated ABA derivative PBI686 (of biological activity comparable to natural ABA) has served as an affinity probe for isolation of ABA-binding proteins. Photoaffinity labeling in conjunction with affinity chromatography (streptavidin-biotin based) was used for specific identification of target proteins from complex mixtures of cytosolic and membrane-bound proteins. Proteins of interest were identified by Mass Spectrometry through peptide mass fingerprinting and MS/MS ion search.

Ribulose bisphosphate carboxylase/oxygenase (Rubisco) was identified as an ABA binding partner, and its interaction with ABA was initially confirmed by its ability to block the photoaffinity labeling reaction with PBI686. In addition, Surface Plasmon Resonance (SPR) experiments with ABA and Rubisco were performed, which provided further evidence for selective interaction between the two binding partners, with a very small preference towards (+)-ABA over (-)-ABA. SPR has also yielded the value of equilibrium dissociation constant (K_D) being 5 nM for (+)-ABA and 7 nM for (-)-ABA. This was further confirmed by [^{3}H] (±)-ABA binding assays, which have also shown that non-radiolabeled (+)-ABA and (-)-ABA (at concentration 1000 fold higher) were able to displace [^{3}H] (±)-ABA from binding to Rubisco. Compounds other than ABA such as PA (phaseic acid) or *trans*-(+)-ABA were not able to displace [^{3}H] (±)-ABA, which has suggested the selectivity of binding.

Further, Rubisco enzymatic activity in the absence of ABA was compared to that in the presence of ABA at various concentrations. The results have clearly indicated the effect of ABA on Rubisco's enzymatic activity. This was reflected on the enzyme's K_m values being increased by seven fold in the presence of 10 mM ABA and 1 mM substrate (RuBP). The interpretation of changes in enzyme kinetics upon inhibition by ABA most resembles allosteric inhibition.

The biological function of this newly discovered interaction is interpreted as ABA's ability to regulate plant growth during abiotic stress by its direct action on the photosynthetic machinery - hypothesis often suggested in the literature.

Acknowledgements

I would like to thank my supervisor Dr. Suzanne Abrams for giving me the opportunity to be a member of her research group and for her advice, suggestions and guidance. My gratitude also goes to my co-supervisor Dr. David Palmer and to Dr. Michele Loewen and Dr. Adrian Cutler for helpful discussions of the results and revisions of this thesis. I also would like to thank other members of my advisory committee Dr. David Sanders and Dr. Matthew Paige for their revisions of my progress reports and suggestions during our meetings.

....to my wife who stood by me through it all

Table of Contents

Table of Figures

List of Abbreviations

2, 4, 5-T	2,4,5-trichlorophenoxyacetic acid
4-Cl-IAA	4-chloroindole-3-acetic acid
7TM	seven transmembrane
A	alanine
ABA	abscisic acid
ABP1	auxin binding protein 1
Ac	acethyl
AHK	Arabidopsis histidine kinase
AHP	arabidopsis histidine phosphor-transfer protein
Ala	alanine
APX	ascorbate peroxidase
Arg	arginine
ATP	adenosine triphosphate
BAK	brassinosteroid-associated kinase
BLAST	basic local alignment search tool
Bmax	maximum bound
BPCS	biotin-tagged castasterone
BR	brassinosteroid
BRI	brassinosteroid insensitive
BSA	bovine serum albumine
C	cysteine
CA1P	2-carboxyarabinol-1-phosphate
$CaCl_2$	calcium chloride
CAN	carbonic anhydrase function
cDNA	complementary DNA
CHCA	α-cyano-4-hydroxycinnamic acid
Ci	currie
CNBr	cyanobromide
CoA	coenzyme A
CSBP	cytokinin specific binding protein
CTBP	2-carboxytetriol-1,4-bisphosphate
CV	coefficient of variation
Cys	cysteine
D	aspartic acid

d.p.m	disintegrations per minute
Da	dalton
DELLA	A family of five protein homologs comprised of GAI, RGA, RGL1, RGL2 and RGL3
DHPC	1,2-Diheptanoyl-sn-glycero-3-phosphocholine
DNA	deoxyrybonucleic acid
DPA	dihydrophaseic acid
DREPP	developmentally regulated endoplasmatic polypeptide
DTT	dithiothreitol
E	glutamic acid
EA	ethylamine
EBD	ethylene binding domain
EDC	1-Ethyl-3-(3-dimethyllaminopropyl)-carbodiimide
EDTA	ethylenediaminetetraacetic acid
EI	enzyme-inhibitor
ELISA	enzyme-linked immuno sorbent assay,
ER	endoplasmatic reticulum
ES	electrospray
F	phenylalanine
FC1	flow cell 1
FC2	flow cell 2
FPLC	fast protein liquid chromatography
g	gram
GA	gibberellic acid
GAP	glyceraldehyde 3-phosphate
GB	gibberrelin
GCPR	G-protein coupled recepror
GID	GA-insensitive dwarf
Gly	glycine
GST	glutathione S-transferase
GTP	guanidine triphosphate
Gu-HCl	guanidine hydrochloride
H	Hill coefficient
HEPES	4-(2-hydroxyethyl)-1-piperazineethanesulfonic acid
His	histidine
HPLC	hight performance liquid chromatography
HRP	horseradish peroxidase
HSL	hormone-sensitive lipase
I	inhibitor, isoleucine
IAA	indole acetic acid

IC50	inhibition constant (50% activity)
ID	isladn domain
INA	isonicotinic acid
JA	jasmonic acid
K	lysine
ka	rate constant for association
KABP	3-ketoarabinol-1,5-bisphosphate
kcal	kilocalories
K_D	equilibrium dissociation constant
kd	rate constant for dissociation
kDa	kilo Dalton
Ki	inhibition constant
K_M	Michaelis-Menten constant
km	coefficient for mass transfer
L	ligand, leucine
LC/MS	liquid chromatography/mass spectrometry
LOX	lipoxygenase
LRR	leucine rich repeat
LS	large subunit
Lys	lysine
M	molar
m/z	mass/charge ratio
mAb	monoclonal antibody
MALDI-TOF	matrix assisted laser desorption ionization-time of flight
MAPK	mitogen-activated protein kinase
MeJA	jasmonic acid methyl ester
mg	miligram
min.	minute
mL	mililiter
mM	milimolar
Mowse	molecular weight search
MS	mass spectrometry
MW	molecular weight
N	asparagine
NAA	1-naphtylacetic acid
NaCl	sodium chloride
NADH	nicotinamide adenine dinucleotide
NH_4HCO_3	ammonium bicarbonate
NHS	N-hydroxysuccinimide

NMR	nuclear magnetic resonance
NRC	national research council
ODPA	oxophytodienoic acid
P	product, protein, proline
P450	cytochrome P450
PA	phaseic acid
PAGE	polyacrylamide gel electrophoresis
PAL	photoaffinity labeling
PBI	plant biotechnology institute
PBS	phosphate buffered saline
PBS-T	phosphate buffered saline with tween
PDBP	D-glycero-2,3-pentodiulose,1,5-bisphosphate
PGA	3-phosphoglyceric acid
Phe	phenylalanine
PMF	peptide mass fingerprinting
ppm	parts per million
PR	pathogen-related protein
Pro	proline
PTB	protein transfer buffer
PUFA	polyunsaturated fatty acids
PVDF	polyvinylidene Fluoride
Q-TOF	quadropole time of flight
R	arginine
Rmax	maximal feasible signal response
ROS	reactive oxygen species
RT	room temperature
RU	resonance unit
Rubisco	ribulose-1,5-bisphosphate carboxylase/oxygenase
RuBP	ribulose-1,2-bisphosphate
S	substrate
SA	salicylic acid
SABP	aslicylic acid binding protein
SAR	systematic acquired resistance
SCF	protein classified as ubiquitin ligase
SDS	sodium dodecyl sulfate
SE	substrate-enzyme
Ser	serine
SPR	surface plasmon resonance
SS	small subunit

T	tryptophan
TCS	two component system
TFA	trifluoroacetic acid
TIR 1	transport inhibitor response 1
TMV	tobacco mosaic virus
Tris	tris-(hydroxymethyl)-aminomethane
Trp	tryptophane
UV	ultraviolet light
V	valine
v/v	volume/volume
Val	valine
Vi	initial velocity
Vmax	maximum velocity
vs.	versus
VSP	vegetative storage protein
W	watt
XuBP	D-xylulose-1,5-bisphosphate
α-NAA	α-naphatalene acetic acid

1. Introduction

1.1. Introduction to plant hormones –roles, effects and signaling mechanisms

Fundamental for the process of plant growth and development are a small number of plant hormones or phytohormones. This group includes auxins, cytokinins, the gibberellins (GAs), abscisic acid (ABA), ethylene, the brassinosteroids (BRs), jasmonates (JA), and salicylic acid (SA), each of which acts at low concentrations to regulate many aspects of plant growth and development.

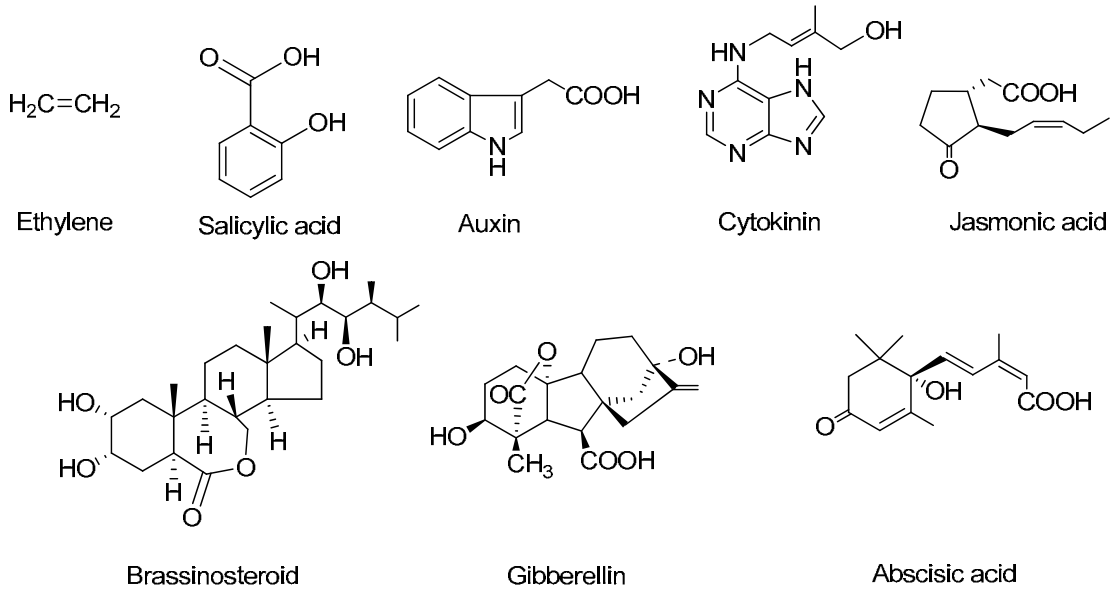

Figure 1. Structures of representative examples of plant hormone classes.

Each hormone is associated with a range of functions in plants. Ethylene gas promotes fruit ripening, senescence, and responses to pathogens and abiotic stresses.[1] Auxin regulates cell division and expansion, vascular differentiation, lateral root development, and apical dominance.[2] Cytokinins are adenine derivatives first identified by their ability to promote cytokinesis, a process in which cytoplasm of a single eukaryotic cell is divided to form two daughter cells.[3] JA modulates pollen development and responses to pathogen infection.[4] The BRs regulate cell expansion and photomorphogenesis (light regulated development).[5] GAs are diterpenoid compounds that promote germination, stem elongation, and the induction of flowering.[6] Salicylic acid (SA) mediates plant defense against pathogens, it is involved in the systemic acquired resistance [SAR], in which a pathogenic attack on older leaves causes the development of resistance in younger leaves.[7] Finally, ABA promotes seed dormancy and most importantly, is involved in several stress signaling pathways.[8]

The transduction pathways are well known for some of them (and will be described further) and still not understood for others. This chapter will briefly introduce each hormone and its binding proteins or receptors (if any) discovered to date. It is important to stress the difference between a receptor and binding protein; although all receptors are binding proteins of a given ligand, not all binding proteins are receptors. The most common characteristics of a receptor are: stereospecificity of ligand binding, reversibility of binding, interaction of a receptor with a ligand initiates cellular response.[9] There are four major classes of receptors: Peripheral membrane receptors, transmembrane receptors, G protein-coupled receptors and metabotropic receptors.

Peripheral membrane receptors are proteins that only temporarily are associated with the membrane. These receptors attach to integral membrane proteins, or penetrate the peripheral regions of the lipid bilayer. The regulatory protein subunits of many ion channels and transmembrane receptors, for example, may be defined as peripheral membrane proteins. Unlike integral membrane proteins, peripheral membrane proteins are usually found in water-soluble fraction of proteins, of all the proteins extracted during a protein purification procedure. The reversible attachment of peripheral receptors to biological membranes was found to regulate cell signaling and many other important cellular events, through various mechanisms.[10] Association between many enzymes and biological membranes often brings them into close proximity with their lipid substrate(s).[11] Membrane binding also promotes dissociation, rearrangement, or conformational changes within many protein structural domains, and downstream activation of their biological activity.[12]

Transmembrane receptors are integral membrane proteins, which are typically located within a cell's plasma membrane.[12] Binding of a signaling molecule on one side of the membrane, transmembrane receptors induce a response on the other side. Because of that transmembrane receptors play a unique and important role in cellular communications and signal transduction. Transmembrane receptors are usually composed of two or more protein subunits which operate collectively and may dissociate when ligands bind. The polypeptide chains of transmembrane receptors cross the lipid bilayer up to seven times.

G protein-coupled receptors (GPCRs), also called seven transmembrane domain receptors, 7TM receptors.[13] They form a large protein family of transmembrane receptors

capable of sensing molecules outside the cell and activating inside signal transduction pathways which lead to cellular responses.[14] G protein-coupled receptors are specific for eukaryotes, (yeast, plants, and animals). Binding of ligands (light sensitive compounds, odors, pheromones, hormones and neurotransmitters) which vary in size (small molecules peptides, proteins) activates these receptors. G protein-coupled receptors are activated by an external signal such as binding of a ligand or other signal mediator, which leads to conformational change in the receptor, hence activation of a G protein. Downstream effect depends on the type of G protein.

Metabotropic receptors belong to a group of membrane receptors located at the surface or in vesicles of eukaryotic cells.[15] Metabotropic receptors are indirectly linked with ion-channels on the plasma membrane of the cell through signal transduction mechanisms, often G proteins. Hence, they are a type of G Protein Coupled Receptor. Metabotropic receptors, when activated, a series of intracellular events are triggered that results in ion channel opening which involve a range of second messenger chemicals.

Ligand-induced conformational changes in receptors result in physiological, metabolic or transcriptional changes which constitute the biological activity of the ligands. Ligand binding proteins on the other hand may exhibit only a few of the functions of receptors. Lack of stereospecificity, enzymatic activity (with exemptions), no association with other signal transduction-related proteins, or any downstream effects of interaction with a ligand, are examples of binding protein features. Enzyme-inhibitor interactions are an example of such non-receptor type of binding.

The following sections will focus on the discoveries of putative receptors or binding proteins (and their associated functions) of all plant hormones.

1.2. Auxins

The term auxin by convention refers to indole-3-acetic acid (IAA) although this particular molecule, structurally resembling tryptophan, represents only one auxin. There are other derivatives of tryptophan also regarded as auxins such as: indole-3-butyric acid (natural hormone), 4-chloroindole-3-acetic acid (4-CI-IAA, natural hormone), and other synthetic compounds that are not derivatives of tryptophan such as 2,4-dichlorophenoxyacetic acid (2,4-D,common synthetic herbicide) or α-naphthalene acetic acid (α-NAA, synthetic hormone). The primary auxin in plants is indole-3-acetic acid (IAA). Its structure is shown in Figure 1. Auxins are often used to promote initiation of adventitious roots and are the active ingredient of the commercial preparations used in horticulture to root stem cuttings.[16,17] They can also be used to promote uniform flowering, to promote fruit set, and to prevent premature fruit drop. Used in high doses, auxin stimulates the production of ethylene. Some synthetic auxins such as 2,4-D and 2,4,5-trichlorophenoxyacetic acid (2,4,5-T) have been used as herbicides. There are other compounds with auxin activity found such as indole-3-butyric acid, phenyl acetic acid, and 4-chloro-IAA but little is known about their physiological functions.[18] Tryptophan was found to be a precursor of IAA in its biosynthesis[19]. IAA occurs not only in the free form but also conjugated to amino acids, peptides, and carbohydrates. These IAA conjugates are biologically inactive and appear to serve as IAA storage forms. IAA was found to have various functions in plant tissues such as inducing transcriptional responses, changes in cell division, expansion and differentiation.[20] Crucial to understanding the molecular bases of auxin action was the elucidation of how auxin is perceived. Literature reports evidence for both plasma membrane and intracellular sites

of auxin perception. Ray *et al.* has reported the auxin receptor called ABP1 (auxin binding protein 1), as a protein that binds biologically active auxins with high affinity.[21-23] ABP1 was isolated by affinity chromatography methods using sepharose 4B covalently modified by tryptophan (coupling of tryptophan to Sepharose 4B was performed according to standard procedure for the covalent attachment of primary amines to CNBr-activated resin)[24] and purified for the first time by Löbler and Klämbt.[25] This led to functional studies of ABP1, examination of its cell biology and its structure. The affinity to auxin 1-naphthylacetic acid (NAA) was found to be 57 nM. The protein sequence of ABP1 reveals little functional information. Consistent with the presence of C-terminal KDEL endoplasmatic retention motif, the majority of ABP1 is ER localized. However, a small fraction escapes to the cell surface, and several lines of evidence implicate plasma membrane associated ABP1 in early auxin-mediated electrophysiologic responses.[21] Genetic approaches to elucidate ABP1 function have found that its over-expression promotes auxin-mediated cell expansion.[26] Furthermore, *Arabidopsis abp1* knock out mutants exhibit an early embryo-lethal phenotype, indicating that ABP1 is an essential gene.[27] However the biological function of ABP1 remains undetermined and it does not appear to be involved in known signaling pathways.

Recent reports have also indicated that the TIR1 (transport inhibitor response) F-box protein is an auxin receptor. It was found that radiolabeled IAA added to crude *Arabidopsis* extracts co-purifies (by immunoprecipitation) with SCF (ubiquitin ligase)^{TIR1} –Aux/IAA complex.[28] Auxin regulates transcription through stimulating the degradation of Aux/IAA proteins.[28,29] There are literature reports that auxin acts by promoting an interaction between the Aux/IAA proteins and the ubiquitin protein ligase SCF^{TIR1}. In

Arabidopsis, the Aux/IAA proteins are encoded by a family of genes comprised of 29 members.[30] Most of these proteins have four common conserved regions designated domains I to IV. Domain II, which includes the conserved amino-acid residues GWPPV, is involved in the degradation of luciferase reporter protein[31] and interacts with SCF^{TIR1}, indicating that domain II is the auxin degron (specific sequence of amino acids in a protein that directs the starting place of degradation).[32] Mutations within domain II result in stabilization of the affected Aux/IAA protein and alter auxin response.[29,33] It is still not understood how auxin promotes the interaction between Aux/IAA and SCF^{TIR1}. Substrate recognition by other cullin-based E3 ligases requires substrate modification such as phosphorylation or proline hydroxylation and glycosylation.[34,35] Recent reports suggest however that none of these mechanisms are involved in auxin-induced Aux/IAA degradation.[32] The current understanding is that the substrate recognition requires an auxin-dependent modification of TIR1 or an associated protein and not the substrate. This concept has been proven by Dharmasiri *et al.* [36] using biochemical methods based on *in vitro* interaction assay between IAA and TIR1 and concludes that auxin regulates degradation of the Aux/IAA proteins by direct binding to TIR1. The interaction of auxins with SCF^{TIR1} was examined by performing competitive binding experiments with active auxins (IAA, 1-NAA, and 2,4-D) and related compounds. The active auxins competed efficiently with [^{3}H]-IAA for binding but benzoic acid and tryptophan-related molecules having no auxin activity – were not capable of competing with [^{3}H]-IAA (Figure 2).

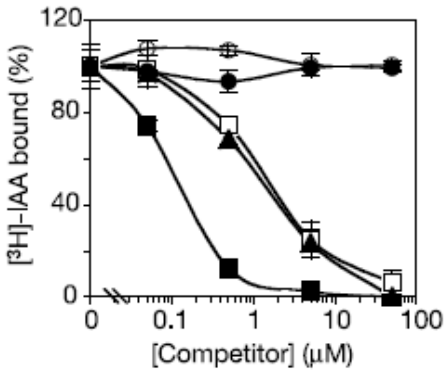

Figure 2. Competition for binding to SCFTIR1 complex incubated with [^{3}H]-IAA with or without cold IAA. Black squares – unlabeled IAA, white squares -2,4-D, black triangles -1-NAA, white circles –benzoic acid, black circles –tryptophan. (figure copied from Dharmasiri *et al.*[36] with permission).

Dharmasiri reports that the auxin receptor binding site is localized within the SCF-TIR1 complex, and Scatchard analysis indicated the equilibrium dissociation constant K_D of the auxin-receptor complex gave a value of 84 nM. It was also demonstrated that IAA has a higher affinity for the receptor than other biologically active auxins such as 2,4-D or 1-NAA. It is concluded that IAA promotes the interaction between Aux/IAA and TIR1 at nanomolar concentrations whereas 2,4-D and 1-NAA are active at micromolar levels. These results provided strong evidence that TIR1 is an auxin receptor which regulates degradation of Aux/IAA proteins and changes in expression of auxin-regulated genes (Figure 6).

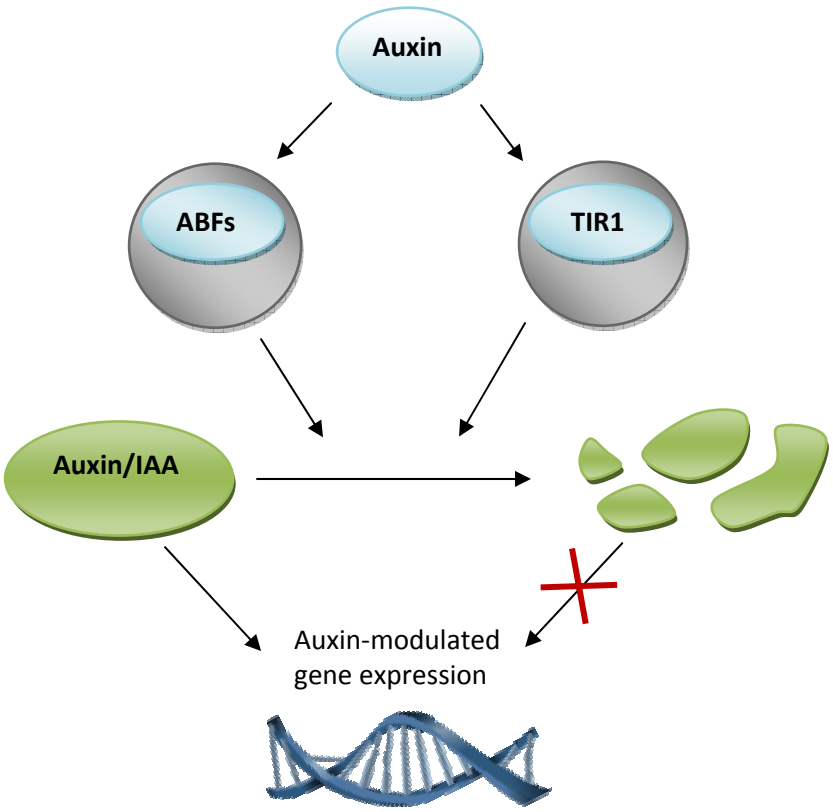

Figure 3. Auxins interact with SCF complexes carrying a transport inhibitor response protein 1 (TIR1) or the related auxin-binding factors (ABFs). This catalyses the destruction of Aux/IAA proteins, which directly inhibit the genes that are responsible for the auxin response. The inhibitory effect of Aux/IAA is thus relieved, allowing auxin responses to occur. (figure and caption adapted from Callis J. *et al.*[37])

To date it is not clear however how auxin stimulates the interaction between SCF^{TIR1} and its substrates. One explanation is that auxin binds TIR1 and induces a conformational change which favors Aux/IAA binding. Alternatively auxin might bind to both TIR1 and the Aux/IAA cooperatively which leads to SCT^{TIR1} – substrate complex stabilization.

SCF family of E3 ligases play an important role in cellular regulation.[38] In a group of characterized SCFs, substrate recognition normally proceeds through phosphorylation

within the substrate degron sequence. The discovery of binding interaction between IAA and SCF^{TIR1} complex brings new input to understanding of SCF^{TIR1} –substrate recognition process and SCF regulation. There are numerous reports suggesting the existence of proteins involved in polar auxin transport (regulated plant hormone transport). It is suggested that it involves proteins located in various parts of the cell such as cytoskeleton, plasma membrane and cell wall.[39] The first auxin transporter protein ZmPIN1a has been recently reported by Gallavotti *et al.*[40]

The structure of auxin-binding protein 1 (ABP1) from maize has been determined by Woo *et al.*,[41] which revealed its auxin-binding site. The structure confirmed that ABP1 belongs to a storage protein superfamily and it is classified as a transmembrane receptor (associated with ER). The binding pocket of ABP1 is of hydrophobic character with a zinc ion deep inside the pocket coordinated to three histidines and one glutamate. Auxin binds within this pocket, with its carboxylate group binding the zinc and its aromatic ring binding hydrophobic residues including Trp151. There is a single disulfide bond between Cys2 and Cys155. No conformational rearrangement of ABP1 was observed when auxin bound to the protein in the crystal, but examination of the structure revealed a possible mechanism of signal transduction. Up till now ABP1 stands as one of the rare examples of a receptor protein that has been crystallized in complex with a plant hormone, revealing its binding site in detail.[42]

1.3. Cytokinins

Cytokinins play an important role in many physiological and developmental processes in the plant, such as regulation of shoot and root growth, leaf senescence,

chloroplast development, stress response and pathogen resistance.[43] Literature provides evidence of two different types of cytokinin hormonal activities in plants. One activity is responsible for regulating cell division and sink strength (as the ability of a sink organ to import assimilates for its growth, development and maintenance), and second activity is based on long-distance signaling, in which cytokinins may serve primarily as a root-to-shoot signal and may regulate physiological (for example nitrogen-dependent) processes.[43]

The most abundant naturally occurring cytokinins are adenine derivatives substituted at N^6-position with an isoprenoid side chain.

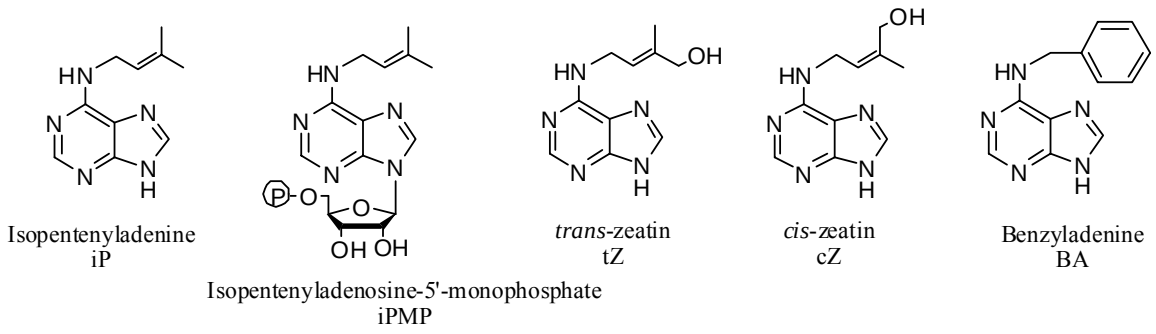

Figure 4. Chemical structures of some naturally occurring cytokinins carrying an isoprenoid or aromatic side chain.

In addition cytokinin molecules carrying an aromatic side chain were detected in several plant species and usually display a high biological activity in different bioassays.[44]

It was found that the cytokinin signal is perceived in *Arabidopsis* by three membrane-located histidine kinase receptors (AHK2, AHK3, CRE1/AHK4) and all of them were identified by genetic methods.[45-47] The cytokinin signaling system consists of two proteins – hence the name two-component system (TCS) – a membrane bound

receptor kinase, which senses the signal and autophosphorylates, and a response regulator, which upon phosphorylation by the receptor kinase, activates the transcription of its target genes or initiates another output reaction[48] After binding of cytokinin to the extracellular ligand-binding domain, the so-called CHASE domain, a dimer of the receptor histidine kinase (AHK) transphosphorylates itself at a conserved histidine residue. The signal is then transferred within the receptor protein to an aspartate residue in the response regulator domain. Subsequently, the phosphoryl group is transferred to a histidine phosphor-transfer protein (AHP), which then translocates to the nucleus, where it activates the B-type response regulators (ARRs) by phosphorylation of an aspartate residue. These response regulators activate the transcription of their genes which regulate the activity of cytokinin signaling and link the cytokinin signaling pathway with other cellular signaling pathways.[49] Cytokinin receptors consist of an input domain, a histidine kinase domain and a receiver domain (similar to other plant histidine kinases). In phylogenetic tree of the *Arabidopsis* histidine kinase domains, all AHK protein, AHK2, AHK3 and CRE/AHK4, cluster together, indicating their close evolutionary relationship.[50] It is generally concluded that cytokinin receptors are located in plasma membrane but so far there is no evidence supporting that.

Figure 5 depicts cytokinin regulated processes associated with given receptors. Biochemical binding assays and response studies performed in heterologous host showed that the cytokinin receptors differ in their binding specificities with different cytokinins. In *in vitro* binding studies CRE1/AHK4 bind the bases tZ and iP (Figure 4) (K_D ~ 4.5 nM) very well.[51]

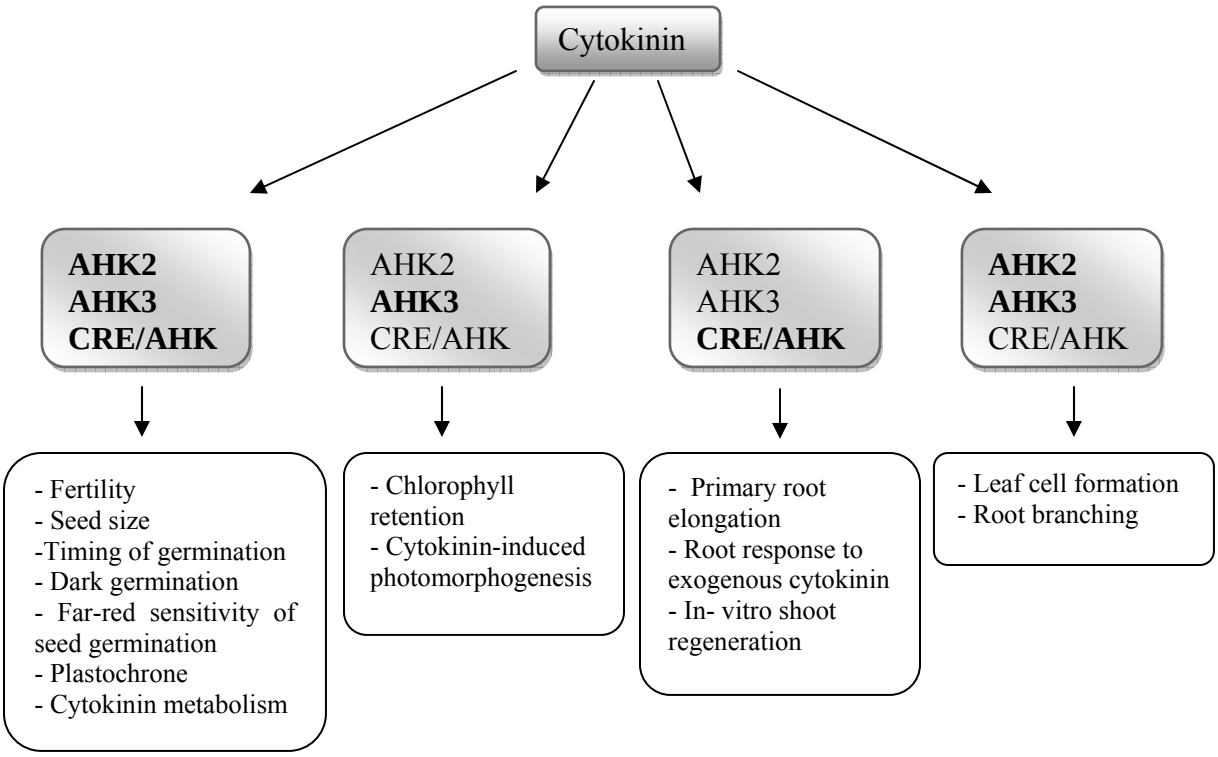

Figure 5. Contributions of different cytokinin receptors and receptor combinations to cytokinin-regulated processes (figure adapted from Riefler *et al.*[52]).

Studies comparing the ligand specificities of CRE1/AHK4 and AHK3 using bacterial assay confirmed the preference of both receptors for the bases of isoprenoid-type cytokinins.[53] In addition it was also reported that CRE1/AHK4 has a narrow spectrum of ligands while AHK3 recognizes a much wider range of cytokinins, with much lower relative affinity.[53] This difference allows for recognition of the different cytokinin signals at the level of receptors and allows various cytokinins to induce partially specific cellular responses.

The Crystal structure of another cytokinin binding protein CSBP (cytokinin specific binding protein) complexed with zeatin has been recently reported by Pasternak *et al.*[54] The binding site consists of an antiparallel β-sheet wrapped around a C-terminal

α-helix, with two short α-helices closing a cavity formed within the protein core. The zeatin molecule was found to be located deep in the cavity with conserved conformation and protein–ligand interactions. Despite the crystal structure and binding affinity of CSBP to zeatin, no function has been assigned to this protein to date.

1.4. Gibberellins

Chemically, all known gibberellins are diterpenoid acids that are synthesized by the terpenoid pathway in plastids and then modified to their biologically-active form in the endoplasmatic reticulum and cytosol. All gibberellins are derived from the ent-gibberelline skeleton, but are synthesized *via ent*-kaurene. The gibberellins were named GA_1....GA_n in order of their discovery. Gibberellic acid, which was the first gibberellin to be structurally characterized, is GA_3 (Figure 1). As of 2003, there were 126 GAs identified from plants, fungi and bacteria. Active gibberellins show many physiological effects, each depending on the type of GA present as well as the species of plant. Some of the physiological processes stimulated by gibberellins are: stem elongation and bolting/flowering in response to long days, breaking of seed dormancy, induction maleness of flowers, seedless fruit development, delay senescence in leaves and citrus fruits.[55] Substantial progress has been made in identification of GA-binding protein and receptors in recent years. In particular a central role of DELLA proteins (family of five homologs comprised of GAI, RGA, RGL1, RGL2 and RGL3) recognized as repressors of GA-mediated responses[56]. Ueguchi-Tanaka *et al.* have also recently reported the identification of a soluble GA receptor from rice[57] through the discovery of gibberellin insensitive gene DWARF1. Biochemical studies have suggested the presence of both

soluble cytoplasmic and plasma membrane-localized GA receptors in plants but the necessary components could not be identified.[58] The identification and characterization of rice GA-insensitive *dwarf (gid)* mutants has proved instrumental in elucidating the GA-signaling cascade. The *gid1* mutants displayed a severe GA-insensitive phenotype, including defects in feedback regulation of GA biosynthesis that result in the accumulation of much higher levels of bioactive GAs than wild-type plants.[57] The *gid1* mutations are recessive, indicating that *GID1* encodes a positive regulator of GA signaling. This is further supported by the demonstration that transgenic plants over-expressing *GID1* exhibit GA-hypersensitive phenotype. The *GID1* gene was isolated by positional cloning and demonstrated to encode a polypeptide of 354 amino acids with significant homology to members of the Hormone Sensitive Lipase (HSL) family.[57] It appears unlikely that GID1 exhibits HSL activity due to the fact that a histidine residue, essential for HSL activity, in GID1 is replaced by valine. Biochemical and genetic evidence indicates strongly that GID1 functions as GA receptor. Thus, recombinant GID1 bound a radiolabeled, bioactive GA analogue, 16,17-dihydro [$^3H_4$]GA_4 with moderate affinity ($K_D \sim 1.4 \times 10^{-6}$ M). GID1 ligand specificity was also examined by competition between [$^3H_4$]-16,17-dihydro-GA_4 and ten GAs (with differing biological activity. Table 1 lists the concentration of each GA required for 50% inhibition (IC_{50}) of [$^3H_4$]-16,17-dihydro GA_4 binding to GST-GID1. GST-GID1 exhibited moderate affinity for biologically active GAs such as GA_4, 15,17-dihydro-GA_4, GA_1 and GA_3, but substantially lower affinity for biologically inactive GAs.

Ueguchi-Tanaka *et al.*[57] have recently reported the study of molecular interactions between GBs and GID1. By replacing conserved residues of GID1 receptor with Alanine,

it was found that there are many regions/blocks in GID1 responsible for GA binding activity. There were 12 blocks essential for GA binding activity. These blocks were scattered throughout the GID1 molecule. This result is consistent with the above prediction that almost the entire GID1 protein is important for its GA binding activity.

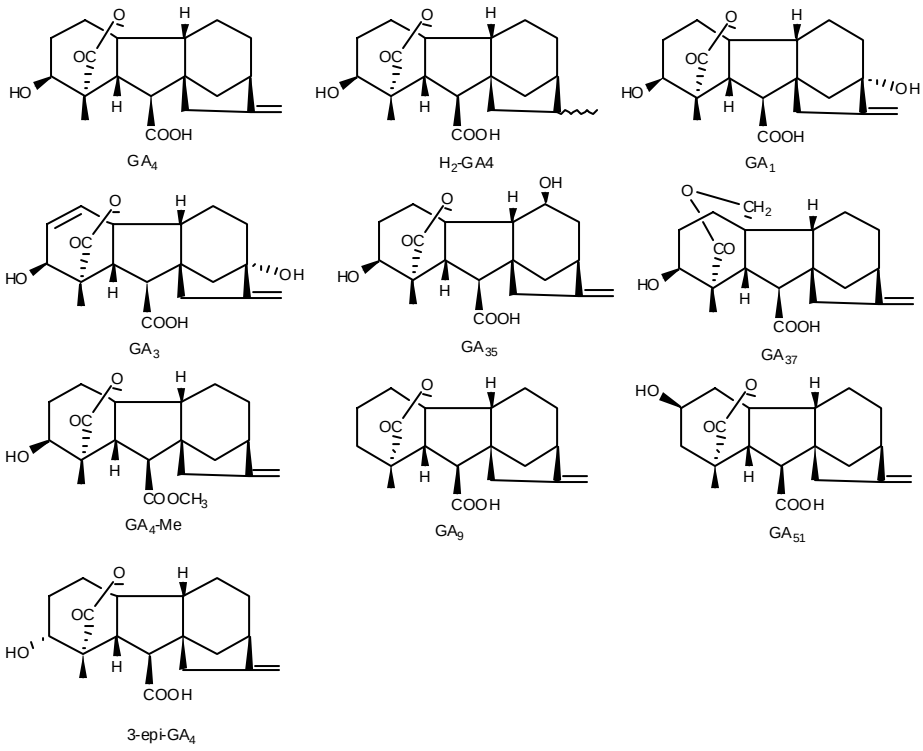

Figure 6. Structures of GAs with different biological activity.

Table 1. Competition for [$^3H_4$]-16,17-dihydro GA_4 binding to GID1 by GAs. (Table adapted from Ueguchi *et al.*[57]).

GAs	IC_{50}	Relative percentage
Biologically active GAs		
GA_4	2×10^{-7} M	100
H_2-GA_4	1×10^{-6} M	20
GA_1	4×10^{-6} M	5
GA_3	4×10^{-6} M	5
Weakly biologically active		
GA_{35}	1×10^{-5} M	2
GA_{37}	2×10^{-5} M	1
Biologically inactive GAs		
GA_4-Me	3×10^{-5} M	0.6
GA_9	2×10^{-4} M	0.1
GA_{51}	$>2 \times 10^{-4}$ M	<0.1
3-*epi*-GA_4	$>2 \times 10^{-4}$ M	<0.1

A simplified model of GA signaling pathway, including biosynthesis and signal transduction is depicted on Figure 7.

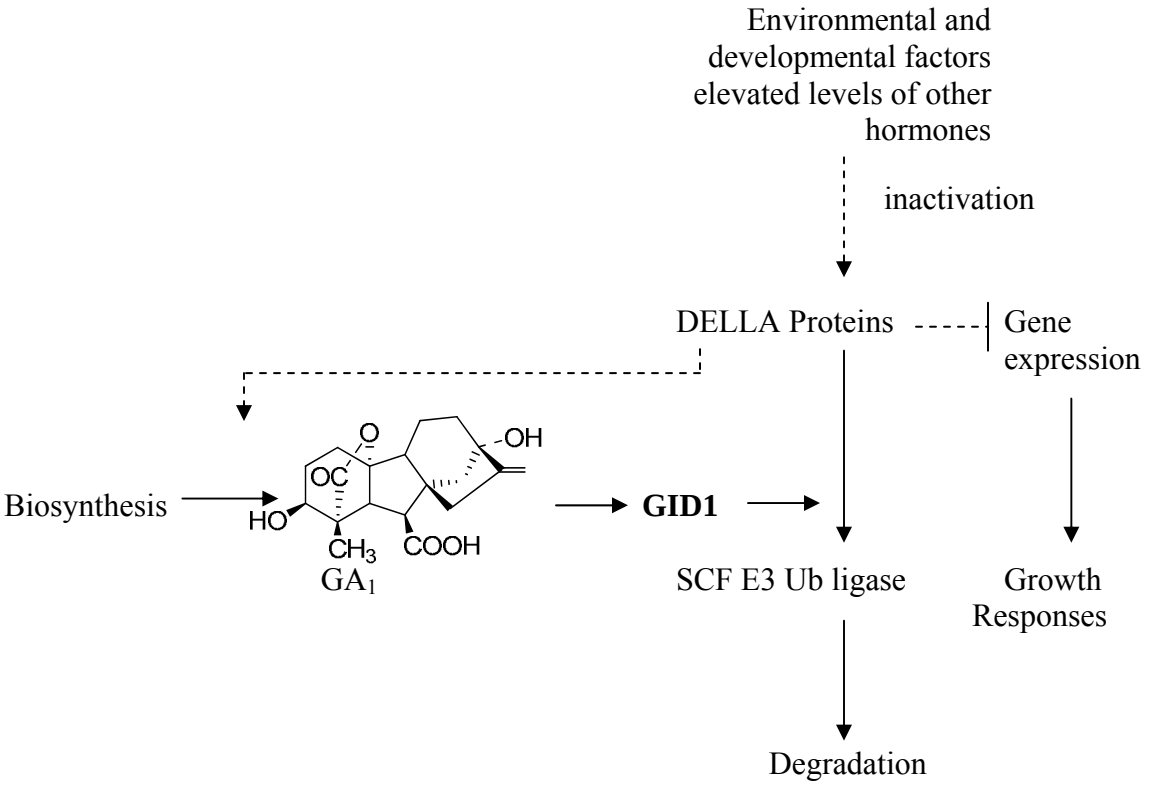

Figure 7. Proposed mechanism of regulation of GA-responsive growth and development.[59] see description in text.

It has been reported[57] that in the absence of bioactive GAs, DELLA proteins repress GA-dependent growth by suppressing the expression of primary GA-response genes. This repression is relieved when GA levels are elevated as a consequence of environmental, developmental and hormonal signals. This occurs either by increased GA biosynthesis or reductions of its inactivation. Elevation of GA levels causes GID1-mediated ubiquitiation of the DELLA proteins through an SCF E3 Ub ligase, followed by degradation by the 25S proteasome. Decreased DELLA protein levels induce changes in the expression of primary GA-response genes, and therefore promotes GA-dependant plant growth and development. These responses include feed back regulation of GA

metabolism, which means that GA signaling leads to down-regulation of the expression of GA-biosynthesis genes, and on the other hand GA-inactivating genes are up-regulated. The possible contribution of membrane receptors, for which there is considerable indirect evidence, remains unclear, and so do immediate targets for DELLA proteins and the mechanism by which they regulate transcription. A major challenge is the identification of genes that are regulated by GA signaling, directly or indirectly, and to determine how their activity translates into the physiological consequences of GA action.

1.5. Ethylene

Ethylene is a gaseous plant hormone that affects numerous developmental processes and vigor responses, including germination, flower and leaf senescence, fruit ripening, leaf abscission, root nodulation, programmed cell death, and responsiveness to stress and pathogen attack.[60,61] A well-known effect of ethylene on plant growth is the so-called "triple response" of etiolated dicotyledonous seedlings. This response is characterized by the inhibition of hypocotyl and root cell elongation, radial swelling of the hypocotyl, and exaggerated curvature of the apical hook. This highly specific ethylene response occurs at an early developmental stage (3 days post-germination), permitting large mutant populations of seedlings to be screened rapidly for ethylene response defects. Over the past decade, genetic screens that are based on the triple-response phenotype have been extensively conducted on *Arabidopsis* by many laboratories. More than a dozen unique mutants have been identified and these can be divided into three distinct categories: constitutive triple-response mutants (i.e. *ethylene overproduction1* [*eto1*], *eto2*, *eto3*, *constitutive triple response1* (ctr1) and *responsive to*

antagonist1 [ran1]/ctr2); *ethylene-insensitive mutants* (i.e. ethylene receptor1 [*etr1*], *etr2*, *ethylene insensitive2* [*ein2*], *ein3*, *ein4*, *ein5*, and *ein6*); and tissue-specific ethylene-insensitive mutants (i.e. *hookless1* [*hls1*], *ethylene insensitive root1* [*eir1*], and several auxin-resistant mutants). Genetic and molecular analyses of the above mutants have defined a mainly linear ethylene response pathway primarily from hormone perception at the membrane to transcriptional regulation within the nucleus.[60-62]

In *Arabidopsis*, ethylene is perceived by a family of five membrane-associated receptors, (ETR1, ETR2, ERS1, ERS2 and EIN4).[63-65] which are highly analogous to bacterial two-component regulators.[66] Based on structural similarities, this receptor group can be divided into two categories. The first is the type-I subfamily, which includes ETR1 and ERS1. These two proteins contain an N-terminal ethylene binding domain (a sensor domain) and also a highly conserved C-terminal histidine (His) kinase domain. Second, type-II receptors which include ETR2, ERS2 and EIN4 share a common N-terminal ethylene-binding domains as well as a degenerate His kinase domain which lacks one or more elements that are necessary for catalytic activity. In addition ETR1 (type-I), ETR2 and EIN4 (type-II) contain an additional receiver domain at C-terminal whose function is still unknown. A major breakthrough in understanding the mechanism of ethylene signaling was the discovery of ethylene perception site which is located at the endoplasmic reticulum (ER).[67,68] Previous reports suggested that the ethylene receptors might be localized at the plasma membrane. Recently however, Arabidopsis ETR1 has been shown credibly, on the bases of both sucrose density-gradient fractionation and immunogold electron microscopy, to associate with the ER. The N-terminal membrane-spanning sensor domain of ETR1 is adequate for the ER association. Ethylene treatment

or introduction of the etr1-1 mutation did not affect the ER localization of ETR1. Importantly, CTR1 (ETR1 binding protein) has also been found to be localized at the ER.[68] CTR1 consists an N- -terminal domain of unknown function, and a C-terminal kinase domain that is most related to Raf-like mitogen-activated protein kinase (MAPK) kinase. Previous yeast two-hybrid and pulldown experiments showed that the amino-terminal domain of CTR1 can interact with the His kinase domains of ETR1 and ERS1.[69] Because CTR1 has no trans-membrane domain or membrane attachment motifs, it is possible that its ER localization might result from direct interaction with the ER-associated receptors. This hypothesis predicts that the removal of ethylene receptors or disruption of the interaction between CTR1 and these receptors would decrease the level of ER-associated CTR1. To test this possibility, a series of single, double, and triple receptor mutants have been examined to assess the effect of functional receptors on the ER localization of CTR1.[68] Whereas most single receptor mutations had little effect on the level of ER-bound CTR1, double and triple combinations of receptor mutations resulted in reduced levels of ER-bound CTR1. Moreover, the levels of ER-bound CTR1 correlated with the strength of the constitutive- ethylene-response phenotypes in the multiple receptor mutants. In addition, a missense mutation in the amino-terminal domain of CTR1 (CTR1-8) was found to disrupt the interaction of CTR1 with ETR1. This mutation did not affect the kinase activity or the level of the CTR1 protein, but conferred phenotypes that were as severe as those of CTR1-kinase-dead mutants. Accordingly, the CTR1-8 protein was primarily soluble, suggesting that an association with ER-bound receptors is required for CTR1 function.[70,71] The proof of CTR1–ETR1 interaction in vivo comes from two lines of evidence. Affinity purification of CTR1 from the

Arabidopsis ER-membrane fraction results in the co-purification of ETR1, demonstrating the presence of ETR1 and CTR1 in the same protein complex.[68] Genetic evidence is also available to support the proposition that CTR1 function may be regulated by its association/dissociation with the ethylene receptors.[72] Figure 8 (adapted from Guo *et al.*[73]) represents a model for signaling by the ethylene receptor-CTR1 complex.

As mentioned before, there are two types of ethylene receptors in *Arabidopsis*. Type-I includes ETR1 and ERS1 which possess a conserved histidine kinase domain (red on Figure 8). Type-II group of receptors which are ETR2, ERS2 and EIN4, include a degenerate histidine kinase domain (orange on Figure 8) which lacks catalytic activity. The N-terminal sensor domains of the receptors contain a copper cofactor required to maintain ethylene binding ability and are ER associated. It was found that the interaction between the N-terminal domain of CTR1 (green on Figure 8) was of higher affinity with type-I receptors than type-II receptors.

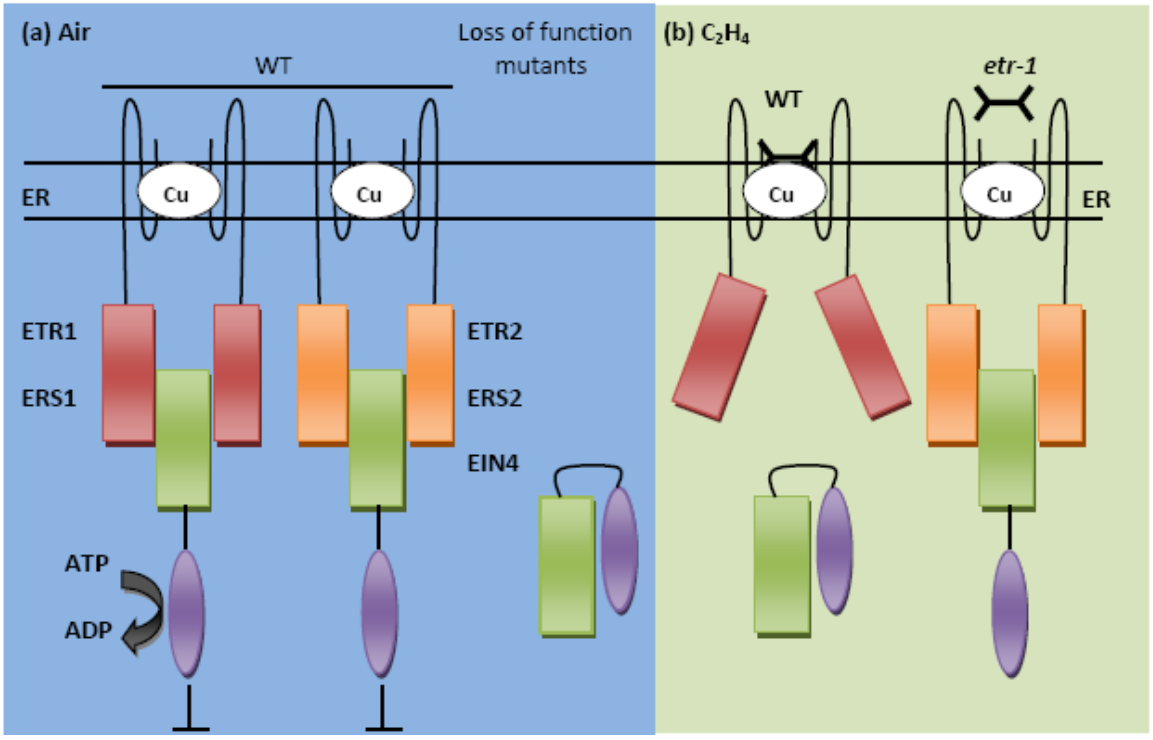

Figure 8. Proposed signaling mechanisms of the ethylene receptors and CTR1 at the ER (figure adapted from Guo *et al.*[73]).

Figure 8a represents a situation in the absence of ethylene where the receptors are in functionally active state and are able to interact with CTR1. Association of CTR1 with ER-bound receptors activates CTR1 and represses the ethylene response through a mechanism that requires its C-terminal domain (Ser/Thr kinase domain, purple on Figure 8). Loss of function in multiple receptors (in LOF mutants) causes the dissociation of CTR1 from the ER. CTR1 is therefore inactivated *via* self-association using a negative regulatory domain (previously shown for Raf kinases). As a consequence, the repression of ethylene responses is relieved. Ethylene, (Figure 8b) when present, binds to the sensor domain of the receptor and leads to conformational changes which inactivate the receptor. CTR1 is released from ER at this point and becomes inactivated. Mutations within the receptor cause disruption in ethylene binding which are assumed to lead to constitutive receptor-CTR1 interaction and the

repression of downstream components in the ethylene signaling pathway. Despite the substantial evidence showing that CTR1 is directly regulated by ethylene receptors, the biochemical basis of such regulation is still elusive. It is also known that ethylene can modulate responses to other plant hormones such as JA, salicylic acid, auxin, ABA, and cytokinin however the mechanisms controlling each of these hormone-hormone interactions are still unkown.[74]

The ethylene binding domain (EBD) found in ETR receptors has been studied in detail by Wang et.al[75] who employed site directed mutagenesis to alter ethylene binding capability of EBD domain. This was achieved by amino acid substitutions in 37 partially or completely conserved residues of the EBD and the effects assayed by ethylene binding and signaling. Mutations within residues located in mid-regions of Helices I and II eliminated ethylene binding and conferred constitutive signaling. This was consistent with the inverse-agonist model of ethylene receptor signaling and suggested that these residues define the ethylene binding pocket. Most mutations clustered near the cytoplasmic ends of Helices I and III, gave normal ethylene binding activity yet still conferred constitutive signaling. Therefore, these residues may play a role in turning off the signal transmitter domain of the receptor. By contrast, only two mutations were loss of function with respect to signaling. These results provided insight into the structure and function of the EBD and indicated a conserved role of the EBD as a negative regulator of the signal transmitter domain.

Wang *et al.*[75] have recently reported the identification of important regions for ethylene binding and signaling in the transmembrane domain of the ETR1 from *Arabidopsis*.

The ethylene binding domain (EBD) of the *Arabidopsis thaliana* ETR1 receptor was modeled as three membrane-spanning helices. Ethylene binding activity was investigated in

different kingdoms and bioinformatic analyses of the EBD were performed. Ethylene binding was found to be restricted to land plants, and also a group of cyanobacteria but was not found in other organisms. Thirty seven amino acid substitutions of partially or completely conserved residues of the EBD were made and the effects assayed against ethylene binding. Mutations of residues within Helices I and II midregions eliminated ethylene binding and conferred constitutive signaling, consistent with the inverse-agonist model of ethylene receptor signaling and also indicated that these residues are part of the ethylene binding pocket. The largest class of mutations, clustered near the cytoplasmic ends of Helices I and III, exhibited normal ethylene binding activity yet still conferred constitutive signaling. It is suggested that these residues play a role in turning off the signal transmitter domain of the receptor. With respect to signaling, only two mutations led to a loss of function. These findings provided more information about the structure and function of the EBD and indicated a conserved role of the EBD as a negative regulator of the signal transmitter domain.

1.6. Jasmonates

Jasmonic acid (JA) and metabolites, such as its methyl ester (MeJA) or amino acid conjugates of JA, all of them named jasmonates were recognized as important signals in plant responses to biotic and abiotic stress.[76] The term jasmonate includes the biologically active intermediates in the pathway for jasmonic acid biosynthesis, as well as the biologically active derivatives of jasmonic acid. These compounds are widely distributed in plants and affect a variety of processes[77] including fruit ripening, production of viable pollen, root growth, tendril coiling, plant response to wounding and abiotic stress, and finally defenses

against insects and pathogens.[78] Jasmonates originate from precursors such as 12-oxophytodienoic acid (ODPA), and dinor-ODPA (dnODPA) which are jointly called octadecanoids. These JA precursors are produced within the lipoxygenase (LOX) pathway which is initiated by oxygenation of free or esterified polyunsaturated fatty acids (PUFAs), leading to many different products collectively named oxylipins. More recently, octadecanoids and some other oxylipins were recognized to be JA-independent signals in plant stress responses. Apart from studies on oxylipin biosynthesis, a growing interest is given to their perception and signal transduction. Transgenic approaches and analyses of mutants led to basic knowledge on JA signaling, specifically cross-talk with other plant hormones (signaling) such as salicylate, ethylene and abscisic acid. Since identification of the first JA-insensitive male sterile mutant[79] the knowledge on the role of jasmonates in developmental processes has been steadily increasing.

The JA signal is assumed to be transduced through the activation of receptors that bind these molecules, however, no receptors have thus far been identified. *Arabidopsis* defense responses are induced by jasmonic acid and ODPA. VSP (vegetative storage protein) transcription and stamen development are induced by jasmonic acid but not by ODPA.[80] This suggests that in *Arabidopsis* , there at least two JA signal transduction pathways, one for recognition of either jasmonic acid or ODPA for defense responses, and a second for recognition of jasmonic acid, but not ODPA, for stamen development. The JA signal pathway regulates aspects of development and diverse responses to stress. A major challenge is to devise assays which will identify genes that perceive the primary stress signal. In tomato, the primary stress signal is transmitted *via* peptide signal molecules, but in *Arabidopsis*, it is not yet known how the wound stress signal is transmitted, and elucidation

of this still remains as a goal of future research.[81] It is still unknown how JAs are perceived, and identification of the JA receptor(s) therefore remains a significant challenge. JA, SA and ethylene signaling pathways interact cooperatively and antagonistically in a variety of responses. A particular challenge is therefore to discover which points of the JA signaling pathway interact with outputs from the SA and ethylene signal pathways, and vice versa. The current understanding of the JA signaling pathway reveals a great complexity, and therein the opportunity for multiple control sites and flexibility of function.[81,82]

1.7. Salicylic acid

Various physiological processes have been associated with SA and include flowering, thermogenesis (heat generation), stomatal closure, and leaf abscission.[83] Exogenous acetylated SA was first shown in tobacco to protect against tobacco mosaic virus (TMV) and was found to be noticeably associated with the induction of pathogen-related proteins (PRs).[84] Also, SA is found in plants after pathogen infection, locally inducing SA endogenous signal for systematic acquired resistance (SAR).[85] These findings initiated studies on molecular mechanism of plant defense. Shortly after the discovery of SA it was recognized as a hormone, and many hypotheses in hormone research were employed to study and understand its molecular action. The primary entry point in such research was the finding of SA receptor. Binding studies in tobacco using radiolabeled SA have revealed the identity of the first receptor/binding protein: catalase SABP (salicylic acid binding protein). The enzyme was found to be inactivated upon binding SA (K_D of 14 μM) which resulted in an increase of intracellular H_2O_2 concentration. This phenomenon was interpreted as activation of defense gene expression or as an antimicrobial barrier at the site of invasion.[86] SA, and its

functional analogue 2,6-dichloroisonicotinic acid were found to be inhibitors of ascorbate peroxidase (APX) which also is considered as H_2O_2-scavenging enzyme. The inhibition of both catalase and APX, but not of guiacol peroxidases, (being involved in cell-wall biosynthesis) supports a model in which SA-induced defense responses are mediated through elevated levels of H_2O_2 or coupled to alterations of the cell redox state.[87] However, the hypothesis that SA acts *via* inhibition of catalase was questioned for several reasons and H_2O_2 was placed upstream of SA in the signal transduction pathway.[88] Shortly after another SABP (SABP2) protein was found in tobacco that exhibits high affinity for SA (K_D of 90 nM).[89] This protein exhibits esterase and an SA-inducible lipase activity.[90] Tobacco SABP2 knock-out mutants exhibited loss in local and systemic-induced resistance to TMV.[90] SABP2 was assigned to the α/β hydrolases superfamily by 3D analysis of its crystal structure. It was also confirmed that it is capable of MeSA binding to the enzyme catalytic site containing Ser-His-Asp motif. It is assumed that SABP2 may participate in the control of intracellular SA levels rather than being a true receptor for SA. That is because MeSA was found to have higher affinity to SABP2 than SA.[91]

Another SABP, SABP3 was found in the soluble fraction of purified tobacco leaf chloroplasts, with carbonic anhydrase function (CAN).[92] SA was found to bind to CAN with moderate affinity (K_D of 3.7 μM) with its enzymatic activity being unaffected by the presence of SA. Binding kinetics of SAPB3 and SA are depicted on Figure 9. Apart from carbonic anhydrase activity CAN also exhibits antioxidant properties. A recombinant SAB3/CAN together with its homologue SABP2 from tobacco complements a yeast mutant sensitive to oxidative stress. CAN knock-out mutants in *Nicotiana bethamiana* exhibited suppressed

response in plant-pathogen interaction. These results lead to the conclusion that, all three proteins interacting with SA have antioxidant activities.

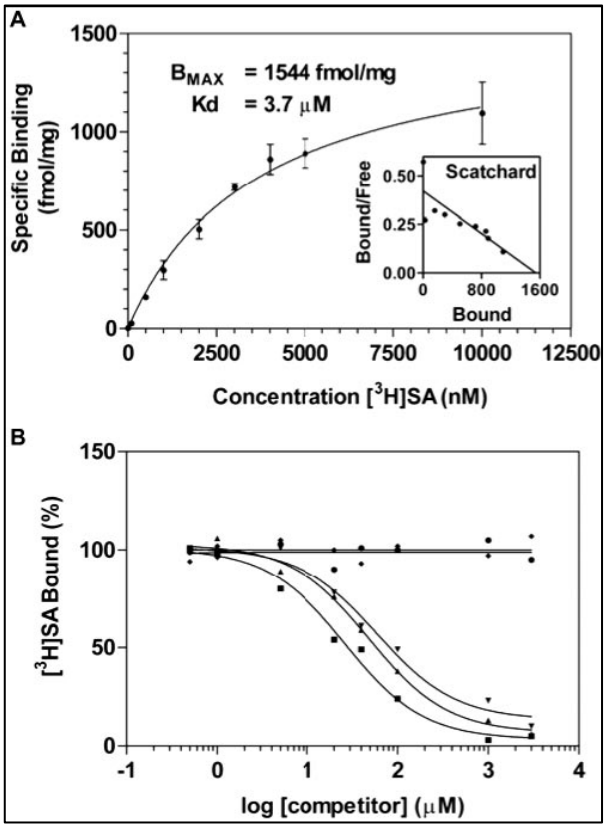

Figure 9. Tobacco leaf chloroplasts contain a specific moderate-affinity SA-binding activity that can be used to discriminate between biologically active and inactive SA analogs. (*A*) Saturation-binding assays showing saturable specific binding of [^{3}H]SA to a soluble chloroplast protein(s). Scatchard analysis of the binding data suggests a single class of binding site. K_D and B_{MAX} values were calculated by using single binding-site hyperbolic nonlinear regression analysis. (*B*) Competition binding assays with SA analogs showing a positive correlation between binding affinity and biological activity. SA (▼) and its active analogs 5-chlorosalicylic acid (■) and 2,6-dihydroxybenzoic acid (▲) showed similar affinity for SABP3 compared with the inactive SA analogs 4-hydroxybenzoic acid (♦) and 4-aminosalicylic acid (●) (figure and caption copied from Slaymaker *at.al*[92] with permission).

Slaymaker *et al.* [92] has proposed that the ability of SA to inhibit both cytosolic and chloroplast antioxidant enzymes might be a part of its molecular action. SA may activate a positive feedback loop for SA production due to its ability to increase the level of reactive

oxygen species (ROS), which can then lead to induction of defense responses following pathogen infection.[92] SA exhibits the ability to form free radicals upon inhibition of heme-containing enzymes, such as peroxidase or catalase. This led to the new "free radical" hypothesis concerning SA action.[93,94] According to that hypothesis, SA action is related to the effect of free radicals on lipid peroxidation, the products of which might activate defense reactions.[95] However, the relationship between free radicals and induction of resistance still needs to be further evaluated.

In summary, the discovery of tobacco CANs as SA-binding proteins which at the same time exhibit antioxidant activity raised new questions regarding SA function in plant defense, as well as CAN function in chloroplasts. Of particular interest was the validation of CAN antioxidant activity in plants, its nature, and finally determination of whether this activity is truly altered by SA. The results reported so far suggest that SA has many effects on the physiology of plants and does that by interacting with multiple effector protein(s) that are not of typical receptor nature.

1.8. Brassinosteroids

Brassinosteroids (BR) are steroidal plant hormones. The first brassinosteroid was discovered in 1973, when it was shown that pollen from *Brassica napus* promotes stem elongation and cell divisions and that the biologically active molecule was a steroid the authors named Brassins.[96] Since their discovery, over 70 BR compounds have been isolated from plants.[97] BRs are involved in numerous plant processes such as: promotion of cell expansion and cell elongation[98] and share a signaling pathway with auxin in this process.[99] BRs were found to have a role in cell division and cell wall regeneration.[98]

Another observed function of BRs is promotion of vascular differentiation; BR signal transduction has been studied during vascular differentiation[100] It is also required for pollen elongation and pollen tube formation.[101] It was also reported that BRs provide protection to plants during abiotic stress such as chilling and drought.[98] BRs induce a signaling cascade at plasma membrane upon binding to BRI1 (Brassinosteroid insensitive 1) receptor. The BRI1 gene encodes a leucine rich repeat receptor-like kinase (LRR-RLK)[102]. Mutants of this gene were identified by genetic screens for plants showing dwarfism and lack of root growth inhibition upon treatment with BRs.[103] The importance of BRI1 in BR signaling has been highlighted in many literature reports, and there is substantial evidence that BRs bind directly to BRI1.[104] Kinoshita *et al.*[104] has confirmed the BR-BRI1 interaction and identified the BR binding site using photoaffinity labeling.

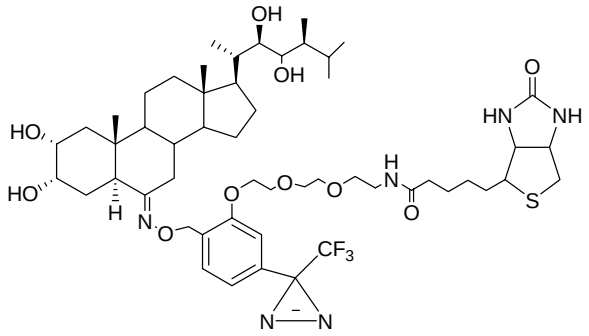

Figure 10. Structure of photoaffnity probe BPCS, castasterone *O*-{2-[2-[2-(2 biotinylaminoethoxy)ethoxy]ethoxy]-4-[3-(trifluoromethyl)-*3H*-diazirin-3-yl].[104]

Biotin-tagged castasterone (BPCS), a biosynthetic precursor of brassinolide (the most active brassinosteroid) with a photoaffinity label (phenyldiazirine) incorporated in its structure was used to identify the BR binding domain within BRI1. The structure of this photoaffinity probe is depicted in Figure 10. Previous studies have shown that the extracellular domain, especially the island domain (ID), might be responsible for BR

perception.[105] In order to identify the BPCS-binding region in BRI1 Kinoshita *et al.*[104] expressed five BRI1 fragments surrounding the ID as glutathione S-transferase (GST) fusion proteins in *E.coli*, and performed photoaffinity crosslinking using three recombinant protein fragments. LRR21-ID-LRR22 and ID-LR22 showed strong binding signals, but the ID alone, LR21-ID and LR22 alone did not bind BPCS. BRR21 alone and the intracellular domain of BRI1, including its serine/threonine kinase domain, also did not bind BPCS. These results indicated that both the ID and LRR22, which immediately flanks the ID on its C-terminal side (ID-LRR22), are crucial for BPCS binding.

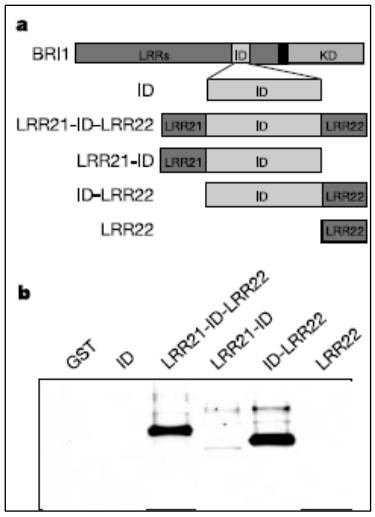

Figure 11. ID-LRR22 in the extracellular domain of BRI1 is sufficient for BPCS binding. **a** – structures of BRI1 and BRI1 fragments. KD, kinase domain. **b**- BPCS binding in BRI1 domains purified from *E.coli* protein bank visualized by biotin-sensitive Western detection system (figure and caption copied from Kinoshita *et al.*[104] with permission).

Binding studies using BPCS, [^{3}H]-labeled brassinolide and recombinant BRI1 fragments showed that the minimal binding domain for bassinosteroids consists of a 70-amino acid domain located between LRR21 and LRR22 in the extracellular domain of BRI1, together with C-terminal flanking LRR (LR22). These results have shown that

brassinosteroids bind directly to the 94-amino acid region comprising ID-LR22 in the extracellular domain of BRI1 and have defined a new binding domain for steroid hormones with K_D = 15-55 nM. Discovery of other LRR-RLKs interacting with radiolabeled BRs and similar to BRI1 suggested that BRI1 is not the only BR receptor.[100] Autophosphorylation of BRI1 was found to be stimulated by BRs, and its status is also modulated through interaction with another LRR-RLK brassinosteroid-associated kinase 1 (BAK1).[106]

Identification of BAK was based on its ability to suppress the *bri1* dwarfing phenotype when over-expressed, and *via* a yeast 2-hybrid screen.[107] Based on that evidence it is postulated that BRs induce BRI1 and BAK1 to form an activated receptor complex *via* the change in phosphorylation status of this complex. This kind of mechanism closely resembles the animal receptor kinase signaling. BAK1 is thought to be a component of the BR receptor complex.[108,109] BAK1 interacts with BRI1 both *in vitro* and *in vivo*, and they phosphorylate each other *in vitro*. Results of both gain-of-function and loss-of function experiments support a positive role for BAK1 in BR signaling.[109] The molecular mechanism by which BR activates the receptor kinases is unclear. However *in vivo* interaction between BRI1 and BAK1 has been confirmed, but the effect of BR on this interaction is not known. Thus, the hypothesis remains to be tested that ligand binding might activate the kinases by inducing receptor heterodimerization, as known for the receptor tyrosine kinases and the transforming growth factor β receptor kinases in animals.[107] Because BR treatment did not increase receptor phosphorylation nor association between BRI1 and BAK1 co-expressed in yeast cells[108], and in addition BR binding activity was not detected for recombinant BRI1 proteins expressed in non-plant cells[105] It is postulated that either proper modification of the receptor kinases or additional proteins are required for BR binding and signaling. The BRS1 serine

carboxypeptidase is thought to be responsible for proteolysis of an extracellular component of the BR receptor complex.[110]

Biochemical purification of all proteins associated with the BRI1–BAK1 receptor kinase complex should provide further insight into the molecular mechanism of the BR receptor function.

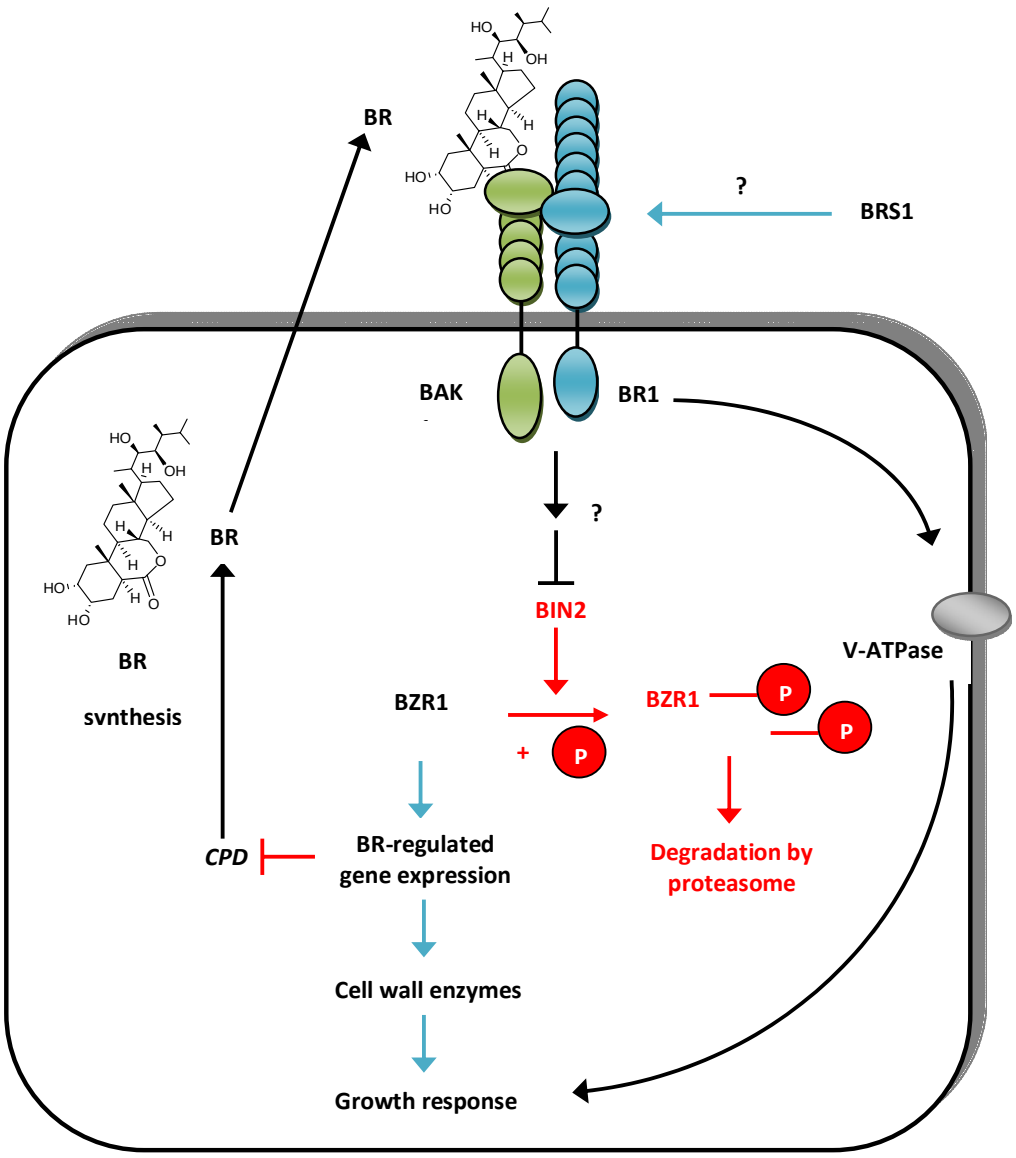

Figure 12. A diagram of the brassinosteroid (BR) signal transduction pathway in *Arabidopsis*. BR is perceived by the receptor complex containing BRI1 and BAK1, which are leucine-rich-repeat receptor-like kinases (LRR-RLKs) that interact with each other. Activation of the receptor kinases by BR binding leads to the dephosphorylation and accumulation of the nuclear proteins BZR1 and BZR2/BES1, possibly by inhibiting the negative regulator BIN2. In the absence of BR, the BIN2 kinase phosphorylates BZR1 and BZR2/BES1, and targets them for degradation by the ubiquitin-dependent proteasome pathway. BZR1 and BZR2/BES1 regulate BR-target genes differently; these targets include the BR biosynthetic gene CPD, which is feedback inhibited by BR through BZR1, and genes encoding enzymes for cell wall synthesis that are probably regulated by both BZR1 and BZR2/BES1. The vacuolar H^+-ATPase (V-ATPase) is also a mediator of certain BR responses. The serine carboxypeptidase BRS1 is proposed to process an unknown extracellular factor that contribute to the activation of the BR receptors. (figure and caption adapted from Wang and He[111])

1.9. Abscisic acid

The plant hormone abscisic acid (ABA) is responsible for many developmental and physiological processes in plants and also it is a key hormone in plant environmental stress response.[112-118] ABA induction of embryo-specific genes in developing seeds leads to accumulation of storage proteins and lipids, desiccation tolerance and prevention of germination. Plant response to environmental stresses, such as drought, high salinity or low temperature results in increase of ABA levels where it is involved in induction of stress-related genes as well as control of water relations by regulation of stomatal closure. In order to understand the physiological changes in plants caused by ABA it is necessary to identify and characterize its binding proteins. A major difficulty with discovering ABA receptors is that no genetic mutations have been identified that are directly related to ABA receptor loss-of-function.

There is little experimental evidence to date that illustrates the nature of ABA perception. Discovery of ABA receptors associated with specific functions would allow the creation of transgenic plants with recombinant ABA receptors. This would allow controlled alterations to ABA perception and plant growth regulation or environmental stress response. In addition from the chemical point of view the structural information about ABA-binding proteins would give an opportunity to develop new ABA-analogs as plant growth regulators.[119,120]

1.9.1. ABA perception

Binding of ABA to its receptor protein(s) is considered as the first step in ABA's signal transduction.[113,121] Three recently reported ABA receptors,[122-124] were disputed due to contradictory results reported by various research groups (see further section for discussion).[125,126]

Neither genetic nor biochemical approaches have identified other protein candidates that would meet the requirements of a functional receptor protein, especially those related to abiotic stress.[127] Several lines of indirect evidence have suggested that there are multiple ABA receptor types.[128] The existence of structurally different ABA-receptor proteins has been suggested by the observation that optically pure ABA isomers can substitute for natural (S)-ABA in some ABA-regulated responses.[129] (R)-ABA and the three isomers (*trans* bond at C-4 C-5, and either a single or double bond at the C-2' C-3' double bond) with the same configuration at C-1' as natural ABA were found to be effective germination inhibitors. Biologically active and inactive ABA (Figure 13) analogs exhibited differential effects on ABA-responsive gene expression, which has been thoroughly studied by Huang *et al.*[130] Schwartz *et al.* [131] suggested on the basis of indirect evidence that both intracellular and extracellular ABA receptors can exist. The intracellular location of ABA-receptor was suggested by the induction of ABA-responses by cytoplasmic application of ABA [132] and identification of ABA-binding sites from cytosolic protein fractions.[133] Many individual components of ABA transduction pathway have been identified but the complete process has not yet been described. Therefore it is unknown what process follows the interaction of ABA with its receptor and if there are any other proteins, which recognize ABA. Although other

plant hormone receptors such as those for auxin and ethylene have been identified, less progress in identification an analysis of ABA receptors is reported. [128,134,135] Shortly after submission of this thesis the discovery of two new ABA receptors have been reported.[149, 168]

1.9.2. ABA-binding proteins in ABA catabolism

Catabolism of ABA has been widely reported and many ABA metabolites (Figure 13) have been fully characterized, although most enzymes that catalyze formation of ABA metabolites are not yet identified and isolated. The principal pathway for enzymatic deactivation of ABA is the most characterized process, catalyzed by cytochrome P450 monooxygenase enzyme, ABA-8'hydroxylase.[136-138] ABA is oxidized on the 8' position, which yields 8'-hydroxy-ABA, which then isomerizes to form the biologically inactive metabolite phaseic acid (PA). The gene encoding ABA-8'-hydroxylase has been cloned and the enzyme was produced in several expression systems (insect cells, yeast) and exhibited its activity towards oxidation of ABA by efficient conversion to phaseic acid (PA).[139] There are other metabolic enzymes in the ABA catabolic pathway such as reductases and monooxygenases which lead to formation of ABA 1',4'-diols and dihydrophaseic acid (DPA) or putative 7'-hydroxylase yielding 7'-hydroxy-ABA respectively. In addition, the enzyme catalyzing ABA glucose ester formation appears to be a conventional glucosyltransferase employing UDP-glucose as co-substrate. [140,141] Zhou *et al.*[142] described a new pathway of ABA oxidation *via* 9'-hydroxylation. This pathway results in the formation of 9'-hydroxy ABA which cyclizes to neo-phaseic acid. This indicates the existence of another ABA metabolic enzyme, ABA-9'-hydroxylase. ABA-8'-hydroxylase and ABA-glucosyltransferase are the only ABA metabolic enzymes identified to date.

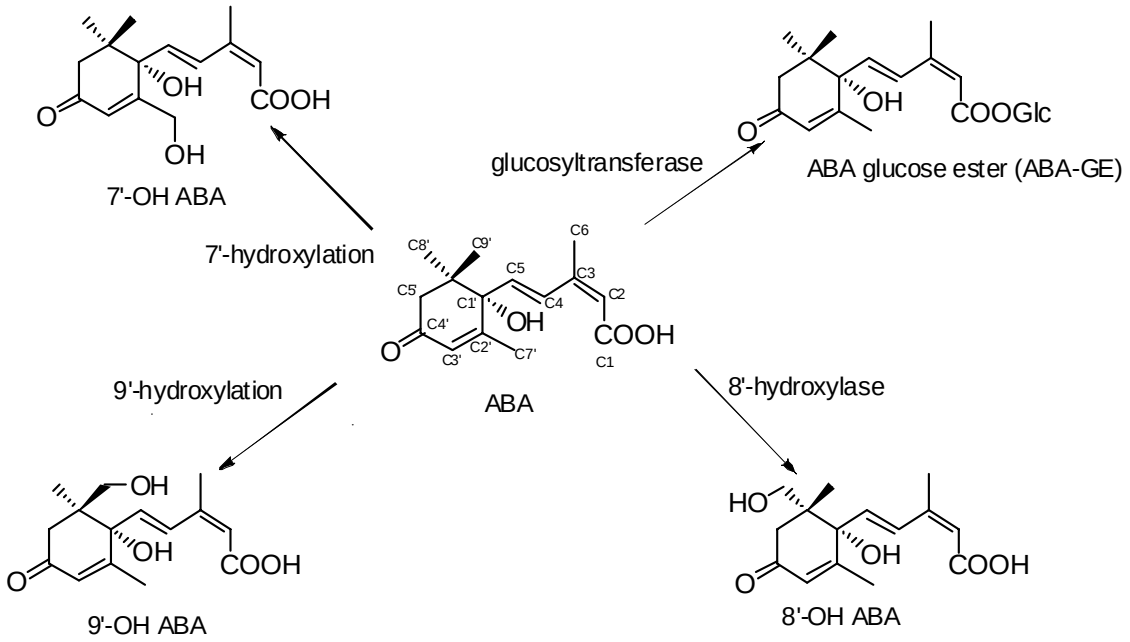

Figure 13. Major ABA catabolic pathways: glucosylation, 8', 7' and 9'-hydroxylation.

1.9.3. ABA-binding proteins and receptors

Transport of ABA across plant cell membranes has been of interest to many scientists for many years. [143-145] There are several proposed mechanisms of ABA transport. It is postulated that ABA accumulates in cells due to acid trapping.[146] This occurs because of the lipophilic character of ABA as a neutral molecule at acidic pH which allows ABA to cross cell membranes from acidic apoplasts into the cytosol. In other words a passive uptake of ABA becomes one of the possible mechanisms.[147] Since ABA accumulates through passive uptake in the cells it implies the existence of a mechanism for subsequent export from the cells. In the absence of an export mechanism, the cells in which ABA is biosynthesized would accumulate ABA to high and undesired levels (in the absence of turnover). By analogy to other hormones like IAA, ABA is expected to have a specific carrier protein (not

reported to date) which actively exports it from the cell. Dietz and Hartung have suggested that ABA-glucose ester is the exported form of ABA.[148] An extracellular glucosidase released ABA from its glucose conjugate. It was shown that barley xylem sap has β-glucosidase activity which releases ABA from its physiologically inactive glucose ester. They hypothesized the possibility of ABA-glucose ester being a long-distance transport form of ABA although there are not characteristics concerning β-glucosidase.

As mentioned previously three new putative ABA receptors have been reported[122,124,149] and those include an RNA binding protein FCA by Razem *et al.* [149] (paper withdrawn), the G-protein coupled receptor GCR2 by Liu *et al.*[122], and finally the Mg-chelatase H subunit reported by Shen *et al.*[124] All three papers have been questioned by various research groups, and some contradictory results to those were recently published.[125,150,151]

Using genetic methods, Shen *et al.*[124] have previously identified an ABA-binding protein from broad bean called ABAR and suggested that this protein may be potentially involved in stomatal signaling because the gene encoding the H subunit of Mg-chelatase (CHLH) was a major component in chlorophyll biosynthesis and plastid-to-nucleus signaling. This group has recently advanced further[124] and showed that *Arabidopsis* ABAR/CHLH binds ABA stereospecifically, mediates ABA signaling in seed germination as well as post-germination growth and stomatal movement, which suggests the possibility that ABAR/CHLH is an ABA receptor. Other functions of CHLH have been previously reported, mostly the enzymatic functions as a subunit of the Mg-chelatase involved in producing photosynthetic apparatus[152] but also this protein has an important function plastid-to-nucleus signaling and its mediation.[153] Shen *et al.* have shown that purified yeast-expressed

Arabidopsis ABAR exhibits specific and saturable binding of ABA, with 1:1 protein:ligand molar ratio, and equilibrium dissociation constant (K_D) of 32 nM.

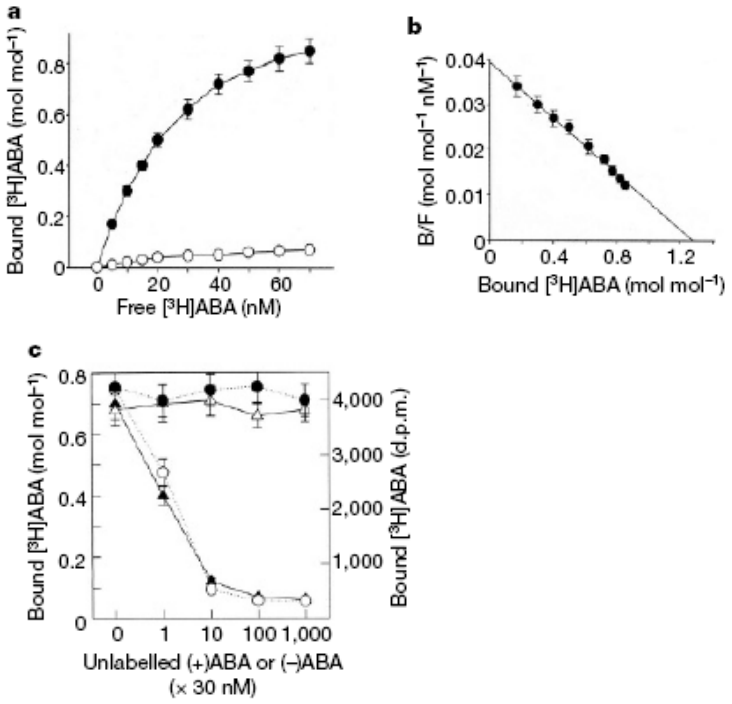

Figure 14. ABAR binds ABA. **a**, Saturable ABA-specific binding (filled circles) to the pure yeast-expressed ABAR. Open circles, non-specific binding. **b**, Scatchard plot of binding data in **a**. B, [^{3}H]ABA bound; F, free [^{3}H]ABA. The parameters of the curve are K_D = 32 nM; B_{max} 51.28 mol mol^{-1}; R^2=0.98. **c**, Displacement of [^{3}H](+)-ABA binding by (+)-ABA and (-)-ABA. Filled triangles, *in vitro* (+)-ABA binding (mol mol^{-1}); open triangles, in vitro (-)-ABA binding (mol mol^{-1}); filled circles, (-)-ABA pull-down assay (d.p.m.); open circles, (+)-ABA pull-down assay (d.p.m.) (figure and caption copied from Shen *et al.*[124]with permission)

Purified ABAR binds ABA stereospecifically, which was confirmed by the efficient displacement of [^{3}H] (+)-ABA binding by the physiologically active form of (+)-ABA but not by less active analogs (-)-ABA and inactive *trans*-ABA.

Muller *et al.* have further evaluated the barley magnesium chelatase and its large subunit (H) in particular.[125] In contrast to Shen *et al.* Muller's findings suggested that ABA had no effect on the magnesium chelatase activity nor did the enzyme show ABA binding ability. Magnesium chelatase mutants showed wild-type response with respect to post-

germination growth and stomatal aperture. It was shown that barley CHLH did not exhibit saturation kinetics with radiolabeled ABA, however the *Arabidopsis* equivalent was found to bind ABA with binding ratio of one ABA molecule per H-subunit and equilibrium dissociation constant of 32 nM. Magnesium chelatase from barley and *Arabidopsis* share 82% sequence identity although the differences in ABA response between the two almost identical proteins cannot be explained at this point. The possibility of CHLH being an ABA receptor is currently unclear. Most recently Pandey *et al.*[154] have reported the discovery of two GPCR-type G proteins (GTG1 and GTG2) as ABA receptors. It was found that *Arabidopsis* mutants lacking both *GTG1* and *GTG2* exhibit, ABA hypersensitivity and bind ABA stereospecifically. Apart from their apparent receptor functions both proteins also show GTPas activity. GDP-bound forms of GTGs showed greater ABA binding than did the GTP-bound forms. It was suggested that GTPase activity of both GTGs can be inhibited by GPA1 and its knockout mutants (*gpa1*) exhibited ABA–hypersensitivity. Pandey *et al.* predict that it is the GTP-bound form of GTG rather than GTP-bound form that is responsible for signal relay. It was postulated that the two new GTG proteins can function as both, G proteins and new membrane ABA receptors. GTG1 and GTG2 showed saturable and specific binding of ABA, and equilibrium dissociation constants of 35.8 nM and 41.2 nM respectively. Both GTG1 and GTG2 showed more efficient ABA binding in the presence of GDP, as compared to binding in the presence of GTP or ATP, which is illustrated in Figure 15.

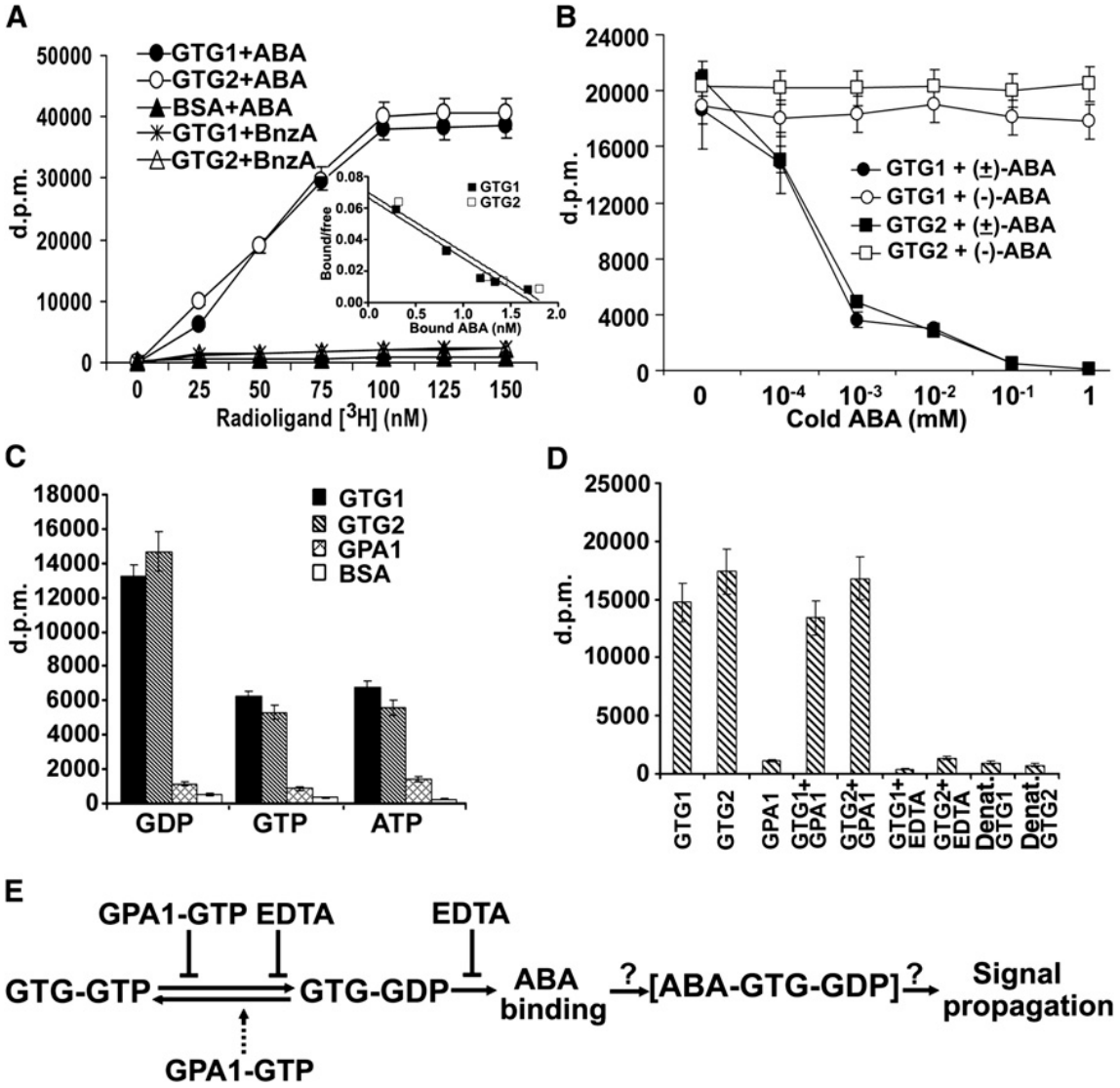

Figure 15. Specific ABA binding by GTG1 and GTG2 reported by Pandey *et al.*.[154] (**A**) Both GTG1 and GTG2 show saturable ABA binding with increasing concentrations of ^{3}H-ABA. No binding was detected when BSA instead of GTG1 or GTG2 was used or by using H-benzoic acid (BnzA) instead of ^{3}H-ABA. Equilibrium dissociation constants for GTG1 are K_D = 35.8 ± 2.6 nM, and for GTG2 K_D= 41.2 ± 3.1 nM. (**B**) ABA binding by GTG1 and GTG2 is competed by (±)-ABA but not by the biologically inactive stereoisomer, (-)-ABA. (**C**) GTG1 and GTG2 bind ABA more efficiently in the presence of GDP (5 mM) as compared with GTP (5 mM) or ATP (5 mM), (**D**) GPA1 does not bind ABA alone nor affects the efficiency of binding of GTG1 or GTG2 when added together in the reaction mix in the presence of 5 mM GDP. No binding of ABA by both GTG1 and GTG2 is observed in the presence of EDTA (2 mM). Also, heat-denatured GTG proteins do not bind ABA. (**E**) proposed model for mechanism of action of GPA1 and GTG proteins. Question marks indicate aspects of the model inferred from, but not directly demonstrated by, experimental results to date. (figure and caption copied from Pandey *et al.*[154] with permission).

Pandey *et al.* suggested that the GTGs are ABA receptors and that GPA1 controls GTG in such way that GTP-bound GPA1 downregulates ABA binding, therefore ABA-signal transduction by the GTGs (Figure 15E). On the other hand, the authors suggest that GDP-bound GTGs bind ABA which induces the ABA signaling cascade.

It was also shown that single *gtg* mutant plants were indistinguishable from wild-type, however the double *gtg1 gtg2* mutant exhibited significant differences, which were mostly related to ABA signaling, both at early and adult stages. The double mutant *gtg1 gtg2* phenotype was complemented with introduction of either the GTG1 or the GTG2 genes, which suggested idleness in GTG function. The *gtg1 gtg2* mutant exhibited hyposensitivity to ABA in seed germination and post-germination growth assays. About 50% of the wild-type *Arabidopsis* seeds germinated on a medium with 1 μM ABA. The germination percentage of *gtg1 gtg2* mutant seeds was 80%. About 40% germination was obtained with 2 μM ABA for *gtg1 gtg2* mutants. At this concentration of ABA no wild-type seeds have germinated.

ABA induction of stomatal closure in *gtg1 gtg2* mutant plants were found to be ABA hyposensitive, and showed only a 17% decrease in stomatal aperture in contrast to an 40% decrease in wild-type plants. On the other hand, ABA inhibition of stomatal opening remained similar to that of wild-type plants.

1.9.4. Affinity-based approaches to identify ABA-binding proteins

Despite numerous attempts to isolate and characterize ABA-binding proteins none of the applied techniques have provided researchers with satisfactory amount of evidence. Many research groups have tried affinity-based methods to purify ABA binding proteins but, although apparently promising results have been obtained, the lack of reproducibility has been a major problem. A primary drawback with affinity approaches (photoaffinity labeling, affinity columns etc.) is that they usually require derivatizing ABA by attachment to an affinity matrix or by photochemical labeling. This can result in a substantial loss in hormonal activity, which is reflected by reduced affinity of the ABA derivative for the receptor protein. This effect has been observed for derivatives in which the free carboxyl group at C-1 is modified. Chemically, C-1 derivatives are the easiest derivatives to make but blocking the carboxyl group to form an ester or compromise hormonal activity.[155,156] Zhang *et al.* [157] has reported isolation of 42-kDa ABA-specific binding protein from epidermis of broad bean leaves. ABA has been linked to sepharose through a C-1 carbon and affinity chromatography was used as a method for capturing ABA binding protein (Figure 16) The function and sequence of the isolated protein have not yet been described.

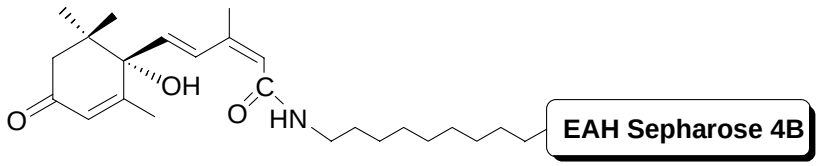

Figure 16. C-1-derivatized ABA by Zhang *et al.*

Other groups have tried to modify ABA at positions chemically available for modification which are also crucial for ABA biological activity. Pedron *et al.* [158] modified ABA at the C-4' and C-1 positions by conjugation to a carrier protein (BSA) that is recognized by anti-BSA antibodies (Figure 17A). The C-4' modification was done by linking through a hydrazone-type bonding which was later reported to be very unstable under biological conditions [159] and may could have been hydrolyzed to yield ABA. The same type of ABA modification was also reported by Yamazaki *et al.*. [160] who used biotinylated ABA (bio-ABA) to attempt to localize ABA-binding proteins on stomatal guard cells (Figure 17B). The putative ABA-binding proteins were visualized by fluorescence microscopy and confocal laser scanning microscopy using "bio-ABA" and fluorescence-labeled avidin. C-4' modification of ABA is likely to reduce ABA's activity. [159]

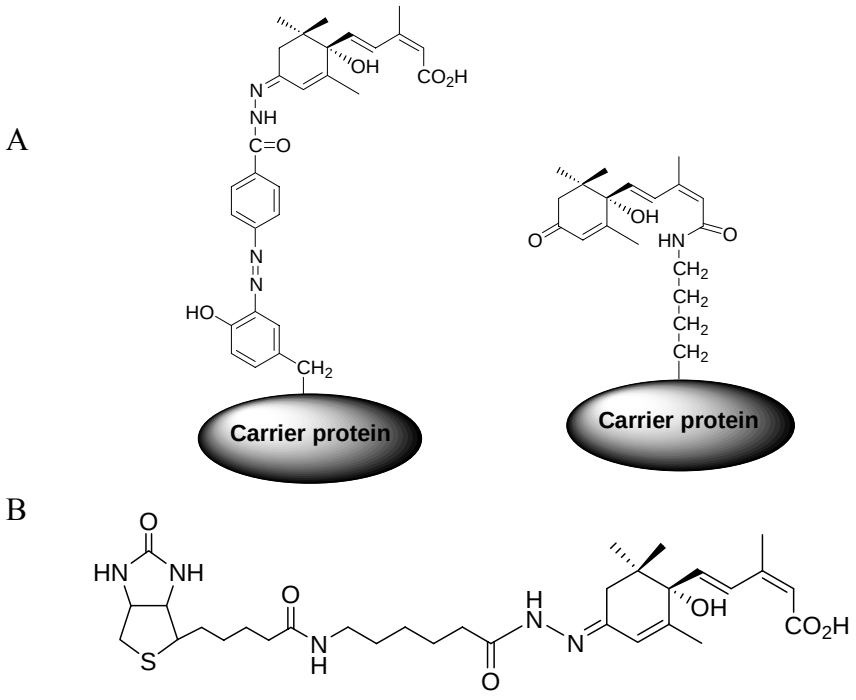

Figure 17. Modification of ABA at C-1 and C-4'. A- carrier protein coupled to ABA *via* C-4' and C-1 by Pedron *et al.* B- biotinylated ABA modified at C-4' by Yamazaki *et al.*[160]

The approach to identification of ABA-binding proteins described in further parts of this thesis is based on development of affinity probes in which modification of ABA molecule will not affect its biological activity. In other words ABA-derivatives (Figure 18) designed for this purpose contain the important features of the ABA molecule. This means that positions which are essential for biological activity such as configuration at C-1', carboxyl (C-1) and ketone (C-4') groups are not modified. A bicyclic analogue of ABA named tetralone-ABA and its derivatives exhibited a high level of activity in biological assays.[161] In tetralone-ABA derivative replacement of vinyl methyl group with an aromatic ring allows the molecule to retain biological activity. The presence of aromatic ring blocks the ring closure subsequent to 8-hydroxylation, a reaction similar to formation of phaseic acid. Biological activity of tetralone-based ABA derivatives prompted the design of a tetralone-based analog containing biotin. The synthesis of tetralone-based biotinylated ABA analogs was previously reported.[162,163] These derivatives were used in this project as organic probes to identify ABA-binding target proteins and their structural features will be further described.

2. Results and Discussion

2.1. Introduction of new multifunctional probe PBI 686, and its validation by affinity chromatography methods using known ABA-binding proteins

Affinity-based methods employing a biologically active derivative of ABA have the potential to identify ABA binding proteins including receptors. To date, probes constructed from derivatives of ABA linked through either the carboxyl group or the ketone have been employed to isolate proteins from plant extracts. [157,158,160] An inherent problem with these probes is that alterations of ABA at C-1 and C-4' result in substantial loss in hormonal activity, presumably because of reduced affinity for ABA receptors. As mentioned previously, Zhang *et al.*[157] reported the isolation of a 42 kDa ABA-binding protein from the epidermis of broad bean leaves by affinity chromatography with ABA linked by an ester to sepharose through C-1. The function and sequence of the isolated protein have not yet been determined.

The first objective of this project was to validate the newly designed probe (PBI 686) and check whether it can be recognized by known ABA-binding proteins.

The second objective was to identify ABA –binding proteins using PBI 686 as a tool which incorporates all the functional groups of ABA required for binding and activity. Structure-activity studies to probe the requirements of the ABA molecule for perception and action in assays in a variety of plant tissues led to the conclusions that the following features of the ABA molecule should be maintained: stereochemistry at C-1', the vinyl carbon group

on the cyclohexenone ring, the acid functional group on the side chain and the ketone on the ring.[164]

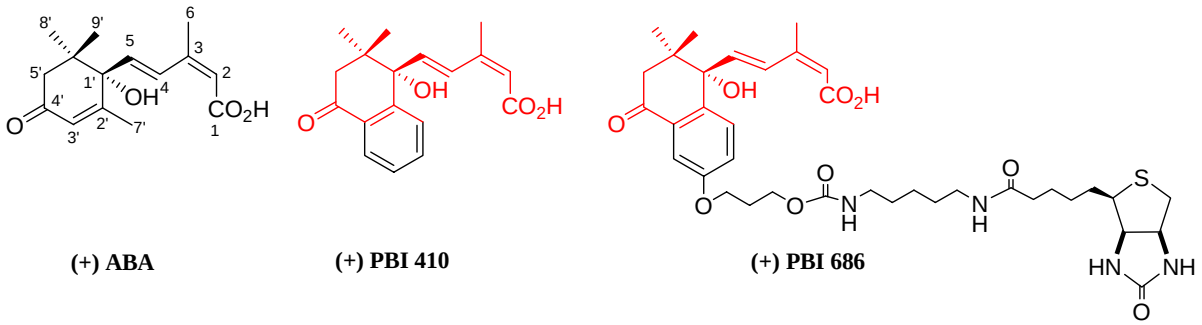

Figure 18. (+)-ABA, and bicyclic analogues PBI 410 and 686.

These requirements are met in a biologically active bicyclic analog PBI 410 (Figure 18), in which an aromatic ring replaced the planar vinyl methyl group.[163] It was anticipated that an affinity probe PBI 686 could be developed with biotin group attached through a tether to the aromatic ring without sacrificing biological activity. The synthesis of a bioactive biotinylated bicyclic ABA probe (PBI 686) was reported earlier.[162] The C-1 carboxylic acid group, vinyl carbon and the C-4' carbonyl group, which are crucial for ABA's activity, remain unmodified.

ABA induces synthesis and modification of genes involved in storage lipid deposition in *Brassica napus*. Cultured microspore-derived embryos of *B. napus* are responsive to ABA and are a convenient system for probing hormonal regulation of gene expression and lipid synthesis.[165] The activity of analog PBI 686 to induce 3-ketoacyl-CoA synthase (*FAE*) expression in microspore-derived embryos of *B. napus* was compared to ABA. At 10 μM, analog PBI 686 was more potent than ABA in inducing mRNA for the *FAE* gene at 72 h, whereas the untreated control at 72 h did not exhibit any signal (Figure 19).

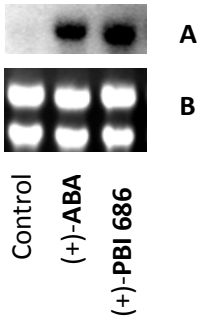

Figure 19. (**A**) Northern analysis of FAE expression with ABA analog treatment (**B**) RNA loading for (+)-ABA and (+) PBI 686. (Experiment performed by Dr. Ashok Jadhav).

An affinity matrix was prepared using the biotinylated probe PBI 686 and streptavidin-linked sepharose, and employed in two experiments validating the probe for binding to ABA–specific proteins. Binding of the probe to an anti-ABA monoclonal antibody (mAb) raised against (+) ABA[166,167] was tested first. According to the literature the anti-(+) ABA mAb did not cross-react with (-)-ABA but the cross-reactivity with (±) PBI410 (Figure 18) was found to be 23% relative to (+)-ABA (100%) and (±)-ABA (50%).[166,167] The mAb was retained by the column upon buffer wash, and was released when racemic ABA was applied as the eluting agent at the same pH (Figure 20, panel A lane 2 vs lane 3). The unmodified column without the probe did not retain the antibody.

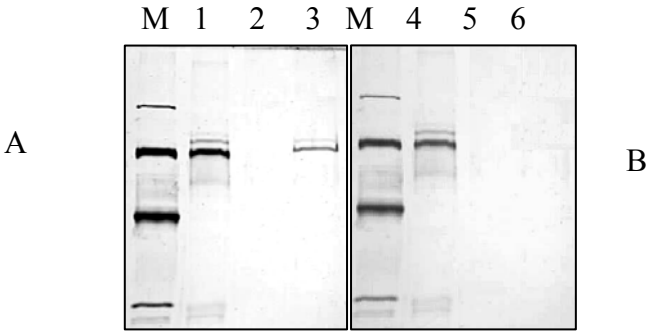

Figure 20. A-SDS-PAGE of fractions collected from column modified with PBI 686 (M) - protein MW standard (from top: 97.4, 66.2, 45.0, 31.0 kDa), (1)- solution of anti-ABA monoclonal antibody, (2) - buffer wash, (3)-5mM (±)-ABA wash, **B**-fractions collected from unmodified column used as control. (4)- solution of anti-ABA monoclonal antibody, (5)-buffer wash, (6)-5 mM (±)-ABA wash.

The affinity probe described above was also used to isolate a membrane-bound protein, ABA-8'-hydroxylase.[139,169] The *Arabidopsis* gene is encoded by CYP707A1, the cDNA open reading frame of which was transferred to pYeDP60 for expression in the WAT11 strain of *Saccharomyces cerevisiae.*[170] The yeast expression vector, pYeDP60, was generously provided by Denis Pompon (CNRS-Centre de Génétique Moléculaire). The solubilized microsomal fraction was applied to the affinity column and the CYP707A1 enzyme was found to be eluted with ABA (Figure 21). No specific binding of proteins to the column in protein preparations from yeast transformed with only the pYePD60 (Figure 21) was observed. BSA, which is present in the microsomal protein extraction buffer in high quantity, was difficult to remove from the column and was therefore found in all column eluates. Q-TOF mass spectrometry (MS/MS ion search with tryptic peptides) confirmed the presence of the ABA 8'-hydroxylase enzyme in crude yeast microsomal extracts as well as in fractions from the column eluted with ABA. Peptide sequences derived from the purified, trypsinized protein were compared with published sequences and as expected, corresponded to CYP707A1. The peptide coverage map and search score chart are presented on Figure 22. Tryptic digest contained a number of peptides which represented 69% of the predicted amino-acid sequence. This is direct evidence that ABA 8'-hydroxylase bound to the probe PBI 686 on the affinity column and validated the probe as being recognized by an authentic ABA-binding protein.

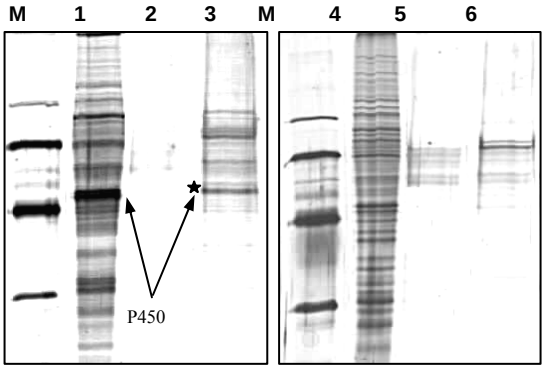

Figure 21. SDS-PAGE of fractions collected from the column modified with PBI 686. (M) – protein MW standard (from top: 97.4, 66.2, 45.0, 31.0 kDa), (1) - crude microsomal protein extract from yeast cells expressing CYP707A1, (2) - buffer wash, (3) -10 mM (±) ABA wash, (4) - crude microsomal protein extract from yeast cells with pYeDP60 (control), (5) - buffer wash, (6) -10 mM (±) ABA wash.

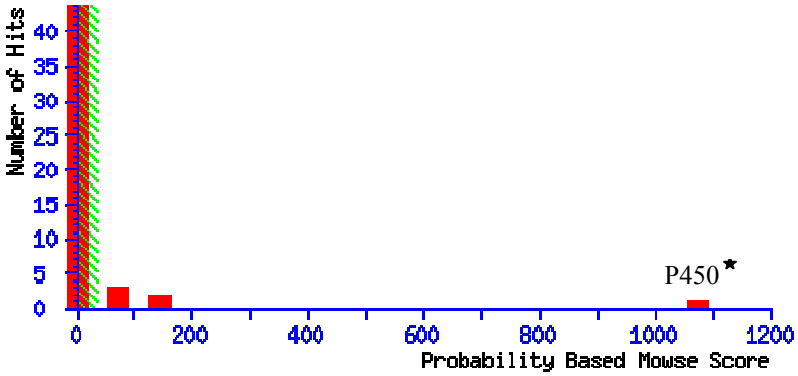

1. gi|18415271 **Mass:** 53288 **Score:** 1073, **Peptides matched:** 37 CYP707A1 (cytochrome P450, family 707, subfamily A); oxygen binding [Arabidopsis thaliana]

P450 peptide coverage map:

```
   1 MDISALFLTL FAGSLFLYFL RCLISQRRFG SSKLPLPPGT MGWPYVGETF
  51 QLYSQDPNVF FQSKQKRYGS VFKTHVLGCP CVMISSPEAA KFVLVTKSHL
 101 FKPTFPASKE RMLGKQAIFF HQGDYHAKLR KLVLRAFMPE SIRNMVPDIE
 151 SIAQDSLRSW EGTMINTYQE MKTYTFNVAL LSIFGKDEVL YREDLKRCYY
 201 ILEKGYNSMP VNLPGTLFHK SMKARKELSQ ILARILSERR QNGSSHNDLL
 251 GSFMGDKEEL TDEQIADNII GVIFAARDTT ASVMSWILKY LAENPNVLEA
 301 VTEEQMAIRK DKEEGESLTW GDTKKMPLTS RVIQETLRVA SILSFTFREA
 351 VEDVEYEGYL IPKGWKVLPL FRNIHHSADI FSNPGKFDPS RFEVAPKPNT
 401 FMPFGNGTHS CPGNELAKLE MSIMIHHLTT KYSWSIVGAS DGIQYGPFAL
 451 PQNGLPIVLA RKPEIEV
```

Figure 22. MS/MS ion search results and peptide sequence coverage map of P450 eluted from the affinity column by (±)-ABA.

2.2. Initial screening for novel ABA-binding proteins in *Arabidopsis* microsomal fractions using PBI686

Using the approach described in previous section it was attempted to isolate new ABA-binding proteins from microsomal protein fractions of *Arabidopsis* (see experimental section) which were applied on streptavidin affinity column previously modified by the probe PBI 686. *Arabidopsis* was chosen due to the fact that entire genome of this plant has been sequenced which also indicates that most proteins are identified for this plant.

Fractions eluted with 10 mM (±)-ABA contained some new candidate proteins. These three most frequently identified are: 83 kDa Cytochrome c oxidase subunit II PS17 (*Arabidopsis thaliana*, gi|109892850) and 107.6 kDa RNA-binding protein of the Puf family (*Arabidopsis thaliana*, gi|9293981), and 60.5 kDa putative phototropic-responsive protein, (*Arabidopsis thaliana*, gi|15229647). All three proteins showed low MS/MS ion search scores, which is most likely due to their low abundance in total protein extracts. This is confirmed by the presence of mostly one tryptic peptide on MS spectrum, thus marginal sequence coverage. Figure 23 illustrates MS/MS ion search results for proteins eluted from affinity column (two fractions) with ABA.

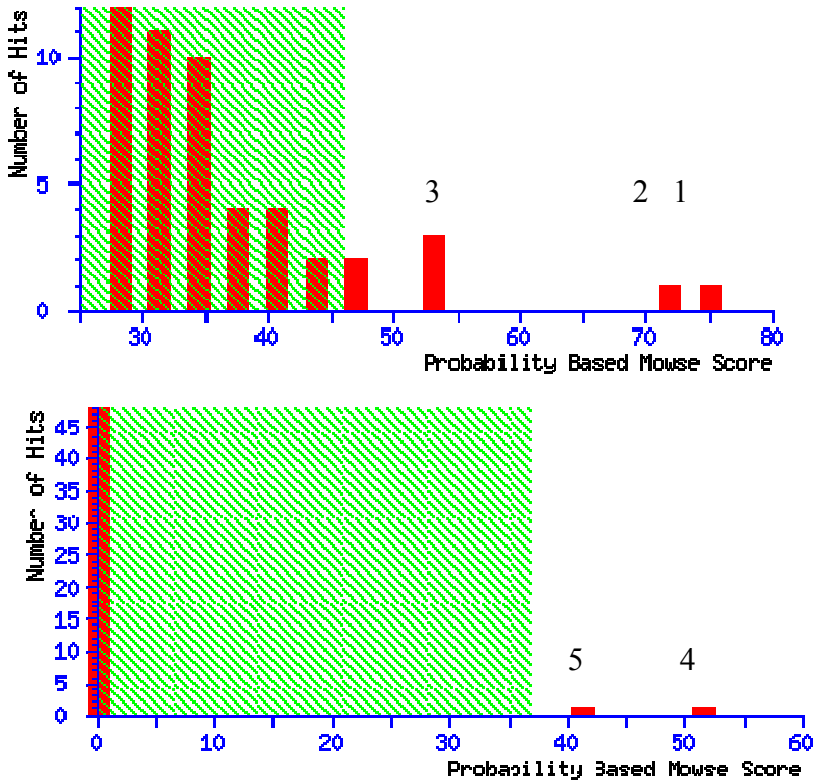

1. gi|109892850 **Mass:** 83100, **Score:** 75, **Peptides matched:** 4,(Putative cytochrome c oxidase subunit II PS17)

2. gi|205830697 **Mass:** 1394, **Score:** 72, Peptides **matched:** 1 , (Unknown protein)

3. gi|15229647 **Mass:** 60495, **Score:** 52, Peptides **matched:** 1 (phototropic-responsive protein, putative [Arabidopsis thaliana])

4. gi|15229647 **Mass:** 60495 **Score:** 52 **Peptides matched:** 1, phototropic-responsive protein, putative [Arabidopsis thaliana]

5. gi|9293981 **Score:** 41 **Peptides matched:** 1, RNA binding protein-like [Arabidopsis thaliana]

Figure 23. MS/MS ion search results (Mascot) of proteins (*Arabidopsis* crude microsomal extract) eluted from the affinity column by ABA.

The five proteins mentioned in Figure 23 are potential candidates; however, their low identity scores were not sufficient to pursue further studies on their interaction with ABA. However the low identity scores should not exclude them from future research, especially because it is expected for potential receptor proteins to be in low abundance in total protein extracts.

Despite the use of large tissue quantities for microsomal protein extractions (50-100 g), attempts to obtain higher amounts of putative ABA-binding proteins were unsuccessful. Therefore, from this point on, photoaffinity labeling was used as an alternative method for identification of putative ABA binding proteins.

2.3. Photoaffinity labeling (PAL) using probe PBI 686

Galardy and co-workers[171] were among the first research groups to introduce the use of aryl ketone derivatives for photolabeling peptides and proteins (e.g bovine serum albumin known to bind carboxyl terminal tetrapeptide of gastrin) with aryl-azido and aryl ketone derivatives of pentagastrin. In addition, the model photoreactions of acetophenone and benzophenone with N-acetylated glycine methyl ester were investigated and the photoaddition products isolated (Figure 24)

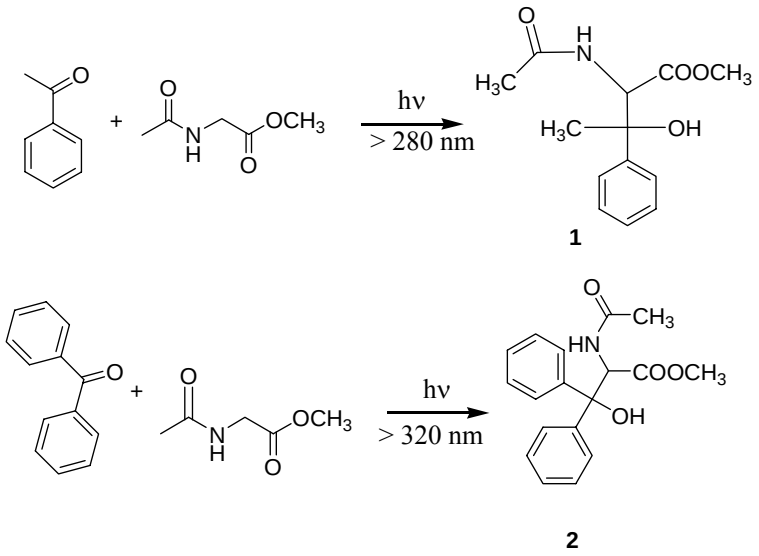

Figure 24. Products of photoaddition reaction of acetophenone and benzophenone to Ac-Gly-OMe reported by Galardy and co-workers.[171]

Products **1** and **2** were isolated and characterized by NMR. Photolysis of acetophenone and Ac-Gly-OMe yielded an insertion product with 6% yield, whereas benzophenone reaction gave compound **2** with 30% yield. Both reactions were run for equivalent times. The isolation of photoaddition products of both acetophenone and benzophenone with Ac-Gly-OMe demonstrated the ability of aryl ketone photoaffinity probes to covalently bind to amino acid residues. The results of these model reactions and the successful labeling of albumin with ketone derivatives of pentagastrin indicated that aryl ketones may be useful photoaffinity probes. It was also suggested that aryl ketones have an advantage over other photoaffinity probes (arylazido) because the ketone triplet state is nearly inert to reaction with water. Thus little ketone photoaffinity label will be lost to hydrolysis in a biological labeling experiment and the label need not be used in excess.

Acetophenones are often reported as polymerization initiators [172,173] and unlike benzophenones, are rarely referred to as protein photochemical labeling reagents. In the literature there are reports on one application of acetophenone as protein labeling reagent.

Zor *et al.* [174] used the acetophenone derivative of Guanidine triphosphate (GTP) as an alternative to its benzophenone equivalent which exhibited a significant loss of binding affinity to the target protein. They used acetophenone-GTP as a photoaffinity label to isolate and identify GTP-binding proteins.

PBI 686 incorporates an acetophenone moiety which similarly to benzophenone reacts exclusively from its corresponding triplet state.[175] As reported previously,[162] the probe PBI 686 was found to be suitable for isolation of new ABA-binding proteins using affinity chromatography approach. This probe incorporates three important functionalities: structural resemblance to ABA with biological activity, a biotin purification handle, and a photo-activable acetophenone moiety. Biological activity has been evaluated [162, 163] and compared to ABA, the functionality of biotin tag has been validated by affinity chromatography with known ABA-binding proteins.[162] This approach was based on isolation of new proteins using non-covalent interactions between PBI686 immobilized on the column and putative ABA – binding proteins in crude cell lysates. It was observed that when using known proteins which were applied on affinity column in large quantities, there was a great loss of binding during the column washings. It was still possible to identify the specific proteins in ABA eluates, however utilizing this method to isolate non-overexpressed, endogenous proteins may not have been a method of choice. It was anticipated that utilizing the probe for photoaffinity labeling would reduce the loss of bound proteins during affinity chromatography. The proposed mechanism (analogous to benzophenone) of photoaffinity labeling which utilizes PBI 686 is depicted on Figure 25.

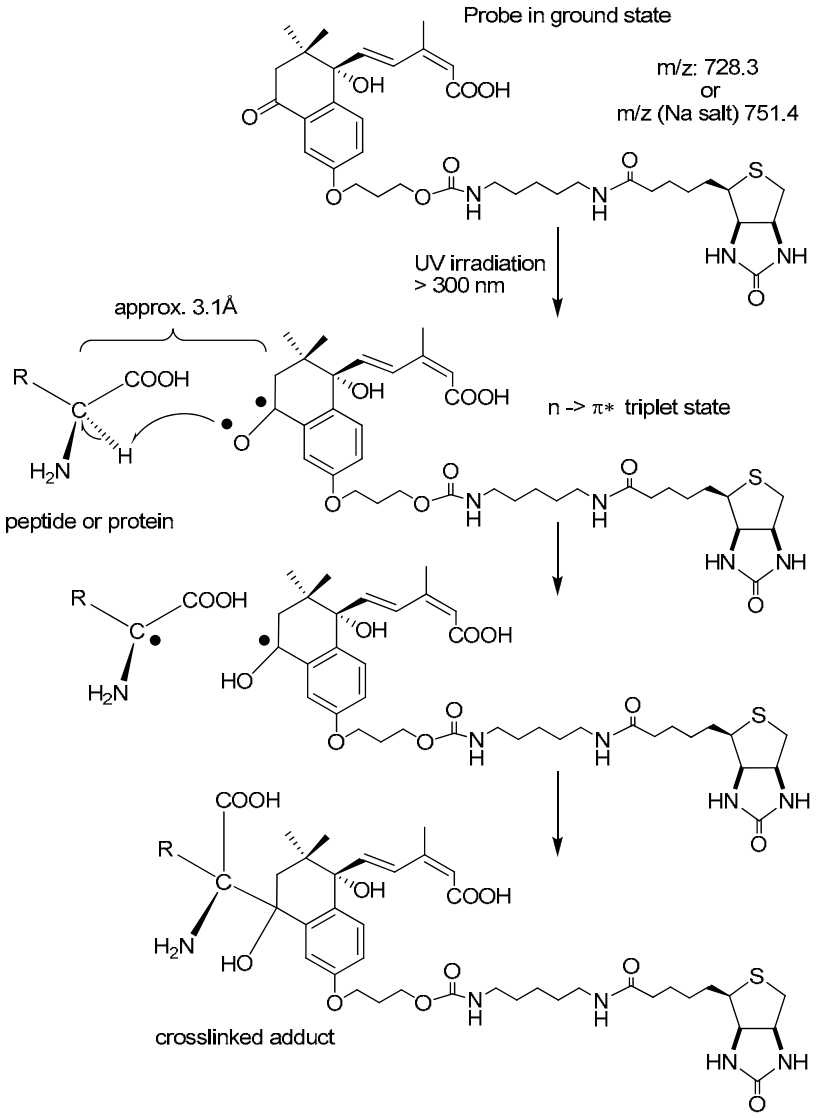

Figure 25. Proposed photoaffinity labeling mechanism of PBI 686.

2.4. PAL labeling of peptides

To validate the photolabeling ability of the probe and identifying labeled proteins by MS methods it was investigated using a model system by studying its reaction with short peptides rather than proteins. Prior to that the MS analysis of the probe under different

ionization conditions (MALDI-TOF, LC/MS) were performed to predict the structure of adducts in terms of their mass increase. The theoretical monoisotopic mass of PBI 686 molecular ion in a positive ionization mode (MALDI-TOF, high resolution, mass accuracy 20 ppm) m/z equals 729.3528 although it was not observed on a MALDI spectrum. Instead a molecular ion representing the sodium adduct m/z = 751.3347 and second, the probe dehydration product m/z = 711.3422 (Figure 26). Additionally low resolution LC/MS experiments (mass accuracy 1Da) were performed (Figure 27) to verify results by MALDI-TOF. In negative ionization mode LC/MS, a peak corresponding to the deprotonated molecular ion appears as m/z = 727. On the other hand the positive ionization mode LC/MS reveals all three: m/z = 711, 729 and 751 ions. The difference between MALDI-TOF (positive mode) and LC/MS (positive mode) is most likely due to the fact that during the collection of MALDI spectrum the sample is ionized from a solid state (co-crystallized with matrix, α-cyano-4-hydroxycinnamic acid) and therefore sodium adducts are observed. In LC/MS spectrometry on the other hand sample is prepared in slightly acidic solution, which reduces the amount of sodium salts.

The subsequent experiments will employ MALDI-TOF as a tool for investigating the crosslinking reaction of PBI 686 and it is therefore important to have the information about the mass of its molecular ion. As discussed above it is expected that the m/z ratio corresponding to PBI686-modified substrates (peptide or protein) will be increased by either 711.3422 or 751.3347 Da. (Figure 27)

Photolabeling with PBI 686 was first investigated by performing reactions with various short synthetic peptides (prepared by Don Schwab, PBI/NRC). Three peptides were used: RPPGF (P1), SVPNSEELRF (P2), TDRAKRKAVSLSKVC (P3). MALDI-TOF spectra of

adducts to individual peptides are presented on Figure 28-32. Each peptide was irradiated with the probe at 1:1 molar ratio (1 mM each in phosphate buffer or methanol: water 50/50) at room temperature with UV light for 20 minutes. The UV light source used was Hanovia medium pressure quartz mercury-vapor lamp (450W) UV power at 1m distance of 300 watts/square inch. The lamp emits UV light in 254 to 350 nm range. The lamp is placed in a quartz immersion well which is cooled by water. Since the probe activation wavelength should be higher than the polypeptide UV absorption (<300 nm), Pyrex filter was used to block lower wavelength light (λ<320 nm). Reaction solutions were placed in Pyrex tubes at 10 cm distance from the lamp. This kind of experiment was expected to provide strictly qualitative information about nature of the binding mode. P1 was reacted with PBI 686 first and MALDI-TOF spectrum (low resolution, linear mode, mass accuracy 300 ppm) of the reaction mixture indicated the presence of crosslinking product (Figure 28). As expected the reaction yielded an adduct ion m/z = 1301.69 corresponding to a single addition of the probe to the peptide, as well as signals corresponding to the residual unreacted PBI 686.

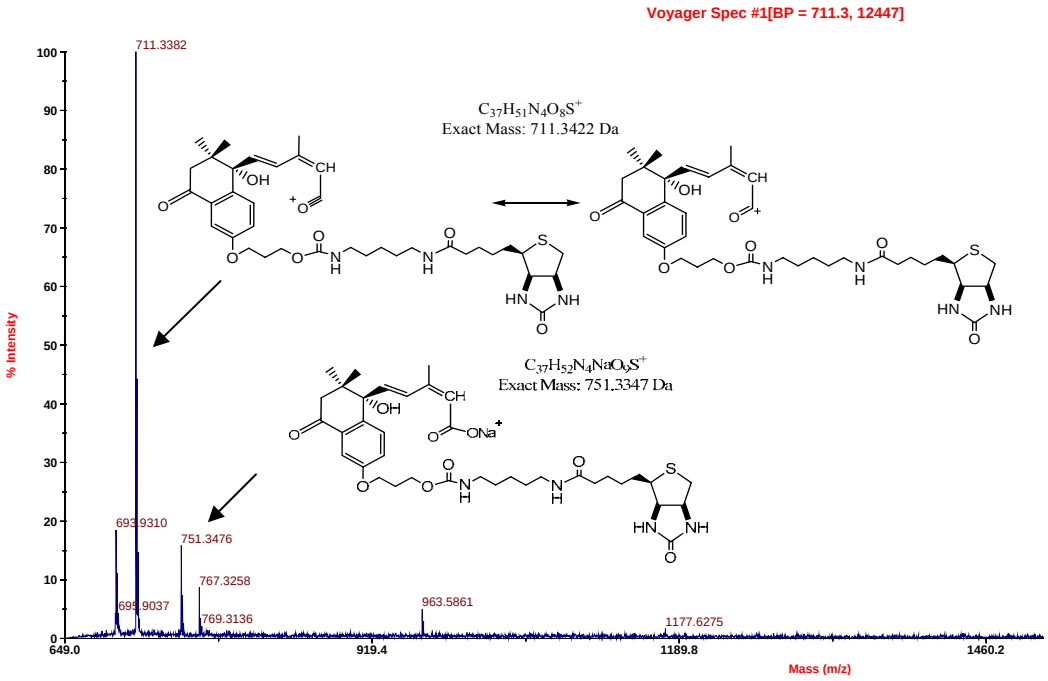

Figure 26. MALDI-TOF spectrum of PBI 686

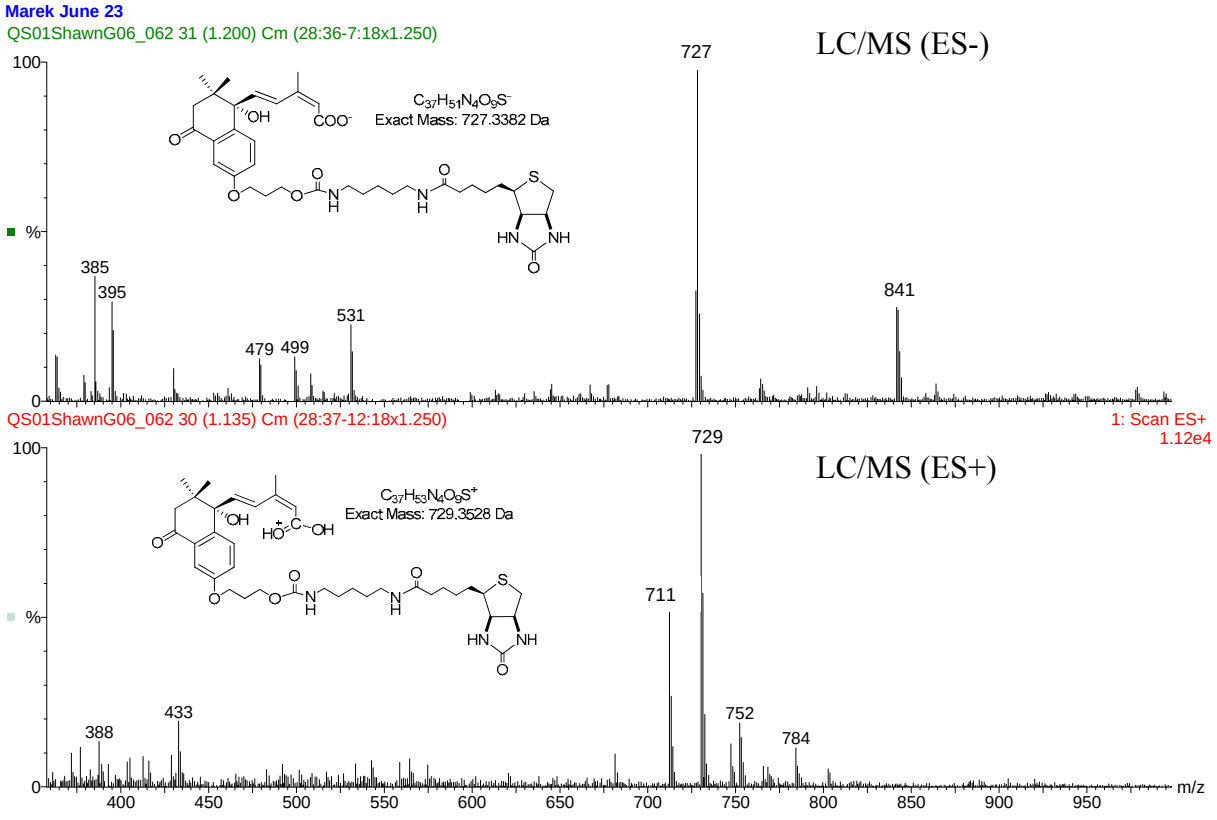

Figure 27. LC/MS spectra of PBI 686 in negative (ES-) and positive (ES+) ionization mode.

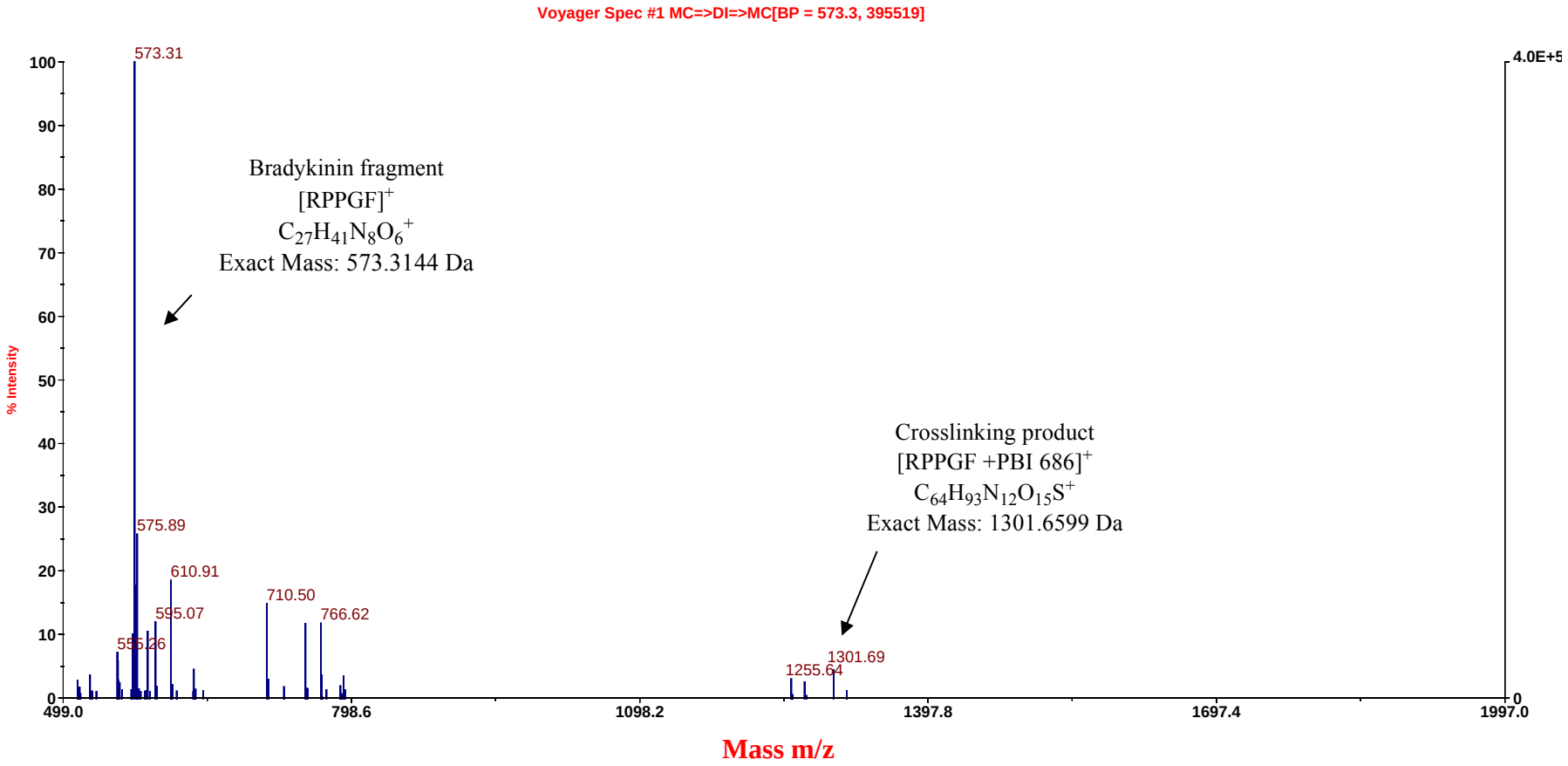

Figure 28. Low resolution (linear mode) MALDI-TOF spectrum of the product resulting from crosslinking reaction between Bradykinin fragment (peptide P1) and PBI686. Spectrum internally calibrated using exact (monoisotopic) mass of Bradykinin fragment, 573.3144 Da. Error calculation: 1301.6599 Da (theoretical) vs. 1301.69 Da (experimental) error = 20 ppm.

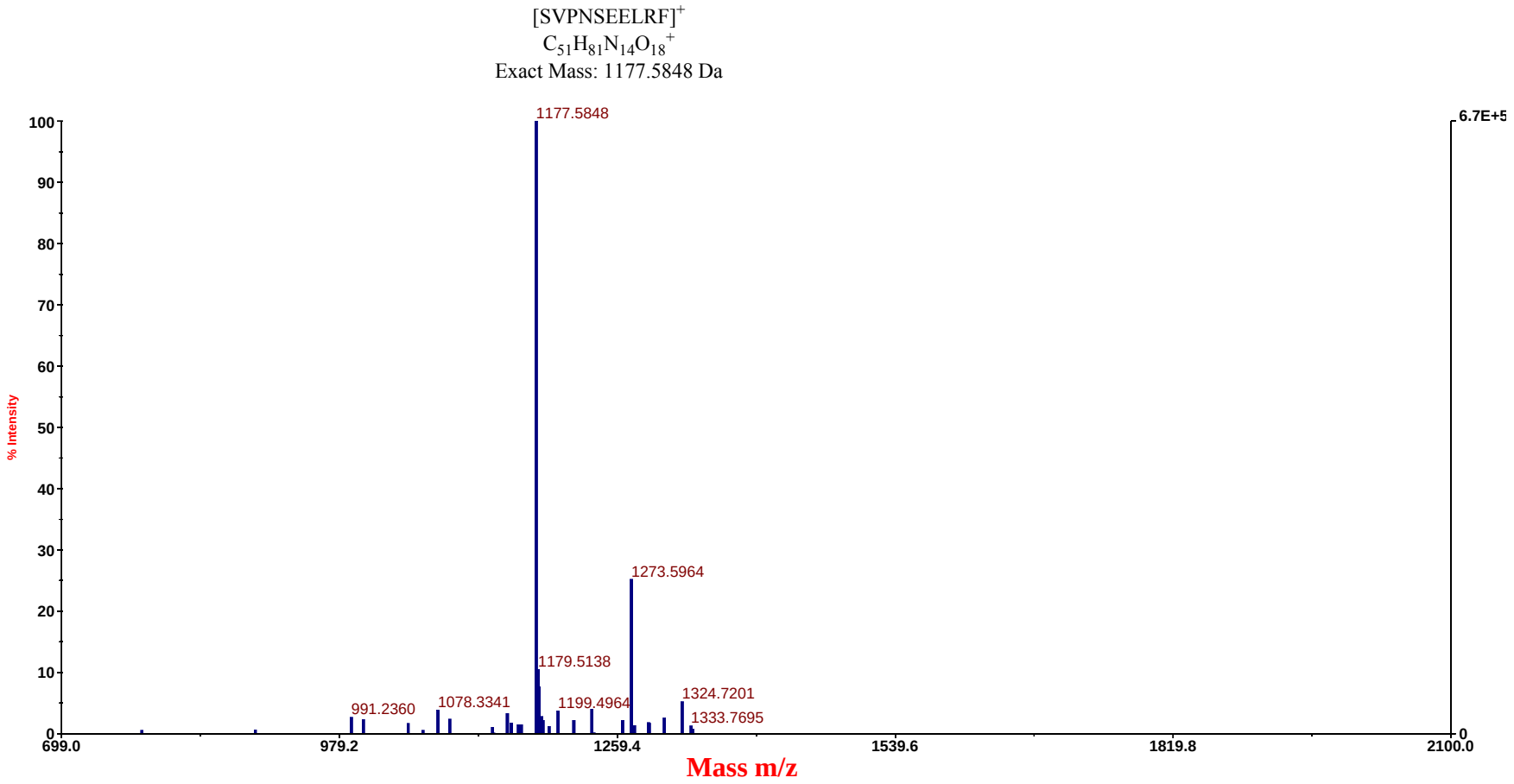

Figure 29. Low resolution (linear mode) MALDI-TOF spectrum of SVPNSEELRF peptide P2 (partially purified). Internal calibration using exact (monoisotopic) mass of SVPNSEELRF 1177.5848 Da. Molecular ion [M+H]+ (external calibration); 1176.6557 Da, data not shown.

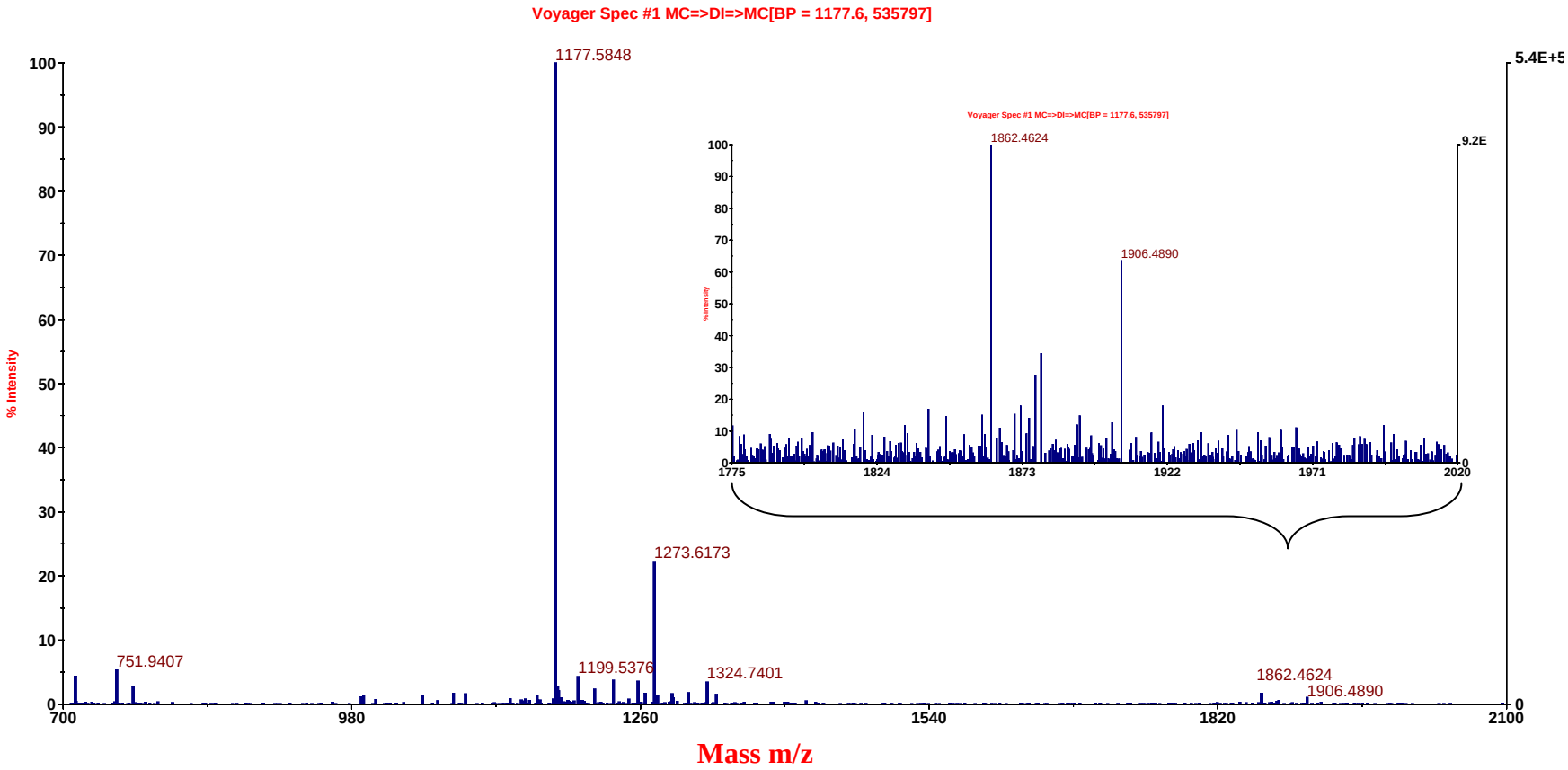

Figure 30. Low resolution (linear mode) MALDI-TOF spectrum of the product resulting from crosslinking reaction between peptide P2 (SVPNSEELRF) and PBI686. Spectrum internally calibrated using exact (monoisotopic) mass of SVPNSEELRF 1177.5848 Da.

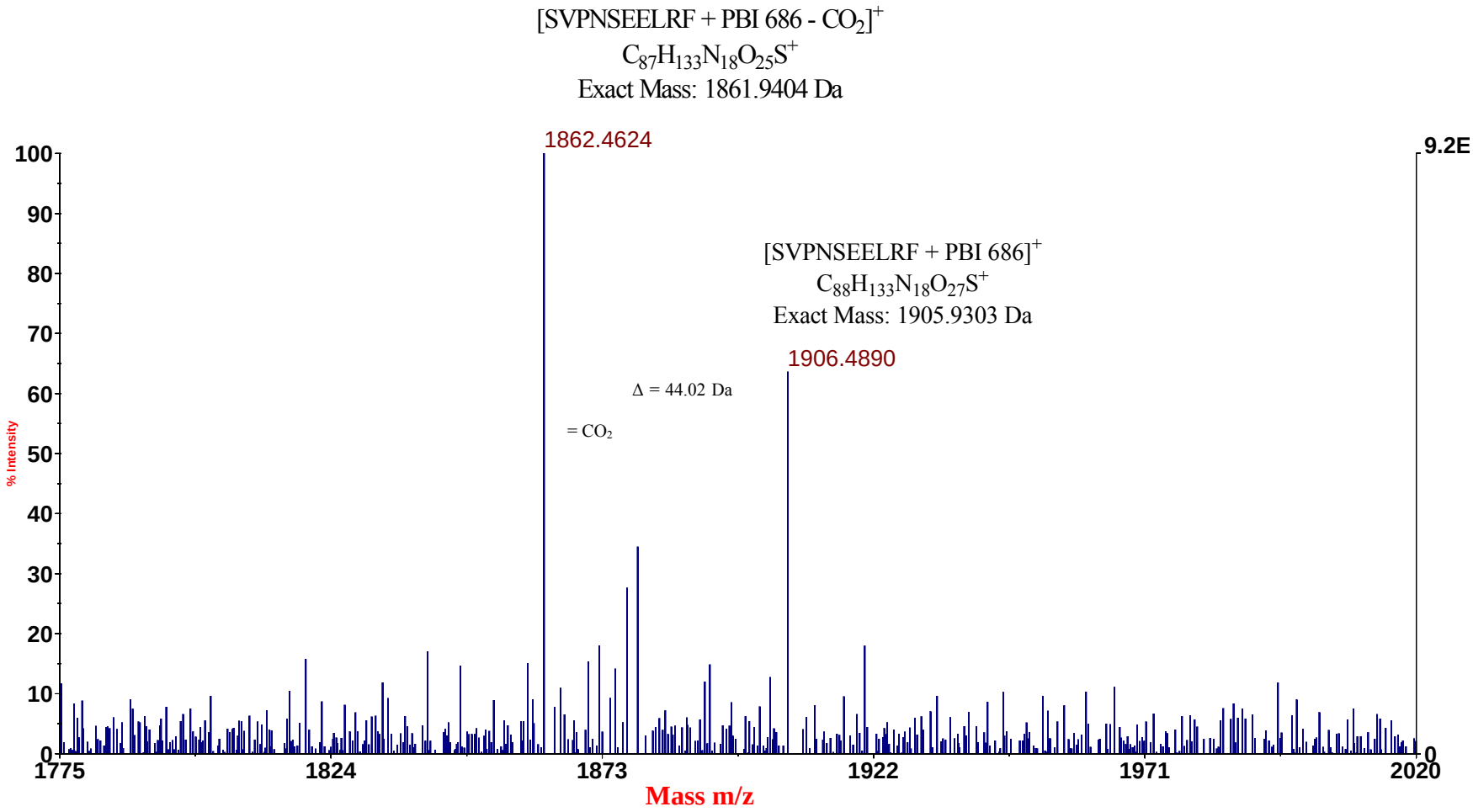

Figure 31. Section of low resolution (linear mode) MALDI-TOF spectrum of the product resulting from crosslinking reaction between peptide P2 (SVPNSEELRF) and PBI686. Spectrum internally calibrated using exact (monoisotopic) mass of P2, 1177.5848 Da. Error calculation: 1861.94 Da (theoretical) vs.1862.46 Da (experimental) error = 280 ppm. 1905.93 Da (theoretical) vs.1906.49 Da (experimental) error = 290 ppm.

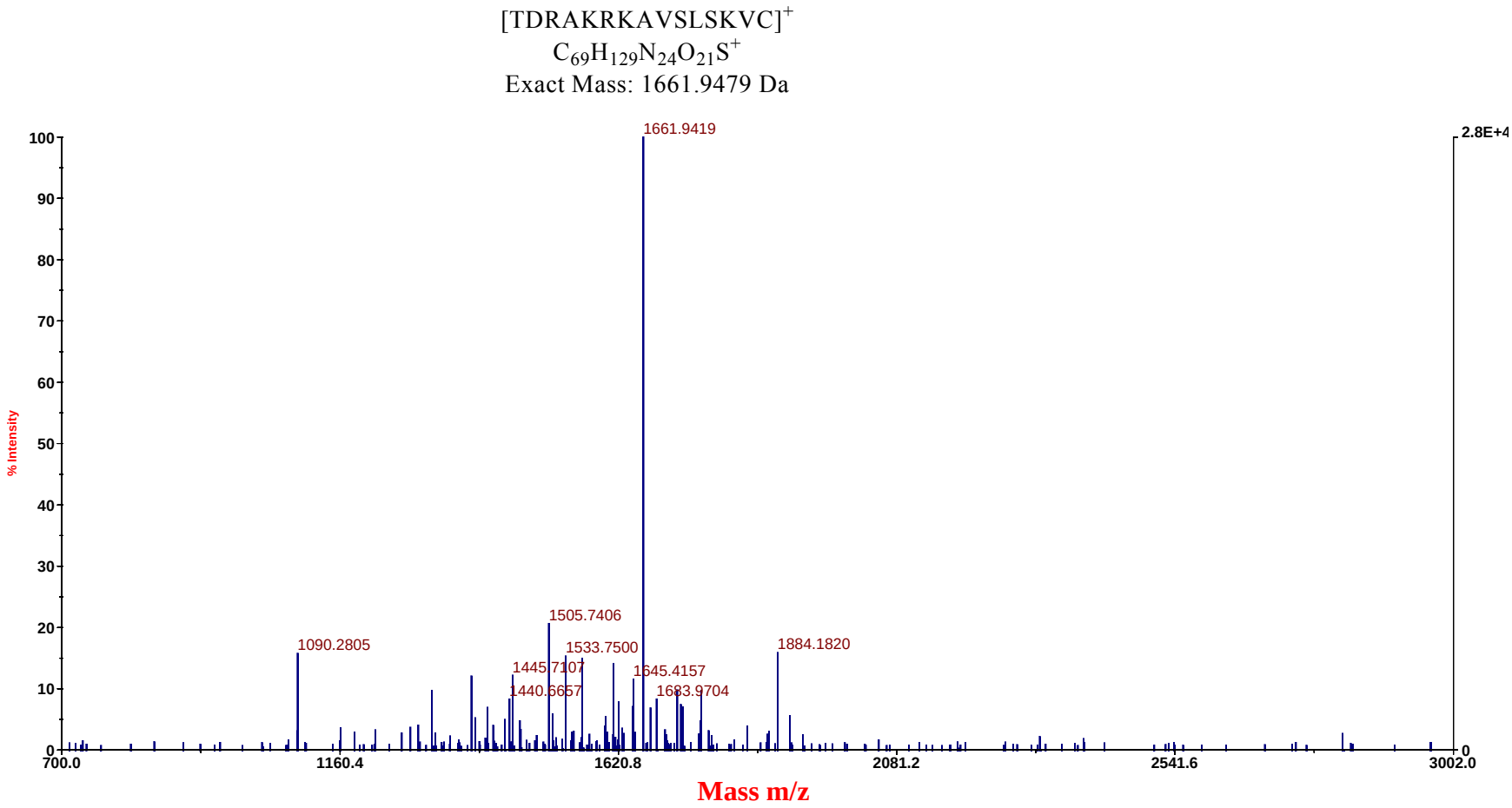

Figure 32. Low resolution (linear mode) MALDI-TOF spectrum of peptide P3 (TDRAKRKAVSLSKVC, partially purified). Spectrum externally calibrated. Error calculation: 1661.9479 Da (theoretical) vs. 1661.9419 Da (experimental) error = 36 ppm.

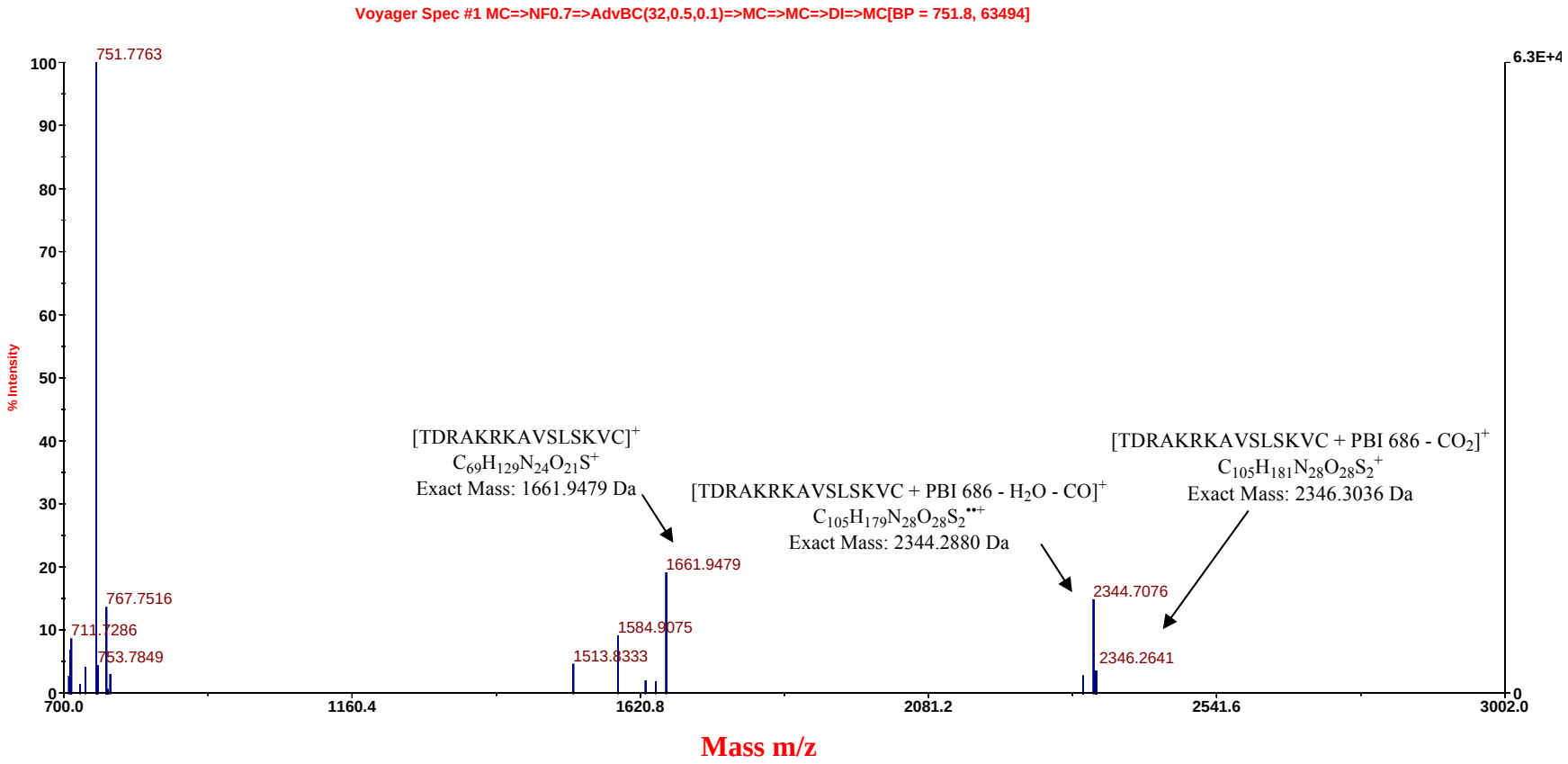

Figure 33. Low resolution (linear mode) MALDI-TOF spectrum of the products resulting from crosslinking reaction between peptide P3 (TDRAKRKAVSLSKVC) and PBI686. Spectrum internally calibrated using exact (monoisotopic) mass of TDRAKRKAVSLSKVC = 1661.9479 Da. Error calculation: 2346.3036 Da (theoretical) vs.2346.2641 Da (experimental) error = 16 ppm 2344.2880 Da (theoretical) vs.2344.7076 Da (experimental) error = 180 ppm.

Based on literature reports it is assumed the reaction yields an insertion product targeting α-C-H bond. The identity of amino acid residue to which the binding occurs cannot be revealed using this technique but on the other hand it was not the objective of this experiment. Low quantities of the product in a crude reaction mixture did not allow their characterization by NMR spectroscopy. However using mass spectra only it was possible to confirm product formation upon UV exposure and establish its molecular weight.

Apart from an adduct, MALDI-TOF spectrum of reaction mixture between P1 and PBI 686 (Figure 28) has also indicated the presence of an additional signal (1255.64 Da) that was 46 Da lower than molecular ion. A difference of 46 mass units could be due to loss of water and carbon monoxide, often observed for carboxylic acids in positive ionization mode.[176]

Peptide P2 (10 amino acid residues SVPNSEELRF) has been also successfully crosslinked with the probe (Figure 29), with the MALDI-TOF spectrum showing new signals in crude reaction mixture. In contrast to peptide P1, adducts of peptide P2 did not exhibit a loss of 46 mass units but rather 44. Figure 29 shows the presence of two types of adduct molecular ions. The first signal m/z = 1906.4890 corresponds to simple PBI686 addition (728 Da mass increase) and the second, m/z = 1862.4624 corresponds to decarboxylated form of the m/z = 1906.4890 product. Decarboxylation of the crosslinking product is not expected to happen during sample ionization. In the literature it is only reported to occur when carboxylic acids are ionized in negative ion mode. It is therefore concluded that the decarboxylation may occur during crosslinking reaction prior to MS sample analysis. Bossio and co-workers [177,178,179] have previously reported that a photoactivated benzophenone is capable of decarboxylating carboxylic acid groups that are in close proximity of a newly formed C-C bond resulting from PAL. Two synthetic peptides (Ac-Bpa-Ala_{10}-Lys and Ac-Bpa-Gly_{10}-

Lys) were modified by benzophenone (Bpa) on the N-terminal amino acid. The photoactivation of benzophenone led to decarboxylation of the C-terminal residue of both peptides. The degree of decarboxylation was found to be 50-fold less for an α-helical alanine-based peptide than for flexible glycine-based peptide. These results suggested that close contact between the photoexcited benzophenone and C terminus is necessary for decarboxylation, implicating hydrogen atom abstraction as the photochemical mechanism.

This confirms the possibility of peptide crosslinking with decarboxylation in these experiments. Although, it seems to be dependent on the structure of the peptide being modified, more specifically on the presence of carboxylic groups in peptide side-chain. Peptide P1 does not have a single amino acid with carboxylic group on its side-chain and the only -COOH group present is the C-terminal one. It can be decarboxylated if the probe binds to the C-terminal residue. This doesn't seem to be the only process in this reaction as the major product signal indicates the presence of non-decarboxylated product (m/z = 1301.6599). In the case of peptide P2, the decarboxylated product is found to be the major one which is explained by the presence of -COOH groups within peptide side chains belonging to two glutamic acid residues. To confirm decarboxylation, an additional experiment was performed with a 15 amino acid residue peptide that also included side chain carboxylic groups in its sequence. Peptide P3 (TDRAKRKAVSLSKVC, Exact mass m/z = 1661.9479, Figure 32) in combination with UV irradiation and PBI 686 clearly yields decarboxylated product (m/z = 2346.2641). In addition 46 mass unit difference of signal m/z = 2344.7076 suggests the presence of a simple adduct with loss of water and carbon monoxide (46 Da loss) which again most likely occurs during sample ionization.

These experiments have established that the probe PBI 686 is capable of reacting with hydrogen atom-donating amino acid residues which results in covalent bond formation. It was also observed that acetophenone moiety incorporated in the probe structure is capable of decarboxylating amino acid residues possessing carboxylic groups on their side-chain.

2.5. Development of experimental conditions for PAL of ABA-binding proteins. Probe validation using anti-ABA monoclonal antibodies

The next step in investigating photoaffinity labeling for future isolation of ABA-binding proteins was determining its specificity. This investigation was undertaken to evaluate the ability of the probe to bind covalently to proteins having an ABA-binding site. For this purpose the binding between the probe and a known ABA-binding protein: the anti-ABA monoclonal antibody[166] (mAb, 60 kDa) produced in mice, was investigated.[180] Application of the ABA monoclonal antibody to quantify levels of ABA by ELISA assays in plant tissues was previously reported.[180]

To evaluate the nature of binding we performed photoaffinity labeling of ABA mAb (source: Dr. Gary Banowetz, National Forage Seed Production Research Center, Oregon, USA) at different protein-ligand molar ratios. Additionally experiments evaluating ligand selectivity towards proteins were performed. This means that apart from ABA mAb, a second protein, (Ovalbumin, 45 kDa) unrelated to ABA was added to the reaction mixture. Figure 34 schematically represents the experiment.

Proteins from the reaction mixture were applied on SDS-PAGE gel which was developed by the far-Western detection system.[181] This detection method is significantly

different from the traditional Western blots. The major difference is that in far-Western system, no primary or secondary antibodies are used. Since proteins photolabeled with PBI 686 carry biotin, this allows direct detection of protein bands by co-incubating the blot membrane with streptavidin-conjugated horseradish peroxidase (HRP). Binding of biotin to this system causes a chemiluminescent reaction of Lumigen PS-3 (Acridan substrate) with HRP. This reaction is based on the oxidation of the cyclic diacylhydrazide.

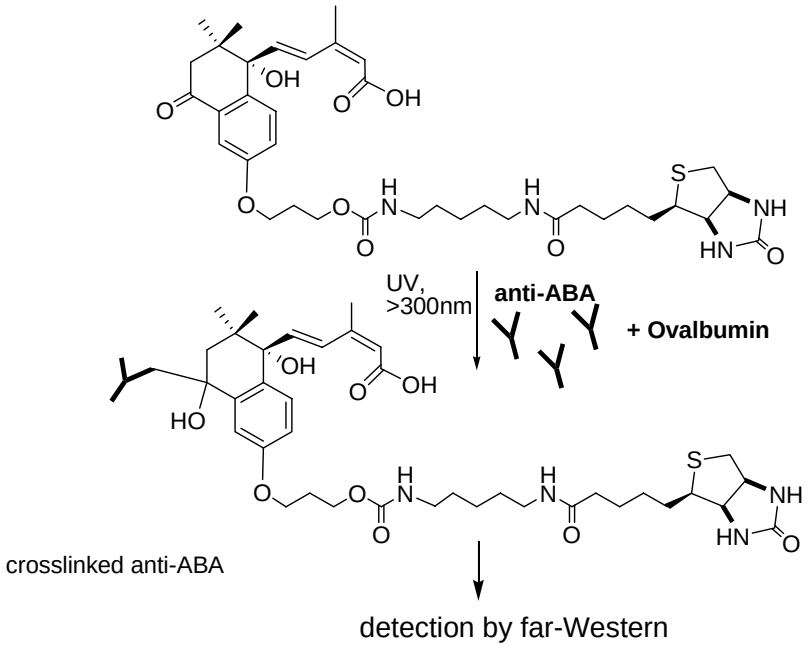

Figure 34. Photoaffinity labeling of ABA mAb.

Combined HRP and peroxide catalyzed oxidation of the Acridan substrate generates thousands of acridinium intermediates per minute. These intermediates react with peroxide (from H_2O_2) under slight alkaline conditions to produce a high intensity chemiluminescence with maximum emission at a wavelength of 430 nm. The resulting light is detected on

autoradiography film. This technique allows detection of bands which correspond to probe-modified proteins. Figure 34 schematically illustrates the experiment.

In the first set of experiments ABA mAb and ovalbumin were mixed at concentration of 30 μg/mL each (molar ratio approx. 1:1) at pH 7.5 in phosphate buffer. PBI 686 was added to a final concentration of 60 μM and with or without (±) ABA at 60 μM. ABA was expected to partially block the specific photoaffinity labeling by competing for ABA binding sites with PBI 686. In this set of experiments the protein-ligand molar ratio was 1:120 (Figure 35A).

In the second set of experiments (Figure 35B) this ratio (protein/ligand) was lowered by increasing the concentration of both proteins (67 μg/mL each) and decreasing the molar concentration of photolabile ligand to 30 μM. In addition three samples contained (±) ABA at 30, 300 μM and 1 mM.

Finally in the third experiment set (Figure 35C), the protein-ligand ratio was further lowered, this time by lowering the concentration of the probe and maintaining the same protein concentration. In this set the protein-ligand ratios ranged from 1:10 to 1:1.

This set of experiments has clearly demonstrated that the molar ratio between protein and photolabile ligand is crucial for specific binding. At high ligand concentrations (protein:ligand 1:120) crosslinking appears between the probe and both proteins ABA mAb and ovalbumin. This indicates that upon UV irradiation, non-specific labeling of ovalbumin is also observed. The amount of non-specific crosslinking decreases as the protein: ligand ratio decreases. At protein:ligand ratio of 1:10 non-specific binding of the probe to ovalbumin becomes negligible (Figure 35C).

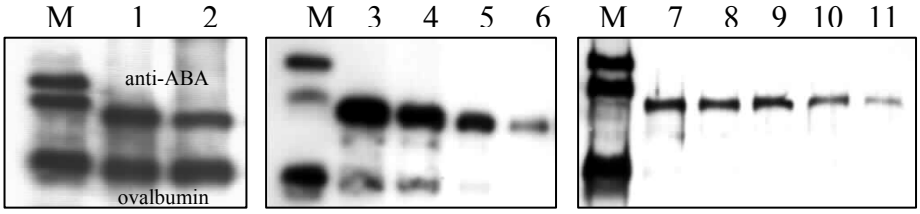

Figure 35. ABA mAb photolabeling by probe PBI686. A-D: far-Western blot analysis of anti-ABA (60 kDa) mixed with Ovalbumin (45 kDa), PBI686 and ABA at different proportions and irradiated with UV. M-protein MW marker (from top 97, 66, 45 kDa).

A - protein:ligand ratio 1:120:
1 – ABA mAb, ovalbumin, 60 μM PBI686.
2 – ABA mAb, ovalbumin, 60 μM PBI686, 60 μM (±) ABA.

B - protein:ligand ratio 1:30:
3 - ABA mAb, ovalbumin, 30 μM PBI686;
4 - ABA mAb, ovalbumin, 30 μM PBI686, 30 μM (±) ABA;
5 - ABA mAb ovalbumin, 30 μM PBI686, 300 μM (±) ABA;
6 - ABA mAb, ovalbumin, 30 μM PBI686, 1mM (±) ABA;

C - protein:ligand ratio 1:10 (7-8), 1:5 (9-10) and 1:1 (11)
7 - ABA mAb, ovalbumin, 10 μM PBI686;
8 - ABA mAb, ovalbumin, 10 μM PBI686, 100 μM (±) ABA;
9 - (protein:ligand ratio 1:5) ABA mAb, ovalbumin, 5 μM PBI686;
10- (protein:ligand ratio 1:5): ABA mAb, ovalbumin, 5 μM PBI686, 100 μM (±) ABA;
11 - (protein:ligand ratio 1:1) - ABA mAb, ovalbumin, 1 μM PBI686.

Far-Western blotting was the only technique that allowed identification of the photoaffinity labeled antibody. Since the yield of this particular photoaffinity reaction is unknown, the analysis of reaction mixtures is only qualitative. The low resolution and sensitivity of MALDI-TOF experiments in high mass range (entire protein, approx 60 kDa) did not allow the determination of the m/z ratio of the adduct signal. Also, a tryptic digest of the antibody would not provide any useful information due to the antibody amino acid sequence not being present protein search databases.

In summary, the experimental conditions used for specific photoaffinity labeling of proteins (such as anti-ABA) included: protein/ligand mole ratio between 1 and 1/5, 1 h incubation time at 4 °C prior to UV-irradiation and 10-20 min UV irradiation with medium pressure UV mercury lamp at lamp-sample distance of 10 cm.

2.6. Photolabeling and identification of cytosolic proteins in *Arabidopsis* leaf extracts

After confirming the ability to carry out selective photoaffinity labeling, the next step was to use this approach to identify new ABA-binding proteins. A procedure was developed and optimized which allowed isolating proteins binding to ABA. A series of experiments were performed with crude protein extracts from *Arabidopsis thaliana* (wild type Columbia) leaf tissue using cytosolic extracts. When microsomal proteins were to be included, the extraction buffer contained non-ionic detergent (DHPC) to keep them solubilized (see next chapter). Usually large amounts of plant tissue (50-100g) were used in order to obtain sufficient protein for analysis after purification. Most commonly, the volume of a total crude extract was >100 mL and proteins were concentrated before incubation with the probe and crosslinking. Ammonium sulfate was used for precipitation as a mild method of protein concentration which allowed maintenance of protein activity, crucial for this experiment. The proteins concentrated by this method were then re-dissolved in a small amount (2-3 mL) of phosphate buffer pH 7.6, with 20 mM NaCl and protease inhibitors. Solutions were then de-salted to remove excess ammonium sulfate then split into several Pyrex test tubes and incubated with PBI686. The incubation period allowed the binding process to reach a steady state equilibrium and was followed by UV irradiation for 15 min. Immediately after

irradiation, the solutions were cooled in an ice bath and applied to a streptavidin affinity column (at 4 °C).

Concentrated crude protein extracts irradiated with PBI686 were applied to a streptavidin sepharose affinity column. This allowed separation of biotinylated proteins from non-labeled ones. Streptavidin exhibits extremely high affinity to biotin which allows the tagged proteins to remain on the column while other proteins can be washed out with running buffer. In the final stage of separation the PBI686-tagged proteins were eluted from the column with denaturing agent: 8M guanidine hydrochloride at pH 2.0. Collected protein fractions were then immediately desalted (PD-10 desalting columns, GE Healthcare) to remove guanidine hydrochloride, and pH was adjusted to 7.6.

Figure 36 represents an FPLC chromatogram from the experiment described above. The crude protein extract containing 50.6 mg of protein was applied, on the column (matrix volume: 1 mL of HiTrap^{TM} sepharose-streptavidin), which was then washed with 25 mL (25 column volumes) of running buffer and finally 8M guanidine hydrochloride (pH 2.2). The fractions from peak at 41 mL were collected, pooled together, concentrated and protein concentration measured (SPN protein assay kit from G-biosciences) resulting in 64 µg of protein.

In the first set of experiments (peak A, Figure 37) 50 g of fresh plant leaf tissue and 10 µM PBI 686 were used, which yielded at least four proteins in eluted fractions.

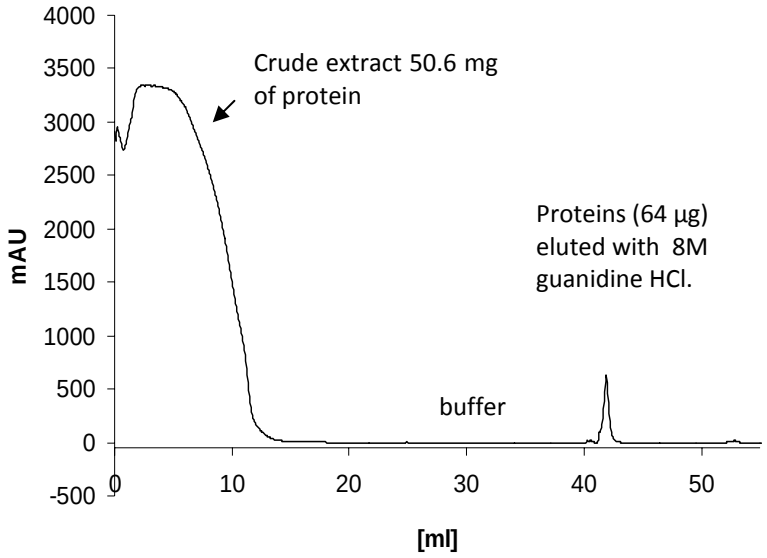

Figure 36. FPLC chromatogram on sepharose-streptavidin matrix. Crude protein extract, UV irradiated in the presence of 10 µM PBI 686.

The second type of experiment (experiment B, peak B, Figure 37) was performed in the presence of 10 µM PBI 686 with addition of 200 µM PBI 410. The structure of the latter is presented in Figure 18. Compound PBI 410 has a high structural resemblance to PBI 686. Both compounds are assumed to have very similar binding affinity to a given protein and more importantly both are photolabile. PBI 410 was added at 20 fold excess (Figure 37-B) with respect to concentration of PBI 686 in order to cause partial blocking of the crosslinking reaction of PBI 686. This effect has in fact been observed by measuring the protein amounts in eluted fractions and simple comparison of FPLC chromatograms (Figure 37). Finally the third experiment (experiment C, peak C, Figure 37) was performed using the same conditions as the above but without addition of PBI 686 or PBI 410. Meaning the crude protein extract was obtained from 50 g of tissue concentrated and irradiated with UV light. It was found that the peak of eluted proteins has further decreased and only 18 µg of protein was collected.

In summary the amount of protein remaining bound to the column matrix is clearly dependent on the presence of the probe. Moreover the competitor PBI 410 is capable of partial blocking the crosslinking reaction which leads to decreased amount of specific proteins in collected fractions.

All of these experiments strongly suggest that among all proteins in crude extracts there are also ones that can specifically bind the probe, and are possibly to be ABA-binding proteins.

At this point it was important to carefully examine the content of the eluted fractions and identify the proteins present by PMF (Peptide Mass Fingerprinting) methods.

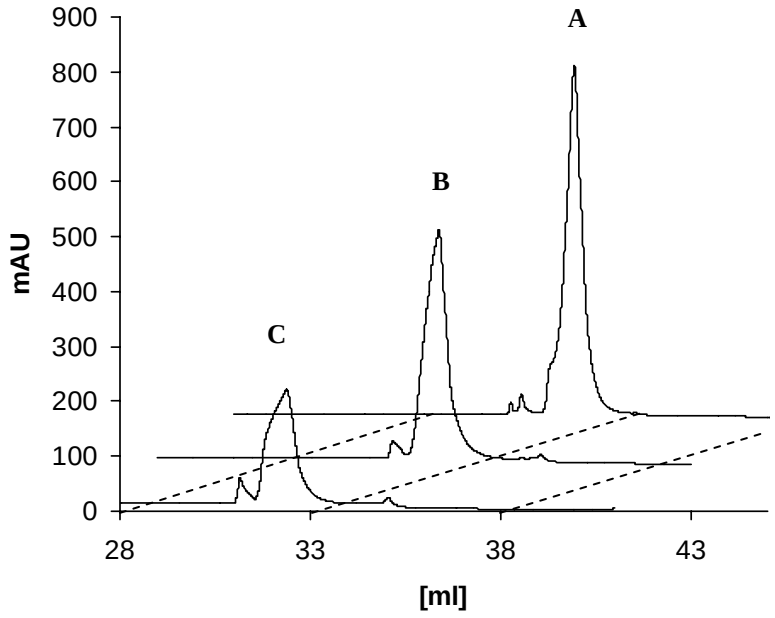

Figure 37. Overlapped (and shifted for clarity) FPLC traces of proteins eluted from the column in the presence (after PAL) and absence of PBI 686. Peak C – non-specific proteins (18 μg) bound to the column matrix in the absence of PBI 686. Peak B – specific and non-specific proteins (24 μg) bound to the column matrix (UV irradiation in the presence of 10 μM PBI 686 and 200 μM PBI 410). Peak A - specific and non-specific proteins (64 μg) bound to the column matrix (UV irradiation in the presence of 10 μM PBI 686 only).

Each fraction (4 mL in total from each experiment, peaks A-C) was first concentrated by Millipore protein concentration devices to 500 µl volume, and then further concentrated by UPPA^{TM} protein concentration system (G-Biosciences) utilizing protein precipitation by organic solvents. Concentrated samples were separated by SDS-PAGE, and gel bands were visualized by both silver staining and far-Western.

Figure 38 shows the silver stained gel and its far-Western equivalent of proteins eluted in peaks A-C onFigure 37.

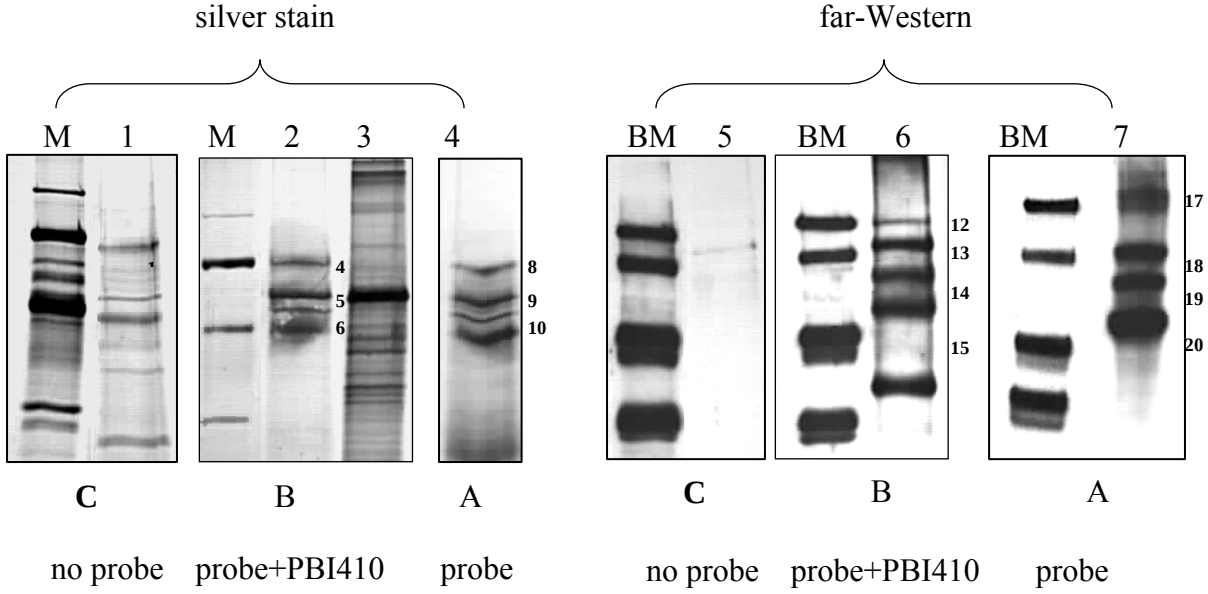

Figure 38. SDS-PAGE separation of proteins found in fractions eluted from affinity column. **A** – **C** peaks from Figure 37. M - protein molecular weight marker (from top: 97, 66, 45, 31 kDa), 1, 5 – proteins from peak C; 2, 6 – proteins from peak B, 3 – crude extract, 4, 7- proteins from peak A. BM – biotinylated protein molecular weight marker (from top: 97, 66, 45, 31 kDa).

These results provided important information about the specificity of photoaffinity labeling. First of all several proteins were identified in peak **C**, which was detected by silver staining (lane C1). None of them, however, were detected by far-Western (lane C5). This

suggests that these proteins are not biotinylated, which was expected since the probe was not present during UV irradiation. Any proteins present in peak **C** can be therefore considered as ones that simply bind the column matrix non-specifically. Identification of all proteins present in bands 1-11 will be discussed further.

Secondly, both silver staining and far-Western indicate the presence of at least four proteins bound to the column after incubation and irradiation with PBI 686. According to silver staining method (Figure 38), it appears that bands **1**, **2**, **3** correspond to the same proteins as in bands **4**, **6** and **7**. Only bands **5** and **9** appear as new protein in peaks **B** and **A** (on Figure 37).

It is difficult to interpret far-Western results by comparing them to silver staining method. It is important to keep in mind that unlike silver staining, the far-Western method is not directly quantitative with respect to protein amounts. On the contrary, the band intensity is proportional to biotin quantity and therefore the extent of biotinylation. A good example of that phenomenon is band **16**, which doesn't appear on silver stained gel but is an intense band by far-Western. In addition there is approximately 100 fold difference in sensitivity between these two techniques with far-Western being more sensitive. Bands **1**-**3** likely do not correspond to the same proteins as any of the bands **12**-**20** detected by far-Western. This is based on comparing lanes **C1** and **C5**, where the same protein sample was analyzed by two different techniques. All three proteins are visible by silver stain and not present on corresponding far-Western, are are most likely not biotinylated. It is suspected that far-Western bands in lanes B6 and C7 are all associated with band B5. Multiplicity of bands on far-Western could be caused by protein degradation or aggregation processes being a result of high intensity UV exposure. Due to 100 fold difference in sensitivity between silver-

staining and far-Western method, only one band is observed on silver-stained gel versus 3-4 bands on far-Western blot. It is also possible that certain protein bands not observed on silver-stained gel are being detected by far-Western blot.

Another band that attracts attention when comparing far-Western analysis is band **16**. It is present in fraction **B** but doesn't appear in fraction **A**. The only explanation at this point would be the possibility of it being a degradation product from one of the higher molecular weight biotinylated protein (bands **12-15**).

To better understand the differences in protein composition in all three peaks (**A-C** Figure 37) bands **1-11** were identified by proteomic methods such as MALDI-TOF coupled peptide mass fingerprinting (PMF) or LC/MS/MS- Q-TOF coupled Mascot MS/MS ion search. The experimental masses of peptides resulting from tryptic digest were compared to peptide masses in a Mascot database. Obtained protein hits were then analyzed by Mascot based Mowse (Molecular Weight SEarch) scoring algorithm. Resulting scores are related to the probability (P) of a given match being a random event according to the following formula: Score = -10*log(P). Also $P = E*N^{-1}$ where E = expect value, N = number of proteins in a database. If during the search 1.5×10^6 proteins fell within the search limits and the significance limit was set to $E< 0.05$ (less than 5% chance the peptide mass match is random) then the cutoff Mascot score would be $S = -10*\log [(1/1.5 \times 10^6) (0.05)] = 74.7$. With today's databases, Mascot scores greater than 76 are significant (with $E < 0.05$). The significance of the result depends on the size of the database being searched. Mascot shades in green the insignificant hits using an $E = 0.05$ cutoff.

In some cases peptide fragments from target proteins were sequenced using LC/MS/MS (Quadropole Time of Flight mass spectrometer – Q-TOF) coupled with Mascot

algorithm (weak bands). The peptide fragment sequences were sent to BLAST to be queried against a protein sequence database. Proteins having the highest number of sequence matches and the highest Mascot score were assigned identity. MS/MS ion search method was used in case of weak gel bands which could not be identified by PMF. MS/MS ion search provides more accurate sequence information as it not only searches for the parent ion of a given peptide but also uses the database to search for daughter ions each associated with a specific peptide fragment. This greatly increases the search scores and hit significance. Silver stained protein bands were cut off the gels, de-stained, trypsin-digested and resulting peptide signals were analyzed.

Bands **3, 7, 11** (Figure 38) were associated with Carboxylic acid hydrolase - **ESM1** from *Arabidopsis thaliana.* The matching results are presented below.

1. **gi|15231805** - ESM1 (EPITHIOSPECIFIER MODIFIER 1);
carboxylic ester hydrolase [Arabidopsis thaliana]
Mass: 44374, **Score:** 1171, **Queries matched:** 69, Sequence coverage **48 %**

2. **gi|18404748** **-** Myrosinase-associated protein,
putative [Arabidopsis thaliana], **Mass:** 43572,**Score:** 426,
Queries matched: 13, Sequence Coverage: **36%**

3. **gi|18406229** - ZW9 [Arabidopsis thaliana], similar to meprin
and TRAF homology domain-containing protein / MATH domain
-containing protein [Arabidopsis thaliana] **Mass:** 45235 **Score:** 412,
Queries matched: 13, Sequence Coverage: **25%**

4. **gi|15235321**- CRU3 (CRUCIFERIN 3);
nutrient reservoir [Arabidopsis thaliana], **Mass:** 58541,
Score: 403, **Queries matched:** 11, Sequence Coverage: **27%**

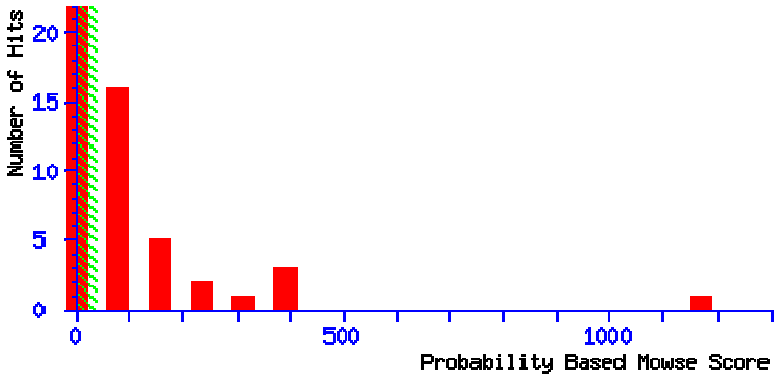

ESM1 (EPITHIOSPECIFIER MODIFIER 1) coverage map:

```
  1 MADNLNLVSV LGVLLVLTIF HNPIIVYAGE GVPNVALFTF GDSYYDAGNK
 51 VFLSQRKDLP QTYWPYGKSR DYPNGKFSDG HIVPDFIADF ISIPNGVLPP
101 VLKPGVDISR GVSFAVADAS ILGAPVESMT LNQQVVKFKN MKSNWNDSYI
151 EKSLFMIYIG TEDYLNFTKA NPNADASAQQ AFVTNVINRL KNDIKLLYSL
201 GASKFVVQLL APLGCLPIVR QEYKTGNECY ELLNDLAKQH NGKIGPMLNE
251 FAKISTSPYG FQFTVFDFYN AVLRRIATGR SLNYRFFVTN TSCCGVGTHN
301 AYGCGKGNVH SKLCEYQRSY FFFDGRHNTE KAQEEMAHLL YGADPDVVQP
351 MTVRELIVYP TGETMREYWE PNNLAIRRRP SRDFYLGLAA YY
```

The BLAST provided 6 significant matches, however the match with the highest score (hit 1) is well distant from all other matches, which gives us a very high confidence in identification of the protein.

Bands **2, 6, 10** were associated with **JR1** (Jacalin lectin family protein) from *Arabidopsis thaliana*.

1. gi|30684083 -JR1(Jacalin lectin family protein),[Arabidopsis thaliana]
Mass: 48524, **Score:** 766, **Queries matched:** 27, Sequence Coverage: **57%**

2. gi|15231805 - ESM1 (EPITHIOSPECIFIER MODIFIER 1);
carboxylic ester hydrolase [Arabidopsis thaliana]
Mass: 44374, **Score:** 358, **Queries matched:** 29, Sequence Coverage: **32%**

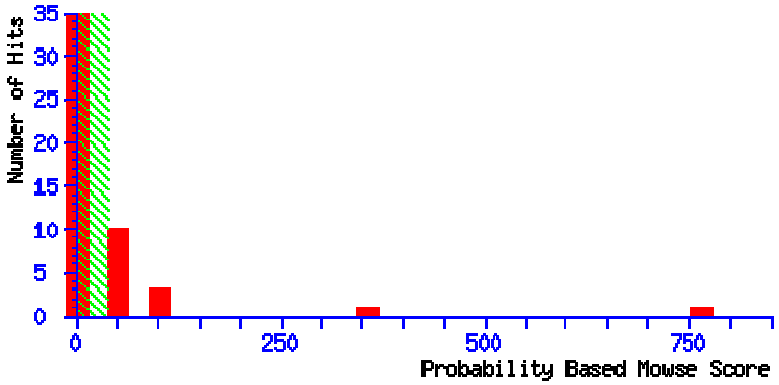

JR1(Jacalin lectin family protein),sequence coverage map (hit 1):

```
  1 MAKKLEAQGG RGGEEWDDGG AYENVKKVYV GQGDSGVVYV KFDYEKDGKI
 51 VSHEHGKQTL LGTEEFVVDP EDYITSVKIY YEKLFGSPIE IVTALIFKTF
101 KGKTSQPFGL TSGEEAELGG GKIVGFHGSS SDLIHSVGVY IIPSTTPLTP
151 PVSGGLTKLE AQGGRGGDVW DDGGAYDNVK KVYVGQGDSG VVYVKFDYEK
201 DGKIVSLEHG KQTLLGTEEF EIDPEDYITY VKVYYEKLFG SPIEIVTALI
251 FKTFKGKTSQ PFGLTSGEEA ELGGGKIVGF HGTSSDLIHS LGAYIIPSST
301 PLTPSSNTIP AQGGDGGVAW DDGVHDSVKK IYVGQGDSCV TYFKADYEKA
351 SKPVLGSDHG KKTLLGAEEF VLGPDEYVTA VSGYYDKIFS VDAPAIVSLK
401 FKTNKRTSIP YGLEGGTEFV LEKKDHKIVG FYGQAGEYLY KLGVNVAPIA
451 K
```

Bands **1**, **4**, **8** were associated with Beta-glucosidase precursor from *Arabidopsis thaliana*.

1. gi|6651430 - Beta-glucosidase homolog [Arabidopsis thaliana],
   Mass: 60904, **Score:** 784, **Queries matched:** 46, Sequence Coverage: **48%**

2. gi|984052 - Thioglucoside Glucohydrolase [Arabidopsis thaliana],
   Mass: 60222, **Score:** 663, **Queries matched:** 31, Sequence Coverage: **52%**

3. gi|5107821 - Arabidopsis thaliana Thioglucosidase
   Mass: 61885, **Score:** 594, **Queries matched:** 16, Sequence Coverage: **35**

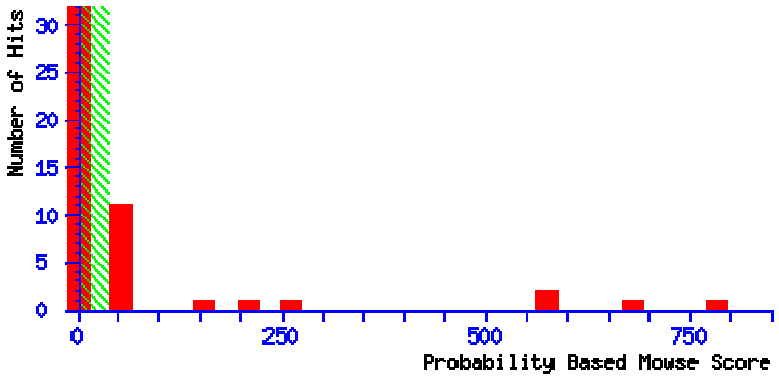

Arabidopsis thaliana, Beta-glucosidase homolog sequence coverage map (hit1):

```
  1 MVRFEKVHLV LGLALVLTLV GAPTKAQGPV CGAGLPDKFS RLNFPEGFIW
 51 GTATAAFQVE GAVNEGCRGP SMWDTFTKKF PHRCENHNAD VAVDFYHRYK
101 EDIQLMKDLN TDAFRLSIAW PRIFPHGRMS KGINKVGVQF YHDLIDELLK
151 NNIIPLVTVF HWDTPQDLED EYGGFLSGRI VQDFTEYANF TFHEYGHKVK
201 HWITFNEPWV FSRAGYDNGK KAPGRCSPYI PGYGQHCQDG RSGYEAYQVS
251 HNLLLSHAYA VDAFRNCKQC AGGKIGIAHS PAWFEPQDLE HVGGSIERVL
301 DFILGWHLAP TTYGDYPQSM KDRVGHRLPK FTEAEKKLLK GSTDYVGMNY
351 YTSVFAKEIS PDPKSPSWTT DSLVDWDSKS VDGYKIGSKP FNGKLDVYSK
401 GLRYLLKYIK DNYGDPEVII AENGYGEDLG EKHNDVNFGT QDHNRKYYIQ
451 RHLLSMHDAI CKDKVNVTGY FVWSLMDNFE WQDGYKARFG LYYIDFQNNL
501 TRHQKVSGKW YSEFLKPQFP TSKLREEL
```

Finally Bands **5** and **9**, were associated with large subunit of ribulose-1,5-bisphosphate carboxylase/oxygenase (Rubisco) from *Arabidopsis thaliana*.

1. gi|7525041 ribulose-1,5-bisphosphate carboxylase/oxygenase large subunit [Arabidopsis thaliana], **Mass:** 53435, **Score:** 1153, **Queries matched:** 82, Sequence Coverage: **49%**

2. gi|2997767 myrosinase-binding protein homolog [Arabidopsis thaliana], **Mass:** 50110, **Score:** 444, **Queries matched:** 7, Sequence Coverage:**21%**

3. gi|7525040 - ATP synthase CF1 beta subunit [Arabidopsis thaliana]
Mass: 53957, **Score:** 286, **Queries matched:** 10, Sequence Coverage: **23%**
The F-ATPase is found in plasma membranes, mitochondrial inner membranes and in chloroplast membranes. Possesses an FTP binding site.

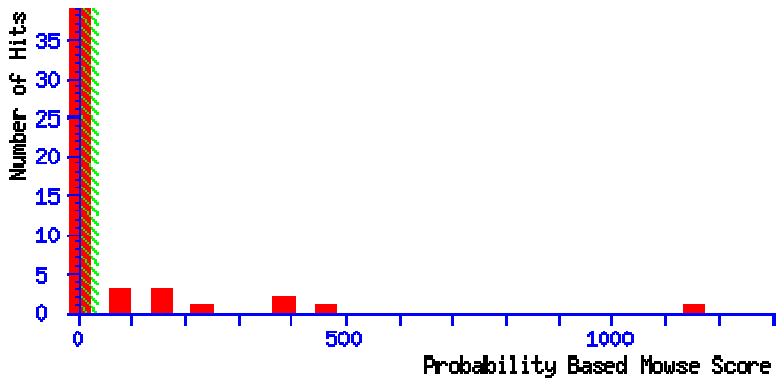

Rubisco, sequence coverage map (hit 1):

```
  1 MSPQTETKAS VGFKAGVKEY KLTYYTPEYE TKDTDILAAF RVTPQPGVPP
```

```
 51 EEAGAAVAAE SSTGTWTTVW TDGLTSLDRY KGRCYHIEPV PGEETQFIAY
101 VAYPLDLFEE GSVTNMFTSI VGNVFGFKAL AALRLEDLRI PPAYTKTFQG
151 PPHGIQVERD KLNKYGRPLL GCTIKPKLGL SAKNYGRAVY ECLRGGLDFT
201 KDDENVNSQP FMRWRDRFLF CAEAIYKSQA ETGEIKGHYL NATAGTCEEM
251 IKRAVFARFL GVPIVMHDYL TGGFTANTSL SHYCRDNGLL LHIHRAMHAV
301 IDRQKNHGMH FRVLAKALRL SGGDHIHAGT VVGKLEGDRE STLGFVDLLR
351 DDYVEKDRSR GIFFTQDWVS LPGVLPVASG GIHVWHMPAL TEIFGDDSVL
401 QFGGGTLGHP WGNAPGAVAN RVALEACVQA RNEGRDLAVE GNEIIREACK
451 WSPELAAACE VWKEITFNFP TIDKLDGQE
```

These results strongly suggest that out of all four proteins eluted from the column only three of them are present in fraction due to their actual binding to the probe. There are also two other proteins which were found in the same band (bands 5 and 9 Figure 38) as Rubisco and those are: a myrosinase-binding protein, and an ATP synthase, both from *Arabidopsis thaliana*. There is a possibility that several proteins are found in one band on the gel due to all of them having close molecular masses. These proteins were also not found in experiments without the probe which indicates the possibility of them being selective towards ABA. All three proteins are also absent in fractions corresponding to control experiments without the probe during UV irradiation (Figure 37A). All other proteins such as ESM1, JR1 and Beta-glucosidase precursor can be considered as non-specific.

In order to check if it is possible to reduce non-specific binding of above proteins to the column matrix pre-elution step during FPLC run was applied. Just like before, the column was loaded with crude, UV-irradiated protein extract, then washed with running buffer (20 column volumes) and was additionally washed with approximately 10 column volumes of 0.1M citric acid at pH 2.0. Under these conditions only biotinylated proteins would still remain on the column and lowered pH by citric acid would elute all other non-specifically bound proteins.

In this experiment crude protein extract from 50 grams of fresh *Arabodopsis* leaf tissue was divided into two equal portions. First portion was irradiated with UV light in the

presence of 100 μM PBI 686. It was then applied to a sepharose-streptavidin affinity column (1 mL volume). Chromatography purifications were run at 1 mL/min flow rate, except during sample injection (0.3 mL/min). It was found that the areas of both peaks A and B were comparable meaning that a substantial amount of proteins are not biotinylated (peak A, Figure 39). Proteins eluted with citric acid should do not carry biotin as its interaction with steptavidin is the strongst known non-covalent interaction ($K_D \sim 10^{-14}$ M) and can only be broken opon streptavidin denturation (heat, denaturating agents).

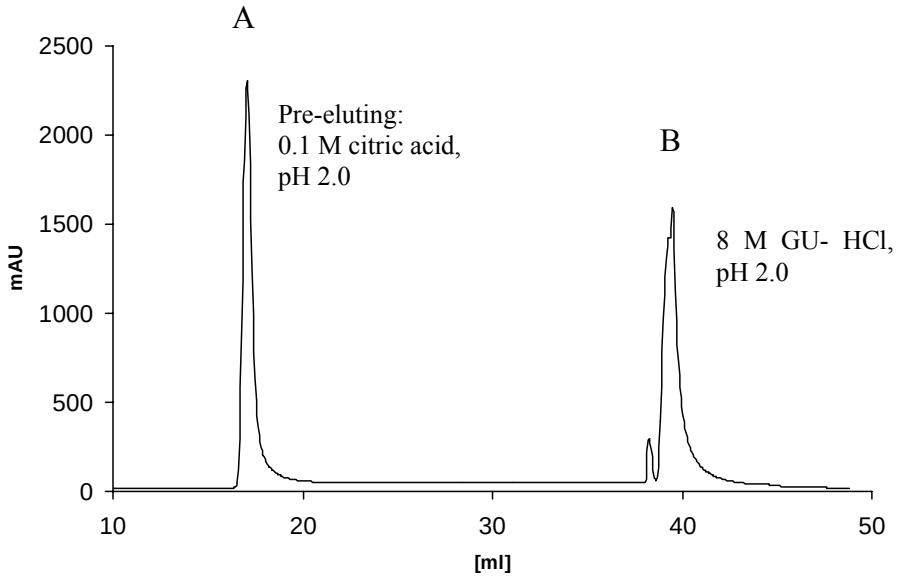

Figure 39. FPLC trace of the experiment with citric acid pre-eluting step. Peak A corresponds to proteins eluted with citric acid. Peak B – biotinylated proteins eluted with Guanidine hydrochloride. A/B peak area ratio = 1.03

The two most effective methods of breaking biotin-streptavidin interaction are treatment with 8M Guanidine hydrochloride at pH 2.0, or boiling the complex with 2% SDS.[182]Common method of pre-eluting of non-specific proteins utilizes a change of pH to either higher or lower than the pH of regular running/binding buffer. The pH of

binding/running buffer in this case was 7.6 and in order to strip off the non-specific proteins, lowering the pH was chosen as a pre-eluting step. Citric acid was used as its buffering capacity (pH 2-6) was suitable for this application.

It was also important to test whether ABA could block the crosslinking reaction and therefore reduce the number of proteins bound to the column. The second portion of the protein cude extract (see previous page) was irradiated with UV light in the presence 100 μM PBI 686 and 5 mM (±) ABA. Figure 40 represents this experiment. The most striking difference between the two experiments with and without ABA is the change of ratio between peak areas (A/B = 1.03, C/D = 3.05). In the latter case the amount of biotinylated proteins has been reduced by almost 70% (peak area relative to pre-eluting peak).

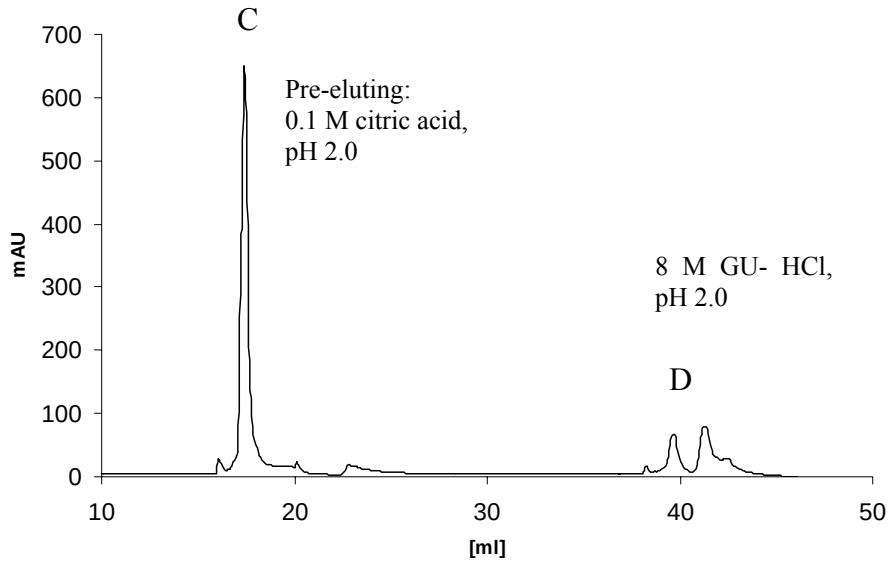

Figure 40. FPLC trace of the experiment with citric acid pre-eluting step and 5 mM (±) ABA during UV irradiaiton. Peak C corresponds to proteins eluted with citric acid. Peak D – biotinylated proteins eluted with Guanidine hydrochloride. C/D peak area ratio = 3.05

This strongly suggests that ABA does in fact block the photoaffinity labeling. Both experiments were performed using the same set of conditions and the same amount of fresh

tissue was used to extract proteins. And if that is the case one could ask a question why both peak areas (A vs. C and B vs. D, Figure 39-40) have decreased in the presence of ABA if only biotinylated protein peak (D) should be reduced? Above situation would only apply if during the photoaffinity labeling reaction all available protein molecules would bind all probe molecules, meaning if the reaction was quantitative. Such condition cannot be applied since the protein/ligand ratio is not known nor is the reaction yield. Therefore after the reaction, both the free protein and ligand will still be present in solution. If such crude reaction mixture is applied on streptavidin affinity column not only biotinylated proteins will retain on the column, but also some non-tagged proteins will bind the probe non-covalently. The free probe will also be captured by streptavidin. In summary one should expect to find potential ABA–binding proteins in both fractions, in peaks A and C (non-covalent binding) and in peaks B and D (probe bound covalently). ABA reduced both peak areas due to both blocking the PAL reaction as well as competing for the non-covalent specific interaction between the protein and the probe. When comparing Figure 39 and Figure 40 it is clear however that there is a dramatic reduction of biotinylated protein (peaks **B** and **D**) in the presence of ABA. In order to confirm that fractions collected from peaks **B** and **D** were analyzed by far-Western blot.\

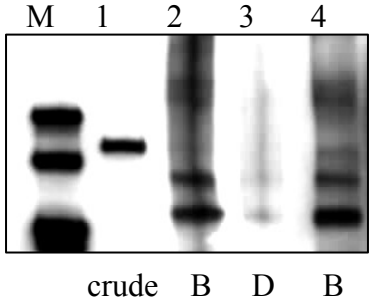

Figure 41. far-Western analysis of fractions collected in peaks B (Figure 39) and D (Figure 40). M – biotinylated protein molecular weight marker (from top: 97, 66, 45, kDa); 1 – non-chromatographed crude protein extract, 2,4 (different gel loadings) – peak B (Figure 39), 3 – peak D (Figure 40).

Far-Western analysis of peaks B and D have confirmed that the crosslinking reaction is blocked by ABA at concentration being fifty fold higher than the concentration of PBI 686. When comparing lanes 2 and 4 on Figure 41 (fractions from two experiments) with lane 3 there is a clear reduction of the amount of biotinylated protein down to the far-Western detection limit.

Lane 1 (Figure 41) represents crude protein extract which was not incubated with PBI 686, non-chromatographed but irradiated with UV light. Initially it was assumed that the protein band appearing in lane 1 was due to a biotinylated protein present in crude extract. However when such extract was affinity chromatographed the protein is no longer found in the eluted fractions (Figure 38A5). This suggests two possibilities. First that this protein is biotinylated and highly concentrated in the crude extract and it is therefore detected on far-Western, whereas when chromatographed it becomes non-detectable due to dilution. Second that it is not biotinylated but rather being non-specifically detected by the far-Western system. Nonspecific protein bands on far-Western blots have been reported.[183,184,185] The

possibility of this protein band being probe-modified can be eliminated since this fraction has not been in contact with the probe.

It was also attempted to compare the effect of (+) and (-)-ABA on crosslinking reaction. For this purpose two parallel experiments using the same conditions were run. The main protein extract was divided into three portions, one UV irradiated in the presence of PBI 686 only, the second and third with PBI 686 with addition of 5 mM (+) or (-)-ABArespectively. Immediately after irradiation protein samples were chromatographed. FPLC chromatograms have shown that the area under peaks eluted with Guanidine hydrochloride from experiment with (+) and (-)-ABA was the same (Figure 42), and again significantly lower than from the corresponding experiment without ABA.

The peak area ratios were the following: A/B/C = 2.60/1.06/1.00 In other words peak area corresponding to experiment with (-)-ABA was only 10% higher than its (+)-ABA equivalent. Proteins in peaks A-C were analyzed by far Western which has confirmed that both enantiomers of ABA effectively block the PAL reaction, and is is further demonstrated on Figure 43.

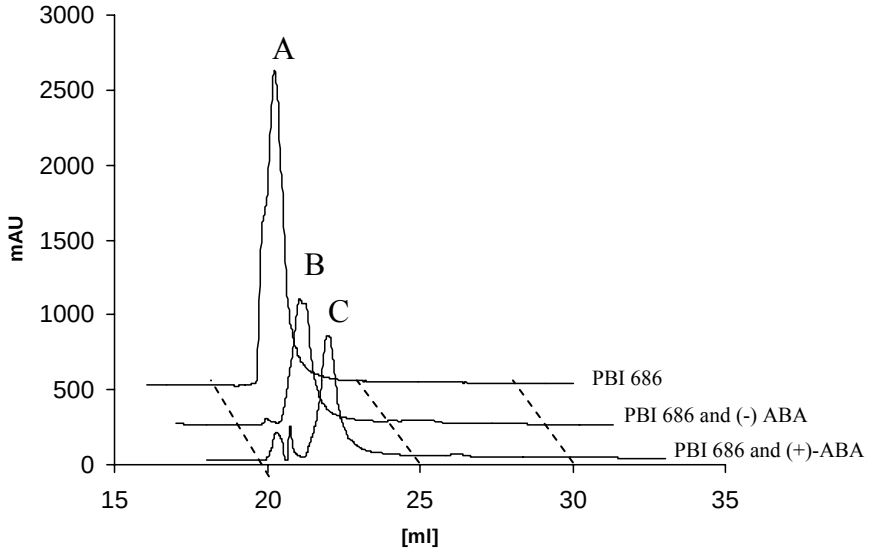

Figure 42. Ovelapped (and shifted for clarity) FPLC traces of proteins eluted from streptavidin affinity column. Peak A – experiment with 100 μM PBI 686 only, peak B - 100 μM PBI 686 and 5 mM (-)-ABA, peak C - 100 μM PBI 686 and 5 mM (+)-ABA.

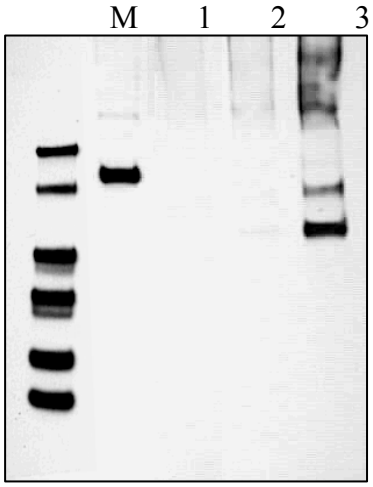

Figure 43. far-Western analysis of fractions collected in peaks A-C (Figure 42). M – biotinylated protein molecular weight marker (from top: 97, 66, 45, 31, 20.1, 14.4 kDa) 1 – non-chromatographed crude protein extract, 2 – peak C – (+)-ABA present (Figure 42), 3 – peak B (-)-ABA present (Figure 42), 4- peak A- no ABA present (Figure 42).

This was the first indication that this potential ABA-binding protein binds ABA with no stereospecific preference. The latter part of the thesis will present further evidence supporting that finding.

At this point identification of all three bands appearing in lane 4 on Figure 43 is necessary. For this purpose, the scale of the experiment was increased to 100 g of fresh tissue in order to obtain sufficient amount of protein in all bands to appear as a band on silver stained gel with band **4-5** (Figure 44) in particular. Protein quantities in bands visible on far-Western blots are usually not sufficient to run peptide mass fingerprinting followed by MALDI-TOF. The crosslinking reaction in a presence of PBI 686 with proteins extracted from 100 g of tissue also yielded three protein bands this time visible on silver stained gel (Figure 44).

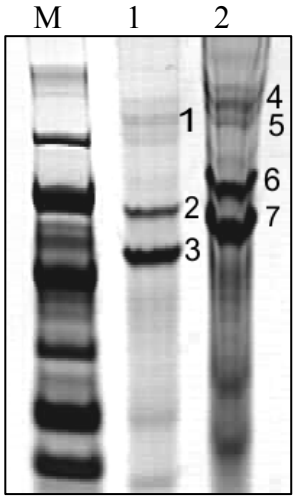

Figure 44. Protein fractions (Figure 42) eluted from FPLC column visualized on a silver-stained gel. M - protein molecular weight marker (from top: 97, 66, 45, 31, 20.1, 14.4 kDa), 1,2 -column fractions (different gel loadings)

Proteins observed in lanes 1 and 2 correspond to column fractions collected during eluting step. Crude cytosolic protein extract was incubated with 100 μM PBI 686, irradiated with UV light and applied on affinity column (pre-eluting step used). All seven protein bands (bands 1-7 Figure 44) were analyzed by MALDI-TOF peptide fingerprinting and/or MS/MS ion search and the results are presented below. All bands but **5** were associated with the

large subunit of Rubisco. Presented below are only the significant Mascot results and peptide coverage map for the highest score hit.

1. gi|7525041
   ribulose-1,5-bisphosphate carboxylase/oxygenase
   large subunit [Arabidopsis thaliana] **Mass:** 53435
   Score: 218, **Queries matched:** 17, Sequence Coverage: **29%**
2. gi|13926229
   F1O19.10/F1O19.10 [Arabidopsis thaliana], (Rubisco small subunit)
   Mass: 14917, **Score:** 179, **Queries matched:** 7 Sequence Coverage: **47%**
3. gi|16195
   ribulose bisphosphate carboxylase [Arabidopsis thaliana]
   Mass: 20586, **Score:** 141, **Queries matched:** 5,Sequence Coverage: **22%**
4. gi|15235321
   CRU3 (CRUCIFERIN 3); nutrient reservoir [Arabidopsis thaliana]
   Mass: 58541, **Score:** 50, **Queries matched:** 2, Sequence Coverage: **4%**

Peptide coverage map for the highest score hit #1:

1 MSPQTETKAS VGFKAGVKEY K**LTYYTPEYE TKDTDILAAF R**VTPQPGVPP
51 EEAGAAVAAE SSTGTWTTVW TDGLTSLDRY KGRCYHIEPV PGEETQFIAY
101 VAYPLDLFEE GSVTNMFTSI VGNVFGFKAL AALRLEDLRI PPAYTK**TFQG**
151 **PPHGIQVER**D KLNKYGRPLL GCTIKPKLGL SAKNYGR**AVY ECLRGGLDFT**
201 **KDDENVNSQP FMR**WRDRFLF CAEAIYK**SQA ETGEIK**GHYL NATAGTCEEM
251 IKRAVFAREL GVPIVMHDYL TGGFTANTSL SHYCR**DNGLL LHIHR**AMHAV
301 IDRQKNHGMH FRVLAKALR**L SGGDHIHAGT VVGK**LEGDR**E STLGFVDLLR**
351 DDYVEKDRSR GIFFTQDWVS LPGVLPVASG GIHVWHMPAL TEIFGDDSVL
401 QFGGGTLGHP WGNAPGAVAN R**VALEACVQA R**NEGR**DLAVE GNEIIR**EACK
451 WSPELAAACE VWK**EITFNFP TIDKLDGQE**

As mentioned before all bands were associated with large (53435 Da) subunit of Rubisco (from *Arabodopsis*) except for band **5** which corresponds to *Arabidopsis* storage protein CRUCIFERIN 3 (CRU3, 58 541 Da). Bands 1,4 and 5 were found to match a set of proteins but their molecular weights did not match the band positions on the gel. An explanation for such phenomenon for bands 1 and 4 (identified as LS of Rubisco) can be found in the literature.

The large subunit of this protein has been often found to form dimers (or aggregates) even after denaturating.[186, 187] Ritamaki *et al.* reported that the separated large subunits of

wheat Rubisco formed non-functional, high-molecular weight aggregates. Treatment with both SDS and thiol reductant was necessary to disrupt the aggregated structures, which indicates that the large subunits had been cross-linked by disulphide bridges. Since added thiol reductant did not prevent aggregation of the separated subunits during attempted reconstitution, oxidation of the sulfhydryl groups apparently took place on contact faces sheltered by the secondary and tertiary structures of the polypeptides. High concentration of large subunits or freezing and thawing of the solution stimulated the formation of disulphide cross-links between the large subunits. The results suggest that large subunits have a tendency to cross-link with disulphide bridges. Luo *et al.*[187] reported that when the unfolded Rubisco in guanidine hydrochloride is diluted at 4 °C, a folding intermediate (Rubisco-I) is rapidly formed, which remains in an unstable monomeric state and gradually develops into folded monomer (Rubisco-M) at 4 °C but undergoes irreversible aggregation at 25 °C.

Refolding of Rubisco-I to Rubisco-M is a very slow process, taking about 20 h for 70% conversion at 4 °C. Rubisco-M is stable at 4 °C and is capable of forming an active dimer spontaneously when incubated at a temperature higher than 10 °C. The dynamic dimerization process has been measured in a temperature range of 4–35 °C by HPLC, and the results demonstrate that the dimerization is strongly facilitated by the temperature.

Two large subunits of Rubisco would have a molar weight 107 kDa. It is therefore concluded that the position of the band above 97 kDa could correspond to the dimer. It has been previously reported that Rubisco is capable of refolding followed by dimer formation.[187,188] It was also reported that both small and large subunits of Rubisco have been found to form aggregates.[186] In addition precursors of large and small subunits can coexist with their corresponding mature forms.[189] There are therefore several different reasons as to why the

large LS of Rubisco could appear as three bands (>100, 60, and 54 kDa, see Figure 44). On the other hand this multiple band appearance of LS has not been observed in crude protein extracts which were not UV-irradiated, which strongly suggests that UV irradiation enhances the processes mentioned above. In fact it was possible to obtain experimental evidence supporting that hypothesis. As observed on Figure 41, 43 and 44, after UV irradiation in the presence of PBI 686 Rubisco LR appears as 2 bands on silver-stained gel and far-Western blot. MALDI-TOF spectra (collected in a typical for tryptic digests 700-3000 ion mass window) of bands 2 and 3 (Figure 44) exhibit the same major fragments as that of non-irradiated protein. However, after careful comparison of MS spectra for bands 2-3 tryptic digests, three new signals were observed. Those signals are: 1351.6470 Da, 1365.6650 Da and 1009.5565 Da. Comparison of both spectra (irradiated and non-irradiated protein) in different mass range windows is shown on Figure 45 and 46.

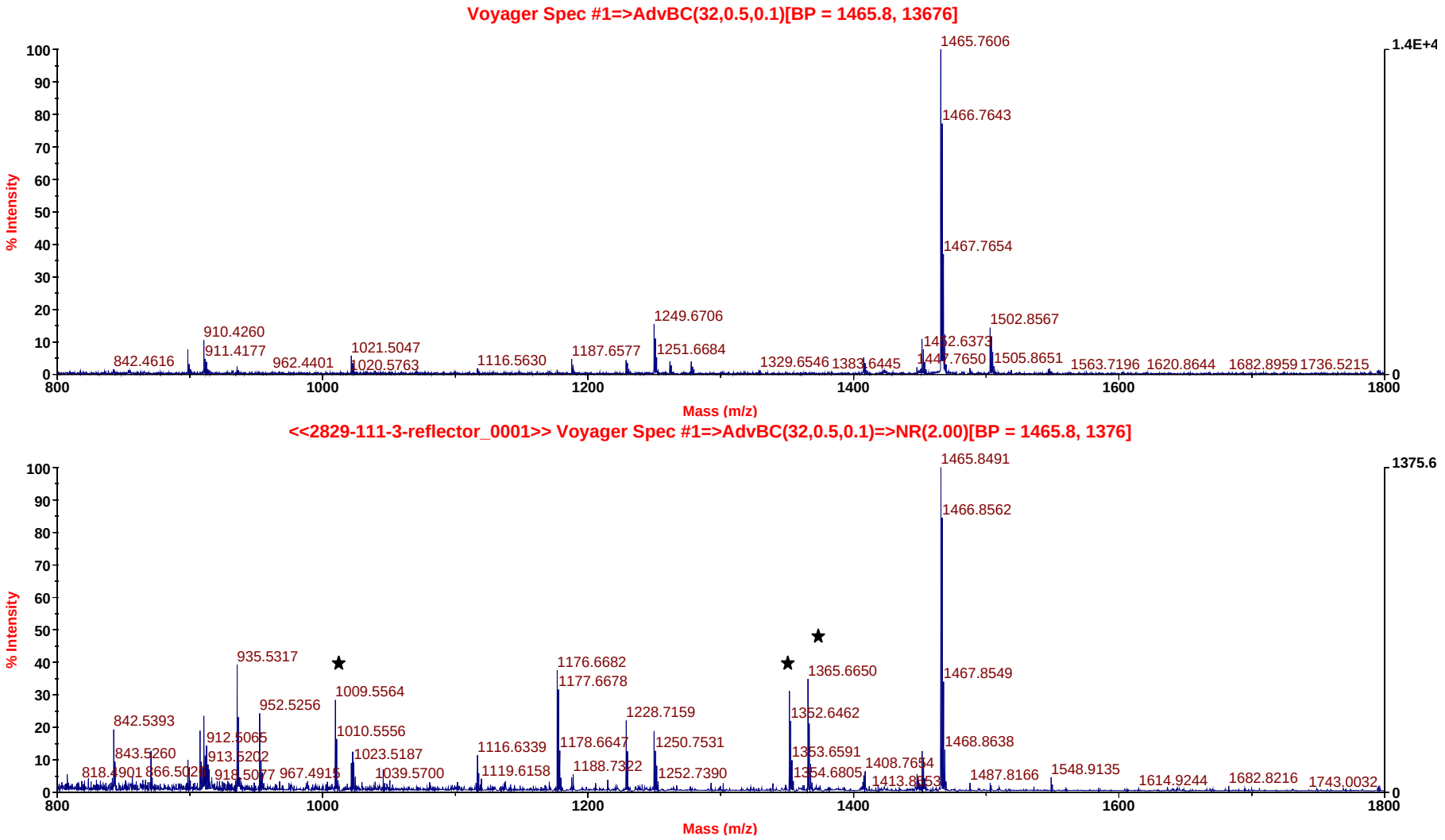

Figure 45. Raw MALDI spectra traces of non-UV irradiated (top trace) and UV-irradiated (bottom trace) and trypsynized Rubisco. High resolution (reflectron) mode, with external calibration and mass accuracy of 20 ppm.

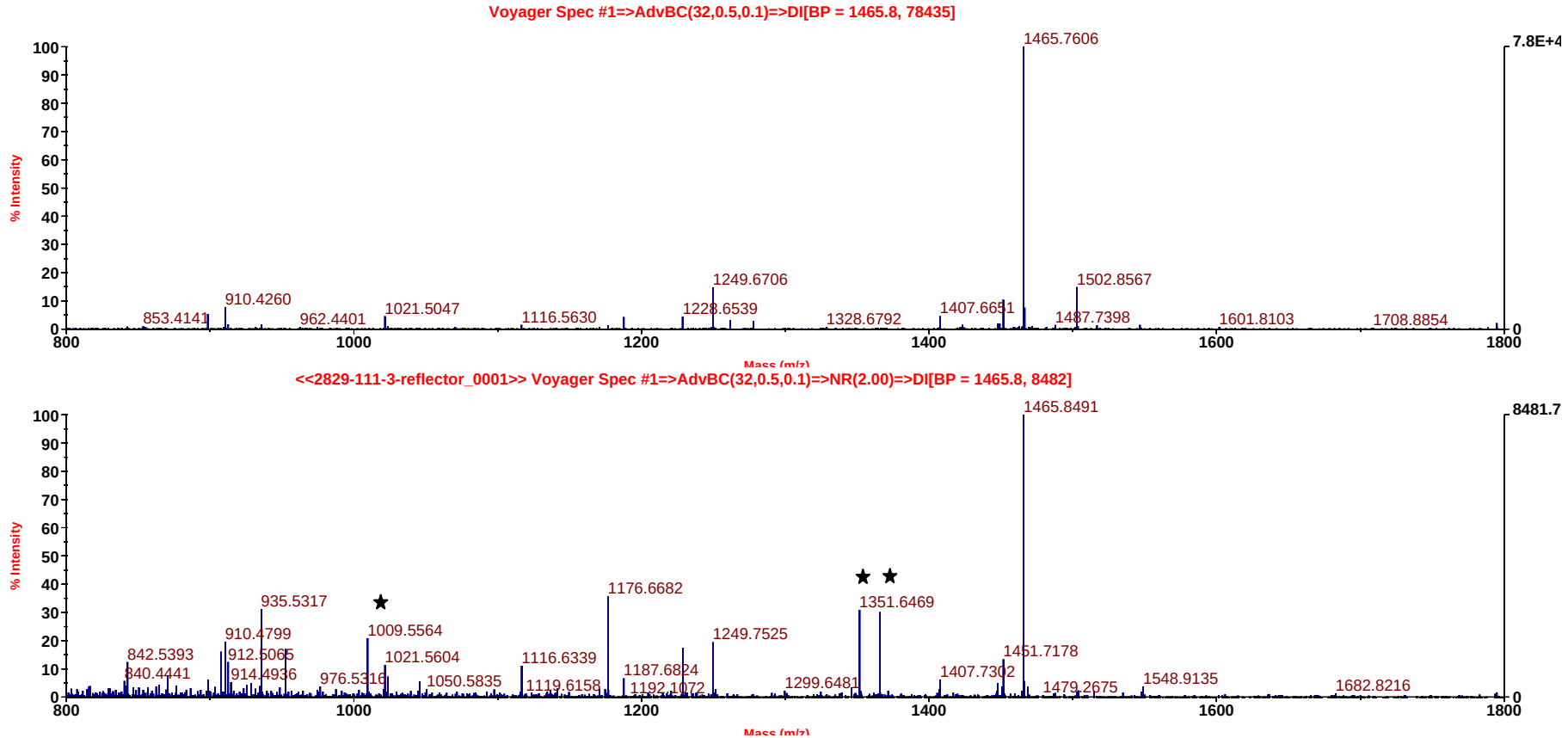

Figure 46. Deisotoped MALDI spectra traces of non-UV irradiated (top trace) and UV-irradiated (bottom trace) and trypsynized Rubisco. High resolution (reflectron) mode, with external calibration and mass accuracy of 20 ppm.

It was initially thought that the new peptide ions observed were associated with PBI 686 adduct. However after thorough examination of MS spectra and analyzing all present peaks (Thanks to Dr. Andrew Ross) and performing a theoretical digest of both large and small Rubisco subunits, it appeared that these peptides belong to the small subunit of the peptide. Although the small subunit's (SS) molecular weight is only 14 kDa, its tryptic peptides were found in a band equivalent to 60 kDa (bands 2 and 6, Figure 44). This indicated that a part of SS is somewhat associated with LS and explains the appearance of Rubisco's LS as two bands after its UV irradiation, one being 54 kDa and second approximately 60 kDa. Combined molecular weight of SS and LS is approximately 70 kDa and appearance of the new Rubisco band (upon UV irradiation) around 60 kDa indicates that only a fragment of approximately 6 kDa of small subunit is covalently attached to the large subunit.

2.7. Photolabeling of purified Rubisco

Having done the photoaffinity labeling with crude extracts and learning that ABA is capable of blocking the probe from labeling Rubisco, further studies on this phenomenon were carried out using purified protein in order to obtain more evidence about ABA interaction with Rubisco. Purified Rubisco was mixed with other purified proteins (non-specific to ABA or probe) all at the same concentration (mg/mL). In such a situation one would expect to observe only the specific protein being labeled, provided the molar ratio between the probe and the proteins does not exceed the previously mentioned value of 1:5 (from photoaffinity labeling of anti-ABA mAb). For such control experiment a mixture of three proteins was used: Rubisco (LS 54 kDa, SS 14kDa), Ovalbumin (45 kDa) and Bovine Serum Albumin (BSA; 66 kDa). The molecular weights of proteins were chosen to be distinctly different to simplify the interpretation of far-Western results.

In sample **1** proteins at 100 μg/mL each (total volume of the reaction mixture 5 mL; protein molar ratio approx 1:1:1) were incubated for 1h at 4 °C with 100 μM PBI 686 and then irradiated for 15 minutes with UV light. Sample **2** was processed in the same way with the exception that concentration of PBI 686 was lowered to 10 μM. Samples **3-4** contained 10 μM PBI686 and 0.5 mM, 1 mM (+)-ABA respectively. Sample **5** contained only UV-irradiated proteins, sample **6** - 10 μM PBI686 but was not irradiated by UV. Figure 47 represents the results by far-Western analysis. Lanes 1-6 correspond to samples 1-6 described above. This experiment indicated that 45 kDa Ovalbumin and 66 kDa BSA did not crosslink with the probe even at its 100 μM concentration (lane 1).

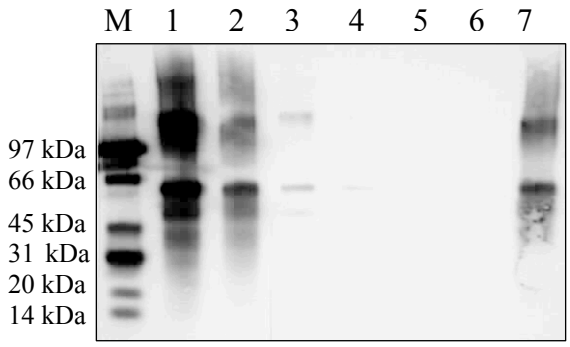

Figure 47. far-Western blot analysis of photoaffinity labeling experiments with purified Rubisco, Ovalbumin and BSA at the same concentration. **1**- 100 μM probe , **2**- 10 μM probe, **3**- 10 μM probe and 0.5 mM (+)-ABA, **4** - 10 μM probe and 1 mM (+)-ABA, 5- UV irradiated proteins only, **6** - 10 μM probe without UV irradiation, **7**- 10 μM probe (detailed description in text).

At 10 μM PBI686 only bands corresponding to Rubisco LS and its dimer are detected (lane 2). The presence of (+)-ABA at both 0.5 mM (50 fold excess) and 1 mM (100 fold excess) almost completely blocked the crosslinking reaction. Lanes 5-6 are negative controls (Figure 47). Lanes 2 and 7 correspond to the same sample.

It was previously observed that tetralone-ABA (PBI 410) was capable of blocking the crosslinking reaction of the probe PBI686 to proteins in crude extracts. Due to the presence of acetophenone moiety in PBI410 it is expected to crosslink in a similar manner with proteins just as well as the actual probe. It was also checked whether PBI410 is capable of blocking the photoaffinity labeling of purified Rubisco and also compare that to the effect of ABA (Figure 48). By comparing lanes 1 vs. 4, 2 vs. 5 and 3 vs. 6 on the above figure it is clear that tetralone-ABA is more efficient in displacing the probe than (+)-ABA. This phenomenon can be explained by the fact that unlike ABA, tetralone-ABA is capable of covalent binding upon UV irradiation (acetophenone moiety). It will therefore be trapped

once bound to the protein and no other competitor will displace it, regardless of its binding affinity and concentration. This experiment has confirmed the initial hypothesis as discussed above (Figure 37).

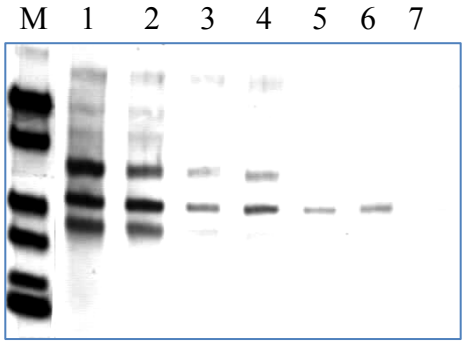

Figure 48. far-Western blot of samples resulting from Rubisco (0.14 mg/mL) crosslinking with the probe (100 μM) in the presence of tetralone-ABA or ABA. M – protein molecular weight marker (from top: 97, 66, 45, 31, 20, 14.4 kDa). **1**-**3** - 100 μM probe + 0.5, 1 and 2 mM (+)-ABA. **4**-**6** - 100 μM probe + 0.5, 1 and 2 mM tetralone-ABA. **7** - 100 μM probe, no UV irradiation.

2.8. Photolabeling and identification of membrane proteins in *Arabidopsis* leaf extracts

In addition to cytosolic proteins, we also wanted to perform initial investigation that would tell us whether there are any hydrophobic proteins found in the crude extract that are capable of binding the probe.

Up to this point, only cytosolic proteins were investigated, and crude protein extracts were not fractionated by ultracentrifugation, nor detergent was added to maintain the microsomal fraction of proteins solubilized. During cytosolic protein extraction, tissue homogenate is first filtered then proteins are precipitated with ammonium sulfate, followed by centrifugation to a pellet. Such pellet is then re-suspended in a small amount of buffer and applied on desalting column. Hydrophobic proteins will remain non-dissolved throughout the extraction process under these conditions. If a non-ionic detergent is added to the extraction buffer, the hydrophobic proteins will be solubilized. In order to compare the two experimental conditions (with or without the detergent) crude tissue homogenate was divided into two equal portions and a non-ionic detergent DHPC (1,2-Diheptanoyl-*sn*-Glycero-3-Phosphocholine) was added to 0.01% w/v concentration to one portion. DHPC preserves the native conformation and therefore the activity of the solubilized proteins.[190]

In the absence of DHPC the protein composition in eluted fractions appeared the same as previously discussed (Figure 38). However in the presence of detergent we observed an additional protein band appearing on both silver-stained gel and far-Western blot (band **1**, Figure 49). The corresponding protein in band 1 was identified by MS/MS ion search method using Q-TOF/MS. Below presented are the results.

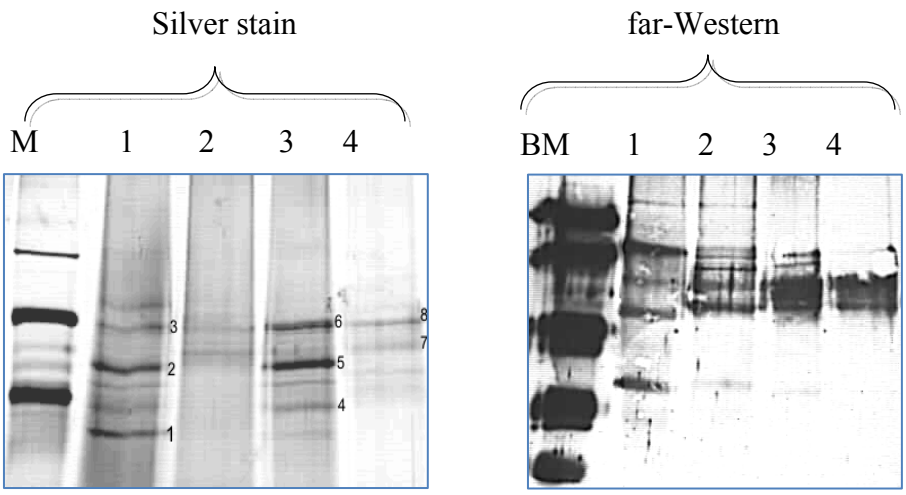

Figure 49. SDS-PAGE separation of proteins found in fractions eluted from affinity column after UV irradiation of detergent-solubilized crude protein lysates in the presence of PBI686. A (silver stain): M- protein molecular weight marker (from top: 97, 66, 45 kDa), 1-2 – proteins eluted in the presence of DHPC detergent during photolabeling reaction; 3-4 proteins eluted in the absence of detergent during photolabeling reaction. B – Corresponding far-Western blot (lanes 1-4 correspond to lanes 1-4 on A).

1. **gi|15235363**
   DREPP plasma membrane polypeptide family protein [Arabidopsis thaliana].
   Mass: 24569, **Score:** 131, **Queries matched:** 10

2. **gi|62319382**
   Fructose bisphosphate aldolase-like protein [Arabidopsis thaliana]
   Mass: 5249, **Score:** 69,**Queries matched:** 2

3. **gi|15232931**
   meprin and TRAF homology domain-containing protein /MATH domain-containing protein [Arabidopsis thaliana] **Mass:** 43031, **Score:** 67, **Queries matched:** 2, Sequence Coverage: **12%**

4. **gi|14334740**
   putative fructose bisphosphate aldolase [Arabidopsis thaliana]
   Mass: 43033, **Score:** 65,**Queries matched:** 5, Sequence Coverage: **12%**

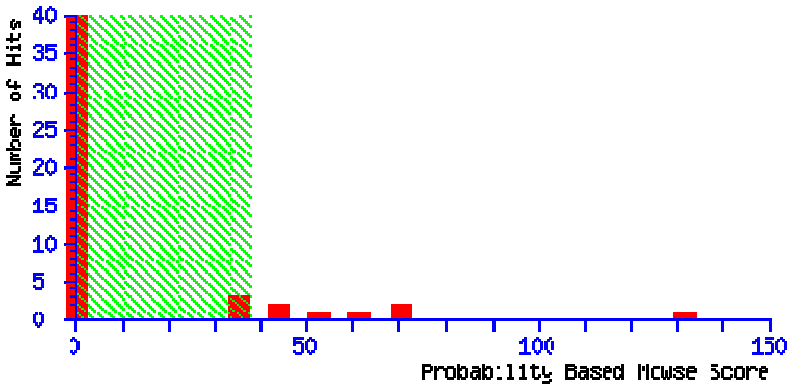

Sequence Coverage for the highest score hit (DREPP): **46%**

```
  1 MGYWNSKVVP KFKKLFEKNS AKKAAAAEAT KTFDESKETI NKEIEEKKTE
 51 LQPKVVETYE ATSAEVKALV RDPKVAGLKK NSAAVQKYLE ELVKIEFPGS
101 KAVSEASSSF GAGYVAGPVT FIFEKVSVFL PEEVKTKEIP VEEVKAEEPA
151 KTEEPAKTEG TSGEKEEIVE ETKKGETPET AVVEEKKPEV EEKKEEATPA
201 PAVVETPVKE PETTTTAPVA EPPKP
```

Band **2** was associated with the large subunit of Rubisco, and band **3** with two other proteins, whose Mascot searches gave very similar scores. A common problem in protein identification using either PMF or MS/MS methods is coexistence of several proteins within one band. If this is the case, the search results usually list several proteins with very similar scores. Below presented is the result of protein identification in band **3** which illustrates this problem.

1. gi|1944432 **ribulose-bisphosphate carboxylase [Arabidopsis thaliana], Mass:** 48008, **Score:** 187, **Queries matched:** 5

2. gi|6651430 **beta-glucosidase homolog [Arabidopsis thaliana], Mass:** 60904, **Score:** 172, **Queries matched:** 6

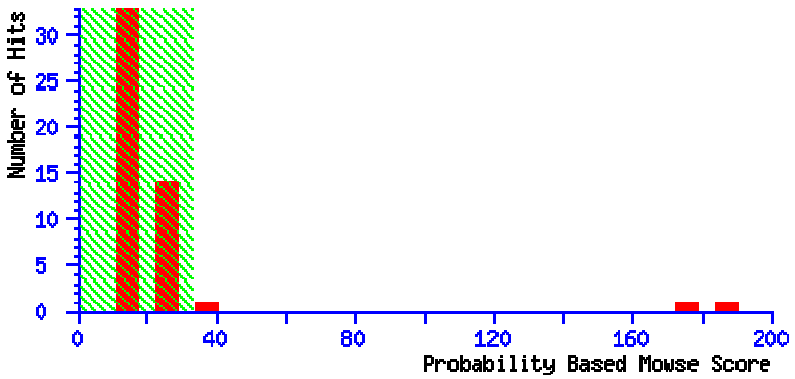

The possibility for band **3** being associated with Rubisco or β-glucosidase is equal. On the other hand if such band appears just below 66 kDa marker lane (Figure 49 A1) it is more likely to be identified as β-glucosidase than Rubisco. As expected bands 4-8 (Figure 49 49A) were as sociated with the same proteins as in the discussion related to the experimental results shown in Figure 38. More specifically band **4** (ESM1- *Arabidopsis thaliana*), band **5** (Rubisco), bands **6** and **8** (β-glucosidase precursor - *Arabidopsis thaliana*). As mentioned before ESM1 and β-glucosidase precursor were disregarded as previously shown non-specific.

In summary proteins which are present in fractions eluted from affinity column due to their possible specific binding with the probe include: Rubisco, Myrosinase-binding protein, ATP synthase, all found in cytosolic extracts, and one membrane protein: DREPP (developmentally regulated endoplasmatic polypeptide).

DREPP is interesting because it is a protein of unknown function, and it is membrane associated. The latter is often a feature of receptor proteins.

DREPP belongs to a small family of plasma membrane proteins first discovered in 1997 by Logan *et al.* [191]. Four highly homologous proteins termed P16-P19 were found to be abundant in the plasma membrane only at a specific developmental stage and in specific leaf-sets. Logan *et al.*[191] reported the cloning of one unknown polypeptide (termed P19) which was one of a pair (the other, P18, displaying 93% identity with P19 in 5 amino acid sequences) that accumulate transiently at floral induction. Cloning and overexpression of a further two plasma membrane polypeptides (P16 and its twin P17) which were abundant in leaves only in the later stages of plant development was also reported. Unexpectedly, these two polypeptides were found to be highly homologous to P18 and P19. On the basis of immunological and sequence data, these four proteins were proposed to be members of a new family of developmentally regulated plasma

membrane polypeptides (DREPP). All four DREPPs share a striking amino acid composition and a structure consisting of a conserved putative trans-membrane domain flanked by a conserved and basic N-terminal region, and by an acidic C-terminal region of more variable length and containing small but highly conserved domains. It was found of particular interest that the expression of DREPP-1/2 during plant development contrasted with that of DREPP-3/4, the former being abundant only in late stages of development while the latter showed a peak in abundance at the time of floral induction. Furthermore, DREPP-1/2 were more abundant in lower leaves, while DREPP-3/4 were more abundant in upper, younger leaves. Sequence analysis provided no clues as to function of each DREPP, but plant DREPP homologues in *Arabidopsis*, rice and tobacco are present as ESTs and no homologues have been identified in other organisms. This suggests DREPPs uniqueness to plants.

Kawamura *et al.* has reported DREPP peptides as cold responsive in: "Mass spectrometric approach for identifying putative plasma membrane proteins of *Arabidopsis* leaves associated with cold acclimation". [192] DREPP peptides were found to be more abundant in cold-treated plants. In addition their experimental molecular weight (35.2 kDa) was found fairly distant from the theoretical one (24.66 kDa). This is consistent with our observation (Figure 49A1). Kawamura has identified DREPP as one of 15 other proteins up-regulated by cold stress among which are found several proteins with calcium-binding ability and which could involve in the increase in freezing tolerance during cold acclimation Tobacco DREPP-like protein contains the possible Glu-rich site at the C-terminus that possesses a sequence similarity to that of the vacuolar Ca^{2+}-binding protein in radish. Taken together with results that the amount of tobacco DREPP-like protein increased temporarily only after 1 day of cold acclimation it is possible that

this protein may be associated with Ca^{2+} signal transduction pathway at the early stage of cold acclimation. There is no other evidence however to support that hypothesis.

Although DREPP's ability to bind ABA has not been further evaluated in this project it remains as one of future directions due to it being one of putative ABA receptors.

2.9. Analysis of the binding interaction between ABA and Rubisco by Surface Plasmon Resonance (SPR)

2.9.1. SPR as a technique chosen for studying ABA-Rubisco interaction

Surface Plasmon Resonance is a label-free technology for monitoring biomolecular interactions as they occur. It is widely used to investigate small molecule-protein and/or protein-protein interactions. The detection principle relies on surface plasmon resonance (SPR), an electron charge density wave phenomenon that arises at the surface of a metallic film when light is reflected at the film under specific conditions. The resonance is a result of energy and momentum being transformed from incident photons into surface plasmons, and is sensitive to the refractive index of the medium on the opposite side of the film from the reflected light. Changes in SPR signal are expressed in resonance units, RU where 1 RU is equivalent to one picogram (of analyte or ligand bound to the surface) per square millimeter of sensor surface. The response is directly proportional to the mass change of the surface. The phenomenon was first observed by Turbadar[193] and fully evaluated by Otto[194] and, Kretschmann.[195] In this project, the Biacore^{TM} SPR system was used to monitor interactions on a biospecific surface by measuring changes in the solute (ABA) concentration at this surface as a result of the interactions. A typical SPR sensogram is depicted on Figure 50.

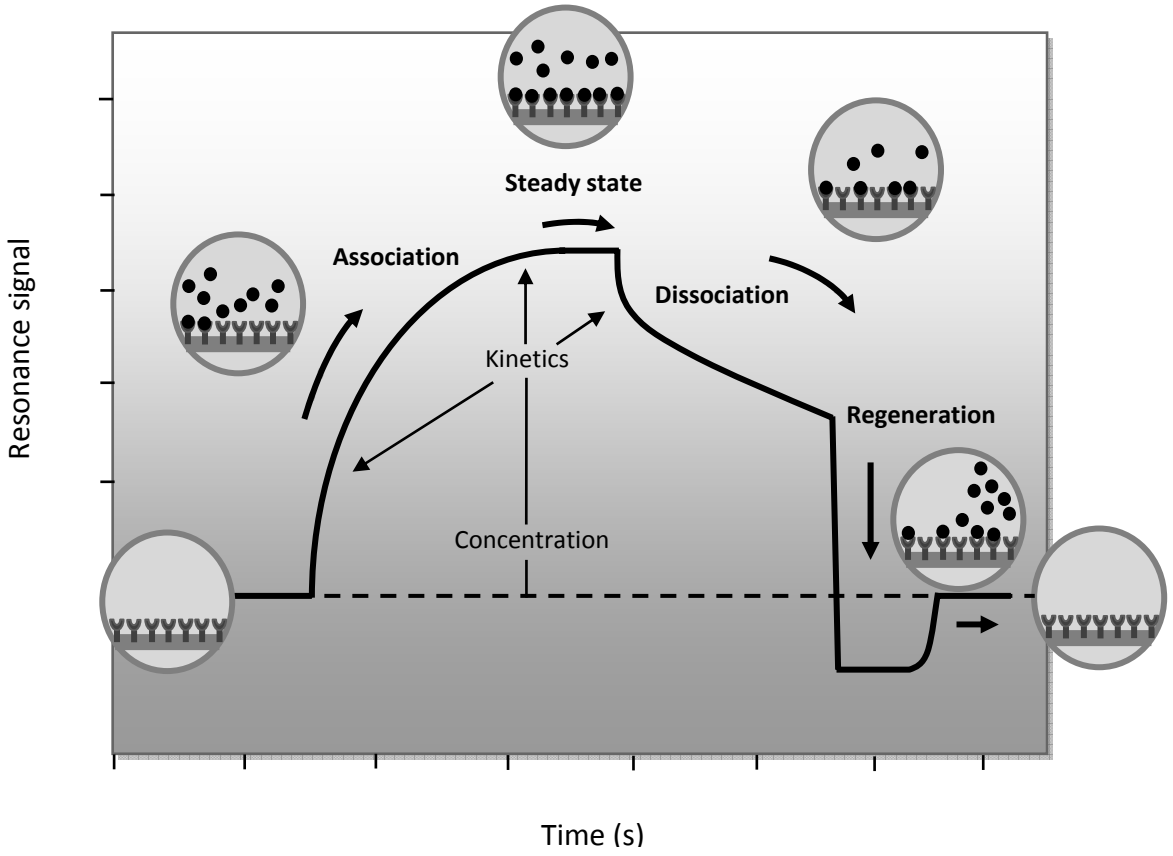

Figure 50. A typical binding cycle observed with an optical biosensor. A protein is immobilized on the sensor surface with appropriate coupling chemistry. At t=0 s buffer is applied to the protein through a micro-fluidic flow cell. At t=100 s a solution of analyte in the running buffer is passed over the protein. As the analyte binds to the surface, the refractive index of the medium adjacent to the sensor surface increases, leading to an increase in the resonance signal. Analysis of this part of the binding curve gives the observed association rate (k_{obs}). If the concentration of the analyte is known, then the association rate constant of the interaction (k_{ass}) can be determined. At equilibrium, by definition, the amount of analyte associating and dissociating with the receptor is equal. The response level at equilibrium is related to the concentration of active analyte in the sample. At t=320 s the analyte solution is replaced by buffer and the receptor–analyte complex is allowed to dissociate. Analysis of this data gives the dissociation rate constant (k_{diss}) for the interaction. Many complexes in biology have considerable half-lives, thus a pulse of a regeneration solution (e.g. high salt, low pH, etc.) is used at t=420 s to disrupt binding and regenerate the free protein. The entire binding cycle is normally repeated several times at varying concentrations of analyte to generate a robust data set for global fitting to an appropriate binding algorithm. The affinity of the interaction can be calculated from the ratio of the rate constants ($K_D=1/K_A=k_{diss}/k_{ass}$) or by a linear or non-linear fitting of the response at equilibrium vs. varying concentration of analyte (figure and caption adapted from Matthew *et al.*[196]).

2.9.2. SPR scouting and protein immobilization

To study the ABA-Rubisco interaction, CM5 (Biacore) sensor chips were used. The free –COOH groups on the unmodified chip were activated with EDC and N-hydroxy-succinimide and then coupled to the protein's free $–NH_2$ groups forming a covalently modified surface. Before the protein was immobilized, a number of scouting experiments were performed. Pre-concentration of the protein in the surface matrix is important for efficient immobilization of macromolecules. This is accomplished by electrostatic attraction between negatively charged sensor surface (carboxymethyl dextran), and a positively charged macromolecule. Because of the electrostatic attraction, it is important to place the macromolecule in a low ionic strength buffer (< 50 mM). The pH at which most protein is depositing on the surface is then used during the immobilization process. The scouting experiments are performed by mixing the protein solution (1:1 ratio by volume) with 10 mM sodium acetate buffer at pH 4.0, 4.5 and 5 correspondingly. The signal intensity during protein injection changes and the magnitude of that change is proportional to the amount of protein being pre-concentrated.

Sodium acetate buffer at pH 5 mixed with the protein solution (pH 7.9) at ratio 1:1 gave the highest signal intensity and therefore was used as the optimal condition for pre-concentrating Rubsico. An example of a scouting experiment is presented on Figure 51.

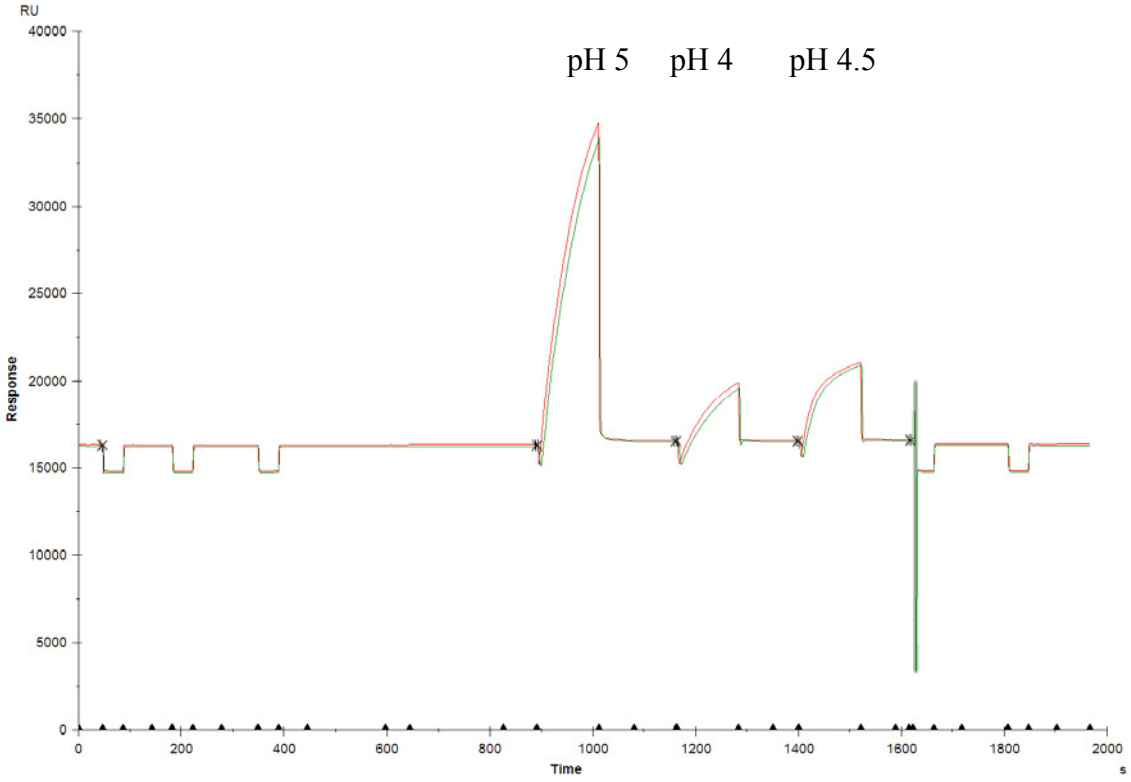

Figure 51. Scouting experiment showing the dependence of protein pre-concentration on pH.

Once the optimal conditions for protein pre-concentration have been established the next step was to immobilize (covalently) the protein on the chip surface. This was done by coupling the protein to the chip surface through a formation of an amide bond. This procedure is depicted on Figure 52.

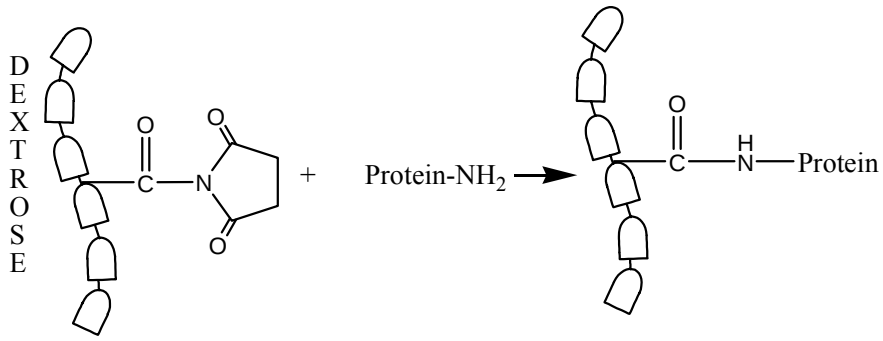

Figure 52. Protein immobilization procedure.

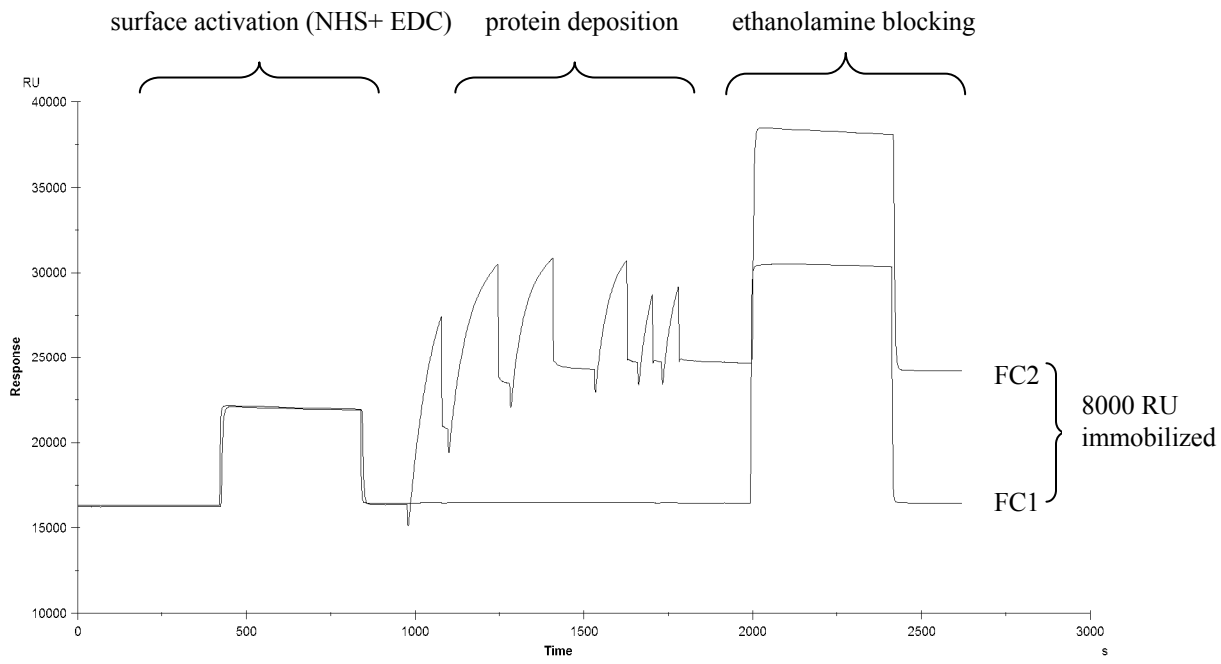

Figure 53. Sensogram representing protein immobilization procedure. FC1- control flow cell, FC2 – modified flow cell.

To avoid coupling of protein to a protein-free reference cell (FC1) it is closed during protein deposition and then re-opened during ethanolamine injection. Since only a certain fraction of all activated carboxyl groups is being modified by the protein, the remaining groups are being blocked by ethanolamine to avoid non-specific binding in further experiments. Protein solution is injected in 1 minute pulses which are repeated until an immobilization level of choice is achieved. The amount of protein to be immobilized depends on the application. For binding specificity measurements, almost any ligand density will be sufficient as long as it gives good signal. Kinetics are investigated with lowest ligand density still giving good response without being disturbed by secondary factors such as mass transfer or steric hindrance. Mass transfer limitation is an important factor which needs to be considered. Binding of analyte (A, immobilized) to the ligand (L, in solution) on the sensor chip can be described as:

$$A_{bulk} \underset{\leftarrow k_m}{\overset{k_m \rightarrow}{\rightleftharpoons}} A_{surface} + L \underset{\leftarrow k_d}{\overset{k_a \rightarrow}{\rightleftharpoons}} AL$$

Where: A_{bulk} = analyte in buffer $A_{surface}$ = analyte at surface of sensor chip, k_m = coefficient for mass transfer, k_a = rate constant for association, k_d = rate constant for dissociation.

The reaction is a two step event. First, the analyte is transferred out of the bulk solution towards the sensor chip surface. Second, the binding of the analyte to the ligand takes place. The first step is also known as mass transfer and is carried out by convection and diffusion.[197] Both events have their own rate constants (k_m and k_a/k_d). The coefficient for mass transfer (k_m) is the same in both directions. With full or partial mass transfer, the diffusion from the bulk to the surface is slower than the rate of binding of the analyte to the ligand creating a shortage of analyte at the surface. The miniaturized flow cell in BIACORE reduces but cannot eliminate the potential contribution of mass transfer processes to the observed binding kinetics. However, there are several ways of reducing the mass transport contribution, one by using low surface density of the protein and if that is not possible due to low signal it is also recommended to perform the experiments using high buffer flow rates. In this project both of these methods were used. For determination of binding specificity high density surface (approx. 8000 RU) was used and for investigating the binding kinetics the surface density was lowered to 4000 RU and high (100 µl/min) buffer flow rates were applied.

2.9.3. SPR experiments with Rubisco and ABA, PA, and PBI 686

Initial experiments with Rubisco immobilized on the surface and (+)-ABA as an analyte provided evidence of specific binding. Low density surface coverage and high concentration of ABA (5 μM) yielded a sensogram with good signal intensity. No signal was observed upon injecting the buffer in which ABA was dissolved. Figure 54 illustrates one such initial experiment.

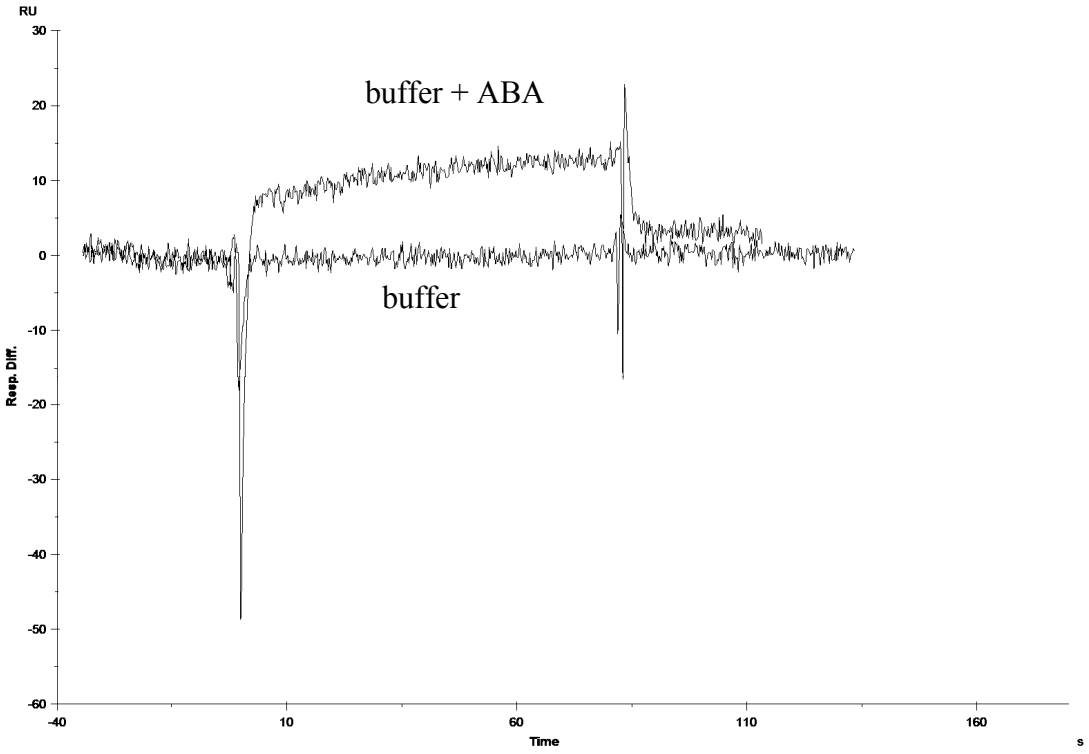

Figure 54. Initial SPR experiment with 4000 RU of protein immobilized and 5 μM (+)-ABA injection vs. buffer injection.

The next step was to check for specificity of binding. For that purpose the signal observed during ABA injection was compared to that of *trans*-cinnamic acid (CA), a molecule unrelated to ABA and its function. Comparison of signals from both ABA and CA is shown on Figure 55.

The lack of any signal observed upon the injection of CA was the first indication that the signal resulting from ABA injection is due to specific interaction with the protein.

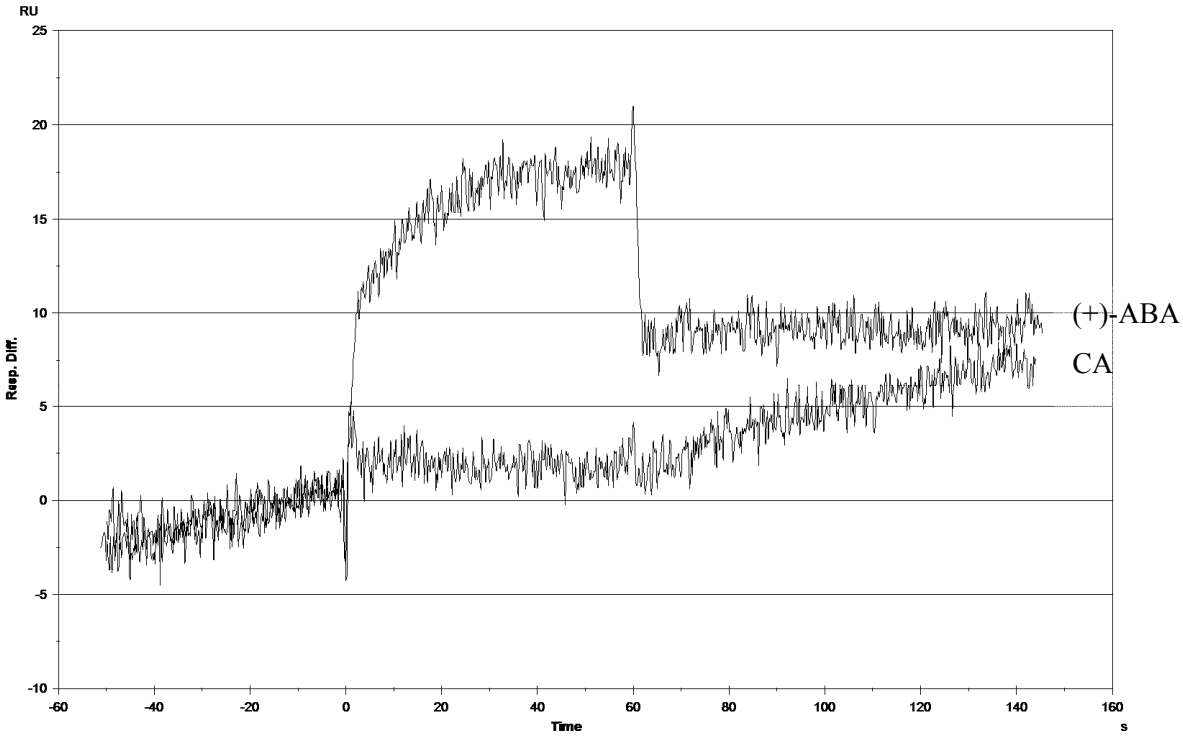

Figure 55. Initial SPR experiment with 4500 RU of protein immobilized and 5 μM (+)-ABA injection vs. 5 μM *trans*-cinnamic acid (CA).

Subsequently the binding of ABA and its analogs/metabolites was further investigated by qualitative comparison of the equilibrium dissociation corresponding to each compound capable of binding Rubisco. (-)-ABA was found to bind yielding a similar signal intensity sensogram when injected at the same concentration as (+)-ABA. This phenomenon is in agreement with previous finding where (-)-ABA blocked photoaffinity labeling of Rubisco as efficiently as (+)-ABA, which was the first indication of Rubisco binding both enantiomers. Although the SPR signal intensity for (-)-ABA seems to be slightly lower than for (+)-ABA. The sensogram in Figure 56 also indicated that the dissociation rate (k_d) of (-)-ABA is detectibly lower than that of (+)-ABA.

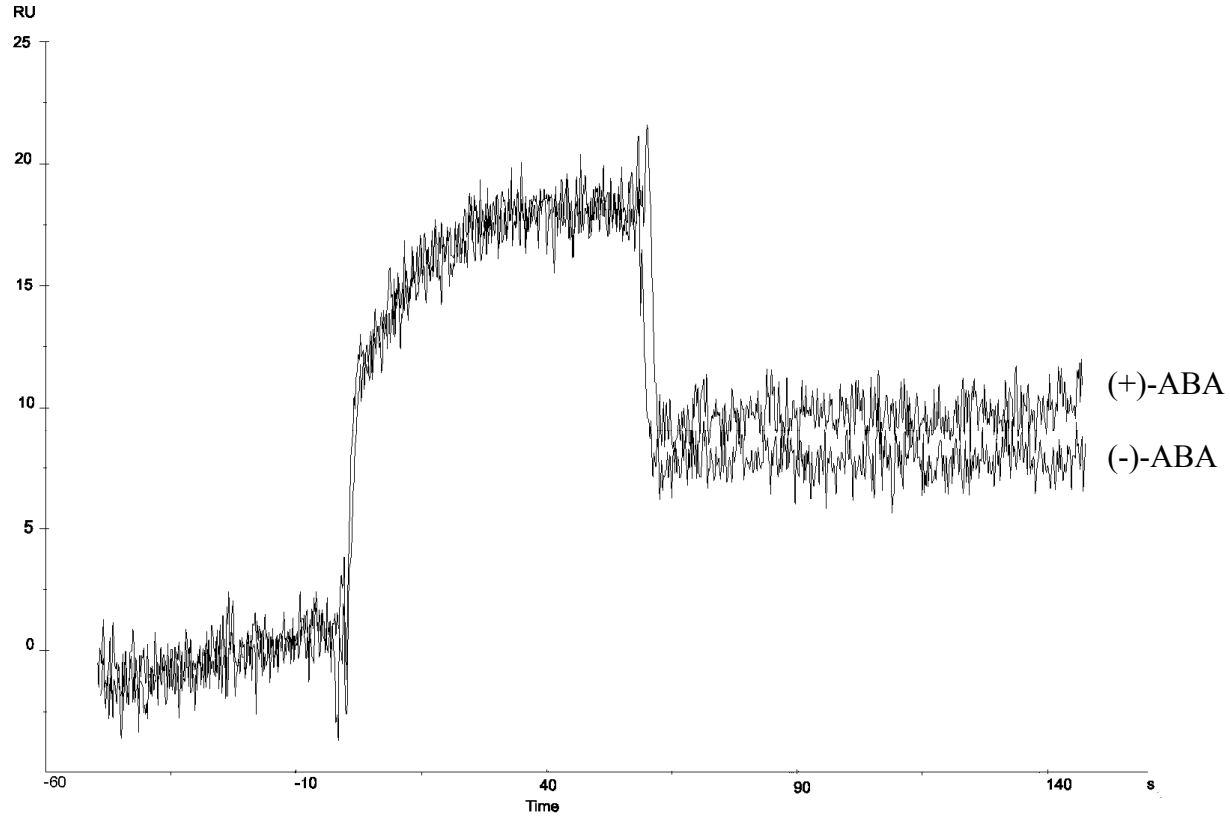

Figure 56. SPR sensograms resulting from 5 μM (+) and (-)-ABA injections. 4500 RU of protein immobilized.

This is observed by the slight shift of the sensogram to the left at the end of injection, which indicates faster dissociation of (-)-ABA than (+)-ABA. In addition slightly more (+)-ABA was found to be retained by the protein after the injection, the difference was minimal but detectable. The ability to bind both ABA enantiomers confirms the selective rather than specific nature of this interaction. PA, a biologically inactive metabolite of ABA was also injected and no signal was observed using the low density surface. The same experiment carried out using the high density surface (8000 RU of protein immobilized) and two different PA concentrations yielded a relatively small signal. This is shown in comparison to the signals observed for (+)-ABA at the same concentrations of both analytes (Figure 57).

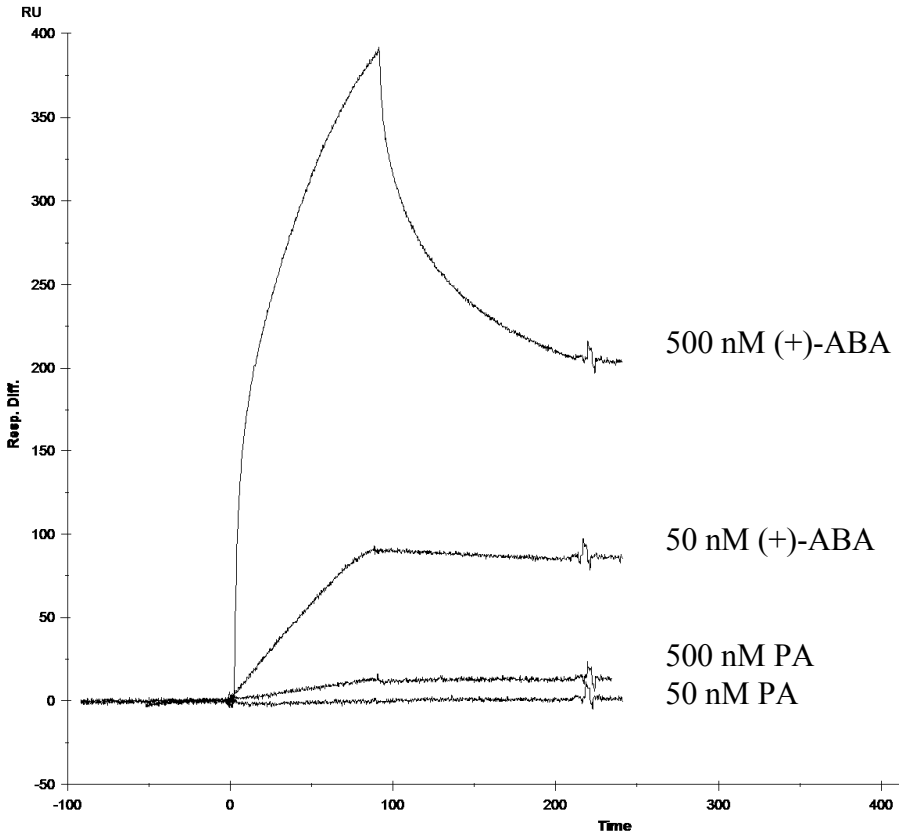

Figure 57. An overlay of SPR sensograms resulting from 50 and 500 nM PA and (+)-ABA. Rubisco surface density 10 000RU.

A dramatic difference between these two molecules was observed which suggests that unlike (+)-ABA, PA binding affinity to Rubisco is significantly lower. This has confirmed the hypothesis that binding of ABA and Rubisco is selective but not stereospecific.

The next step in this study was a quantitative evaluation of binding kinetics between (+)-ABA, (-)-ABA, PA and the probe PBI 686. Kinetic evaluations of ABAs were done using low density surfaces (4000-4500 RU) and high buffer flow rates (100 µl/min). For PA and PBI 686 high surface densities were used as no signal was observed at lower densities. For these two latter compounds mass transport correction was utilized for kinetics evaluation to minimize the impact of mass transport on evaluation of binding parameters.

Binding kinetics of (+)-ABA were evaluated using 5 sensor chips. Equilibrium dissociation constants were obtained using BiaEvaluation software, using 1:1 Langmuir fit algorithm which yielded the best fit. Equilibrium dissociation constants are calculated from the dissociation/association rate ratio (k_d/k_a). An example of SPR sensogram obtained for (+) and (-)-ABA using a chip surface density of 4500RU is presented on Figure 58. Results from five different chips (for (+)-ABA) were averaged yielding the following equilibrium dissociation constant: K_D (+)-ABA = 5.3 ± 1.6 nM. Equilibrium dissociation constant for (-) -ABA was also evaluated using one sensor chip and it was K_D (-)-ABA = 7.1 nM.

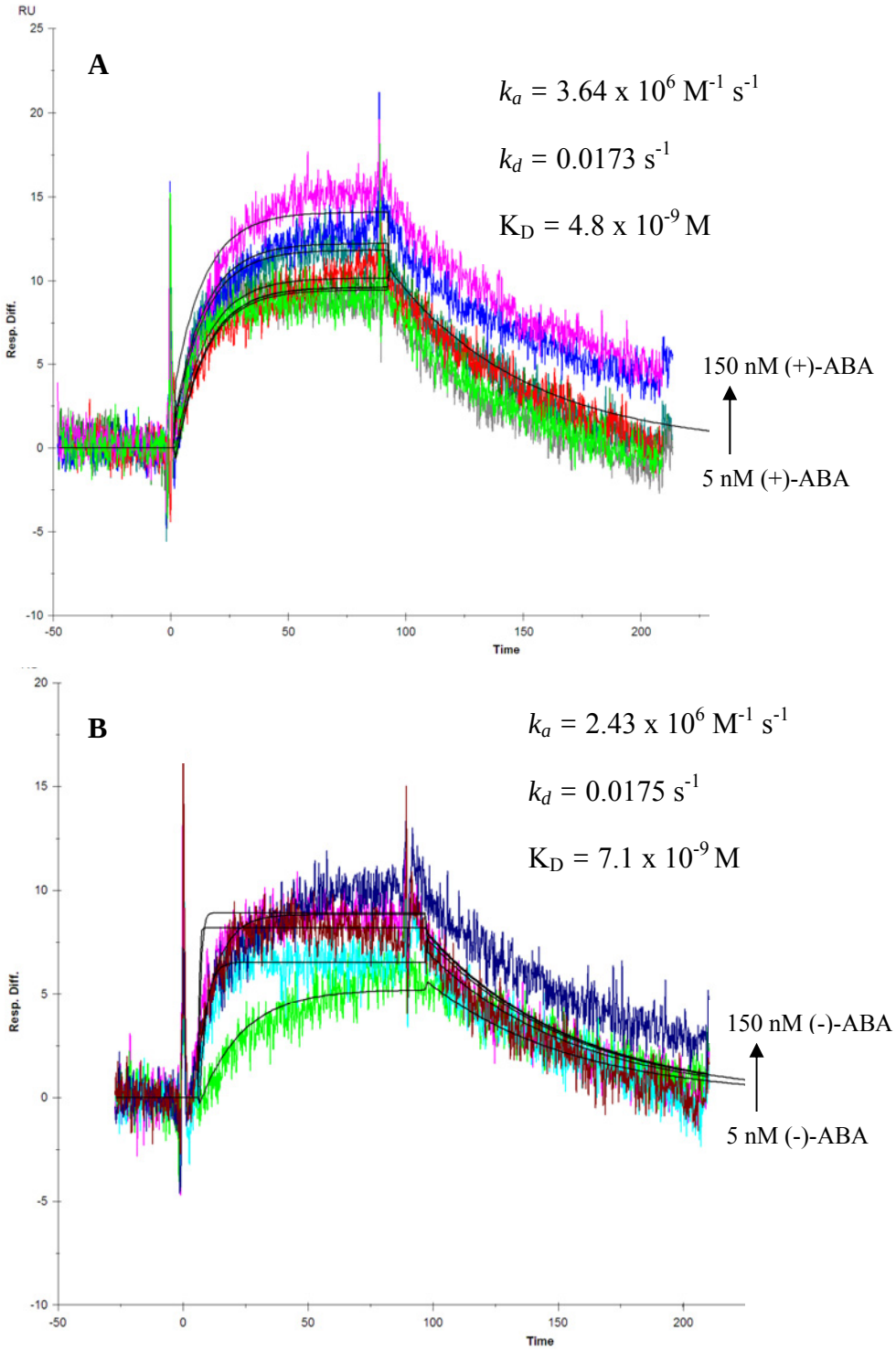

Figure 58. SPR sensograms resulting from **A** - (+) and **B** - (-)-ABA injections. ABA concentrations ranging from 0.2 to 50 nM. Rubisco surface density 4500 RU.

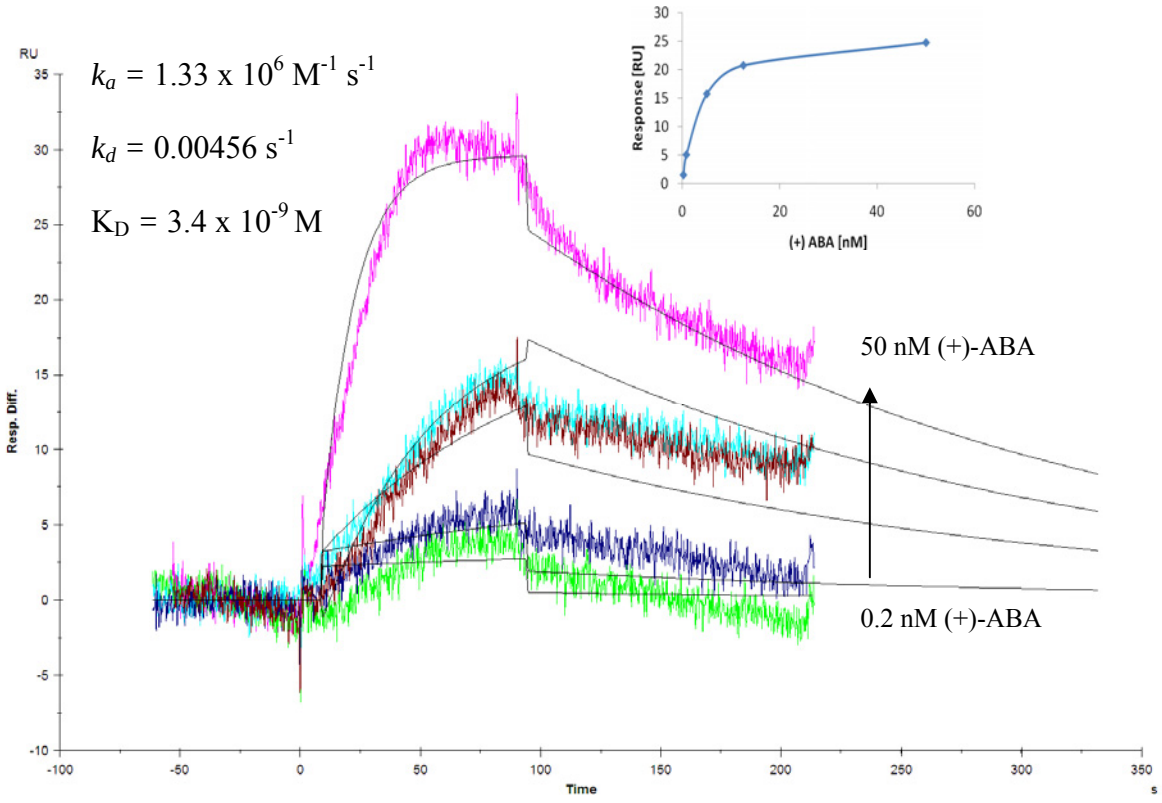

Figure 59. SPR sensograms resulting from (+)-ABA injections. ABA concentrations ranging from 0.2 to 50 nM. Rubisco surface density 8000 RU.

Table 2. Kinetic parameters resulting from SPR measurements on five Rubisco-crosslinked CM5 sensor chips for (+)-ABA interactions.

Sensor chip #	k_a [M^{-1} s^{-1}]	k_d [s^{-1}]	K$_D$ [nM]
1	3.64 x 10^6	1.73 x 10^{-2}	4.76
2	1.84 x 10^4	1.02 x 10^{-4}	5.55
3	1.33 x 10^6	4.56 x 10^{-3}	3.42
4	1.30 x 10^6	6.33 x 10^{-3}	4.86
5	8.36 x 10^5	6.59 x 10^{-3}	7.88
Average (± stdev.)	1.42 ± 1.35 x 10^6	6.98 ± 6.33 x 10^{-3}	5.29 ± 1.64

R_{max} is the maximal feasible signal in Response Units (RU) which is dependent on the number of binding places (ligand concentration and valency (V) and the size (MW) relation between ligand and analyte. Where R_L is the surface density

$$\mathbf{R_{max} = (MW_A / MW_L) \times R_L \times V_L}$$

It was previously found that ABA binds to large Rubisco subunits (LS), and there are eight LS in the entire protein complex. Assuming that one molecule of ABA binds to one LS and protein surface density is 4500 RU, the theoretical R_{max} value would be:

$$\mathbf{R_{max} = (264\ g\ mol^{-1} / 560\ 000\ g\ mol^{-1}) \times 4500\ RU \times 8 = 17\ RU}$$ (Figure 58)

For protein surface density of 8000 RU:

$$\mathbf{R_{max} = (264\ g\ mol^{-1} / 560\ 000\ g\ mol^{-1}) \times 8000\ RU \times 8 = 30\ RU}$$ (Figure 59)

Observed R_{max} values (sensograms from Figure 58) are approximately 15 and 11 RU for (+) and (-)-ABA correspondingly. R_{max} observed on Figure 59 on the other hand is approximately 30 RU, and the surface density is doubled (8000 RU). The experimental R_{max} (surface density 4500 RU, Figure 58) suggests that the protein: ligand ratio is approximately 1:7. Experimental R_{max} value was found to be very close to the theoretical one and indicated protein:ligand ratio 1:8. The experimental signal intensity being lower (Figure 58) than the theoretical one, is most likely due to the fact that a fraction of binding sites do not have binding functionality or are not accessible to ABA during the experiment.

The above results suggest that each large Rubisco subunit binds one molecule of ABA, and that assumption is based on the fact that all large subunits are identical, previous finding that only large subunits are capable of binding ABA and finally supported by the experimental evidence by SPR.

Binding kinetics of other compounds such as PA and PBI 686 were also evaluated. PA was found to bind at high concentrations yielding the signal when using high density surfaces (8000 RU). The equilibrium dissociation constant of PA was found to be 46 µM, which is 9200 fold higher than that of ABA (5 nM). This confirms the previous finding of PA binding affinity to Rubisco being dramatically lower than ABA.

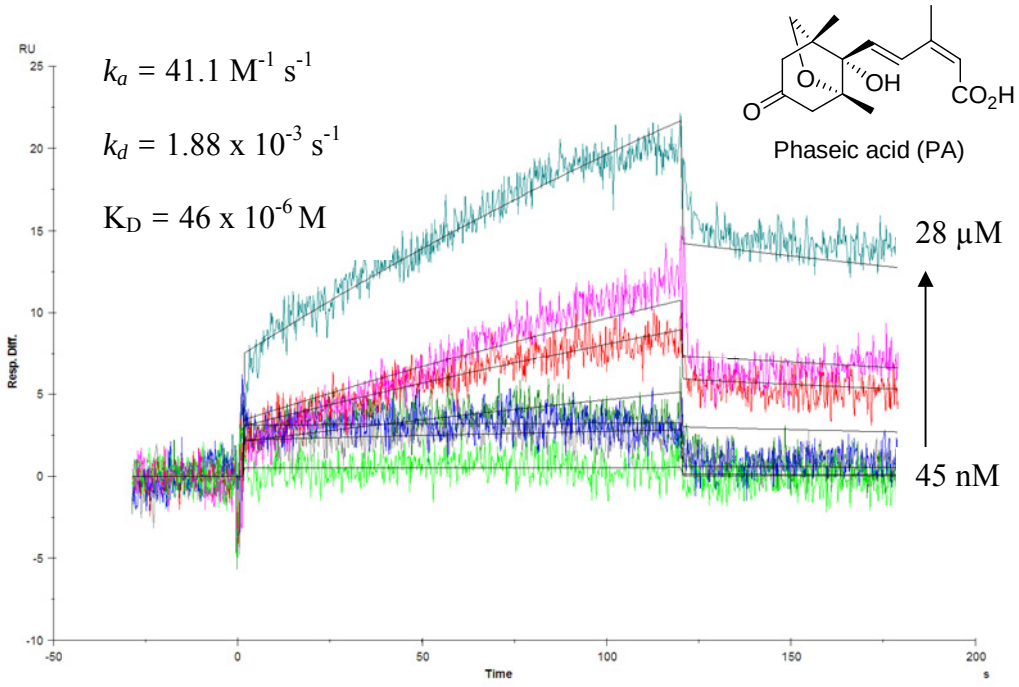

Figure 60. SPR sensogram resulting from PA injections ranging from 0.045 µM to 28 µM. Surface density 8000 RU.

It was also of interest to evaluate the binding kinetics of the probe PBI 686 since it was used as a tool for isolation of Rubisco from crude extracts and exhibited selective binding capability to Rubisco.

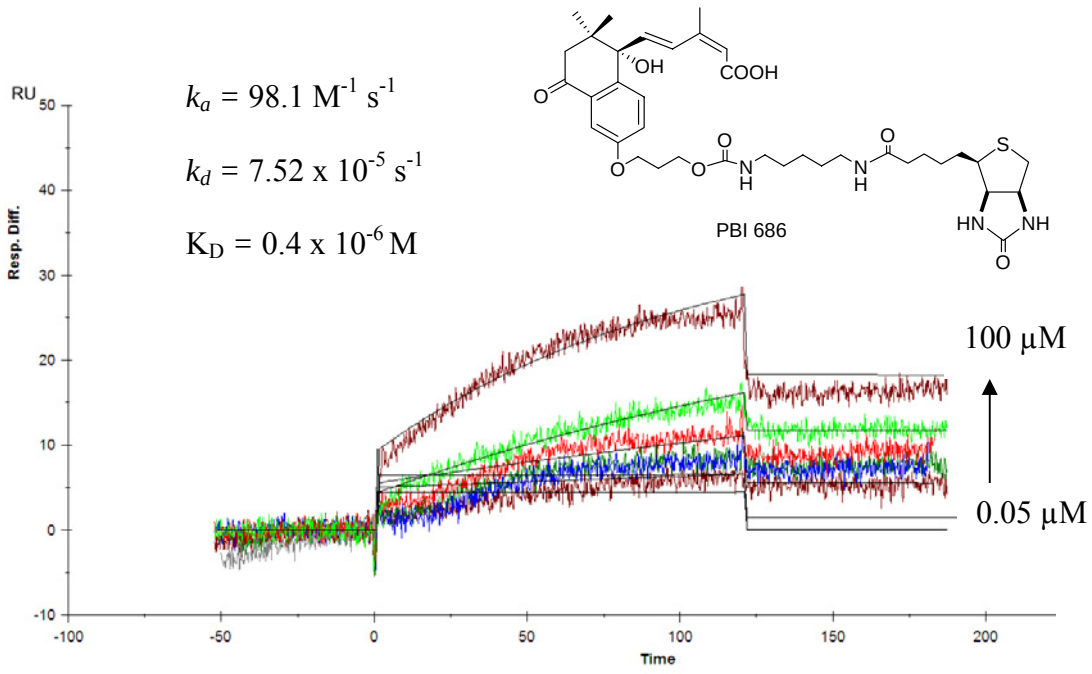

Figure 61. SPR sensogram resulting from PBI 686 injections ranging from 0.05 µM to 100µM. Surface density 8000 RU.

The above experiment (Figure 61) indicated that the affinity of PBI686 to Rubisco is relatively high, and unlike PA, PBI 686 exhibits a low equilibrium dissociation constant of 0.4 µM, which is 77 fold higher than that of ABA but 115 fold lower than PA.

In summary, testing Rubisco-ABA interaction by SPR has provided good and reproducible data, and yielded kinetic parameters indicating high affinity of both ABA enantiomers to Rubisco. Interaction of PA was also investigated, and the results suggested PA affinity being 9200 fold lower than that of ABA, which is an important finding in relevance to physiological meaning. PA is a biologically inactive metabolite of ABA and its affinity to Rubisco is too low for it to have any physiological relevance in plants, in other words an equilibrium dissociation constant of PA being on the order of 46 µM would have

little impact on Rubisco as concentrations of PA in plant tissues do not exceed 10 μM threshold.

A reverse approach which involves immobilization of the probe on the chip surface and running solution of Rubisco through the system did not provide acceptable results due to high background signal caused by non-specific binding of the protein to the chip surface.

In this project SPR was used as one of the methods for studying Rubisco-ABA interaction and the resulting K_D value will be then further confirmed by an alternative method such as radioligand binding assays.

2.9.4. Literature examples of studying protein-small molecule interactions by SPR

There are many literature examples of investigating small molecule-protein interactions that rely on SPR as a technique for determination of binding kinetics.[198,199] Casper et.al[198] has investigated the interaction between small molecule inhibitors and p38α mitogen-activated protein kinase. This research group has developed a real-time, label free method to study protein kinase inhibitor binding kinetics using SPR. Utilizing p38α mitogen-activated protein kinase as a model system, they studied the binding properties of two known small molecule p38α inhibitors (Figure 62). Direct coupling of p38α to the biosensor surface in the presence of a reversible structure-stabilizing ligand produced greater than 90% active protein on the biosensor surface. The dissociation and kinetic constants derived using Biacore method were in very good agreement with values determined by other solution-based methods.[200,201]

p38α kinase is a well characterized target for inflammatory disease therapy. It is widely expressed in many mammalian tissues and is activated as a part of signal transduction

cascades that respond to inflammatory stimuli. The kinetic parameters were evaluated at various temperatures, from SPR sensograms using BiaEvaluation software. The average equilibrium dissociation constants describing SB-203580/p38α interaction were found to be dependent on temperature and were 3.8, 6.7 11.5 and 29 nM at 5, 15, 25, and 35°C correspondingly.

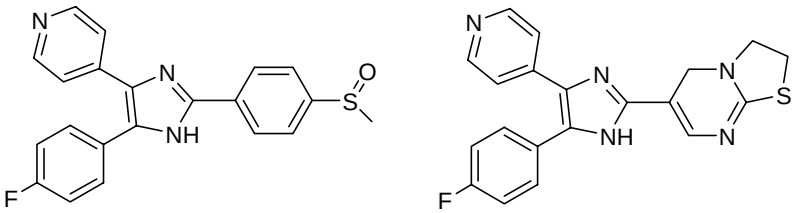

Figure 62. Chemical structures of two known p38α protein kinase inhibitors[198]

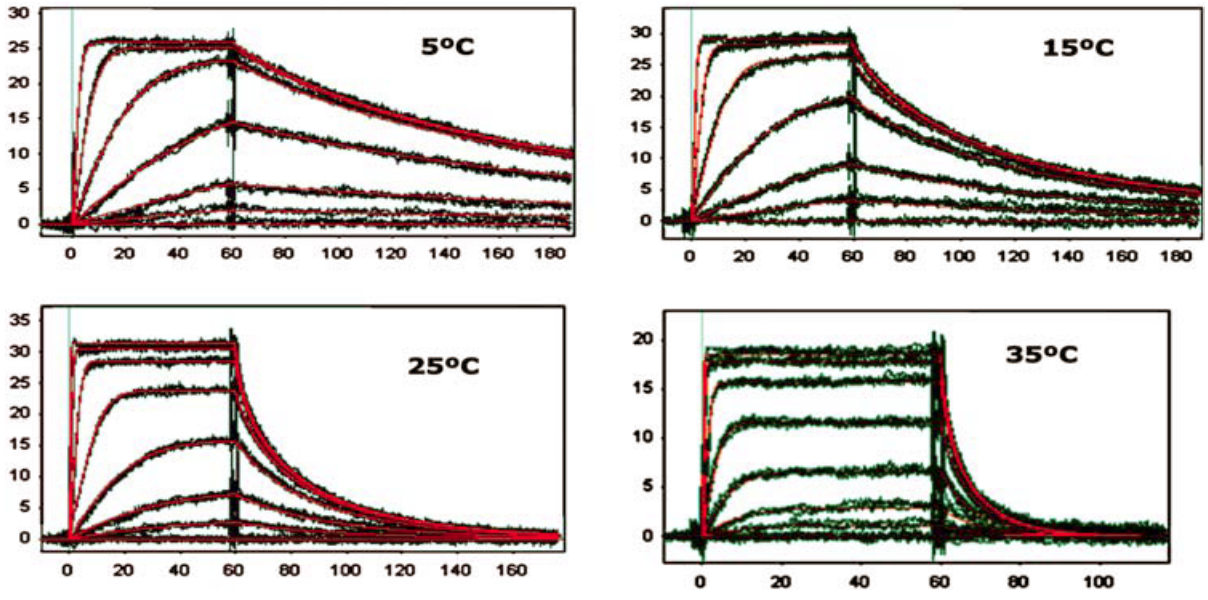

Figure 63. Temperature dependence of SB-203580 binding to p38α protein kinase (figure copied from[198] with permission).

In this project it was not possible to evaluate the kinetics of Rubisco-ABA interaction at various temperatures due to incapability of the instrument used to run experiments at variable temperatures.

2.9.5. SPR vs. other techniques

In 2004, a number of authors performed studies to establish the reliability of information obtained using SPR biosensor technology.[202] These investigations determined the reproducibility of kinetic and affinity parameters reported by different researchers and compared the affinities obtained from kinetic and equilibrium analyses, as well as those measured using the biosensor and solution-based methods. As illustrated on Figure 64, the kinetic parameters obtained by SPR are in good agreement with other techniques.

The year 2004 also saw 36 different investigators analyze an identical small molecule/enzyme interaction under similar conditions[203] in order to test the experimental variability associated with Biacore analysis. Acetazolamide (222 g/mol) binding to carbonic anhydrase II (CAII; 30,000Da) was chosen as a model system. Both reagents were stable and their interaction posed a challenge to measure because of the low molecular weight of the small molecule that was used as the analyte and the fast association rate constant. Each investigator created three different density surfaces of CAII and analyzed interaction of an identical dilution series of acetazolamide (ranging from 4.1 to 1000 nM) with these. The greatest variability in the results was observed during the enzyme immobilization step since each investigator provided their own surface activating reagents. Variability in the quality of the acetazolamide binding responses was likely a product of how well the investigators' instruments had been maintained.

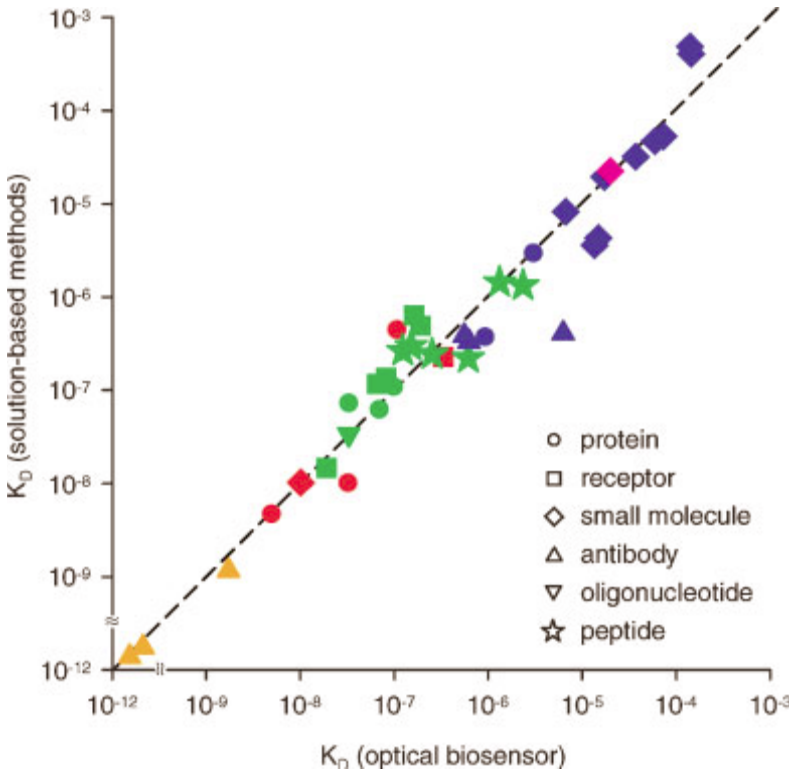

Figure 64. Plot of equilibrium dissociation rate determined for a variety of biological systems (denoted by the different symbols) by both SPR and analytical centrifugation (blue), isothermal calorimetry (green), fluorescence (red), NMR (pink), or KinExA (orange), The diagonal dashed line represents a correlation of 1. constants (figure copied from[202] with permission).

To determine the reaction kinetics, the responses from the different density surfaces were fit globally to a 1:1 interaction model that included a term for mass transport. The averaged association and dissociation rate constants were $(3.1 \pm 1.6) \times 10^{-6}\ M^{-1}\ s^{-1}$ and $(6.7 \pm 2.5) \times 10^{-2}\ s^{-1}$, respectively, which corresponded to an average equilibrium dissociation constant (K_D) of $(2.6 \pm 1.4) \times 10^{-8}$ M. The results provide a benchmark of variability in interpreting binding constants from the biosensor and highlight keys areas that should be considered when analyzing small molecule interactions.[202,203]

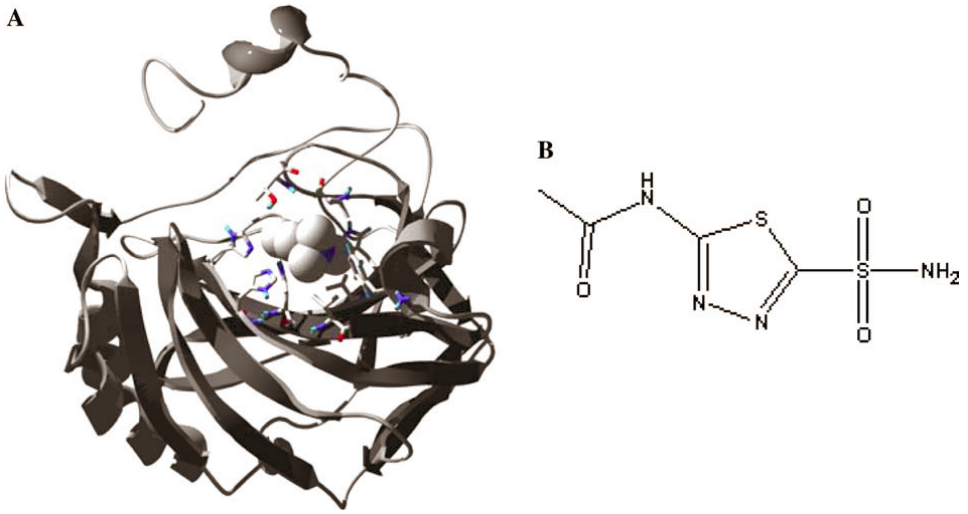

Figure 65. Enzyme/inhibitor model system. (A) Ribbon diagram of the crystal structure of carbonic anhydrase II bound with a sulfonamide inhibitor. (B) Chemical structure of the CAII inhibitor acetazolamide that was used in the analysis. (figure copied from[203] with permission).

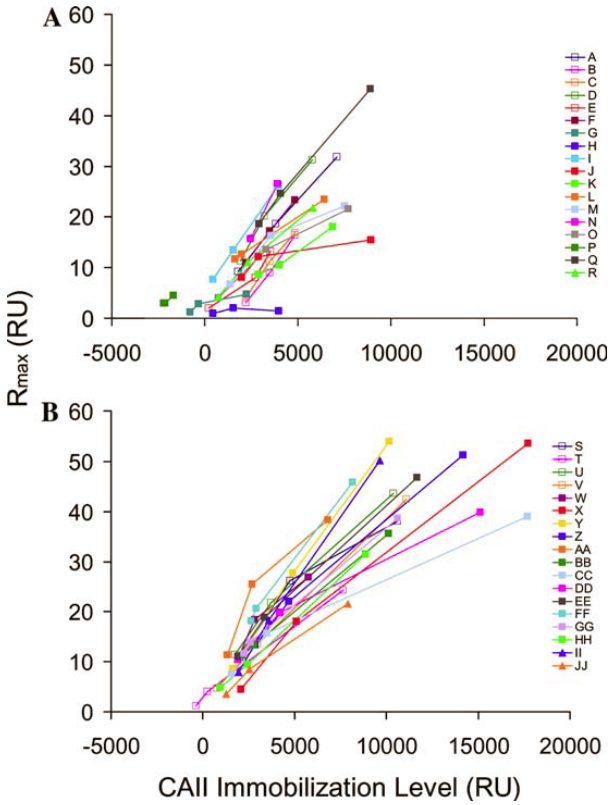

Figure 66. Correlation of maximum binding response with the CAII immobilization level. The maximum binding response obtained on each surface versus the amount of CAII immobilized on the flow cell for group 1 (A) and group 2 (B) (figure copied from[203] with permission).

Thirty-six different Biacore users were provided similar samples of an analyte and ligand, along with a detailed protocol on how to set up and carry out their analysis[203]. Each investigator immobilized CAII enzyme at three different surface densities and analyzed the binding of acetazolamide over a 250-fold concentration range in triplicate. The participants evaluated the interaction under the same buffer conditions, at 25 °C. Data collected from the experiments were processed and analyzed in an identical manner. The results presented here

provide a foundation to compare the ability of various users and the quality of data obtained from different instrument platforms. Applying SPR biosensors to study small molecules reacting with larger biomolecules is still relatively new. Small molecule interactions can be challenging to characterize because the signals are inherently smaller than those observed for protein/protein interactions, due to the low mass of the analyte. Proper analysis of a small molecule system requires careful instrument preparation, experimental design, and data analysis. It also requires a high-density surface for detecting the small molecule binding which can introduce mass transport effects. The distribution of the dissociation rate constants is shown in B, where the average was (6.7 ± 2.5) × 10-2 s^{-1} and corresponds to a CV (coefficient of variation) of 37% The histogram plot shown in Figure 67C indicates the distribution of the equilibrium dissociation constants. The interaction affinity was determined by the quotient $K_D = k_d/k_a$, and an average of (2.6 ±1.4) × 10^{-8} M was determined for the K_D of the binding interaction.

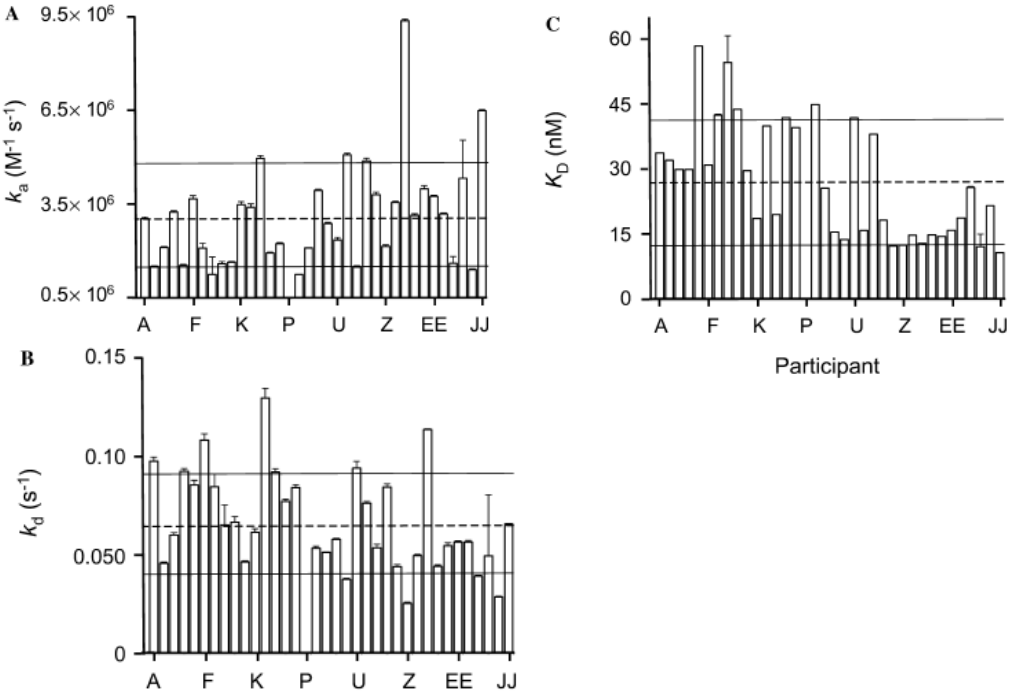

Figure 67. Distribution of the kinetic rate constants and equilibrium dissociation constant for each of the participants. (A) Histogram plot of the association rate constant determined from the fit of each data set. (B) Histogram plot of the dissociation rate constant determined by the fit of each data set. (C) Histogram plot of the equilibrium dissociation constant determined from the fit of each data set. The black dashed horizontal line indicates the average of the constants and the solid black horizontal lines denote the boundaries of the calculated standard de*via*tion. The error bars for each participant denote the standard de*via*tion for nonlinear least squares analysis (figure copied from Matthew *et al*).[196]

2.10. Rubisco – structure and enzymatic activity

Rubisco catalyses the carboxylation of D-ribulose-1,5-bisphosphate (RuBP).[204-208] This conversion of inorganic CO_2 into carbohydrate is considered a rate-limiting step in the synthesis of most of the world's biomass. Rubisco is a key enzyme in the Calvin cycle which catalyzes the first step of carbon fixation, a process by which the atoms of atmospheric carbon dioxide are made available to plants in the form of energy-rich molecules such as sucrose. The enzyme can catalyze both the carboxylation or the oxygenation of ribulose-1,5-bisphosphate (RuBP) with carbon dioxide or oxygen correspondingly. Rubisco is very important in terms of biological impact because it catalyzes the most commonly-used chemical reaction by which inorganic carbon enters the biosphere. It is also the most abundant protein in leaf chloroplasts, and it is often referred to as the most abundant protein on Earth.[204] Given its important role in the biosphere, it is an important target of genetic engineering to create crop plants that would contain more efficient Rubisco.

Rubisco is the major enzyme in Calvin cycle – a series of reactions during which carbon dioxide and water are used to produce organic compounds. This reaction is also called "carbon fixation". Calvin cycle is illustrated in Figure 68.

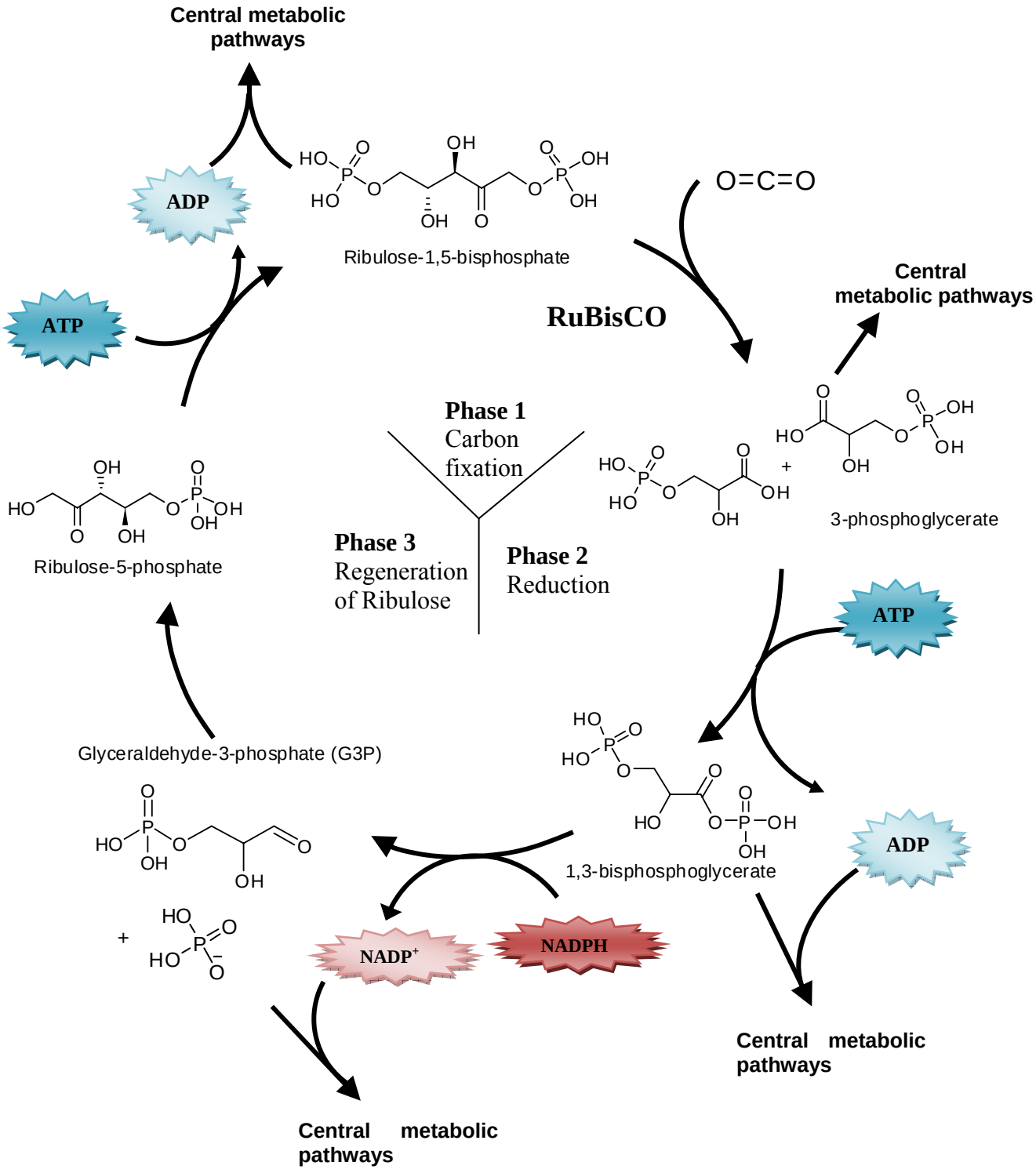

Figure 68. Calvin cycle.

Rubisco is made of 8 large subunits of 54 kDa each and eight small subunits of 14 kDa each. In spite of its biological importance, Rubisco is an inefficient catalyst, particularly at lowered CO_2 concentrations. Its turnover number of 3 s^{-1} is situated at the bottom end of turnover number range (10-1000 s^{-1}) for most enzymes.[207] In addition, the efficiency of Rubisco-catalyzed carbon assimilation is further limited by the fixation of O_2, which can compete with CO_2 for addition to ribulose-P2. It is not clear why such an important enzyme is so slow and nonspecific.[209] There is also a great amount of uncertainty in the literature about how Rubisco is regulated, especially under abiotic stress conditions such as drought and high temperature.[204,205,210-212] It has been established that Rubisco activity is modulated *in vivo* by reaction with CO_2 and Mg^{2+} to carbamylate a lysine residue in the catalytic site, or by binding of inhibitors within the catalytic site. Binding of inhibitors blocks either activity or the carbamylation of the Lysine201 residue crucial to activity. During the night, 2-carboxyarabinol-1-phosphate (CA1P) is formed which was found to bind tightly to Rubisco, and reduce catalytic activity. The mechanisms of Rubisco regulation have been recently reviewed by Parry *et al.*[213] Rubisco activity *in vivo* can be regulated by several possible mechanisms. First, carbamylation of catalytic lysine residue followed by stabilization of the resulting carbamate product by Mg^{2+} ion, which leads to formation of catalytically active ternary complex (Enzyme-CO_2-Mg^{2+}), and a second type of regulation could proceed through the tight binding of low molecular weight inhibitors (I). The inhibitors can either bind before (Enzyme-I) or after carbamylation (Enzyme-CO_2-Mg^{2+}-I), and block the active site of the enzyme by limiting the substrate binding or carbamylation reaction. Rubisco activase is required to remove the bound inhibitors from the catalytic site of carbamylated or decarbamylated forms of Rubisco. The activase becomes responsible in this way for maintaining Rubisco active and free of inhibitors.

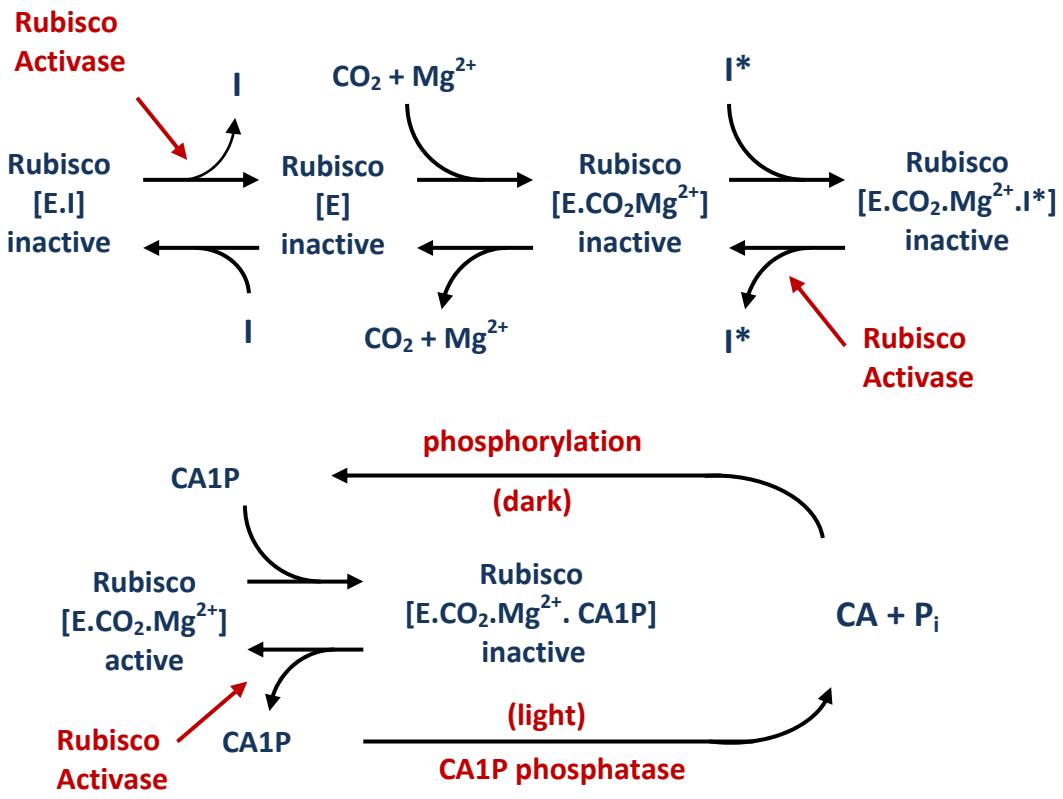

Figure 69. A- Principles of Rubisco catalytic activity regulation, proposed by Perry *et al.* [E]- unmodified (decarbamylated) enzyme, [E.I] – decarbamylated enzyme with RuBP bound at active sites – in this context RuBP acting as an inhibitor [I]; [E.CO_2.Mg^{2+}], complex with catalytically active site; [E.CO_2.Mg^{2+} I*] – carbamylated enzyme with catalytic site occupied by tight binding inhibitor (I* = CAP1, PDBP and/or KABP). B- reversible inhibition of carbamylated Rubisco by CAP1, showing light-dependent removal and dephosphorylation of CA1P, performed by Rubisco activase and CA1P phosphatase, respectively. CA is rephosphorylated to CA1P during dark period (figure and caption adapted from Parry *et al.* [213]).

Crystallographic data provided evidence that most structural changes after substrate binding occur in loop 6 (Figure 71), which is located at the mouth of a large subunit alpha/beta barrel, in which this loop folds or slides over the active site and loses its mobility. This allows two conformations, with residues on the C-terminal tail and the loops on N-terminal domain of the adjacent large subunit being responsible for maintaining the closed conformation. The cleavage of the C2-C3 bond upon reaction between bound RuBP and CO_2

leads to active site opening. It is postulated that a number of naturally existing sugar-phosphates which are assumed to be tight-binding inhibitors and structurally similar to the substrate, force the active site of Rubisco to adopt a closed conformation, which is a current rationale for Rubisco regulation. Structures of naturally occurring inhibitors isolated to date are presented on Figure 70.

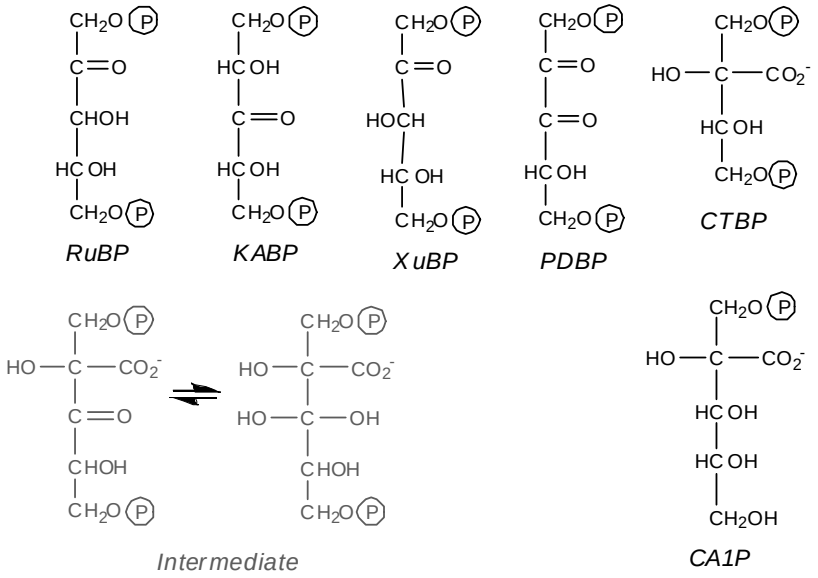

Figure 70. Naturally occurring Rubisco inhibitors identified up to date[213]. RuBP – ribulose-1,5-bisphosphate; KABP – 3-ketoarabinol-1,5-bisphosphate; XuBP – D-xylulose-1,5-bisphosphate, PDBP – D-glycero-2,3-pentodiulose-1,5-bisphosphate; CTBP – 2-carboxytetritol-1,4-bisphosphate; CA1P – 2-carboxy-D-arabinol-1-phosphate (figure adapted from Parry *et al.*[213]).

Capturing of tight-binding inhibitors is challenging. Prolonged dialysis or gel filtration are often insufficient to release them from the catalytic site of purified Rubisco. It is also proposed that other sugar phosphates and some inorganic anions also interact with the catalytic site *in vitro* which can affect the carbamylation reaction. These are often called effectors and act as competitive inhibitors with respect to RuBP. The literature presents a

striking lack of experimental evidence for most compounds referred to as inhibitors. No kinetic parameters of inhibition/binding such as inhibition constant K_i or equilibrium dissociation constant K_D are yet reported.

Marcus *et al.*[214,215] reported allosteric effects of orthophosphate ion on cyanobacterial Rubisco. X-ray analysis of the enzyme in complex with orthophosphate revealed that this anion binds at three sites: two sites are those normally occupied by 1P and 5P (groups of RuBP and the third site (the "latch site") in the pocket made of positively charged residues, which is involved in active-site closure during catalysis. The role of the latch site and 5P sites was examined in terms of cyanobacterium Rubisco activation and catalysis by site-directed mutagenesis. Mutations at both sites abolished the P_i-stimulated Rubisco activation. Substitution of residues at the 5P site, but not the latch site, significantly exaggerated the P_i inhibition of Rubisco catalysis. Point mutations within the latch site decreased the catalytic turnover and increased Rubisco K_m (RuBP) which was probably due to alterations in catalytic site closure.

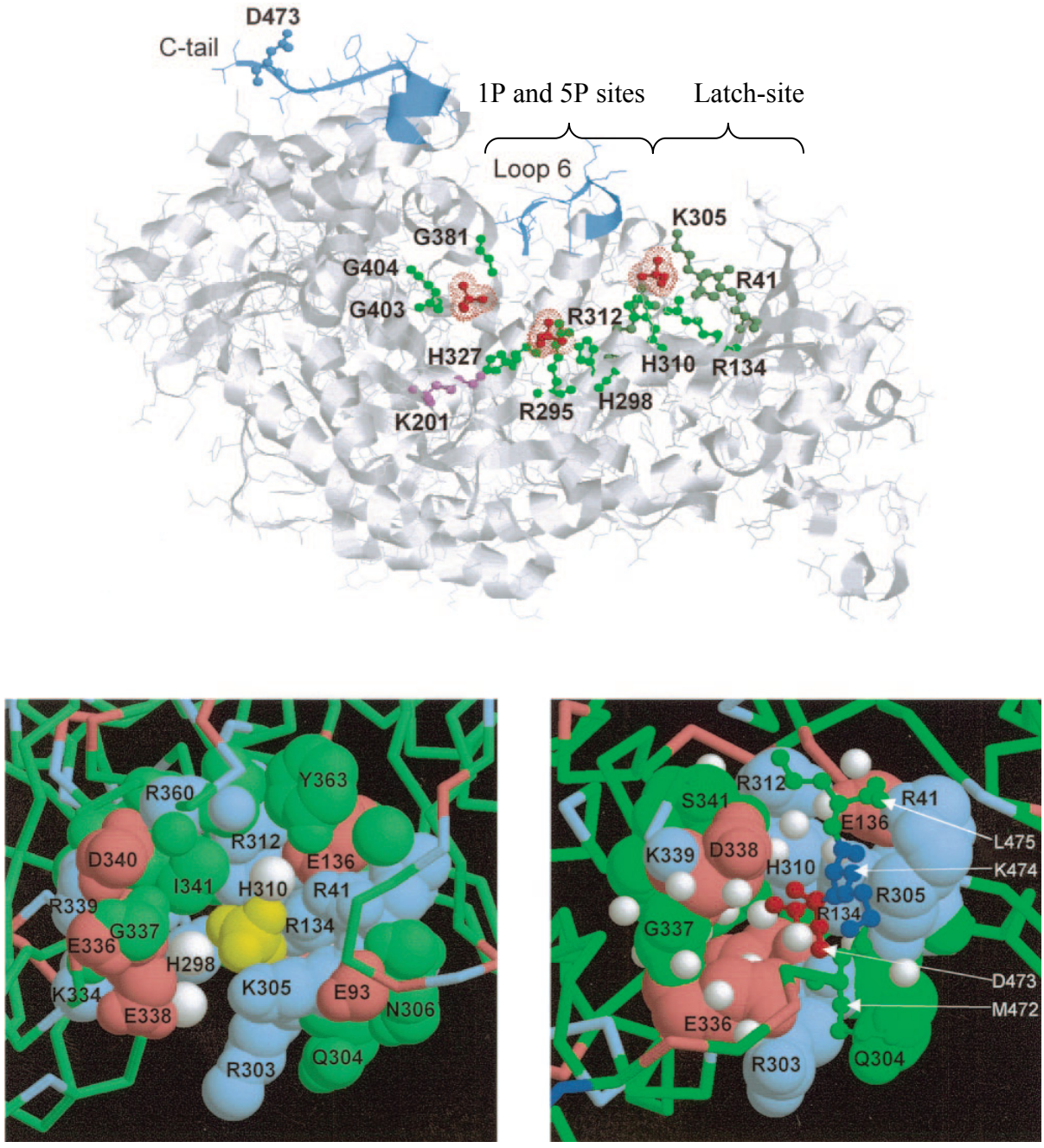

Figure 71. A- diagram of the three Phosphate (P_i)-binding sites in Rubisco large subunit. Three P_i ions are in red, and residues directly associated with P_i are in green. Lys201 residue is in magenta. Moving elements (C-tail and loops 6) participating in closure of the catalytic site are in blue. B- space-filled model of P_i bound to the latch site if tobacco Rubisco (figure and caption copied from Marcus *et al.* [215] with permission).

The inhibition of Rubisco by P_i was found to be competitive with respect to RuBP. The inhibitory effect was elevated upon point mutations at the 5P site. However mutations on the latch site had no effect on the phosphate inhibition constant.

Table 3. Kinetic properties of Rubisco mutants.

Protein	Site	k_{cat} (min^{-1})	K_m(RuBP) (μM)	$K_i(P_i)$ (mM)
Wild type		545	140	5.8
R134A	Latch	178	212	6.0
K305E	Latch	185	242	5.7
K305A	Latch	177	199	NM
H310D	Latch	185	387	NM
H310A	Latch	540	179	NM
H298A	5P	43	267	6.3
H327Q	5P	92	490	0.67

Regardless of the minor effects on the rate of photosynthesis (indicated by K_i), in most cases the mutations at the latch site reduced catalytic turnover (k_{cat}) by two-thirds, and increased the K_m (RuBP). These findings indicate that the mutations at the latch site affect the k_{cat} and K_m (RuBP) of Rubisco by affecting the mechanism of the catalytic site closure.

The latch site has been proven to be an important structural feature of the enzyme, especially in terms of enzyme regulation by affecting the access to the catalytic site. This suggests that binding of ABA to the latch site could have a significant impact on Rubisco regulation.

In order to visualize the binding site of ABA, docking experiments of ABA to Rubsico large subunit were performed using AutoDock software. Energy optimized ABA structure

was obtained using Chem3D software and Rubisco (large subunit from *Nicotiana tabacum*) crystallographic data obtained from the RSCB PROTEIN DATABANK (PTB file: 1EJ7).

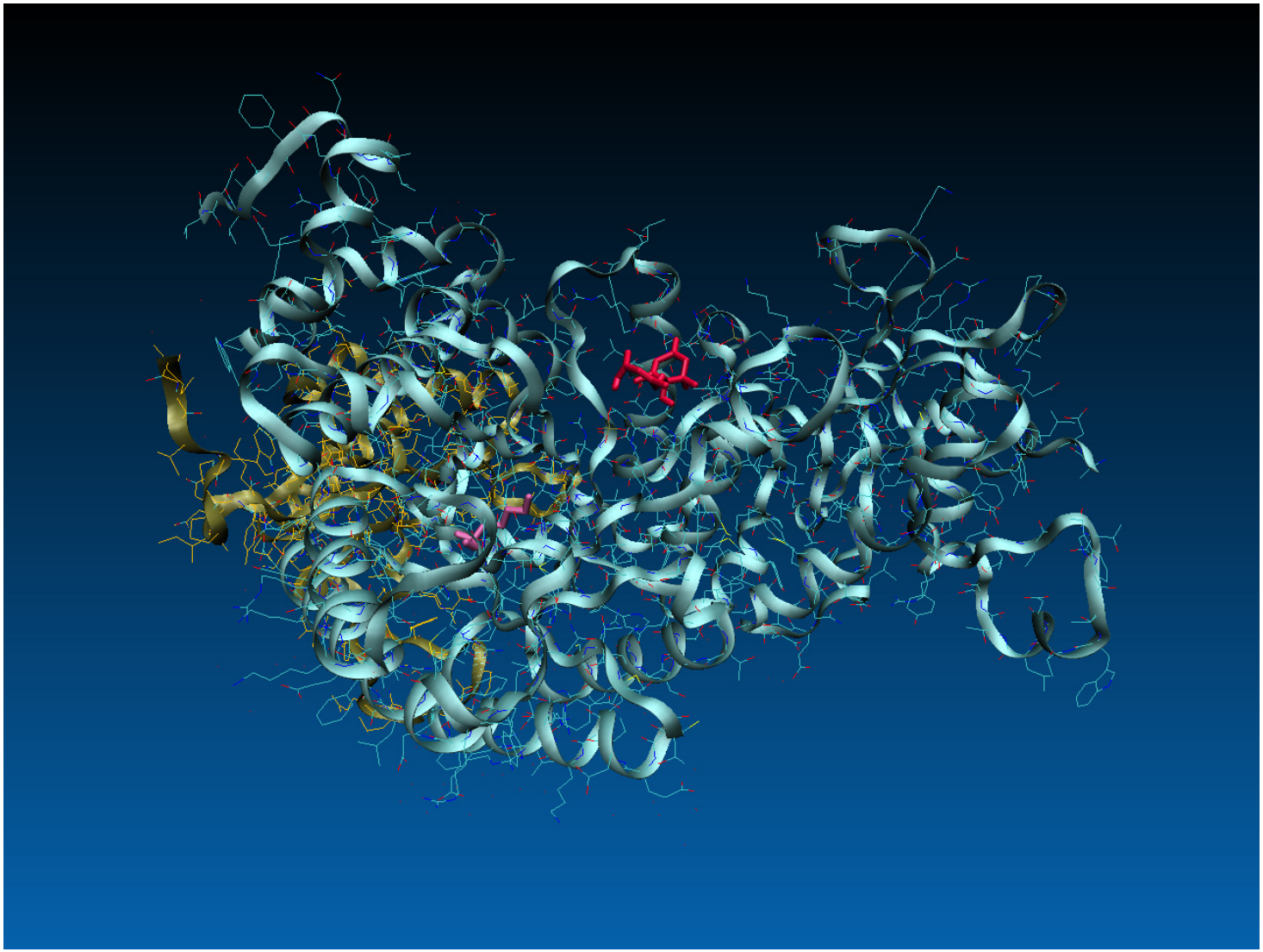

Figure 72. View of ABA (red) docked into the latch site of Rubisco large subunit. Catalytic residue Lys201 (pink).

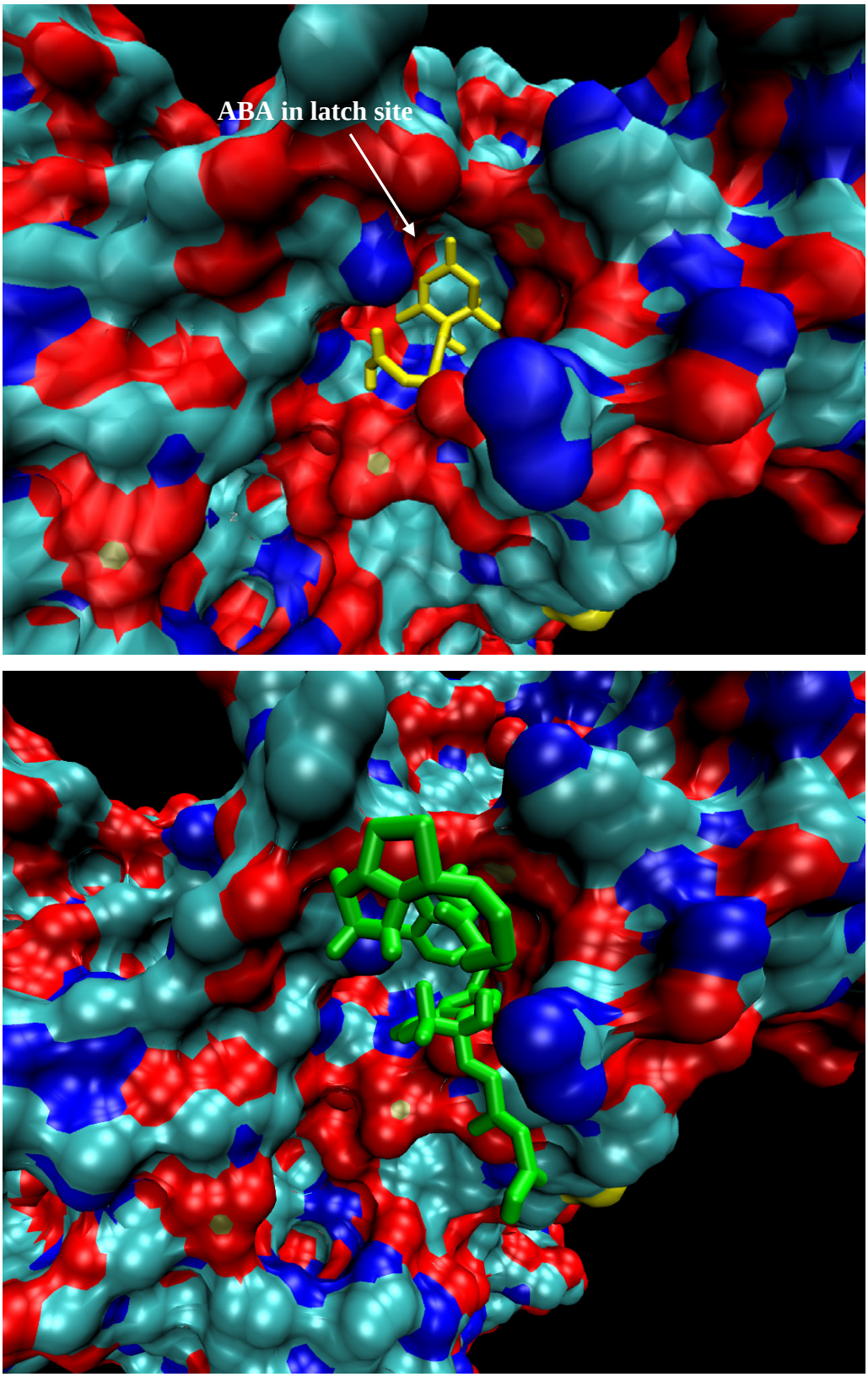

Figure 73. Surface view on ABA (top), and PBI 686 (bottom) docked in Rubisco latch site.

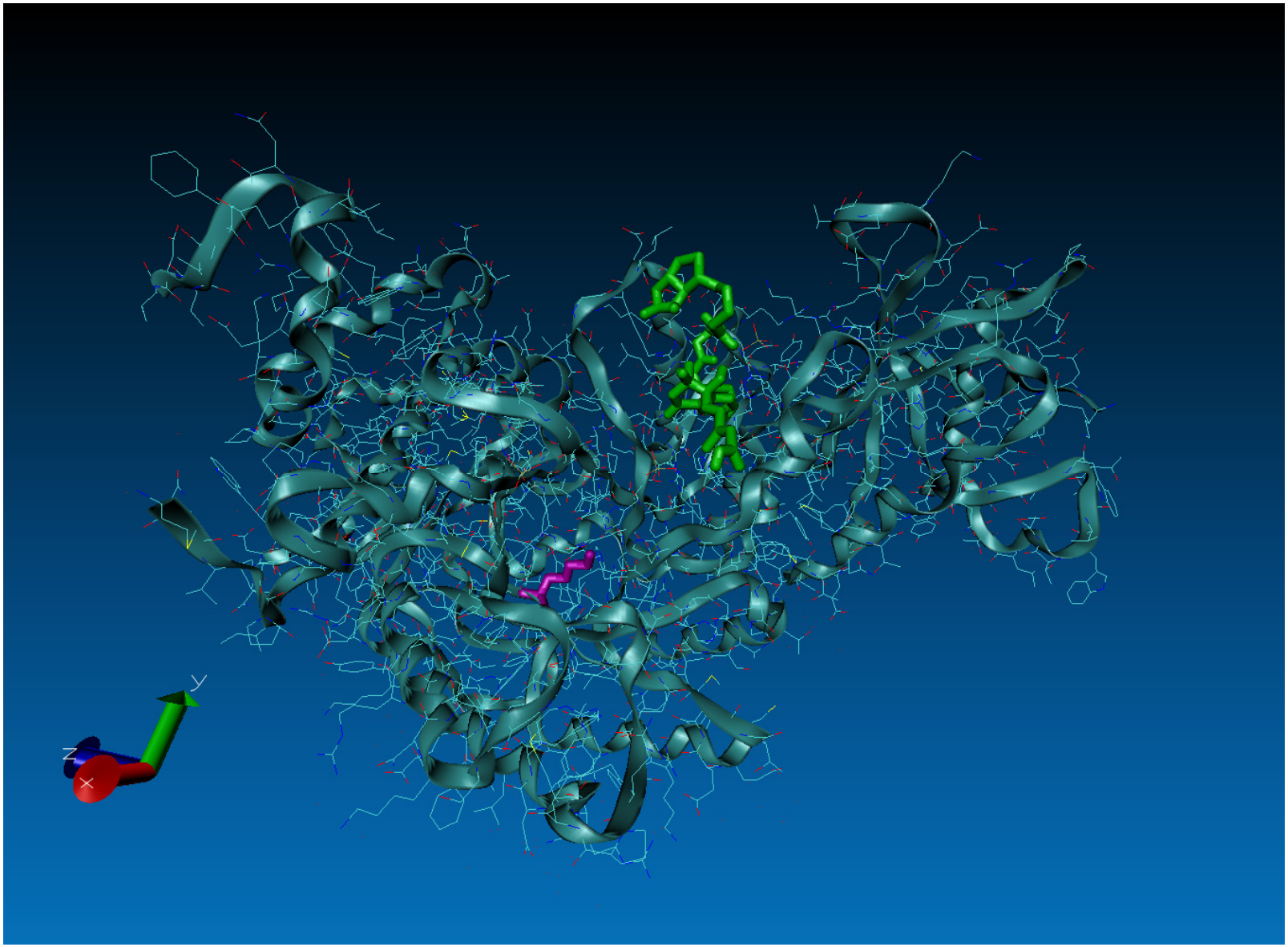

Figure 74. View of PBI686 (green) docked into the latch site of the Rubisco large subunit. Catalytic residue Lys201 is shown in pink.

Table 4. Binding energies and corresponding inhibition constants predicted by AutoDock software.

Compound	Binding Energy (kcal/mol)	Predicted K_i
(+)-ABA	-5.4	108 μM
PA	-3.8	1.6 mM
trans-(+)-ABA	-5.1	185 μM
PBI 686	-6.4	22.2 μM

Predicted binding energy for ABA being lower than its structural analogs PA and *trans*-(+)-ABA is in agreement with binding experiments using radiolabeled ABA, described in later sections of the thesis. The binding energy of PBI686 being lower than that of ABA, may be due to the probe's additional interactions with Rubisco (such as H-bonding of biotin moiety) not attributed to its ABA-like structural features.

In summary, the software-predicted binding pocket of ABA within the Rubisco latch site suggests the possible function of ABA in contributing to the process of catalytic site opening and/or closure.

2.10.1. Effect of ABA on Rubisco enzymatic activity

In order to investigate the significance of ABA binding to Rubisco, the enzyme catalytic activity was measured in the presence of ABA and compared to that in the absence of ABA. This was evaluated by coupling the activity of the enzyme (the conversion of RuBP to 3-phosphoglycerate) to NADH oxidation using PGA kinase and GAP dehydrogenase.[206] The oxidation of NADH was monitored spectrophotometrically (λ = 340 nm) over time for 5 min. The reaction was initiated by addition of Rubisco and the A_{340} was measured at 5 s

intervals. Absorbance values were converted to NADH concentration using an extinction coefficient of 6.22 mM^{-1}. The coupled enzyme assay employed is depicted in Figure 75.

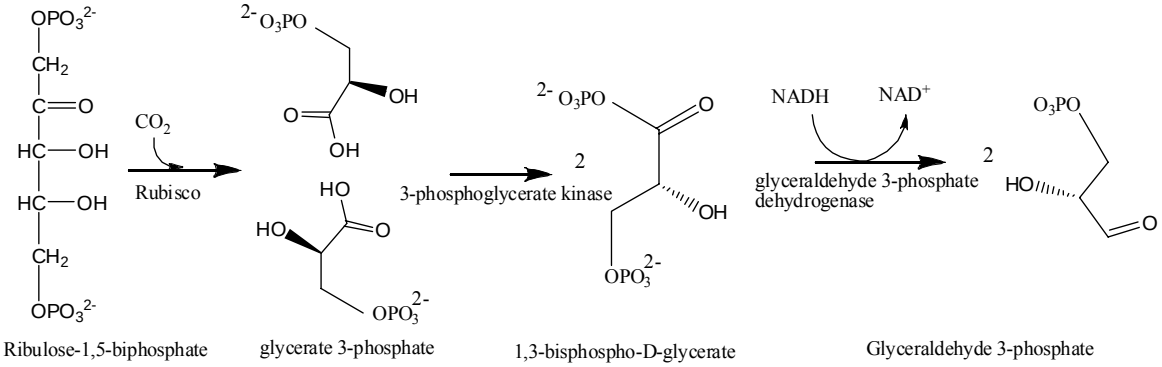

Figure 75. Coupled enzyme Rubisco activity assay.

A series of experiments were performed using the above system. An example of one reaction showing the difference in initial reaction rates (V_i) observed in the presence and absence of ABA, at a fixed substrate concentration is presented below.

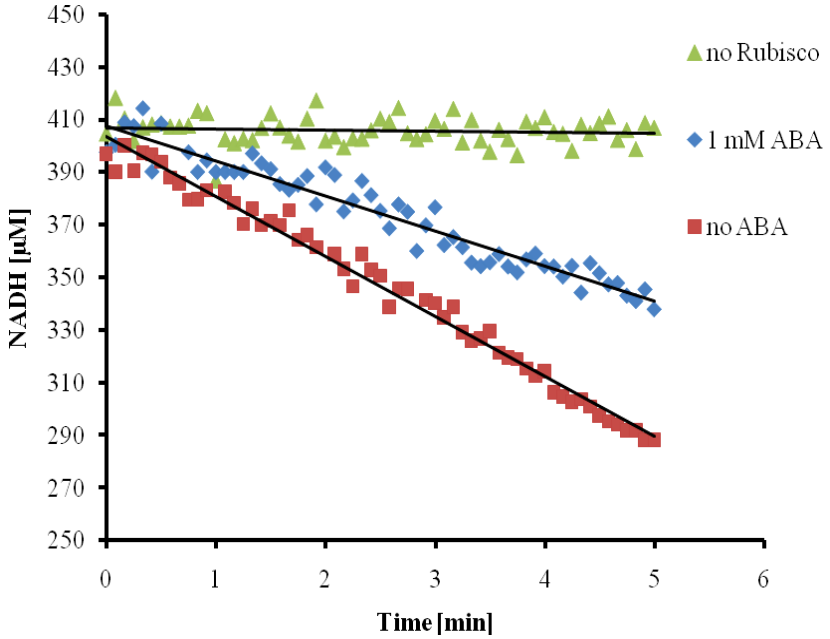

Figure 76. Change of NADH concentration against time. Rate of NADH oxidation, evaluated from the slope corresponds to the rate of Rubisco catalysis reaction.

The slopes on the plot of [NADH] vs. time correspond to the rate of NADH oxidation expressed in nmol/min. This rate can be extrapolated to the velocity of CO_2 incorporation by Rubisco. The rates of CO_2 can be calculated by division of NADH oxidation rate by factor of two; due to the fact that there are two molecules of NADH oxidized per one molecule of RuBP (see

Figure 75). In the presence of ABA, Rubisco rate of CO_2 incorporation is clearly reduced which indicates the inhibitory effect of ABA. Since there are two enzymes other than Rubisco used in this assay, it was important to perform a control experiment and check if ABA can inhibit these enzymes. If ABA does not affect the activity of other enzymes this would assure that reduced NADH oxidation rates in the presence of ABA are only due to changes in Rubisco kinetics. This control experiment was done by eliminating Rubisco and RuBP from the assay, adding 3-phosphoglyceric acid (3-PGA) instead, and monitoring the NADH oxidation rates in the presence and absence of ABA. It showed that ABA does not inhibit PGA kinase nor GAP dehydrogenase and the slope remains unaffected in the presence of 10 mM ABA. The results of NADH oxidation assay with and without ABA and at fixed, 500 μM 3-phosphoglyceric acid concentration are listed in Table 5.

Table 5. Results of control experiments of NADH oxidation assay without Rubisco and RuBP.

no ABA		**10 mM ABA**	
slope x 10^{-4}	velocity [nmol/min]	slope x 10^{-4}	velocity [nmol/min]
2.86	17.16	3.15	18.90
3.51	21.06	3.46	20.76
3.56	21.08	3.49	20.94
Average: 3.31	**19.77**	**3.36**	**20.20**

Subsequently, Rubisco activity changes in the presence of ABA at different concentrations were further evaluated. First, kinetic parameters were calculated by measuring

rates at various RuBP concentrations, from 10 μM to 1200 μM (10, 20, 50, 100, 200, 400, 800, 1200 μM) in the absence of ABA. Subsequently, rates were measured with the addition of ABA (1, 2, 5, and 10 mM). Plots of initial velocity (V_i) vs. substrate concentration (RuBP) show a significant change in the presence of ABA in a concentration dependent manner (Figure 78).

Non-linear regressions were performed by GraphPad Prism™ software which was able to fit the experimental data into two different models. One is a competitive inhibition model based on the Michaelis-Menten kinetic equation. The second, based on a sigmoidal shape of V_i vs. [RuBP] plot, is an allosteric inhibition model, with Hill coefficient being >1. Based on the goodness of both fits, a comparison of both models indicated that allosteric inhibition is preferred. When comparing V_i vs. [RuBP] plot curves for an experiment without ABA to the one in the presence of 10 mM ABA it becomes noticeable that the curve adopts a sigmoidal shape which is a strong indication of allostery.

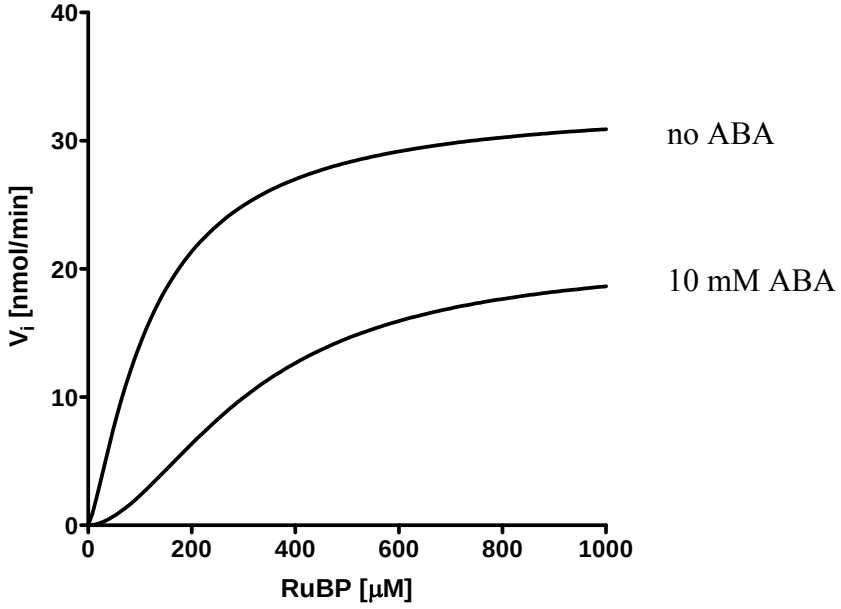

Figure 77. Initial velocity V_i vs. substrate concentration [RuBP] plot showing the shapes of fit curves obtained in the presence and absence of ABA.

Table 6. Comparison of kinetic parameters obtained by fitting the experimental values into competitive and allosteric inhibition models using GraphPad Prism enzyme kinetics evaluation. Vmax – maximum reaction velocity, K_{prime} – parameter related to the K_m, but not equal the substrate concentration needed to achieve a half-maximum enzyme velocity. H-hill coefficient. P- probability of the measurements being a coincidence.

Comparison of Fits					
Null hypothesis		Competitive inhibition			
Alternative hypothesis		Allosteric sigmoidal			
P value		0.0034			
Conclusion (alpha = 0.05)		Reject null hypothesis			
Preferred model		**Allosteric sigmoidal**			
Allosteric sigmoidal	no ABA	1 mM ABA	2 mM ABA	5 mM ABA	10 mM ABA
Best-fit values					
V_{max} [nmol/min]	32.98	30.92	28.59	24.29	20.98
H	1.298	1.330	1.426	1.604	1.805
K_{prime}	527.8	925.6	1374	7549	32736
Std. Error					
V_{max} [nmol/min]	1.045	1.331	1.499	2.259	2.042
H	0.1067	0.1306	0.1915	0.3232	0.3777
K_{prime}	240.5	539.9	1191	12060	64202
Goodness of Fit					
R^2	0.9968	0.9961	0.9930	0.9869	0.9869
Absolute Sum of Squares	3.257	3.578	6.096	7.773	5.630
Competitive inhibition					
Best-fit values					
V_{MAX} [nmol/min]	36.29	35.51	33.48	32.41	33.28
K_m [µM]	156.9	237.4	230.4	479.2	779.8
K_i [µM]	1930	1930	1930	1930	1930
Std. Error					
K_m [µM]	15.55	15.55	15.55	15.55	15.55
K_i [µM]	251.6	251.6	251.6	251.6	251.6
V_{max}	1.003	1.003	1.003	1.003	1.003
Goodness of Fit					
R^2	0.9897	0.9891	0.9761	0.9680	0.9736
Absolute Sum of Squares	10.37	10.12	20.74	19.02	11.35

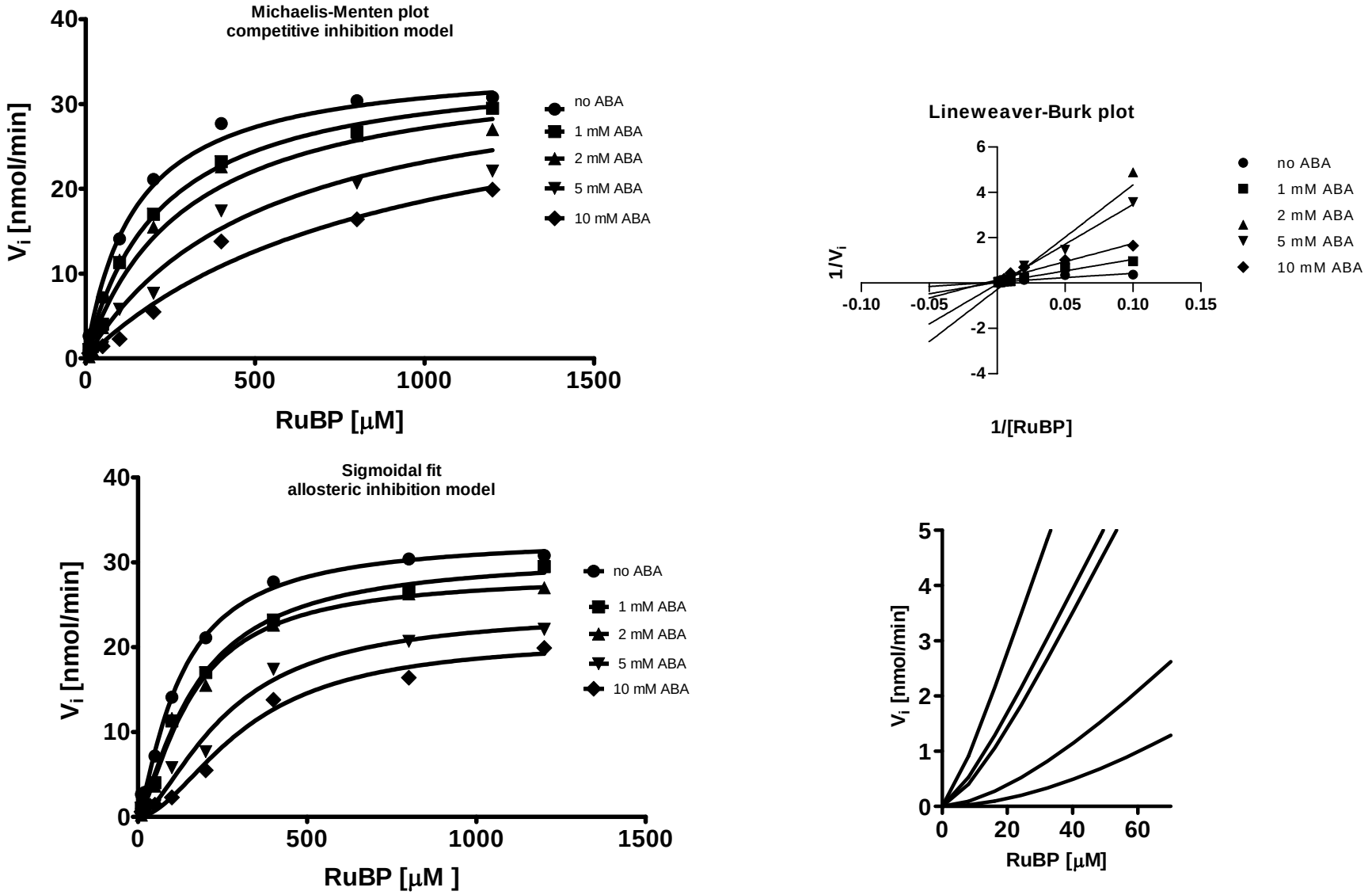

Figure 78. A - Initial velocity (V_i) vs. substrate concentration [RuBP] plot at various ABA concentrations (competitive inhibition model, Michaelis-Menten equation), **B**- the corresponding double reciprocal plot, **C**- V_i vs. [RuBP] plot showing sigmoidal fit (allosteric inhibition model), **D**- shape of plot C at low RuBP concentrations. Points represent data, lines represent fits.

Let us briefly compare the two proposed mechanisms. There are two kinds of competitive inhibition: first the classical competition for the active site binding, and second competitive inhibition by conformational change.

In most cases, a competitive inhibitor is a compound which structurally resembles the substrate of the enzyme. Because of this similarity the inhibitor binds to the active site in place of the substrate. The competitive inhibitor binding site does not always have to be the same as the active site. Upon binding, the inhibitor blocks substrate access to the active site, so that it can no longer bind to it. Both substrate and inhibitor compete for binding to the enzyme.

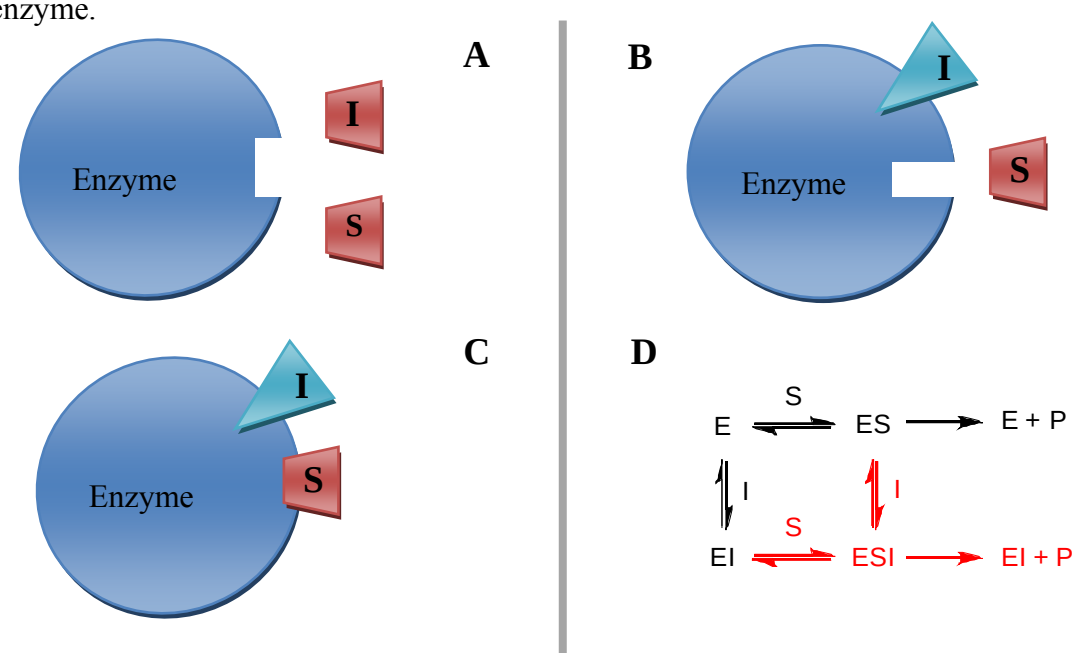

Figure 79. A- competitive inhibition, **B**- allosteric inhibition. **C**- allosteric (mixed) inhibition) **D**- diagram representing two different types of inhibition, black path- classical competitive, red path – allosteric (mixed) inhibition, the ESI complex may or may not be a dead-end complex. Competitive inhibition occurs when substrate (S) and inhibitor (I) both bind to the same site on the enzyme. In effect, they compete for the active site and bind in a mutually exclusive fashion. (**A**). There is another type of inhibition that would give the same kinetic data. If S and I bound to different sites, and S bound to E and produced a conformational change in E such that I could not bind (and vice versa), then the binding of S and I would be mutually exclusive. This is called allosteric competitive inhibition (**B**). In mixed inhibition, the inhibitor also binds to a site different from the active site where the substrate binds, however the inhibitor can bind to either free enzyme or the enzyme-substrate complex (**C**).

Allosteric inhibition concerns a protein containing two or more distinct binding sites which interact functionally with each other. The binding of an inhibitor at one site alters the properties of the substrate-binding site.

Most allosteric proteins are allosteric enzymes, in that they are capable of catalyzing reactions but some, such as hemoglobin, are simply binding proteins.

Allosteric inhibitors and activators are commonly referred to as *allosteric effectors***.** Alteration of the rate of enzyme catalyzed reactions by inhibition and activation is the basis of methods controlling the metabolism. Figure 80 below demonstrates the way in which effectors change the kinetic plot of a typical allosteric enzyme.

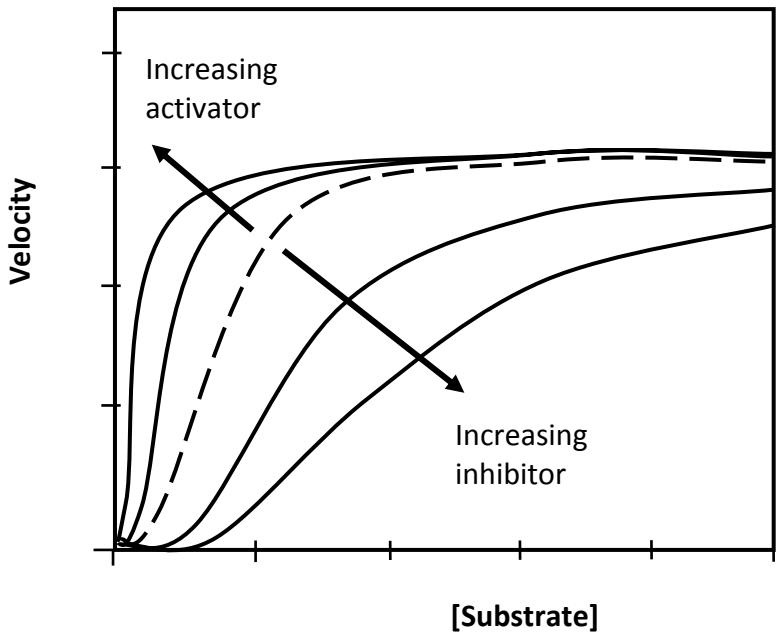

Figure 80. V_i vs. [Substrate] plot showing the effect of allosteric activator and inhibitor.

The central line in the graph shows a typical sigmoid plot in the absence of any effector. The presence of an activator increases the reaction rate at any given substrate concentration, whereas an inhibitor decreases the reaction rate. The inhibitor has increased

the sigmoid shape, lengthening the toe, and the activator has caused the opposite effect. This means that an allosteric inhibitor increases the concentration of the substrate required to achieve the original reaction velocity while an activator decreases it. It is also important to mention that there are two kinds of allosteric interactions: homotropic and heterotropic. In homotropic allosteric interaction the activity of the enzyme is regulated by its substrate. Homotropic modulators are often allosteric activators, which means that they typically up-regulate the activity of the enzyme. They can do so by inducing the conformational change of the multi-subunit allosteric protein from the inactive state (Tense state) to the active state (Relaxed state). A heterotropic allosteric interaction is considered when the activity of the enzyme is regulated by a molecule other than the protein's substrate.

When the mechanism of ABA-Rubisco inhibition was being analyzed it became apparent that the inhibition constant K_i of 1.93 mM resulting from competitive inhibition model was substantially different from previously obtained equilibrium dissociation constant K_D of 5 nM. The inhibition constant was calculated using the following equations.

$$K_{m\,obs} = K_m \cdot \left\langle \frac{1 + [ABA]}{K_i} \right\rangle \qquad \mathbf{A}$$

$$V_i = \frac{V_{max} \cdot [RuBP]}{K_{m\,obs} + [RuBP]}$$

$$V_i = \frac{V_{max} \cdot [RuBP]^h}{K_{prime} + [RuBP]^h} \qquad \mathbf{B}$$

Figure 81. Equations used to calculate kinetic parementers for A-classical competitive, B- allosteric competitive inhibition with substrate cooperativity.

It is important to mention that if ABA binds to an allosteric site in Rubisco, it is possible that its equilibrium dissociation constant will be different in the absence than that in the presence of the substrate. This could provide an explanation of the difference between K_D measured in the absence of RuBP being 5 nM and K_i measured in the presence of RuBP being 1.93 mM. The resuts indicate that upon binding of RuBP, Rubisco affinity for ABA is dramatically reduced. It was therefore not possible to achieve complete Rubisco inhibition in the presence of ABA at concentrations as high as 10 mM, as this concentration is only five fold higher than K_i. The solubility of ABA at concentrations above 10 mM was a limitation of this experiment.

It is also important to note that the concentration of enzyme used for the *in vitro* activity assays is relatively higher than *in vivo*. More specifically, the concentration of Rubisco used in the assay was approximately 0.71 μM (each complex has 8 active sites), and therefore it would take 5.7 μM ABA to obtain enzyme-inhibitor molar ratio of 1/1. In other words in each assay sample, ABA being at 1 mM concentration is only in 175 fold molar excess. In addition, Michaelis-Menten plot indicated that the substrate saturates Rubisco at 0.8 mM concentration where enzyme velocity plateaus. Competitive effect of ABA with respect to the substrate RuBP is only observed when ABA concentration is greater than its competitor's.

Local concentrations of ABA in plants range from nanomolar to micromolar and never reach milimolar levels.[225-227] This remains in conflict with previously mentioned K_i value being 1.93 mM. There are two possible explanations to this problem, first the concentrations of Rubisco and ABA as well as their molar ratio *in vivo* are unknown and might be very different than that used *in vitro* and therefore cannot be compared. The experiments were performed on the "large scale" meaning that substantial amounts of the enzyme its substrate and lastly high concentrations ABA had to be used in order to observe and measure changes in NADH oxidation. Second, K_i value obtained experimentally might be biased by experimental conditions being much different than those *in vivo*. And third, it might be possible that ABA acts on photosynthesis by fine regulation of Rubisco activity, and not inhibiting the enzyme completely. At micromolar concentrations of ABA, Rubisco activity would be still lowered, (ABA's effect on the enzyme activity is observed), but the extent of inhibition remains putative. Complete inhibition of Rubisco by ABA may not be desirable for the plant because functioning Rubisco is crucial for plant's survival. Even small changes in

the activity of the major photosynthetic enzyme still could have a significant impact on its growth and adaptation to stress.

As previously discussed, it is likely that the ABA binding site is remote from the enzyme catalytic site. This indicates that ABA inhibition of Rubisco can be due to conformational change of the enzyme. If the ABA binding site is located in the latch-site (part of loop 6), a channel though which the substrate gains access to the active site, the binding of ABA could produce allosteric competitive inhibition kinetics. In addition, conformational changes within loop 6 of Rubisco large subunit lead to opening or closure of the catalytic site, [214,215] behavior similar to multiple-unit allosteric enzymes. In addition, the allosteric model of inhibition gave a better goodness of fit for non-linear regression performed by GraphPad Prism (see Table **6**)

Allosteric inhibition is often reported for enzymes consisting of multiple identical subunits.[228-230] In addition allosteric enzymes are usually positioned at key metabolic steps which can be regulated to activate or inhibit whole pathways. Aspartate transcarbamoylase can serve as an example of multiple-unit enzyme, regulated by allosteric mechanism.[231,232]

Aspartate transcarbamoylase plays an important role in biosynthesis of pyrimidine nucleotides. The structure and allosteric properties of the enzyme have been very extensively studied. It catalyses a reaction between aspartic acid and carbamoyl phosphate to generate N-carbamoyl aspartate with the release of inorganic phosphate.

The complete, active enzyme consists of 12 different subunits. It contains two catalytic components each made up of three identical subunits. These components are arranged next to each other effectively forming the two main faces of the whole enzyme. The rest of the enzyme is composed of three regulatory components each comprising two subunits. These

components form the corners of the enzyme which has a roughly triangular shape. The catalytic and regulatory components can be separated. If they are, the catalytic components are found to be capable of catalyzing the reaction in the usual way except that they have no allosteric properties. They show no sign of substrate cooperativity and no reaction with allosteric effectors. The regulatory components are unable to carry out catalysis, but can bind the usual effectors of ATCase, CTP (an inhibitor) and ATP (an activator).

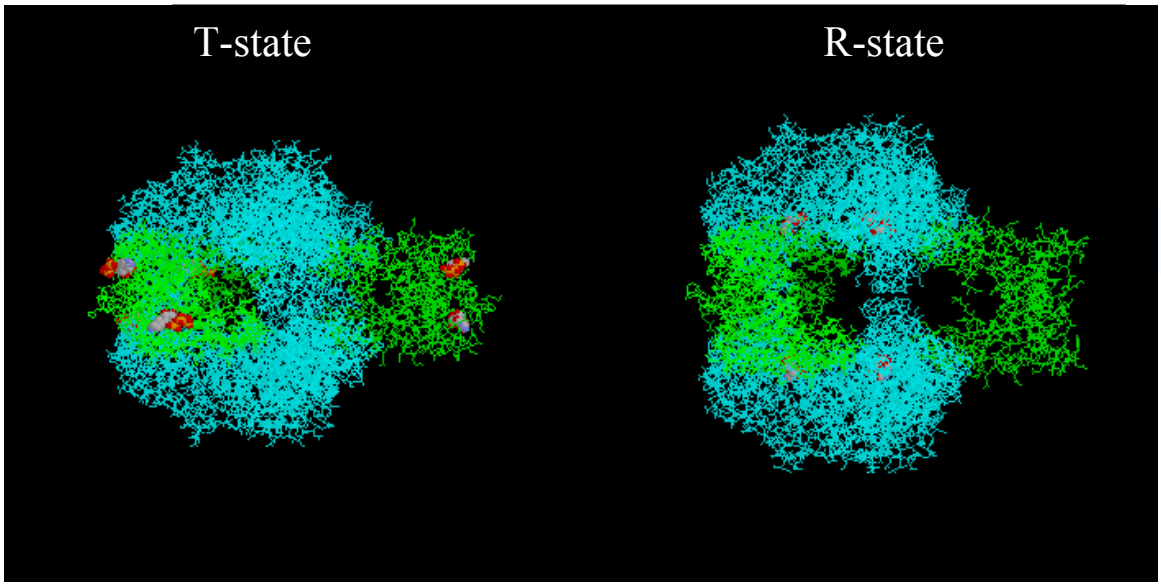

Figure 82. Tense (T) and relaxed (R) states of aspartate transcarbamoylase. T-state shown with allosteric inhibitor bound to regulatory subunits, R-state shown with substrate bound to catalytic subunits.

Figure 82 represents two different states ATCase can adopt. One of them is the enzyme with the inhibitor CTP bound to it. This maintains it in the tense, low substrate affinity state. The other one has a substrate analogue bound which maintains it in the relaxed, high affinity state. It is noticeable that the relaxed enzyme is "swollen" compared with the tense one, with the two catalytic components pushed further apart. The substrate is deeply buried within the

overall enzyme structure, it's almost invisible; presumably this swelling makes the active site more accessible to it which explains why the affinity for the substrate is increased. Upon binding of allosteric inhibitor, it is expected that the substrate affinity will be lowered which would then be reflected by a significant change in K_m.

A similar scenario could be applied in case of Rubisco which is similar to aspartate transcarbamoylase in terms of its architecture, meaning both enzymes consist of multiple identical subunits, divided into two different functionalities. Significant reduction of Rubisco activity in the presence of ABA is observed which clearly indicates the effect of ABA on the enzyme catalytic efficiency. The only difference from the carbamoylase example is the binding site of ABA which was found to be located within the same subunit (large subunit) of Rubisco as its catalytic site. It is known that Rubisco adopts two different conformations (open and closed) of the large subunit. The open conformation corresponds to activated enzyme, and the closed conformation to deactivated enzyme. Changes within loop 6 are responsible for the regulation of substrate's access to the active site. Similarly to aspartate transcarbamoylase, deactivated Rubisco could correspond to the tense state, and activated form to relaxed state. ABA binding to Rubisco in the tense state would be consistent with allosteric inhibition model. It is important to mention that all ABA binding studies were performed with deactivated Rubisco, meaning in the absence of both substrates CO_2 and RuBP. In addition, the ABA docking studies were also performed with the inactivated Rubisco structure, and AutoDock was able to find the binding site within the enzyme's latch site. An allosteric inhibition model of Rubisco by ABA is consistent with numerous reports in the literature, suggesting the presence of allosteric regulatory sites within the enzyme.[206,233]

As mentioned before, Perry *et al.* [205,213,234] studied tobacco Rubisco activity during abiotic stress and have suggested that the enzyme activity under drought stress is not primarily the result of changes in activation by CO_2 and Mg^{2+} but due rather to the presence of tight-binding inhibitors. The amounts of inhibitor present in leaves of droughted tobacco based on the decrease in Rubisco activity per mg soluble protein were found to be much greater than the amounts of the known inhibitors (CA1P and "daytime inhibitor") that can be recovered in acid extracts. This suggests the presence of other inhibitor(s) that were not discovered to date.

Parry *et al.* have indicated the presence of Rubisco inhibitor during drought stress[205] that was undetectable (using methods reported) in plants under normal growing conditions. This finding is consistent with the fact that ABA levels are elevated during drought stress[235-243] and suggests a possibility that is functions as a "stress inhibitor" of Rubisco.

In addition there are numerous reports on simultaneous and independent effects of abscisic acid on stomata and the photosynthetic apparatus.[244-247] Some studies with intact leaves have shown that ABA appears to affect growth by reducing photosynthesis, not only by closing the stomata but also by affecting the photosynthetic machinery. There is also evidence to suggest that there is a direct effect of water stress on the photochemical process and/or Calvin cycle of photosynthesis. Daley *et al.*[248] reported the effect of ABA on photosynthesis by measuring leaf gas exchange. The results showed that C_i (CO_2 concentration in leaves) remained unchanged while leaf carbon dioxide assimilation declined upon exogenous ABA treatment. This result led to the conclusion that the effect of ABA on photosynthesis must also be mediated through non-stomatal factors such as a direct effect on photosynthetic machinery. Lauer and Boyer *et al.* [249] have developed a system which allowed

measurement of internal CO_2 concentration. With this method they found that when plants were subjected to drought stress, stomatal conductance and biochemical activity for photosynthesis were simultaneously reduced. The role of ABA in the regulation of photosynthesis may also depend on how leaf water deficit is developed. Decrease of stomatal conductance caused by increase of xylem ABA usually occurred before a decrease in leaf water potential[250-252] and any inhibition of photosynthesis at that time should be attributed to the effect of ABA.

Raschke *et al.* also reports that stomata closure and reduction of photosynthesis are two simultaneous and independent effects of ABA. Saturation curves of photosynthesis with respect to the partial pressure of CO_2 in the intercellular spaces indicated that application of ABA causes a reduction of the initial slope of the saturation curve which indicates diminished carboxylation efficiency and causes a reduction of the level of CO_2-saturated rate of assimilation which indicates a reduction of Rubisco regeneration capacity.

Based on measurements of Rubisco activity at various CO_2 and RuBP concentrations Bota *et al.*[253] conclude that the reduction of RuBP/CO_2 content has a minimal impact on photosynthesis and that Rubisco activity becomes noticeably impaired only under severe drought conditions. The lack of Rubisco sensitivity to lowered substrate concentrations could be explained by increased/positive catalytic site cooperativity caused by ABA bound to allosteric sites. In other words ABA would increase enzyme affinity for the substrate through improvement of cooperativity between catalytic sites located in adjacent subunits. During severe stress, ABA concentrations are substantially increased; RuBP and CO_2 concentrations on the other hand are dramatically reduced. In this situation ABA binding to the allosteric sites could induce positive substrate cooperativity and help to maintain photosynthesis at

minimal sustainable level during abiotic stress. Photosynthesis is progressively diminished during drought, but the mechanistic basis for this reduction remains unclear. While many authors suggest that diffusional (stomatal and mesophyll) limitations are most important for most drought situations,[254] other reports suggest that decreased Rubisco activity[205] and impaired capacity for RuBP regeneration as the main cause,[255] are the main limitations to photosynthesis under drought conditions.

In summary, all above literature reports indicate the dual action of ABA on photosynthesis, one through stomata closure, and a second through direct biochemical effect on photosynthesis. Based on experimental evidence obtained in this project it can be concluded that binding of ABA to Rubisco leads to the inhibition of the enzyme which mostly resembles competitive allosteric inhibition with positive substrate cooperativity. This interaction could directly contribute to regulation of photosynthesis, especially under severe stress conditions where endogenous ABA concentration is significantly increased.

2.11. Studies of ABA and Rubisco interaction by [^{3}H]-ABA binding assays

Radioligand binding assays are most often used in receptor binding studies to determine the affinity of various drugs/ligands for a receptor as well as the binding site density (B_{max}) of receptor families and their subtypes in different tissues or samples[256]. Receptor binding studies help in mapping the distribution of receptors in different areas of the body, as well as the effects of physiological and pathological conditions on the expression of the receptors. This methodology can also be used to study the interaction of other proteins with their corresponding ligands.[257] The reason why it is most often utilized

for receptor binding assays is because it allows quick and preliminary identification of a given receptor in a mixture with other proteins or tissue samples.[258]

There are two types of binding experiments: saturation and competition.[259] Saturation experiments are used to determine the ligand affinity (K_D) for a given receptor as well as B_{max} (maximum amount of radioligand bound per unit of tissue) in various tissues or samples. The latter one is not relevant however in cases where assays are performed with purified protein. Competition studies on the other hand can be used for measuring the affinity of various unlabelled ligands for a given protein/receptor. The basis of the protein binding study is the binding of ligand (L) to the protein (P). The ligand-protein complex is classically referred to as Bound, meaning the amount of ligand that is bound to the receptor. The unbound ligand (L) is referred to as Free, meaning the amount of ligand that is free and able to interact with the protein. The parameter measured is the amount of radioactive ligand that is bound to the protein. This requires separation of the free ligand from the bound ligand after the reaction has reached steady-state conditions (Figure 83). K_D is a measure of the affinity of a ligand for a given protein and is equal to k_a/k_d, where k_a is the association rate constant and k_d is the dissociation rate constant.

$$\text{Protein (P)} + \text{Ligand (L)} \underset{k_d}{\overset{k_a}{\rightleftharpoons}} \text{Protein-Ligand Complex (LR)}$$

$$\text{Receptor (R)} + \text{Free (F)} \underset{k_d}{\overset{k_a}{\rightleftharpoons}} \text{Bound (B)}$$

Figure 83. Basic concepts in protein-ligand binding studies.

K_D is the concentration of radioactive ligand required to occupy 50 % of the receptors in a given tissue sample or if the experiment is performed with purified protein it corresponds

to 50% of all binding sites. It is important to note at this point that the approach assumes 100 % binding capacity of the protein, in other words that all binding sites for a given ligand are functional during the assay and that there is no loss of such binding functionality upon separation of bound ligand from the free ligand.[260] The latter is often a major problem which will be discussed further. Scheme on Figure 84 depicts the major steps that need to be undertaken in radioligand binding assay.

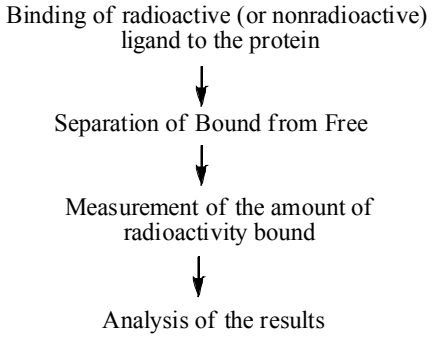

Figure 84. Steps undertaken in radioligand-binding assay.

The radioactive ligand used should have high affinity for the protein being studied and high specific activity (30 Ci/mmol or higher). The higher the ligand affinity for a given protein, the easier it is to measure the equilibrium dissociation constant. Higher affinity ligands have lower dissociation constants, which allows reasonable time for the experiment to be performed without significant loss of bound ligand during sample preparation.

Isotopes such as [^{3}H] or [^{125}I] are most often used due to their high specific activity rather than low specific activity isotopes such as [^{14}C]. The amount of protein used in the assay is based on the affinity of the radioligand for the protein, the specific activity of the radioligand and the ligand/protein binding ratio. Ideally, 100 to 500 disintegrations per minute (dpm) which is well above background should be due to ligand bound to the protein

of interest at the lowest concentration of radioligand used in the assay. The amount of signal corresponding to bound radioligand can be enhanced by either increasing the protein concentration or using radioactive ligand with higher specific activity. Less than 10% of total radioligand added should be bound to the protein because the equations for analysis of saturation experiment are based on the assumption that the free concentration of ligand does not change.

The protein is incubated with radioactive ligand until steady-state conditions are reached. The time required to reach a steady-state may be minutes to hours. The incubations can be done at various temperatures depending on the stability of the radioactive ligand and the protein. It should be noted that the affinity of the protein for the radioligand may be temperature-dependent.

Once steady-state conditions have been reached, the bound radioactive ligand is separated from the free ligand using various techniques, such as filtration, centrifugation or precipitation. The important principle to keep in mind is that the method needs to be rapid to minimize ligand dissociation from the receptor. This is often a major obstacle as the separation of bound from free ligand disturbs the steady-state equilibrium in a very short time. The amount of ligand dissociated depends on the time of the separation as well as on the type of separation. When radioligand binding assays are performed with membrane proteins a filtration method is often used. It functions by trapping the protein-ligand complex on the filter, whilst allowing the free ligand to pass through. In this project the filtration method itself could not be employed due to the fact that Rubisco is a soluble protein, and therefore a precipitation followed by filtration method was chosen. The amount of radioactive ligand bound can be determined by scintillation counting. When using the filter to

separate bound from free, the filter is simply placed in a scintillation fluid and incubated for at least 12h.

Protein binding data is analyzed by non-linear regression analysis using Microsoft Excel and/or GraphPad Software. In saturation experiment, various concentrations of the radioligand are incubated with the same amount of protein, producing increasing concentrations of the protein-ligand complex. The equation for the resulting hyperbola is:

$$\text{Bound} = \frac{B_{max} \times \text{Free}}{K_D + \text{Free}}$$

As the concentration of radioactive ligand increases, a point is reached where the amount of ligand bound no longer increases. The amount of bound radioactivity accounts for the ligand bound specifically and non-specifically and it is called total binding.

Radioactive ligands usually bind to more than one type of binding site. The site that is being studied is referred to as the specific site, or specific binding. All other binding sites are referred to as non-specific sites. Some non-specific binding sites are saturable others are not. In order to distinguish binding to specific sites from binding to non-specific sites, a second set of incubations is run simultaneously using radioactive ligand and unlabeled ligand at a concentration sufficient to block the binding of the radioactive ligand to the specific sites, but not the non-specific sites. The amount of radioactive ligand bound in the presence of unlabeled ligand is referred to as the total binding. Binding in the presence of the unlabeled ligand is referred to as non-specific binding. The difference between the two corresponds to specific binding.

In this project the separation of free from bound radioligand was done in two steps. First Rubisco-[^{3}H] (±)-ABA complex was applied on SPN™ spin columns (G-biosciences)

and then precipitated using chilled proprietary solvent buffer (OrgoSol^{TM}, G-biosciences) specifically developed for efficient precipitation of protein solutions with minimal disruption to the protein structure and biological activity. Precipitated protein remains on the column which is then washed twice with cold OrgoSol^{TM} buffer to remove unbound [^{3}H] (±)-ABA. The column matrix was then placed in a scintillation fluid and incubated overnight. Subsequently, the radioactivity corresponding to bound [^{3}H] (±)-ABA was measured using the scintillation counter. Total binding was measured after incubating Rubisco with [^{3}H] (±)-ABA at various concentrations.

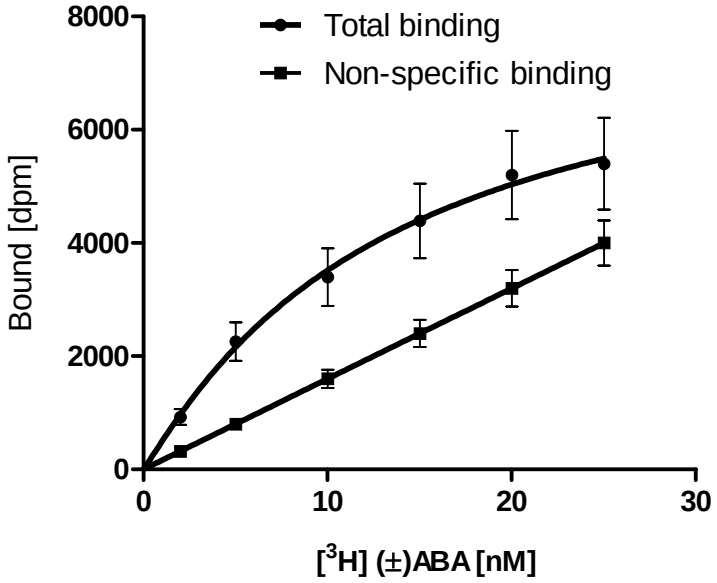

Figure 85. Total and non-specific binding of [^{3}H] (±)-ABA to Rubisco.

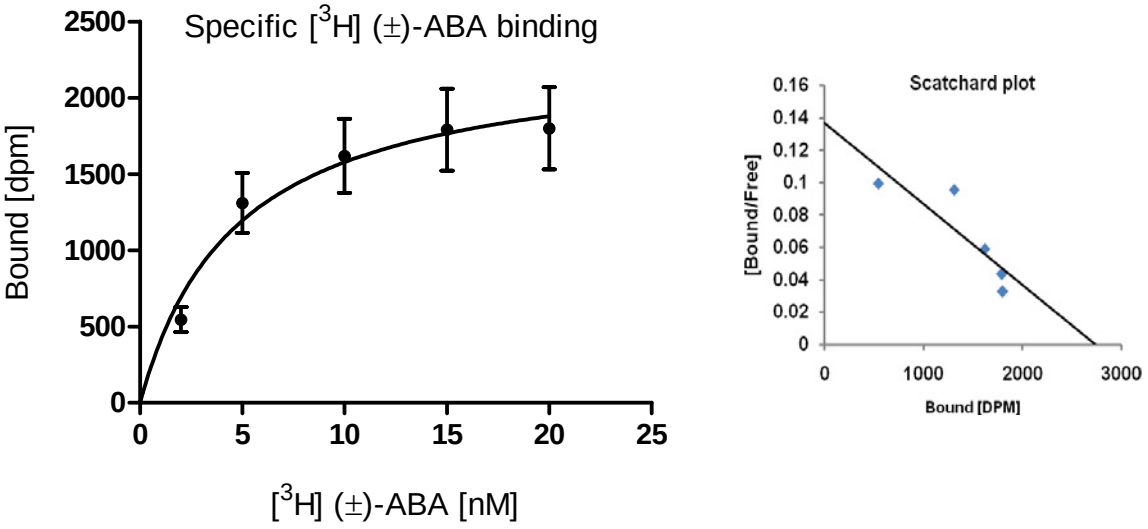

Figure 86. Saturation curve and Scatchard plot representing specific binding of [^{3}H] **(±)**-ABA, as a difference between total and non-specific binding signal.

The non-specific binding was measured by addition of 10,000 fold excess of non-radiolabeled (cold) ABA. The amount of non-specific binding was composed of [^{3}H] (±)-ABA remaining on the column matrix (90% of non-specific signal) after the washings and [^{3}H] (±)-ABA remaining bound to the protein in the presence of 10 000 fold excess of cold ABA. It is noticeable that the total binding curve on Figure 85 begins to level off at 25 nM [^{3}H] (±)-ABA but the difference between total and non-specific signal becomes lower than at 25 nM than it is at 20 nM concentration. Unlike non-specific binding, the specific binding is saturable and at certain concentration no more signal will be observed, the non-specific signal however is non-saturable and keeps rising with concentration. At a certain point these two lines will intersect and the difference between specific and non-specific signal will begin to decline. For that reason the saturation curve representing the specific bound signal only was constructed using [^{3}H] (±)-ABA concentrations up to 20 nM. The equilibrium dissociation constant (K_D) was evaluated using GraphPad Prism^{TM} software using non-linear regression and was found to be 4.7 (± 1.3) nM. The percentage of bound [^{3}H] (±)-ABA

(bound/free) did range from 3% to a maximum of 10 % (Scatchard plot, Figure 86) and therefore no signal depletion was accounted for during data analysis. All analyses presented depend on the assumption that a very small fraction of the ligand binds to the protein. It is therefore assumed that the free concentration of ligand is approximately equal to the concentration added. If a fraction larger than 10% of added radioligand is bound by the protein, then ligand depletion needs to be accounted for and incorporated in non-linear regression equations.[261]

From previous studies it became apparent that Rubisco binds ABA in a selective (nonstereospecific) manner and therefore in all radioligand binding assays, racemic [^{3}H] ABA was used rather than (+) and (-) [^{3}H] ABA separately.

Literature provides examples of radioligand binding assays with recent report of ABA receptor proteins and their equilibrium dissociation constants evaluated by this technique.

Pandey *et al.* has reported two proteins (see Figure 15) GRG1 and GTG2 which showed saturation kinetics with [^{3}H] (±)-ABA and equilibrium dissociation constants of 35.8 nM and 41.2 nM respectively. The binding was found to be stereospecific which was confirmed by the inability of (-)-ABA to displace [^{3}H] (±)-ABA.

Liu *et al.*[122] has reported the binding of G protein-coupled receptor as the first plasma membrane ABA receptor with K_D value being 20.1 nM and ligand/protein molar binding ratio of 0.8 mol mol^{-1} protein. These results have been disputed by Gao *et al.*[262] who showed that GCR2 is not a 7- trans-membrane G protein coupled receptor as claimed by Liu *et al.* In addition the SPR studies on interaction between GCR2 and GPA1 by Liu have been contradicted by Johnson *et al.*[263] who has also suggested that GCR2 is not plant specific but rather a plant homolog of bacterial lanthionine synthetase.

Shen *et al.* reported an Mg-chelatase H subunit form barley as an abscisic acid receptor, exhibiting high affinity (K_D = 32 nM) and specificity of binding towards (+)-ABA and ligand/protein molar binding ratio of 1.28 mol mol^{-1} protein. This report was contradicted by Mueller and Hanson[125] who reported that barley Mg-chelatase did not bind ABA, they also found that *Arabidopsis* equivalent did show saturation kinetics. The inconsistency of results obtained with two different plant species is being investigated.

When analyzing the experimental conditions used in previously reported radioligand binding assays of ABA receptors it becomes noticeable that often more protein than ligand is used in the assays. The mole ratio protein to ligand used in the assay by Shen *et al.* it is 235/1. This raises a question whether reporting the protein ligand binding stoichiometry is appropriate. In order to determine the binding molar ratio it would be necessary to run binding assays with an excess of ligand rather than protein. Determination of binding ratio is a difficult task due to two factors. First, a substantial loss of bound ligand during the separation of "bound" from "free". This step disturbs the steady state equilibrium and leads to a significant loss of bound ligand. Second it is often reported that receptor or other proteins studied retain only a fraction of binding functionality and therefore it is often required to use more (non- stoichiometric amounts) protein in order to maintain the amount of bound ligand at the detectable level. Waldo *et al.*[260] have studied agonist binding to purified human P2Y receptor protein and reported that the density of binding sites in purified protein was only 10-15% of the theoretical binding, and reported experimental evidence for the loss of binding functionality during protein purification and loss of bound ligand during the separation of "free" from "bound". The evaluation of binding stoichiometry carries smaller error in case the radioligand binding assays are performed with tissue expressed and

non-purified protein although the extent of ligand loss during "free" from "bound" separation remains unchanged.

In this project greater amount of protein than ligand was used due to Rubisco fractional binding functionality and loss of bound ligand during the separation of "free" from "bound" [^{3}H] (±)-ABA. The protein precipitation and subsequent washings greatly reduced the amount of bound ABA although its fraction remaining bound throughout the procedure was sufficient to obtain substantial signal due to selective binding and allowed the construction of saturation plot and evaluation of equilibrium dissociation constant. This experiment was not however used to evaluate the stoichiometry of binding for reasons discussed above. This information was provided by Surface Plasmon Resonance experiments indicating the Rubisco/ABA molar binding ratio of approximately 1:8, which is rationalized by the presence of 8 large identical subunits being the only part of the entire protein complex capable of binding ABA.

The final step in evaluating the binding between ABA and Rubisco utilizing radioisotope was the determination of binding specificity. Such experiment was performed by preparing mixtures of the protein and [^{3}H] (±)-ABA at the saturating concentration (25 nM, Figure 86) and addition of non-radiolabeled (+)-ABA, (-)-ABA, PA and *trans*- (+)-ABA at 100, 1000 and 10,000 fold excess with respect to [^{3}H] (±)-ABA. Samples were treated in the same way as the ones used for constructing the saturation curve (Figure 86). Bound [^{3}H] (±)-ABA was separated from free [^{3}H] (±)-ABA by two OrgoSol^{TM} washings of the SPN column matrix as described previously. The displacement of radiolabeled ABA by any compound listed above would indicate its ability for selective binding to Rubisco. Lack of

[^{3}H] (±)-ABA displacement by compounds other than ABA indicates the selectivity of ABA-Rubisco interaction. Figure 87 represents the results.

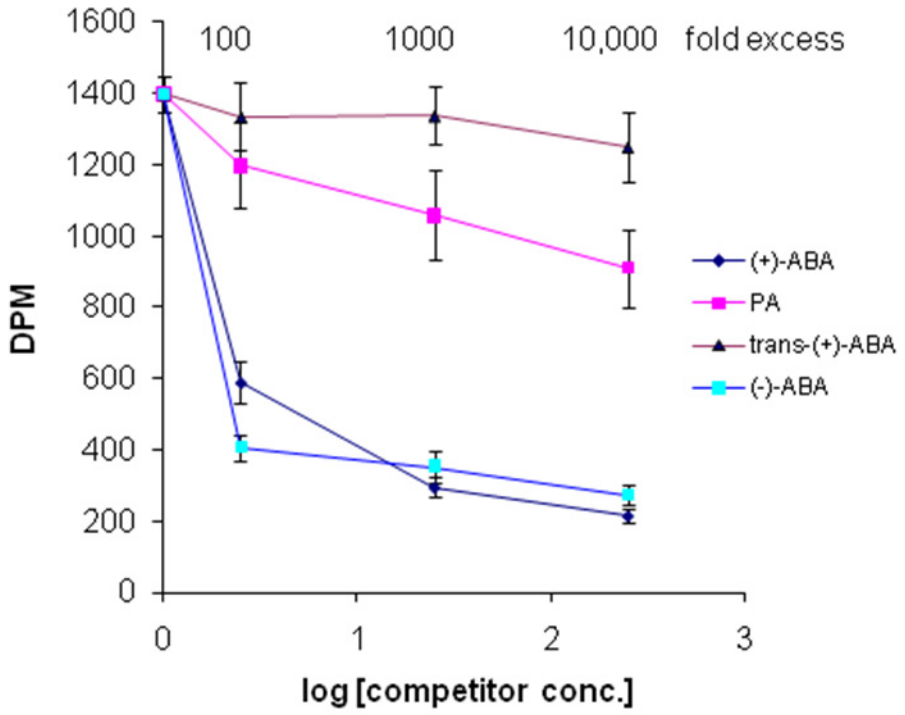

Figure 87. Displacement of [^{3}H] **(±)**-ABA by non-radiolabeled (+)-ABA, (-)-ABA, PA and *trans*-(+)-ABA.

As mentioned before, Rubisco exhibits binding capability for both (+) and (-)-ABA as observed by SPR, and also by photoaffinity labeling experiments where (+) and (-)-ABAs both blocked the PAL reaction. This is confirmed here by the ability of both enantiomers to displace [^{3}H] (±)-ABA as demonstrated on Figure 87. It is also noticeable and consistent with previous SPR experiments that PA only exhibits weak affinity for Rubisco. It is not however able to displace [^{3}H] (±)-ABA completely even at 10,000 fold excess with respect to ABA. *Trans*-(+)-ABA is almost completely incapable of ABA displacement. No signal due to

binding of of *trans*-(+)-ABA was observed by SPR (data not shown). The consistency of results obtained by SPR with radioligand binding technique is particularly satisfying and provides strong evidence for selective binding between ABA and Rubisco.

3. Experimental Procedures

3.1. Gel electrophoresis

Acrylamide gels were used for electrophoresis in denaturing conditions (SDS-PAGE). The concentration of a stacking gel was 4%, and the running gel 10%, the thickness of a gel was 1 mm. Running buffer for electrophoresis contained of: 0.1 M Tris, 1.0 M Glycine, 0.5% SDS. Samples were mixed with Laemmli buffer (4% SDS, 20 % Glycerol, 10% 2-mercaptoethanol, 0.004% bromophenol blue, 0.125 M Tris-HCl) then boiled for 5 minutes and vortexed.

3.2. Gel silver staining

Gels were stained using FOCUS-FAST silver kit from G-biosciences. After electrophoresis, the gel was fixed in a solution containing 30% ethanol and 10 glacial acetic acid. After 30 minutes the gel was washed twice, 5-10 minutes, in 10% ethanol, and then washed three times 5-10 minutes with de-ionized water. The gel was then soaked in prepared Silver Stain solution (Genotech) for 20-30 minutes with gentle rocking. After staining it was quickly rinsed with de-ionized water and soaked in Developer-Sensitizer solution (provided in the kit) for the amount of time required to observe all protein bands. As soon as the intensity reached an acceptable level, the development was stopped decanting the developer solution and soaking the gel in 2% acetic acid.

3.3. Far-Western blotting

After electrophoresis the gel was soaked in Protein Transfer Buffer (PTB) (3.03 g Trizma-base, 14.4 g Glycine, 200 mL methanol, 650 mL de-ionized water) for 10-20 minutes. Sheet of Hybond-P PVDF membrane (Amersham Bioesciences) of the same size as the gel was cut and soaked for 10 seconds in methanol and washed 5 minutes in water followed by equilibration in PTB for at least 10 minutes. The membrane and the gel were then assembled in electroblotting cassette and placed in the blotting unit filled with PTB. The assembly was placed in a cooler to prevent overheating. In addition an ice block was immersed in the electroblotting unit. Protein transfer into the membrane was done either for 30 minutes at 120V or overnight at 20V.

After blotting the membrane was soaked in a phosphate buffered saline solution (PBS-T) with 0.1% v/v Tween (pH 7.5) and 3% w/v BSA with gentle rocking for 1h. The membrane can also be stored in this solution. The blot was then washed with PBS-T two times 5 minutes. Streptavidin-HRP conjugate was then diluted 1:1000 in PBS-T to a final volume of 5 mL. Washed blot was incubated on an orbital shaker with Streptavidin-HRP solution for 1h at RT. The membrane was then briefly rinsed with PBS-T with two changes of buffer and then washed again for 15 minutes, followed by rinsing for 3 x 5 minutes with fresh changes of wash buffer at RT. Extensive washing is crucial for eliminating the background signal. The blot was then removed from the wash buffer the excess of which was drained onto a paper towel. The membrane was placed protein side up on a sheet of SaranWrap^{TM}. 5 mL of previously mixed detection reagents (ECL plus Western Blotting Detection Reagents, Amersham Biosciences) were poured on the membrane and incubated

for 5 minutes at RT. The membrane was then dried and placed on a fresh piece of SaranWrap^{TM,} wrapped up and air bubbles gently removed. Wrapped blot was then placed protein side up in an x-ray film cassette and a sheet of Hyperfilm ECL (Amersham Bioseciences) was placed on top of the membrane in a dark room. The exposure time depends on the amount of biotinylated proteins loaded into the gel. (usually 10-30 seconds). After which the film was developed and proteins modified by PBI686 were identified. Biotinylated marker (ECL protein marker, Amersham Biosciences) was used as molecular weight reference.

3.4. Protein extraction procedure

Proteins were maintained in their native form throughout the experiment to maintain proper folding. For that reason proteins are not frozen, no ionic detergents are added and protein extracts are kept at 0-4ºC.

First 40-80 g of fresh aerial tissue wild of type *Arabidopsis* (Columbia, grown in a growth chamber using 12 h photoperiod and temperature of 23-25°C) leaf tissue was ground with glass beads (500 micron, Aldrich) in 100 mM Sodium Phosphate buffer at pH 7.6 with 0.33 M sucrose, 40 mM ascorbate and 0.5 EDTA and protein inhibitor cocktail (Complete^{TM} Roche). The homogenate was filtered through cheesecloth and centrifuged at 20,000 g for 10 min. The supernatant was collected (200 and 400 mL) and proteins were concentrated by precipitation with 75% ammonium sulfate. The precipitated proteins were centrifuged at 5000g for 30min and re-dissolved in 3-6 mL of phosphate buffer (pH 7.6) with 0.3% non-ionic detergent DHPC (1,2-Diheptanoyl-s*n*-Glycero-3-Phosphocholine) (Avanti Polar Lipids)

to help re-solubilize hydrophobic proteins. At this point the protein concentration of such solubilized crude extract is in 3-6 mg/mL range (concentration determined using SPN^{TM} Protein Assay kit from G-biosciences). To remove any remaining ammonium sulfate the extract was then run through desalting column (PD-10 Amersham Biosciences). Before analysis samples were concentrated using the protocol supplied with UPPA- Protein - Concentrate^{TM} kit from G-biosciences.

3.5. Heterologous expression of CYP707A1 in yeast

The full-length cDNA of CYP707A1 (Dr. Adrian Cutler's laboratory, PBI/NRC) in pBluescript sk- was excised with and KpnI/SstI and isolated using Qiagen's gel extraction kit. The yeast expression vector, YeDP60, was generously provided by Denis Pompon (CNRS-Centre de Génétique Moléculaire). Upon sequencing, the multiple cloning site (MCS) of YeDP60 was found to contain a start codon and 2 *Cla*I sites after the *Bam*HI site at the 5' end. The entire MCS was removed and replaced with the MCS from pUC19. The open reading frame of CYP707A1 from the pBluescript construct was directionally cloned into the modified YeDP60 vector using the enzyme pairs indicated above. The resulting constructs were used to transform the WAT11 strain of *Saccharomyces cerevisae* (Pompon et al., 1996). Transformants were grown overnight in selection media (SC-URA with 2% glucose, 60mg/l adenine and 40mg/l tryptophan), collected by centrifugation and resuspended in YPG media (1% yeast extract, 1% bactopeptone, 2% glucose) and grown for a further 24 hours at 28°C. The yeast was pelleted by centifugation, washed three times with inducing media (YPL - 1% yeast extract, 1% bactopeptone, 2% galactose) and used to

inoculate YPL media to a final optical density of 0.5. The yeast were grown in inducing media for a further 16 hours before microsomal extraction.

3.6. Yeast microsome preparation

Yeast microsomes were prepared following the methods outlined by Urban et al. [28] with the following modifications: Yeast cells (with YeDP60 and CYP707A1) were harvested by centrifugation at 10,000g for 10 minutes and washed in ice-cold, filter-sterilized extraction buffer (0.1%BSA, 0.33M Sucrose, 40mM ascorbate, 20mM EDTA, 200mM potassium phosphate buffer, pH 7.6). The pellet was resuspended (0.3g/ml) in extraction buffer and PMSF was added to a final concentration of 0.5mM. Cell walls were disrupted using an ice cooled bead beater with 0.45mm-0.5mM glass beads. Cells were pulverized three times at one minute each allowing extract to cool between treatments. Cell extract was collected and centrifuged at 10,000g for ten minutes. The supernatant was collected and microsomes precipitated on ice for 30 minutes after the addition of PEG3500 (10g/ml) and NaCl (0.15M). Extracts were centrifuged at 13,000rpm in a Sorval SS-34 rotor for 20 minutes at 4°C. Microsomal pellet was resuspended in cold 100mM potassium phosphate buffer and 40mM ascorbate and protein content determined using Biorad protein determination kit.

Shortly before applying the extract on the affinity column 1 ml of 1 % DHPC detergent from Avanti Polar Lipids was added in order to completely dissolve proteins.

3.7. Isolation of 8'-ABA-hydroxylase from yeast microsomes using affinity probe PBI 686

Microsomes isolated from yeast suspension cultures overexpressing both ABA-8'hydroxylase gene (CYP707A1) and one not overexpressing this protein (YeDP60) as control were re-dissolved in 1% CHAPS detergent in affinity binding buffer (see above). Each solution was run through a separate probe-modified affinity column (5 ml volume, pre-conditioned as described above) three times at 0.4 ml/min. Then the columns were washed three times with 20 ml of binding buffer followed by washing with 5 mM (±) ABA. The three buffer wash fractions as well as ABA wash fractions were collected and concentrated down to 100µl using Amicon Ultra-4 centrifugal Filter Devices purchased form Millipore. The concentrated fractions were then checked for the presence of proteins by SDS-PAGE.

3.8. UV crosslinking of anti-ABA monoclonal antibodies

A mixture of anti-ABA mAb and ovalbumin (in phosphate buffer pH 7.6) at 30 µg/mL each, was combined with PBI 686 at different concentrations (1µM, 5µM, 10µM, 30µM, and 60µM) in 2.0 mL volume for each sample. In addition another set of samples were prepared where (±) ABA was added at concentration from 10 to 50 times higher than PBI 686. Samples were then placed in Pyrex glass test tubes and irradiated by UV light using Hanovia medium pressure mercury lamp for 10 min at RT at the distance of 10 cm from the lamp. Immediately after irradiation samples were placed on ice or frozen and further analyzed by far-Western (see Figure 35).

3.9. UV crosslinking of peptides with PBI686

Three different peptides were UV-irradiated in the presence of PBI686. Peptide #1 TDRAKRKAVSLSKVC (MW = 1660.94), Peptide # 2 (fragment of bradykinin): Arg-Pro-Pro-Gly-Phe (MW = 572.65), peptide # 3: adrenocorticotropic hormone) Ser-Tyr-Met-Glu-His-Phe-Arg-Trp-Gly-Lys-Pro-Val-Gly-Lys-Lys-Arg (MW = 2093.40). A solution of each peptide was mixed with PBI686 at 1 mM concentration (peptide: probe molar ratio 1:1). The mixtures were irradiated with UV light for 15 minutes. Another set of peptide solutions was prepared and without addition of PBI686 and also UV- irradiated.

Samples were then analyzed by MALDI-TOF spectrometry in linear (low resolution), positive ionization mode (

Figure 28-32), using MALDI-TOF MS equipped with a nitrogen laser (337 nm; Voyager-DE STR; Applied Biosystems, Foster City, CA, USA). The sample matrix used was α-Cyano-4-hydroxycinnamic acid

3.10. UV crosslinking of proteins from plant extracts

10 mL of a clear solution resulting from extraction procedure (section 3.4) was split into 5 Pyrex glass test tubes. Three of them contained the probe PBI 686 at 100 μM concentration, and the remaining two were used as negative control. One contained no probe, and one contained the probe but was set aside and not exposed to UV light. Such mixture was incubated for 1h on ice and then irradiated (except for one) with high- intensity UV light

using Hanovia medium pressure mercury lamp for 15 min at RT at the distance of 10 cm from the lamp. Immediately after irradiation samples were placed on ice. Proteins covalently linked with the probe were then separated from non-modified proteins by affinity chromatography (section 3.9). Another set of samples was prepared as above with an addition of (+)-ABA to 1 mM final concentration before UV exposure.

3.11. Photoaffinity labeling of purified Rubisco by PBI 686

Ribulose-1,5-bisphosphate carboxylase/oxygenase (Rubisco) purchased from Aldrich was used for photoaffinity crosslinking with the probe PBI686. Rubisco, ovalbumin and BSA were combined in one solution at 100 μg/mL each. Proteins were dissolved in 100 mM phosphate buffer, 0.15 M NaCl, pH 7.6. Six samples were prepared, each containing the protein and the following: #1- 100 μM PBI686, #2- 10 μM PBI686, #3- 10 μM PBI686 + 0.5 mM (+)-ABA, #4- 10 μM PBI686 + 1 mM (+)-ABA, #5 – proteins only, #6- 10 μM PBI686. All samples but #6 were then irradiated with UV light for 5 minutes, quickly cooled and analyzed by far-Western (see Figure 47-48).

3.12. Affinity chromatography

Affinity chromatography was done using HiTrap streptavidin matrix column and AKTA^{TM} Explorer FPLC system (Amersham Bioesciences). The column (1 mL matrix volume) was first conditioned by running 30 mL of running buffer (20 mM sodium phosphate, 0.15 M NaCl, pH 7.5) at 1 mL/min flow rate. Then 5-10 mL of the extract (30-60

mg of protein) was injected on the column at 0.3 mL/min. After injection another 30-50 mL of buffer was run through the system to wash out unbound proteins, followed by 10 mL of 0.1 M Citric Acid (pH 2) to strip off the non-specifically bound proteins. Chromatography is then finalized by running 8M Guanidine-HCl (Aldrich) at pH 2 and collected fractions (1 mL each) were immediately run through PD-10 desalting columns (GE Healthcare) to remove Gu-HCl and bring pH to 7.6. Proteins from collected fractions were then concentrated using Amicon™ Ultrafree filtering devices (Millipore). Samples were then further concentrated using UPPA- Protein -Concentrate™ kit (Genotech).

3.13. Surface Plasmon Resonance (SPR)

SPR was performed using CM5 sensor chips (Biacore) and Biacore X SPR instrument. All buffers were filtered and degassed prior to use. Free carboxyl groups on the chip surface were activated with EDC and N-hydroxy-succinimide and then coupled to the protein's free -NH_2 groups. The following procedure was used to immobilize protein (ligand) on the chip surface. First scouting experiments on an unmodified chip were done to find optimal pH for protein pre-concentration on the chip surface by inducing electrostatic interactions. Optimal pre-concentration was found when protein solution (0.5 mg/mL in 10 mM HEPES, pH 7.9) was mixed with Sodium acetate buffer at pH 5 at ratio 1:1. Once optimal pH for immobilization was found the chip surface was then washed by several 1 minute injections of 0.05 % SDS then 50 mM NaOH followed by several 100 µl injections of running buffer (10 mM HEPES, 100 mM NaCl, 10 mM $MgCl_2$, pH 8). The chip surface was then activated by injecting a 1:1 mixture of NHS and EDC (running both chip cells open). NHS/EDC

activation mixture is injected for 7 minutes at 5 µl/min flow rate. Then flow cell 1 (FC1) was closed and ligand solution (mixture of protein solution with Sodium Acetate pH 5) was injected in manual mode (1 minute pulses) 4-6 times on flow cell 2 (FC2). The injector was washed and subsequently a solution of ethylamine (EA) was injected on both flow cells for 7 minutes. At this point 4000-8000 resonance units (RU) were immobilized (compare FC1 and FC2 baselines).

It is important to perform chip activation and ligand immobilization in less than 10 minutes. Once the surface was activated the protein had to be injected immediately. The pH of protein solution is lowered just before the injection to prevent protein damage.

High density surface (8000 RU immobilized) is only recommended if a given experiment is only expected to determine if the ligand binds the analyte. Experiments yielding binding kinetics information use lower density surfaces and therefore fewer protein injections on the chip surface during immobilization would be required (4000 RU). Signal from the unmodified cell is automatically subtracted from the modified cell signal. It is also very important to maintain the composition of the running buffer identical to the buffer in which the sample is injected. If the two buffers were slightly different a bulk buffer shift will be observed during the injection. The magnitude of a bulk shift is usually several times higher than the signal due to binding of analyte with the ligand. It is therefore required to test the system by injecting running buffer as a sample several times to check for bulk shift. If a buffer injection doesn't disturb the baseline, then the actual sample of an analyte ((+)ABA, (-)-ABA, PA, trans-ABA, PBI686 or cinnamic acid) was injected at various concentrations ranging from 5 nM to 5 µM and a flow rate of 50-100 µl/min. The injection was run until signal saturation, usually between 100 -120 s. As soon as signal saturated, injections were

stopped and running buffer was run again at 100 µl/min. If during analyte dissociation the signal did not return to the baseline within 3-5 minutes the undissociated analyte was then stripped from the surface by injecting of 2.5 M NaCl for 30 seconds followed by running buffer. If this procedure still did not remove all analyte from the surface, NaCl injections were repeated several times. Also the system was washed with running buffer to remove analyte remaining in the injector component.

Sensograms obtained during analyte concentration were analyzed by Biacore evaluation software, yielding K_D values, calculated from the ratio between association rate ($k_{a)}$ and dissociation rate (k_d). Analytes were injected at different concentrations (usually 100 fold difference between the lowest and the highest concentration). Langmuir binding fit model was used for data evaluation and no mass transfer was observed when injecting buffer at different flow rates. Five CM5 chips were used to evaluate dissociation constant (K_D) of ABA binding to Rubisco and all K_D values were averaged yielding 5 (± 2) nM value.

3.14. Protein identification using MALDI-TOF peptide mass fingerprinting (PMF)

Protein bands visible on silver-stained gels were excised and then subjected to alkylation and tryptic digestion using a modified procedure of Jensen *et al.*. (1999). The gel pieces containing proteins were washed two times with a solution containing 20 mM EDTA and 100 mM NH_4HCO_3 in 30% (v/v) acetonitrile, dried and then re-hydrated with a reducing solution (10 mM EDTA, 10 mM dithiothreitol, and 100 mM NH_4HCO_3) for 1 h at 60°C. After cooling to room temperature, the gel pieces were dried and then re-hydrated with alkylating solution (10 mM EDTA, 10 mM iodoacetamide, and 100 mM NH_4HCO_3) for 30

min at room temperature. The gel pieces were washed two times with water and were then minced. The minced gel pieces were dried and then re-hydrated in a digestion solution containing 100 mM NH_4HCO_3 and 10 mM $CaCl_2$ with 0.1±0.2 mg of trypsin at 37°C overnight. After the trypsin digestion, the minced gel pieces were separated from the digestion solution and successively washed with 0.1% (v/v) trifuoroacetic acid (TFA), 0.1% TFA in acetonitrile, 0.1% TFA in 50% (v/v) acetonitrile, and 0.1% TFA in acetonitrile at room temperature in order to further extract the peptides from the minced gel pieces. Pooled extracts (including the digestion solution and both the aqueous and organic washes) were concentrated using a centrifugal concentrator and then desalted by a ZipTipC18 (Millipore, Billerica, MA, USA). Trypsin-digested peptide masses were measured using a MALDI-TOF MS equipped with a nitrogen laser (337 nm; Voyager-DE STR; Applied Biosystems, Foster City, CA, USA). A solution of peptides was mixed with the same volume of a matrix solution consisting of saturated α-cyano-4-hydroxycinnamic acid (CHCA) in 50% (v/v) acetonitrile/0.1% (v/v) TFA. After the peptides were co-crystallized with CHCA by evaporating organic solvents, the peptide masses of the peptides were measured. All MALDI spectra were externally calibrated using a standard peptide mixture: angiotensin I, angiotensin II, neurotensin, and adrenocorticotropic hormone fragment 1±17 (Sigma). Monoisotopic masses from all spectra recorded for a given peptide were selected and analyzed. Matching of experimental mass spectra with theoretical mass spectra obtained from various Arabidopsis databases was performed using a sequence database search program, MASCOT PMF. Database queries were carried out for monoisotopic masses using the following parameters: peptide mass tolerance of ±50 p.p.m. (p.p.m = [experimental mass (in Daltons) - theoretical mass/theoretical mass], expressed in parts per million), equivalent to

0.1 Da for a 2-kDa peptide; the maximum number of missed tryptic cleavages of 1 or 2; and modifications, including conversion of oxidation of Met. The maximal molecular mass was restricted to 300 kDa for the protein over 60 kDa, 100 kDa for the protein below 60 kDa or, sometimes, 50 kDa for the protein below 30 kDa to avoid hits of very large proteins. No strict pI filters were applied to find possible breakdown products, unexpected splicing, or post-translational modification such as phosphorylation.

3.15. Rubisco Activity Assays

Stock solution of pre-purified Rubisco (Sigma) from spinach was prepared by dissolving 2-5 mg of protein in a buffer containing 15 mM $MgCl_2$ and 25 mM $NaHCO_3$ at pH 8.0. Each assay (total volume, 1.0 mL) contained 50 mM Bicine (pH 8.0), 15 mM MgCl2, 10 mM NaCl, 5 mm DTT, 5 mM phosphocreatine, 5 mM ATP, 5 mM phosphoenolpyruvate, and 25 mM $NaHCO_3$. This mixture was prepared before each set of experiments using distilled water. Five minutes before initiating the reaction with activated Rubisco, stock solutions were added to produce final concentrations as follows: 0.1 -1 mM RuBP (10 samples at 0.1 mM intervals), 0.4 mM NADH, 20 units mL^{-1} of glyceraldehyde-3-phosphate dehydrogenase, 20 units mL^{-1} of 3-phosphoglycerate kinase, and 2 units mL^{-1} of creatine phosphokinase. Following the addition of Rubisco to a final concentration of 0.3 mg mL^{-1}, NADH concentration was measured spectrophotometrically (λ = 340 nm) over time for 5 min. A340 was measured at 5s intervals and recorded. Absorbance values were converted to NADH concentrations using an extinction coefficient of 6.22 mM^{-1}. Reaction rates were evaluated from the slope of absorbance vs. time curve and plotted against concentration of Rubisco substrate (RuBP). Initial velocity (V_i) vs. substrate concentration [RuBP] plot was

constructed using GrapPad Prism™ software which based on experimental reaction rates (V_i) and RuBP concentrations and fitted the experimental date into two different inhibition models (competitive and allosteric) All experiments were performed in the absence of ABA (control) and with ABA at four concentrations: 1, 2, 5 and 10 mM.

3.16. [^{3}H] (±)-ABA binding assays

3.16.1. Hot saturation

Stock solution of pre-purified Rubisco (Sigma) was prepared by dissolving 2-5 mg of protein in binding buffer (50 mM Bicine, 15 mM $MgCl_2$, 20 mM NaCl, pH 7.9) and placed on ice. Total volume for each assay sample was 30 µL and each contained approx 30 µg of protein. Protein solution was mixed with ^{3}H (±)-ABA (specific activity 37 Ci mmol $^{-1}$ hot: cold ratio 1.8:1, purchased from GE biosciences). Radioactive ABA was added at different concentrations: 2, 5, 10, 15, 20, 25 nM. In addition another set of samples containing 2-25 nM (±) [^{3}H] (±)-ABA and 500 µM [^{1}H] (+)-ABA were prepared. Samples containing 30 µg of protein, [^{3}H] (±)-ABA with and without [^{1}H] (+)-ABA were incubated at RT for 30 minutes then amounts of bound [^{3}H] (±)-ABA were measured. The following method was used to separate the bound from unbound [^{3}H] (±)-ABA. 15 µL samples from each reaction were transferred into SPN columns (G-biosciences), allowed to soak into the column matrix. Subsequently 100 µL of cold (chilled at -20° C) non-denaturing and precipitating OrgoSol™ buffer (G-biosciences) was added to the column. Samples were quickly paced in centrifuge and spun at 12,000 rpm for 10 seconds and another 100 µL portion of cold OrgoSol™ buffer was added to the column, and centrifuged again for 20 seconds at 12,000 rpm. Column

matrix from each sample was then removed from the column and placed in scintillation *via*ls containing Aqasol™ scintillation fluid. Column matrices containing protein with bound [^{3}H] (±)-ABA were then soaked in scintillation fluid for at least 24 hours followed by counting radioactivity using Beckman Cutler Multi Purpose Scintillation Counter. A set of control samples not containing the protein but different concentrations of [^{3}H] (±)-ABA were also prepared and counted. Radioactivity remaining on the column matrix in the absence of protein was used as background and subtracted from samples containing the protein (matrix non-specific binding). Signal corresponding to specific ABA binding was calculated from the difference between samples with [^{3}H] (±)- ABA and those containing 1000 fold excess of non-radiolabeled (+)-ABA. Each sample was replicated 5-10 times and readings averaged.

3.16.2. Cold saturation

Cold saturation was performed similarly to hot saturation. The concentration of [^{3}H]-(±)-ABA was 25 nM in all samples, and non-radiolabeled (+)-ABA was added to each sample at increasing concentrations ranging from 10 to 10000 fold higher than radiolabeled ABA. The same procedure was applied when using non-radiolabeled (-)-ABA, PA, and *trans*-ABA. Similarly to the above specific binding was calculated from the difference between readings from samples with [^{3}H] (±)-ABA and samples containing both hot and cold ABA. Each sample was replicated 5-10 times and the readings averaged.

4. Conclusions and future work

The primary objective of this project was isolation and identification of new ABA-binding proteins in plants. This was to be achieved by employing a biologically active ABA derivative, which served as both an affinity and a photoaffinity probe. It has been proven that this probe was recognized by known ABA-binding proteins. Subsequently the probe was used to isolate putative ABA–binding proteins, and this led to the discovery of Rubisco as a new ABA binding protein, among several other potential candidates. The binding of ABA to Rubisco was confirmed by various techniques and it was found that in addition to specific binding, ABA also affects Rubisco's enzymatic activity. This suggests that ABA may act as modulator of photosynthesis through the inhibition of this enzyme.

Ability of non-radioactive (+) and (-)-ABA to displace [^{3}H] (±)-ABA, indicated that Rubisco binds ABA in a non-stereospecific manner. However the that fact that PA and *trans*-(+)-ABA were incapable of [^{3}H] (±)-ABA displacement, suggest that certain structural features present in ABA are required for binding. Modifications of ABA 8' carbon (present in PA) or changes in its side-chain configuration (present in *trans*-ABA) eliminate binding. Following this, the investigation of the binding ability of other ABA metabolites or synthetic analogs remains within future research directions. Screening a number of ABA analogs could possibly provide more information about the structural requirements of Rubisco towards its ABA-like binding partners.

There are several other questions to be answered by future research work. First, is the exact location of ABA binding site within the multi-subunit protein. This could be achieved through either co-crystallization ABA and Rubisco and detailed crystallographic studies of the complex, or further MS analysis of Rubisco-PBI686 tryptic digests.

ABA-binding site identification by MS methods would be possible though performing experiments using precursor ion scanning in a low energy collision-induced dissociation mode. This can be done by obtaining an MS/MS fragmentation pattern of PBI686 and choosing product ions highly characteristic for the probe (reporter ions). Trypsin digestion of PBI686-tagged-Rubisco would result in a mixture of peptides and also containing PBI686-tagged-peptide(s). The peptide mixture could be then subjected to MS/MS analysis and searched for PBI686 reporter ions. These reporter ions are also precursors of the probe-peptide adducts. Precursor ions could then be associated with the parent ion of the adduct and allow identification of the MS signals belonging to PBI686-tagged peptide(s). MS/MS analysis of these "new" peptides through *de novo* sequencing would reveal the identity of amino acid residue being covalently modified by PBI686. This approach could lead to identification of ABA binding site within Rubisco complex. In addition, the finding of ABA binding site would allow creating recombinant Rubisco and alterations in plant sensitivity to ABA under abiotic stress conditions.

Using the approach described above it would also be possible to identify other putative ABA-binding proteins/receptors as well as their ABA-binding sites. In addition to binding studies, the MS methods could be employed to identify the ABA-binding sites of other proteins (e.g. DREPP) identified in this project.

5. References

(1) Chang, C.; Meyerowitz, E. M. The ethylene hormone response in Arabidopsis: a eukaryotic two-component signaling system. *Proc. Natl. Ac. Sci.* **1995**, *92*, 4129-4133.

(2) Teale, W. D.; Paponov, I. A.; Palme, K. Auxin in action: signalling, transport and the control of plant growth and development. *Nat. Rev. Mol. Cell. Biol.* **2006**, *7*, 847-859.

(3) Sakakibara, H. Cytokinins: Activity, Biosynthesis, and Translocation. *Ann. Rev. Pl. Biol.* **2006**, *57*, 431-449.

(4) Creelman, R. A.; Mullet, J. E. Bosynthesis and actcion of jasmonates in plants. *Ann. Rev. Pl. Phys. Pl. Mol. Biol.***1997**, *48*, 355-381.

(5) Li, J.; Chory, J. Brassinosteroid actions in plants. *J. Exp. Bot.* **1999**, *50*, 275-282.

(6) Yamaguchi, S. Gibberellin Metabolism and its Regulation. *Ann. Rev. Pl. Biol.* **2008**, *59*, 225-251.

(7) Aldesuquy, H. S. Regulating effect of salicylic acid on germination of Lupinus termis seedlings. *Acta Bot. Hung.***2000**, *42*, 15-27.

(8) Nambara, E.; Nakabayashi, K. Perception and signal transduction of abscisic acid (ABA). *Shokubutsu no Seicho Chosetsu* **2003**, *38*, 58-64.

(9) Lazareno, S. Quantification of receptor interactions using binding methods. *J. Rec. Sig. Trans.* **2001**, *21*, 139 - 165.

(10) Cafiso, D. S. *Structure and interactions of C2 domains at membrane surfaces*; John Wiley & Sons, 2005.

(11) Johnson, J. E.; Cornell, R. B. Amphitropic proteins: regulation by reversible membrane interactions. *Mol. Membr. Biol.* **1999**, *16*, 217-235.

(12) Thuduppathy, G. R.; Craig, J. W.; Kholodenko, V.; Schon, A.; Hill, R. B. Evidence that membrane insertion of the cytosolic domain of Bcl-xL is governed by an electrostatic mechanism. *J. Mol. Biol.* **2006**, *359*, 1045-58.

(13) Jackson, M. B.; Attwood, P. A.; Brailsford, R. W.; Coupland, D.; Else, M. A.; English, P. J.; Summers, J. E. Hormones and root-shoot relationships in flooded plants - an analysis of methods and results. *Plant and Soil* **1994**, *167*, 99-107.

(14) King, N.; Hittinger, C. T.; Carroll, S. B. Evolution of Key Cell Signaling and Adhesion Protein Families Predates Animal Origins. *Science* **2003**, *301*, 361-363.

(15) Antunes, V. R.; Machado, B. H. Antagonism of glutamatergic metabotropic receptors in the NTS of awake rats does not affect the gain of the baroreflex. *Autonomic Neuroscience* **2003**, *103*, 65-71.

(16) Grossmann, K. Mediation of herbicide effects by hormone interactions. *J. Pl. Gr. Reg.* **2003**, *22*, 109-122.

(17) Grossmann, K.; Hansen, H. Auxin herbicides: The janus face of active ingredients. *Biologie in Unserer Zeit* **2003**, *33*, 12-20.

(18) Normanly, J.; Slovin, J. P.; Cohen, J. D. Rethinking Auxin Biosynthesis and Metabolism. *Plant Phys.* **1995**, *107*, 323-329.

(19) Bialek, K.; Michalczuk, L.; Cohen, J. D. Auxin Biosynthesis during Seed Germination in Phaseolus vulgaris. *Plant Phys.* **1992**, *100*, 509-517.

(20) Hedden, P.; Thomas, S. G. *Plant Hormone Signaling*; Wiley-Blackwell: Harpenden, UK, 2006; Vol. 24.

(21) Napier, R. M.; David, K. M.; Perrot-Rechenmann, C. A short history of auxin-binding proteins. *Plant Mol. Biol.* **2002**, *49*, 339-48.

(22) Ray, P. M. Specificity of Auxin-binding Sites on Maize Coleoptile Membranes as Possible Receptor Sites for Auxin Action. *Plant Phys.* **1977**, *60*, 585-591.

(23) Ray, P. M. Auxin-binding Sites of Maize Coleoptiles Are Localized on Membranes of the Endoplasmic Reticulum. *Plant Phys.* **1977**, *59*, 594-599.

(24) Kim, Y. S.; Kim, D.; Jung, J. Isolation of a novel auxin receptor from soluble fractions of rice (Oryza sativa L.) shoots. *FEBS Lett.* **1998**, *438*, 241-4.

(25) Lobler, M.; Klambt, D. Auxin-binding protein from coleoptile membranes of corn (Zea mays L.). I. Purification by immunological methods and characterization. *J.Biol.Chem.* **1985**, *260*, 9848-53.

(26) Jones, A. M.; Im, K. H.; Savka, M. A.; Wu, M. J.; DeWitt, N. G.; Shillito, R.; Binns, A. N. Auxin-dependent cell expansion mediated by overexpressed auxin-binding protein 1. *Science* **1998**, *282*, 1114-7.

(27) Chen, J.-G.; Ullah, H.; Young, J. C.; Sussman, M. R.; Jones, A. M. ABP1 is required for organized cell elongation and division in Arabidopsis embryogenesis. *Genes* **2001**, *15*, 902-911.

(28) Kepinski, S.; Leyser, O. The Arabidopsis F-box protein TIR1 is an auxin receptor. *Nature* **2005**, *435*, 446.

(29) Gray, W. M.; Kepinski, S.; Rouse, D.; Leyser, O.; Estelle, M. Auxin regulates SCF(TIR1)-dependent degradation of AUX/IAA proteins. *Nature* **2001**, *414*, 271-6.

(30) Liscum, E.; Reed, J. W. Genetics of Aux/IAA and ARF action in plant growth and development. *Plant Mol. Biol.* **2002**, *49*, 387-400.

(31) Ramos, J. A.; Zenser, N.; Leyser, O.; Callis, J. Rapid Degradation of Auxin/Indoleacetic Acid Proteins Requires Conserved Amino Acids of Domain II and Is Proteasome Dependent. *Plant Cell* **2001**, *13*, 2349-2360.

(32) Kepinski, S.; Leyser, O. Auxin-induced SCF TIR1 Aux/IAA interaction involves stable modification of the SCF TIR1 complex. *Proc. Natl. Ac. Sci.***2004**, *101*, 12381-12386

(33) Ouellet, F.; Overvoorde, P. J.; Theologis, A. IAA17/AXR3: Biochemical Insight into an Auxin Mutant Phenotype. *Plant Cell,* **2001**, *13*, 829-842.

(34) Deshaies, R. J. SCF and Cullin/Ring H2-based ubiquitin ligases. *Annu. Rev. Cell Dev. Biol.* **1999**, *15*, 435-67.

(35) Schulman, B. A.; Carrano, A. C.; Jeffrey, P. D.; Bowen, Z.; Kinnucan, E. R. E.; Finnin, M. S.; Elledge, S. J.; Harper, J. W.; Pagano, M.; Pavletich, N. P. Insights into SCF ubiquitin ligases from the structure of the Skp1-Skp2 complex. *Nature*, **2000**, *408*, 381.

(36) Dharmasiri, N.; Dharmasiri, S.; Estelle, M. The F-box protein TIR1 is an auxin receptor. *Nature* **2005**, *435*, 441.

(37) Callis, J. Plant biology Auxin action. *Nature* **2005**, *435*, 436-437.

(38) Pickart, C. M. Mechanisms underlying ubiquitination. *Annu. Rev. Biochem.* **2001**, *70*, 503-33.

(39) Swanson, S. J.; Bethke, P. C.; Jones, R. L. Barley aleurone cells contain two types of vacuoles: characterization of lytic organelles by use of fluorescent probes. *Plant Cell* **1998**, *10*, 685-698.

(40) Gallavotti, A.; Yang, Y.; Schmidt, R. J.; Jackson, D. The Relationship between Auxin Transport and Maize Branching. *Plant Phys.* **2008**, *147*, 1913-1923.

(41) Woo, E. J.; Marshall, J.; Bauly, J.; Chen, J. G.; Venis, M.; Napier, R. M.; Pickersgill, R. W. Crystal structure of auxin-binding protein 1 in complex with auxin. *Embo J.*. **2002**, *21*, 2877-85.

(42) Bertosa, B.; Kojic-Prodic, B.; Wade, R. C.; Tomic, S. Mechanism of auxin interaction with Auxin Binding Protein (ABP1): a molecular dynamics simulation study. *Biophys. J.* **2008**, *94*, 27-37.

(43) Mok, D. W.; Mok, M. C. Cytokinin Metabolism And Action. *Annu Rev Plant Phys. Plant Mol. Biol.* **2001**, *52*, 89-118.

(44) Strnad, M. The aromatic cytokinins. *Physiol. Plant.* **1997**, *101*, 674.

(45) Hwang, I.; Sheen, J. Two-component circuitry in Arabidopsis cytokinin signal transduction. *Nature* **2001**, *413*, 383.

(46) Inoue, T.; Higuchi, M.; Hashimoto, Y.; Seki, M.; Kobayashi, M.; Kato, T.; Tabata, S.; Shinozaki, K.; Kakimoto, T. Identification of CRE1 as a cytokinin receptor from Arabidopsis. *Nature* **2001**, *409*, 1060.

(47) Suzuki, T.; Miwa, K.; Ishikawa, K.; Yamada, H.; Aiba, H.; Mizuno, T. The Arabidopsis sensor His-kinase, AHk4, can respond to cytokinins. *Plant Cell Physiol.* **2001**, *42*, 107-13.

(48) West, A. H.; Stock, A. M. Histidine kinases and response regulator proteins in two-component signaling systems. *Trends Biochem. Sci.* **2001**, *26*, 369-76.

(49) Heyl, A.; Schmulling, T. Cytokinin signal perception and transduction. *Curr. Opin. Plant Biol.* **2003**, *6*, 480-8.

(50) Yonekura-Sakakibara, K.; Kojima, M.; Yamaya, T.; Sakakibara, H. Molecular Characterization of Cytokinin-Responsive Histidine Kinases in Maize. Differential Ligand Preferences and Response to cis-Zeatin. *Plant Phys.* **2004**, *134*, 1654-1661.

(51) Yamada, H.; Suzuki, T.; Terada, K.; Takei, K.; Ishikawa, K.; Miwa, K.; Yamashino, T.; Mizuno, T. The Arabidopsis AHK4 Histidine Kinase is a Cytokinin-Binding Receptor that Transduces Cytokinin Signals Across the Membrane. *Plant Cell Physiol.* **2001**, *42*, 1017.

(52) Riefler, M.; Novak, O.; Strnad, M.; Schmulling, T. Arabidopsis Cytokinin Receptor Mutants Reveal Functions in Shoot Growth, Leaf Senescence, Seed Size, Germination, Root Development, and Cytokinin Metabolism. *Plant Cell* **2006**, *18*, 40-54.

(53) Spichal, L.; Rakova, N. Y.; Riefler, M.; Mizuno, T.; Romanov, G. A.; Strnad, M. Two Cytokinin Receptors of Arabidopsis thaliana, CRE1/AHK4 and AHK3, Differ in their Ligand Specificity in a Bacterial Assay. *Plant Cell Physiol.* **2004**, *45*, 1299.

(54) Pasternak, O.; Bujacz, G. D.; Fujimoto, Y.; Hashimoto, Y.; Jelen, F.; Otlewski, J.; Sikorski, M. M.; Jaskolski, M. Crystal Structure of Vigna radiata Cytokinin-Specific Binding Protein in Complex with Zeatin. *Plant Cell* **2006**, *18*, 2622-2634.

(55) Davies, P. J. *Plant Hormones: Physiology, Biochemistry and Molecular Biology.*, 1995. Academic Press.

(56) Thomas, S. G.; Sun, T.-p. Update on Gibberellin Signaling. A Tale of the Tall and the Short. *Plant Phys.* **2004**, *135*, 668.

(57) Ueguchi-Tanaka, M.; Ashikari, M.; Nakajima, M.; Itoh, H.; Katoh, E.; Kobayashi, M.; Chow, T. Y.; Hsing, Y. I.; Kitano, H.; Yamaguchi, I.; Matsuoka, M. Gibberellin Insensitive dwarf1 encodes a soluble receptor for gibberellin. *Nature* **2005**, *437*, 693-8.

(58) Nakajima, M.; Takita, K.; Wada, H.; Mihara, K.; Hasegawa, M.; Yamaguchi, I.; Murofushi, N. Partial purification and characterization of a gibberellin-binding protein from seedlings of Azukia angularis. *Biochem. Biophys. Res. Commun.* **1997**, *241*, 782-6.

(59) Nakashita, H. Regulation of disease resistance by plant hormones. *Shokubutsu Saibo Kogaku Shirizu* **2004**, *19*, 147-149.

(60) Bleecker, A. B.; Kende, H. Ethylene: a gaseous signal molecule in plants. *Annu. Rev. Cell Dev. Biol.* **2000**, *16*, 1-18.

(61) Johnson, P. R.; Ecker, J. R. The ethylene gas signal transduction pathway: a molecular perspective. *Annu. Rev. Genet.* **1998**, *32*, 227-54.

(62) Stepanova, A. N.; Ecker, J. R. Ethylene signaling: from mutants to molecules. *Curr. Opin. Plant Biol.* **2000**, *3*, 353-60.

(63) Sakai, H.; Hua, J.; Chen, Q. G.; Chang, C.; Medrano, L. J.; Bleecker, A. B.; Meyerowitz, E. M. ETR2 is an ETR1-like gene involved in ethylene signaling in Arabidopsis. *Proc. Natl. Ac. Sci.* **1998**, *95*, 5812-7.

(64) Hua, J.; Sakai, H.; Nourizadeh, S.; Chen, Q. G.; Bleecker, A. B.; Ecker, J. R.; Meyerowitz, E. M. EIN4 and ERS2 are members of the putative ethylene receptor gene family in Arabidopsis. *Plant Cell* **1998**, *10*, 1321-32.

(65) Chang, C.; Kwok, S. F.; Bleecker, A. B.; Meyerowitz, E. M. Arabidopsis ethylene-response gene ETR1: similarity of product to two-component regulators. *Science* **1993**, *262*, 539-44.

(66) Chang, C.; Stadler, R. Ethylene hormone receptor action in Arabidopsis. *Bioessays* **2001**, *23*, 619-27.

(67) Chen, Y. F.; Randlett, M. D.; Findell, J. L.; Schaller, G. E. Localization of the ethylene receptor ETR1 to the endoplasmic reticulum of Arabidopsis. *J.Biol.Chem.* **2002**, *277*, 19861-6.

(68) Gao, Z.; Chen, Y. F.; Randlett, M. D.; Zhao, X. C.; Findell, J. L.; Kieber, J. J.; Schaller, G. E. Localization of the Raf-like kinase CTR1 to the endoplasmic reticulum of Arabidopsis through participation in ethylene receptor signaling complexes. *J. Biol. Chem* **2003**, *278*, 34725-32.

(69) Clark, K. L.; Larsen, P. B.; Wang, X.; Chang, C. Association of the Arabidopsis CTR1 Raf-like kinase with the ETR1 and ERS ethylene receptors. *Proc. Natl. Acad. Sci.* **1998**, *95*, 5401-6.

(70) Stepanova, A. N.; Alonso, J. M. Arabidopsis Ethylene Signaling Pathway. *Sci. Signl.* **2005**, *2005*, cm4.

(71) Yafan Huang, Biochemical and functional analysis of CTR1, a protein kinase that negatively regulates ethylene signaling in *Arabidopsis*. *Plant J.* **2003**, *33*, 221-233.

(72) Huang, Y.; Li, H.; Hutchison, C. E.; Laskey, J.; Kieber, J. J. Biochemical and functional analysis of CTR1, a protein kinase that negatively regulates ethylene signaling in *Arabidopsis*. *Plant J.* **2003**, *33*, 221-233.

(73) Guo, H.; Ecker, J. R. The ethylene signaling pathway: new insights. *Curr. Op. Plant Biol.* **2004**, *7*, 40-49.

(74) Alonso, J. M.; Stepanova, A. N.; Leisse, T. J.; Kim, C. J.; Chen, H.; Shinn, P.; Stevenson, D. K.; Zimmerman, J.; Barajas, P.; Cheuk, R.; Gadrinab, C.; Heller, C.; Jeske, A.; Koesema, E.; Meyers, C. C.; Parker, H.; Prednis, L.; Ansari, Y.; Choy, N.; Deen, H.; Geralt, M.; Hazari, N.; Hom, E.; Karnes, M.; Mulholland, C.; Ndubaku, R.; Schmidt, I.; Guzman, P.; Aguilar-Henonin, L.; Schmid, M.; Weigel, D.; Carter, D. E.; Marchand, T.; Risseeuw, E.; Brogden, D.; Zeko, A.; Crosby, W. L.; Berry, C. C.; Ecker, J. R. Genome-Wide Insertional Mutagenesis of Arabidopsis thaliana. *Science* **2003**, *301*, 653.

(75) Wang, W.; Esch, J. J.; Shiu, S.-H.; Agula, H.; Binder, B. M.; Chang, C.; Patterson, S. E.; Bleecker, A. B. Identification of Important Regions for Ethylene Binding and Signaling in the Transmembrane Domain of the ETR1 Ethylene Receptor of Arabidopsis. *Plant Cell* **2006**, *18*, 3429-3442.

(76) Ellard-Ivey, M.; Douglas, C. J. Role of Jasmonates in the Elicitor- and Wound-Inducible Expression of Defense Genes in Parsley and Transgenic Tobacco. *Plant Phys.* **1996**, *112*, 183.

(77) Creelman, R. A.; Mullet, J. E. Biosynthesis and action of jasmonates in plants. *Ann. Rev. Pl.Physi. Pl. Mol. Biol.* **1997**, *48*, 355-381.

(78) Farmer, E. E.; Ryan, C. A. Octadecanoid Precursors of Jasmonic Acid Activate the Synthesis of Wound-Inducible Proteinase Inhibitors. *The Plant Cell* **1992**, *4*, 129.

(79) Feys, B. J. F.; Benedetti, C. E.; Penfold, C. N.; Turner, J. G. Arabidopsis Mutants Selected for Resistance to the Phytotoxin Coronatine Are Male Sterile, Insensitive to Methyl Jasmonate, and Resistant to a Bacterial Pathogen. *The Plant Cell* **1994**, *6*, 751.

(80) Ishiguro, S.; Kawai-Oda, A.; Ueda, J.; Nishida, I.; Okada, K. The DEFECTIVE IN ANTHER DEHISCENCE1 Gene Encodes a Novel Phospholipase A1 Catalyzing the Initial Step of Jasmonic Acid Biosynthesis, Which Synchronizes Pollen Maturation, Anther Dehiscence, and Flower Opening in Arabidopsis. *The Plant Cell* **2001**, *13*, 2191.

(81) Virginia Balbi, A. D. Jasmonate signalling network in *Arabidopsis thaliana*: crucial regulatory nodes and new physiological scenarios. *New Phytol.* **2008**, *177*, 301-318.

(82) Takahashi, H.; Kanayama, Y.; Zheng, M. S.; Kusano, T.; Hase, S.; Ikegami, M.; Shah, J. Antagonistic Interactions between the SA and JA Signaling Pathways in Arabidopsis Modulate Expression of Defense Genes and Gene-for-Gene Resistance to Cucumber Mosaic Virus. *Plant and Cell Physiol.* **2004**, *45*, 803.

(83) Raskin, I. Salicylate, A New Plant Hormone. *Plant Phys.* **1992**, *99*, 799-803.

(84) White, R. F. Acetylsalicylic acid (aspirin) induces resistance to tobacco mosaic virus in tobacco. *Virology* **1979**, *99*, 410-2.

(85) Durrant, W. E.; Dong, X. Systemic acquired resistance. *Ann. Rev. Phytopathol.* **2004**, *42*, 185-209.

(86) Chen, Z.; Silva, H.; Klessig, D. F. Active oxygen species in the induction of plant systemic acquired resistance by salicylic acid. *Science* **1993**, *262*, 1883-1886.

(87) Durner, J.; Klessig, D. F. Inhibition of ascorbate peroxidase by salicylic acid and 2,6-dichloroisonicotinic acid, two inducers of plant defense responses. *Proc. Natl. Ac. Sci.* **1995**, *92*, 11312-11316

(88) Mauch-Mani, B.; Metraux, J.-P. Salicylic Acid and Systemic Acquired Resistance to Pathogen Attack. *Ann. Bot.* **1998**, *82*, 535-540.

(89) Du, H.; Klessig, D. F. Identification of a Soluble, High-Affinity Salicylic Acid-Binding Protein in Tobacco. *Plant Phys.* **1997**, *113*, 1319-1327.

(90) Kumar, D.; Klessig, D. F. High-affinity salicylic acid-binding protein 2 is required for plant innate immunity and has salicylic acid-stimulated lipase activity. *Proc. Nat. Acad. Sci.* **2003**, *100*, 16101-6.

(91) Seskar, M.; Shulaev, V.; Raskin, I. Endogenous Methyl Salicylate in Pathogen-Inoculated Tobacco Plants. *Plant Phys.* **1998**, *116*, 387-392.

(92) Slaymaker, D. H.; Navarre, D. A.; Clark, D.; del Pozo, O.; Martin, G. B.; Klessig, D. F. The tobacco salicylic acid-binding protein 3 (SABP3) is the chloroplast carbonic anhydrase, which exhibits antioxidant activity and plays a role in the hypersensitive defense response. *Proc. Natl. Ac. Sci.*. **2002**, *99*, 11640-11645

(93) Durner, J.; Klessig, D. F. Inhibition of ascorbate peroxidase by salicylic acid and 2,6-dichloroisonicotinic acid, two inducers of plant defense responses. *Proc. Natl. Ac. Sci.* **1995**, *92*, 11312.

(94) Durner, J.; Klessig, D. F. Salicylic Acid Is a Modulator of Tobacco and Mammalian Catalases. *J. Biol. Chem.* **1996**, *271*, 28492-28501.

(95) Farmer, E. E.; Weber, H.; Vollenweider, S. Fatty acid signaling in Arabidopsis. *Planta* **1998**, *206*, 167-74.

(96) Mitchell, J. W.; Mandava, N.; Worley, J. F.; Plimmer, J. R.; Smith, M. V. Brassins - a New Family of Plant Hormones from Rape Pollen. *Nature* **1970**, *225*, 1065.

(97) Bajguz, A. Metabolism of brassinosteroids in plants. *Plant Phys. Biochem.* **2007**, *45*, 95-107.

(98) Clouse, S. D.; Sasse, J. M. Brassinosteroids: Essential Regulators of Plant Growth and Development. *Ann. Rev. Pl. Phys. Pl. Mol. Biol.***1998**, *49*, 427-451.

(99) Nemhauser, J. L.; Mockler, T. C.; Chory, J. Interdependency of brassinosteroid and auxin signaling in Arabidopsis. *PLoS Biol.* **2004**, *2*, 258.

(100) Cano-Delgado, A.; Yin, Y.; Yu, C.; Vafeados, D.; Mora-Garcia, S.; Cheng, J.-C.; Nam, K. H.; Li, J.; Chory, J. BRL1 and BRL3 are novel brassinosteroid receptors that function in vascular differentiation in Arabidopsis. *Development* **2004**, *131*, 5341-5351.

(101) Hewitt, F. R.; Hough, T.; O'Neill, P.; Sasse, J. M.; Williams, E. G.; Rowan, K. S. Effect of Brassinolide and other Growth Regulators on the Germination and Growth of Pollen Tubes of *Prunus avium* using a Multiple Hanging-drop Assay. *Func. Plant Biol.* **1985**, *12*, 201-211

(102) Chory, J.; Nagpal, P.; Peto, C. A. Phenotypic and Genetic Analysis of *det2*, a New Mutant That Affects Light-Regulated Seedling Development in Arabidopsis. *Plant Cell* **1991**, *3*, 445-459.

(103) Clouse, S. D. Brassinosteroid signal transduction: clarifying the pathway from ligand perception to gene expression. *Mol. Cell* **2002**, *10*, 973-82.

(104) Kinoshita, T.; Cano-Delgado, A.; Seto, H.; Hiranuma, S.; Fujioka, S.; Yoshida, S.; Chory, J. Binding of brassinosteroids to the extracellular domain of plant receptor kinase BRI1. *Nature* **2005**, *433*, 167.

(105) Wang, Z.-Y.; Seto, H.; Fujioka, S.; Yoshida, S.; Chory, J. BRI1 is a critical component of a plasma-membrane receptor for plant steroids. *Nature* **2001**, *410*, 380.

(106) Wang, X.; Goshe, M. B.; Soderblom, E. J.; Phinney, B. S.; Kuchar, J. A.; Li, J.; Asami, T.; Yoshida, S.; Huber, S. C.; Clouse, S. D. Identification and Functional Analysis of in Vivo Phosphorylation Sites of the Arabidopsis Brassinosteroid-Insensitive1 Receptor Kinase. *Plant Cell* **2005**, *17*, 1685-1703.

(107) Li, J.; Wen, J.; Lease, K. A.; Doke, J. T.; Tax, F. E.; Walker, J. C. BAK1, an Arabidopsis LRR receptor-like protein kinase, interacts with BRI1 and modulates brassinosteroid signaling. *Cell* **2002**, *110*, 213-22.

(108) Nam, K. H.; Li, J. BRI1/BAK1, a receptor kinase pair mediating brassinosteroid signaling. *Cell* **2002**, *110*, 203-12.

(109) Li, J. Brassinosteroids signal through two receptor-like kinases. *Curr. Opin. Plant Biol.* **2003**, *6*, 494-9.

(110) Li, J.; Lease, K. A.; Tax, F. E.; Walker, J. C. BRS1, a serine carboxypeptidase, regulates BRI1 signaling in Arabidopsis thaliana. *Proc. Natl. Ac. Sci.* **2001**, *98*, 5916-5921

(111) Wang, Z. Y.; He, J. X. Brassinosteroid signal transduction--choices of signals and receptors. *Trends Plant Sci.* **2004**, *9*, 91-6.

(112) Addicott, F. T.; Carns, H. R. History and introduction to abscisic acid. *Abscisic Acid* **1983**, 1-21.

(113) Zeevaart, J. A. D.; Creelman, R. A. Metabolism and physiology of abscisic acid. *Ann. Rev. Pl.Physi. Pl. Mol. Biol.***1988**, *39*, 439-73.

(114) Sanchez-Serrano, J. J.; Amati, S.; Ebneth, M.; Hildmann, T.; Mertens, R.; Pena-Cortes, H.; Prat, S.; Willmitzer, L. The involvement of ABA in wound responses of plants. *Abscisic Acid* **1991**, 201-16.

(115) McCarty, D. R. Genetic control and integration of maturation and germination pathways in seed development. *Ann. Rev. Pl.Physi. Pl. Mol. Biol.***1995**, *46*, 71-93.

(116) Rock, C. D.; Quatrano, R. S. The role of hormones during seed development. *Plant Hormones (2nd Edition)* Spinger Netherlands **1995**, 671-97.

(117) Ueno, O. Induction of Kranz anatomy and C4-like biochemical characteristics in a submerged amphibious plant by abscisic acid. *Plant Cell* **1998**, *10*, 571-583.

(118) Albinsky, D.; Masson, J. E.; Bogucki, A.; Afsar, K.; Vass, I.; Nagy, F.; Paszkowski, J. Plant responses to genotoxic stress are linked to an ABA/salinity signaling pathway. *Plant J.* **1999**, *17*, 73-82.

(119) Wilen, R.; Gusta, L.; Lei, B.; Abrams, S.; Ewan, B. Effects of abscisic acid (ABA) and ABA analogs on freezing tolerance, low-temperature growth, and flowering in rapeseed. *J. Pl. Gr. Reg.* **1994**, *13*, 235-241.

(120) Rajasekaran, L. R.; Blake, T. J. New plant growth regulators protect photosynthesis and enhance growth under drought of jack pine seedlings. *J. Pl. Gr. Reg.* **1999**, *18*, 175-181.

(121) Zeevaart, J. A. D. Abscisic acid metabolism and its regulation. *New Comp. Biochem.* **1999**, *33*, 189-207.

(122) Liu, X.; Yue, Y.; Li, B.; Nie, Y.; Li, W.; Wu, W.-H.; Ma, L. A G Protein-Coupled Receptor Is a Plasma Membrane Receptor for the Plant Hormone Abscisic Acid. *Science* **2007**, *315*, 1712-1716.

(123) Razem, F. A.; El-Kereamy, A.; Abrams, S. R.; Hill, R. D. The RNA-binding protein FCA is an abscisic acid receptor. *Nature (London, United Kingdom)* **2006**, *439*, 290-294. (paper retracted)

(124) Shen, Y.-Y.; Wang, X.-F.; Wu, F.-Q.; Du, S.-Y.; Cao, Z.; Shang, Y.; Wang, X.-L.; Peng, C.-C.; Yu, X.-C.; Zhu, S.-Y.; Fan, R.-C.; Xu, Y.-H.; Zhang, D.-P. The Mg-chelatase H subunit is an abscisic acid receptor. *Nature* **2006**, *443*, 823.

(125) Muller, A. H.; Hansson, M. The barley magnesium chelatase 150-kDa subunit is not an abscisic acid receptor. *Plant Phys.* **2009**, pp.109.135277.

(126) Gao, Y.; Zeng, Q.; Guo, J.; Cheng, J.; Ellis, B. E.; Chen, J.-G. Genetic characterization reveals no role for the reported ABA receptor, GCR2, in ABA control of seed germination and early seedling development in Arabidopsis. *Plant J.* **2007**, *52*, 1001-1013.

(127) McCourt, P.; Creelman, R. The ABA receptors -- we report you decide. *Curr. Opin. Plant Biol.* **2008**, *11*, 474-8.

(128) Finkelstein, R. R.; Gampala, S. S. L.; Rock, C. D. Abscisic acid signaling in seeds and seedlings. *Plant Cell* **2002**, *14*, S15-S45.

(129) Walker-Simmons, M. K.; Anderberg, R. J.; Rose, P. A.; Abrams, S. R. Optically pure abscisic acid analogs. Tools for relating germination inhibition and gene expression in wheat embryos. *Plant Phys.* **1992**, *99*, 501-7.

(130) Daiqing Huang, M. R. J., Weiren Wu, Stephen J. Ambrose, Andrew R. Ross, Suzanne R. Abrams, Adrian J. Cutler, . Structural analogs of ABA reveal novel features of ABA perception and signaling in Arabidopsis. *Plant J.* **2007**, *50*, 414-428.

(131) Schwartz, A.; Wu, W.-H.; Tuker, E. B.; Assmann, S. M. Inhibition of inward K+ channels and stomatal response by abscisic acid: an intracellular locus of phytohormone action. *Proc. Natl. Ac. Sci.* **1994**, *91*, 4019-23.

(132) Allan, A. C.; Trewavas, A. J. Abscisic acid and gibberellin perception: inside or out? *Plant Phys.* **1994**, *104*, 1107-8.

(133) Zhang, D.-P.; Chen, S.-W.; Peng, Y.-B.; Shen, Y.-Y. Abscisic acid-specific binding sites in the flesh of developing apple fruit. *J. Exp. Bot.* **2001**, *52*, 2097-2103.

(134) Finkelstein, R. R.; Rock, C. D. In *The Arabidopsis Book* 2002.

(135) Christmann, A.; Grill, E.; Meinhard, M. In *Topics in Current Genetics*; Hirt, H., Shinozaki, K., Eds.; Springler-Verlag: Berlin 2003, 2003; Vol. 4.

(136) Krochko, J. E.; Abrams, G. D.; Loewen, M. K.; Abrams, S. R.; Cutler, A. J. (+)-Abscisic acid 8'-hydroxylase is a cytochrome P450 monooxygenase. *Plant Phys.* **1998**, *118*, 849-860.

(137) Wang, Z.; Mambelli, S.; Setter, T. L. Abscisic acid catabolism in maize kernels in response to water deficit at early endosperm development. *Ann. Bot. (Oxford, United Kingdom)* **2002**, *90*, 623-630.

(138) Cutler, A. J.; Squires, T. M.; Loewen, M. K.; Balsevich, J. J. Induction of (+)-abscisic acid 8' hydroxylase by (+)-abscisic acid in cultured maize cells. *J. Exp. Bot.* **1997**, *48*, 1787-1795.

(139) Saito, S.; Hirai, N.; Matsumoto, C.; Ohigashi, H.; Ohta, D.; Sakata, K.; Mizutani, M. Arabidopsis CYP707As encode (+)-abscisic acid 8'-hydroxylase, a key enzyme in the oxidative catabolism of abscisic acid. *Plant Phys.* **2004**, *134*, 1439-49.

(140) Xu, Z.-J.; Nakajima, M.; Suzuki, Y.; Yamaguchi, I. Cloning and characterization of the abscisic acid-specific glucosyltransferase gene from Adzuki bean seedlings. *Plant Phys.* **2002**, *129*, 1285-1295.

(141) Jackson, R.; Li, Y.; Lim, E.-K.; Bowles, D. J.; (The University of York, UK). Application: WOWO, Patent #: 2002-GB4143 2003023035, v 2003, p 37.

(142) Zhou, R.; Cutler, A. J.; Ambrose, S. J.; Galka, M. M.; Nelson, K. M.; Squires, T. M.; Loewen, M. K.; Jadhav, A. S.; Ross, A. R. S.; Taylor, D. C.; Abrams, S. R. A new abscisic acid catabolic pathway. *Plant Phys.* **2004**, *134*, 361-369.

(143) Hartung, W.; Slovik, S. Physicochemical properties of plant growth regulators and plant tissues determine their distribution and redistribution: stomatal regulation by abscisic acid in leaves. *New Phytol.* **1991**, *119*, 361-82.

(144) Windsor, M. L.; Milborrow, B. V.; McFarlane, I. J. The uptake of (+)-S- and (-)-R-abscisic acid by suspension culture cells of hopbush (Dodonaea viscosa). *Plant Phys.* **1992**, *100*, 54-62.

(145) Perras, M. R.; Abrams, S. R.; Balsevich, J. J. Characterization of an abscisic acid carrier in suspension-cultured barley cells. *J. Exp. Bot.* **1994**, *45*, 1565-73.

(146) Hartung, W.; Wilkinson, S.; Davies, W. J. Factors that regulate abscisic acid concentrations at the primary site of action at the guard cell. *J. Exp. Bot.* **1997**, *49*, 361-367.

(147) Veen, H.; Frissel, M. J. Simulation of hormone transport in petiole segments of Coleus. *Physiol. Plant.* **1975**, *34*, 208-15.

(148) Dietz, K.-J.; Sauter, A.; Wichert, K.; Messdaghi, D.; Hartung, W. Extracellular b-glucosidase activity in barley involved in the hydrolysis of ABA glucose conjugate in leaves. *J. Exp. Bot.* **2000**, *51*, 937-944.

(149) Y. Ma, I. Szostkiewicz, A. Korte, D. Moes, Y Yang, A. Christmann, and E. Grill. Science **2009** *324* 1064-1068.

(150) Jang, Y. H.; Lee, J. H.; Kim, J. K. Abscisic acid does not disrupt either the Arabidopsis FCA-FY interaction or its rice counterpart in vitro. *Plant Cell Physiol.* **2008**.

(151) Dulson, J.; Bewley, J. D.; Johnston, R. N. Abscisic acid is an endogenous inhibitor in the regulation of mannanase production by isolated lettuce (Lactuca sativa cv Grand Rapids) endosperms. *Plant Phys.* **1988**, *87*, 660-5.

(152) Walker, C. J.; Willows, R. D. Mechanism and regulation of Mg-chelatase. *Biochem. J.* **1997**, *327 (Pt 2)*, 321-33.

(153) Mochizuki, N.; Brusslan, J. A.; Larkin, R.; Nagatani, A.; Chory, J. Arabidopsis genomes uncoupled 5 (GUN5) mutant reveals the involvement of Mg-chelatase H subunit in plastid-to-nucleus signal transduction. *Proc. Natl. Acad. Sci.* **2001**, *98*, 2053-8.

(154) Pandey, S.; Nelson, D. C.; Assmann, S. M. Two Novel GPCR-Type G Proteins Are Abscisic Acid Receptors in Arabidopsis. *Cell* **2009**, *136*, 136-148.

(155) Walton, D. C.; Sondheimer, E. Activity and metabolism of [14C]-(+-)-abscisic acid derivatives. *Plant Phys.* **1972**, *49*, 290-2.

(156) Walton, D. C. Structure-activity relationships of abscisic acid analogs and metabolites. *Abscisic Acid*, Praeger, New York, N.Y **1983**, 113-46.

(157) Zhang, D.-P.; Wu, Z.-Y.; Li, X.-Y.; Zhao, Z.-X. Purification and identification of a 42-kilodalton abscisic acid-specific-binding protein from epidermis of broad bean leaves. *Plant Phys.* **2002**, *128*, 714-725.

(158) Pedron, J.; Brault, M.; Nake, C.; Miginiac, E. Detection of abscisic-acid-binding proteins in the microsomal protein fraction of Arabidopsis thaliana with abscisic-acid-protein conjugates used as affinity probes. *Eur. J. Biochem.* **1998**, *252*, 385-390.

(159) Hite, D. R. C.; Outlaw, W. H., Jr.; Seavy, M. A. Substitution of hydrazones for the 4' carbonyl on abscisic acid rendered it ineffective in a rapid stomatal-opening-inhibition bioassay. *Physiol. Plant.* **1994**, *92*, 79-84.

(160) Yamazaki, D.; Yoshida, S.; Asami, T.; Kuchitsu, K. Visualization of abscisic acid-perception sites on the plasma membrane of stomatal guard cells. *Plant J.* **2003**, *35*, 129-139.

(161) Nyangulu J., M.; Nelson K.M.; Rose P.A.; Gai, Y.; Loewen, M.; Lougheed, B.; Quail, J. W.; Cutler A. J.; Abrams S.R. Synthesis and biological activity of tetralone abscisic acid analogues. *Org. Biomol. Chem.* **2006**, *4*, 1400-12.

(162) Nyangulu, J. M.; Galka, M. M.; Jadhav, A.; Gai, Y.; Graham, C. M.; Nelson, K. M.; Cutler, A. J.; Taylor, D. C.; Banowetz, G. M.; Abrams, S. R. An affinity probe for isolation of abscisic acid-binding proteins. *J. Am. Chem. Soc.* **2005**, *127*, 1662-1664.

(163) Nyangulu, J. M.; Nelson, K. M.; Rose, P. A.; Gai, Y.; Loewen, M.; Lougheed, B.; Quail, J. W.; Cutler, A. J.; Abrams, S. R. Synthesis and biological activity of tetralone abscisic acid analogues. *Org. Biomol. Chem.* **2006**, *4*, 1400-1412.

(164) Walker-Simmons, M. K.; Rose, P. A.; Shaw, A. C.; Abrams, S. R. The 7'-methyl group of abscisic acid is critical for biological activity in wheat embryo germination. *Plant Phys.* **1994**, *106*, 1279-84.

(165) Zou, J.; Abrams, G. D.; Barton, D. L.; Taylor, D. C.; Pomeroy, M. K.; Abrams, S. R. Induction of lipid and oleosin biosynthesis by (+)-abscisic acid and its metabolites in microspore-derived embryos of Brassica napus L. cv Reston. Biological responses in the presence of 8'-hydroxy abscisic acid. *Plant Phys.* **1995**, *108*, 563-71.

(166) Banowetz, G. M.; Hess, J. R.; Carman, J. G. A monoclonal antibody against the plant growth regulator, abscisic acid. *Hybridoma* **1994**, *13*, 537-41.

(167) Walker-Simmons, M. K.; Reaney, M. J. T.; Quarrie, S. A.; Perata, P.; Vernieri, P.; Abrams, S. R. Monoclonal antibody recognition of abscisic acid analogs. *Plant Phys.* **1991**, *95*, 46-51.

(168) Sang-Youl Park, Pauline Fung, Noriyuki Nishimura, Davin R. Jensen, Hiroaki Fujii, Yang Zhao, Shelley Lumba, Julia Santiago, Americo Rodrigues, Tsz-fung F. Chow, Simon E. Alfred, Dario Bonetta, Ruth Finkelstein, Nicholas J. Provart, Darrell Desveaux, Pedro L. Rodriguez, Peter McCourt, Jian-Kang Zhu, Julian I. Schroeder, Brian F. Volkman, and Sean R. Cutler. Science **2009** *324*, 1068-1071.

(169) Cutler, A. J.; Rose, P. A.; Squires, T. M.; Loewen, M. K.; Shaw, A. C.; Quail, J. W.; Krochko, J. E.; Abrams, S. R. Inhibitors of Abscisic Acid 8'-Hydroxylase. *Biochemistry* **2000**, *39*, 13614-13624.

(170) Pompon, D.; Louerat, B.; Bronine, A.; Urban, P. Yeast expression of animal and plant P450s in optimized redox environments. *Meth. Enzymol.* **1996**, *272*, 51-64.

(171) Galardy, R. E.; Craig, L. C.; Jamieson, J. D.; Printz, M. P. Photoaffinity Labeling of Peptide Hormone Binding Sites. *J. Biol. Chem.* **1974**, *249*, 3510-3518.

(172) John, G.; Morita, M. Synthesis and Characterization of Photo-Cross-Linked Networks Based on L-Lactide/Serine Copolymers. *Macromolecules* **1999**, *32*, 1853-1858.

(173) Kell, A. J.; Workentin, M. S. Aryl Ketone Photochemistry on Monolayer Protected Clusters: Study of the Norrish Type II Reaction as a Probe of Conformational Mobility and for Selective Surface Modification. *Langmuir* **2001**, *17*, 7355-7363.

(174) Zor, T.; Halifa, I.; Kleinhaus, S.; Chorev, M.; Selinger, Z. m-Acetylanilido-GTP, a novel photoaffinity label for GTP-binding proteins: synthesis and application. *Biochem. J.* **1995**, *306 (Pt 1)*, 253-8.

(175) Turro, N. J. *Modern Molecular Photochemistry* University Science Books, Sausalito, California, 1991.

(176) Clipston, N. L.; Jai-nhuknan, J.; Cassady, C. J. A comparison of negative and positive ion time-of-flight post-source decay mass spectrometry for peptides containing basic residues. *Int. J. Mass Spectr.* **2003**, *222*, 363.

(177) Bossio, R. E.; Hudgins, R. R.; Marshall, A. G. Gas Phase Photochemistry Can Distinguish Different Conformations of Unhydrated Photoaffinity-Labeled Peptide Ions. *J. Phys. Chem. B* **2003**, *107*, 3284-3289.

(178) Sobczak, M.; Wagner, P. J. Light-Induced Decarboxylation of (o-Acylphenyl)acetic Acids. *Org. Lett.* **2002**, *4*, 379-382.

(179) Martinez, L. J.; Scaiano, J. C. Transient Intermediates in the Laser Flash Photolysis of Ketoprofen in Aqueous Solutions: Unusual Photochemistry for the Benzophenone Chromophore. *J. Am. Chem. Soc.* **1997**, *119*, 11066-11070.

(180) Walker-Simmons, M. K.; Rose, P. A.; Hogge, L. R.; Abrams, S. R. Abscisic acid: ABA immunoassay and gas chromatography/mass spectrometry verification. *Meth. Mol. Biol.* **2000**, *141*, 33-47.

(181) Schwartz, C. J.; Sampson, H. M.; Hlousek, D.; Percival-Smith, A.; Copeland, J. W.; Simmonds, A. J.; Krause, H. M. FTZ-Factor1 and Fushi tarazu interact via conserved nuclear receptor and coactivator motifs. *Embo J.* **2001**, *20*, 510-9.

(182) Savage, M. D.; Mattson, G.; Desai, S.; Nielander, G. W.; Morgensen, S.; Conklin, E. J. *Avidin-Biotin Chemistry: A Handbook* Pierce Chemical Company, Rockford, Illinois, 1992.

(183) Delom, F.; Chevet, E. In vitro mapping of calnexin interaction with ribosomes. *Biochem. Biophys. Res. Comm.* **2006**, *341*, 39.

(184) Qadota, H.; Mercer, K. B.; Miller, R. K.; Kaibuchi, K.; Benian, G. M. Two LIM Domain Proteins and UNC-96 Link UNC-97/PINCH to Myosin Thick Filaments in Caenorhabditis elegans Muscle. *Mol. Biol. Cell* **2007**, *18*, 4317-4326.

(185) Zakaria, S.; Gomez, T. S.; Savoy, D. N.; McAdam, S.; Turner, M.; Abraham, R. T.; Billadeau, D. D. Differential Regulation of TCR-mediated Gene Transcription by Vav Family Members. *J. Exp. Med.* **2004**, *199*, 429-434.

(186) Rintamaki, E. Formation of Disulphide Cross-Linked Aggregates of Large Subunit from Higher Plant Ribulose-1, 5-Bisphosphate Carboxylase-Oxygenase. *J. Exp. Bot.* **1989**, *40*, 1305-1313.

(187) Luo, S.; Wang, Z.-Y.; Kobayashi, M.; Nozawa, T. The Dimerization of Folded Monomers of Ribulose 1,5-Bisphosphate Carboxylase/Oxygenase. *J. Biol. Chem.* **2001**, *276*, 7023-7026.

(188) Cohen, I.; Sapir, Y.; Shapira, M. A conserved mechanism controls translation of Rubisco large subunit in different photosynthetic organisms. *Plant Phys.* **2006**, *141*, 1089-97.

(189) John R., E.; Saskia, M., Van der Vies. The Rubisco subunit binding protein. *Photosynth. Res.* **1988**, *16*, 101-115.

(190) Fernandez, C.; Hilty, C.; Wider, G.; Wuthrich, K. Lipid-protein interactions in DHPC micelles containing the integral membrane protein OmpX investigated by NMR spectroscopy. *Proc. Natl. Acad. Sci. U S A* **2002**, *99*, 13533-7.

(191) Logan, D. C.; Domegue, O.; Teyssendier de la Serve, B.; Rossignol, M. A new plasma memberne polypeptides differentially regulated during plant development. *Biochem. Mol. Biol. Int.* **1997**, *43*, 1051-1062.

(192) Kawamura, Y.; Uemura, M. Mass spectrometric approach for identifying putative plasma membrane proteins of Arabidopsis leaves associated with cold acclimation. *Plant J.* **2003**, *36*, 141-154.

(193) Turbadar, T. Complete Absorption of Plane Polarized Light by Thin Metallic Films. *J. Mod. Opt.* **1964**, *11*, 207 - 210.

(194) Otto, A. Excitation of nonradiative surface plasma waves in silver by the method of frustrated total reflection. *Zeitschrift für Physik A Hadrons and Nuclei* **1968**, *216*, 398.

(195) Kretschmann, E.; Ferrell, T. L.; Ashley, J. C. Splitting of the Dispersion Relation of Surface Plasmons on a Rough Surface. *Phys. Rev. Lett.* **1979**, *42*, 1312.

(196) Matthew, A. C. Advances in membrane receptor screening and analysis. *J. Mol. Recogn.* **2004**, *17*, 286-315.

(197) Glaser, R. W. Antigen-Antibody Binding and Mass Transport by Convection and Diffusion to a Surface: A Two-Dimensional Computer Model of Binding and Dissociation Kinetics. *Anal. Biochem.* **1993**, *213*, 152.

(198) Casper, D.; Bukhtiyarova, M.; Springman, E. B. A Biacore biosensor method for detailed kinetic binding analysis of small molecule inhibitors of p38[alpha] mitogen-activated protein kinase. *Anal. Biochem.* **2004**, *325*, 126.

(199) Thurmond, R. L.; Wadsworth, S. A.; Schafer, P. H.; Zivin, R. A.; Siekierka, J. J. Kinetics of small molecule inhibitor binding to p38 kinase. *Eur. J. Biochem.* **2001**, *268*, 5747-5754.

(200) Szafranska, A. E.; Dalby, K. N. Kinetic mechanism for p38 MAP kinase α. A partial rapid-equilibrium random-order ternary-complex mechanism for the phosphorylation of a protein substrate. *FEBS J.* **2005**, *272*, 4631-4645.

(201) Borsch-Haubold, A. G.; Pasquet, S.; Watson, S. P. Direct Inhibition of Cyclooxygenase-1 and -2 by the Kinase Inhibitors SB 203580 and PD 98059. SB 203580 Also Inhibits Thromboxane Synthase. *J. Biol. Chem.* **1998**, *273*, 28766-28772.

(202) Rebecca L. Rich, D. G. M. Survey of the year 2004 commercial optical biosensor literature. *J. Mol. Recogn.* **2005**, *18*, 431-478.

(203) Cannon, M. J.; Papalia, G. A.; Navratilova, I.; Fisher, R. J.; Roberts, L. R.; Worthy, K. M.; Stephen, A. G.; Marchesini, G. R.; Collins, E. J.; Casper, D.; Qiu, H.; Satpaev, D.; Liparoto, S. F.; Rice, D. A.; Gorshkova, II; Darling, R. J.; Bennett, D. B.; Sekar, M.; Hommema, E.; Liang, A. M.; Day, E. S.; Inman, J.; Karlicek, S. M.; Ullrich, S. J.; Hodges, D.; Chu, T.; Sullivan, E.; Simpson, J.; Rafique, A.; Luginbuhl, B.; Westin, S. N.; Bynum, M.; Cachia, P.; Li, Y. J.; Kao, D.; Neurauter, A.; Wong, M.; Swanson, M.; Myszka, D. G. Comparative analyses of a small molecule/enzyme interaction by multiple users of Biacore technology. *Anal. Biochem.* **2004**, *330*, 98-113.

(204) Portis, A. R., Jr.; Parry, M. A. Discoveries in Rubisco (Ribulose 1,5-bisphosphate carboxylase/oxygenase): a historical perspective. *Photosynth. Res.* **2007**, *94*, 121-43.

(205) Parry, M. A.; Andralojc, P. J.; Khan, S.; Lea, P. J.; Keys, A. J. Rubisco activity: effects of drought stress. *Ann. Bot.* **2002**, *89 Spec No*, 833-9.

(206) Lan, Y.; Mott, K. A. Determination of Apparent Km Values for Ribulose 1,5-Bisphosphate Carboxylase/Oxygenase (Rubisco) Activase Using the Spectrophotometric Assay of Rubisco Activity. *Plant Phys.* **1991**, *95*, 604-609.

(207) McNevin, D.; von Caemmerer, S.; Farquhar, G. Determining RuBisCO activation kinetics and other rate and equilibrium constants by simultaneous multiple non-linear regression of a kinetic model. *J. Exp. Bot.* **2006**, *57*, 3883-3900.

(208) Taylor, T. C.; Andersson, I. The structure of the complex between rubisco and its natural substrate ribulose 1,5-bisphosphate. *J. Mol. Biol.* **1997**, *265*, 432.

(209) Greene, D. N.; Whitney, S. M.; Matsumura, I. Artificially evolved Synechococcus PCC6301 Rubisco variants exhibit improvements in folding and catalytic efficiency. *Biochem. J.* **2007**, *404*, 517-24.

(210) Parry, M. A.; Keys, A. J.; Foyer, C. H.; Furbank, R. T.; Walker, D. A. Regulation of Ribulose-1,5-Bisphosphate Carboxylase Activity by the Activase System in Lysed Spinach Chloroplasts. *Plant Phys.* **1988**, *87*, 558-561.

(211) Jensen, R. G. Activation of Rubisco regulates photosynthesis at high temperature and CO2. *Proc. Natl. Acad. Sci.* **2000**, *97*, 12937-8.

(212) Kane, H. J.; Wilkin, J.-M.; Portis, A. R., Jr.; John Andrews, T. Potent Inhibition of Ribulose-Bisphosphate Carboxylase by an Oxidized Impurity in Ribulose-1,5-Bisphosphate. *Plant Phys.* **1998**, *117*, 1059-1069.

(213) Parry, M. A. J.; Keys, A. J.; Madgwick, P. J.; Carmo-Silva, A. E.; Andralojc, P. J. Rubisco regulation: a role for inhibitors. *J. Exp. Bot.* **2008**, *59*, 1569-1580.

(214) Marcus, Y.; Gurevitz, M. Activation of cyanobacterial RuBP-carboxylase/oxygenase is facilitated by inorganic phosphate via two independent mechanisms. *Eur. J. Biochem.* **2000**, *267*, 5995-6003.

(215) Marcus, Y.; Altman-Gueta, H.; Finkler, A.; Gurevitz, M. Mutagenesis at Two Distinct Phosphate-Binding Sites Unravels Their Differential Roles in Regulation of Rubisco Activation and Catalysis. *J. Bacteriol.* **2005**, *187*, 4222-4228.

(216) Cornish-Bowden, A. *Fundamentals of Enzyme Kinetics*; 3rd ed.; Portland Press: London, 2004.

(217) Laden, B. P.; Porter, T. D. Inhibition of human squalene monooxygenase by tellurium compounds: evidence of interaction with vicinal sulfhydryls. *J. Lipid Res.* **2001**, *42*, 235-240.

(218) Hogg, P. J.; Owensby, D. A.; Chesterman, C. N. Thrombospondin 1 is a tight-binding competitive inhibitor of neutrophil cathepsin G. Determination of the kinetic mechanism of inhibition and localization of cathepsin G binding to the thrombospondin 1 type 3 repeats. *J. Biol. Chem.* **1993**, *268*, 21811-21818.

(219) Antunes, F.; Marinho, H. S.; Barreto, M. C.; Pavão, M. L.; Pinto, R. E. Diagnosis of enzyme inhibition based on the degree of inhibition. *Biochim. Biophys. Act. (BBA) - General Subjects* **2003**, *1624*, 11.

(220) Adade, A. B.; Chignell, D.; Vanderkooi, G. Local anesthetics: A new class of partial inhibitors of mitochondrial ATPase. *Journal of Bioenergetics and Biomembranes* **1984**, *16*, 353.

(221) Baici, A. Graphical and statistical analysis of hyperbolic tight-binding inhibition. *Biochem. J.* **1987**, *244*, 793-6.

(222) Turner, J. J.; Gerrard, J. A.; Hutton, C. A. Heterocyclic inhibitors of dihydrodipicolinate synthase are not competitive. *Bioorg. Med. Chem.* **2005**, *13*, 2133.

(223) Ananthan, S.; Saini, S. K.; Khare, R.; Clayton, S. D.; Dersch, C. M.; Rothman, R. B. Identification of a novel partial inhibitor of dopamine transporter among 4-substituted 2-phenylquinazolines. *Bioorg. Med. Chem. Lett.* **2002**, *12*, 2225.

(224) Dickenson, C. J.; Dickinson, F. M. Inhibition by ethanol, acetaldehyde and trifluoroethanol of reactions catalysed by yeast and horse liver alcohol dehydrogenases. *Biochem. J.* **1978**, *171*, 613-27.

(225) Correia, M. J.; Pereira, J. S. The control of leaf conductance of white lupine by xylem ABA concentration decreases with the severity of water deficits. *J. Exp. Bot.* **1995**, *46*, 101-10.

(226) Dodd, I. C.; Tan, L. P.; He, J. Do increases in xylem sap pH and/or ABA concentration mediate stomatal closure following nitrate deprivation? *J. Exp. Bot.* **2003**, *54*, 1281-1288.

(227) Okuda, H.; Kihara, T.; Iwagaki, I. Effects of cropping on photosynthesis, dark respiration, leaf ABA concentration, and inflorescence induction in satsuma mandarin. *J. Jap. Soc. Hort. Sci.* **1995**, *64*, 9-16.

(228) Maillet, E. L.; Pellegrini, N.; Valant, C.; Bucher, B.; Hibert, M.; Bourguignon, J. J.; Galzi, J. L. A novel, conformation-specific allosteric inhibitor of the tachykinin NK2 receptor (NK2R) with functionally selective properties. *Faseb J* **2007**, *21*, 2124-34.

(229) Changeux, J.-P.; Edelstein, S. J. Allosteric Mechanisms of Signal Transduction. *Science* **2005**, *308*, 1424-1428.

(230) Koshland, D. E.; NÃ©methy, G.; Filmer, D. Comparison of Experimental Binding Data and Theoretical Models in Proteins Containing Subunits. *Biochemistry* **1966**, *5*, 365-385.

(231) Gibbons, I.; Yang, Y. R.; Schachman, H. K. Cooperative interactions in aspartate transcarbamoylase. 1. Hybrids composed of native and chemically inactivated catalytic polypeptide chains. *Proc. Natl. Acad. Sci. U S A* **1974**, *71*, 4452-6.

(232) Gouaux, J. E.; Lipscomb, W. N. Three-dimensional structure of carbamoyl phosphate and succinate bound to aspartate carbamoyltransferase. *Proc. Natl. Ac. Sci.***1988**, *85*, 4205-4208.

(233) Yokota, A.; Higashioka, M.; Wadano, A. Cooperative Binding of Carboxyarabinitol Bisphosphate to the Regulatory Sites of Ribulose Bisphosphate Carboxylase/Oxygenase from Spinach. *J. Biochem.* **1991**, *110*, 253-256.

(234) Parry, M. A. J.; Andralojc, P. J.; Parmar, S.; Keys, A. J.; Habash, D.; Paul, M. J.; Alred, R.; Quick, W. P.; Servaites, J. C. Regulation of Rubisco by inhibitors in the light. *Plant Cell Environment* **1997**, *20*, 528.

(235) Maidebura, E. V.; Chernyad'ev, I. I.; Kosakovskaya, I. V. Change in the level of abscisic acid and activity of D-ribulose-1,5-diphosphate carboxylase-oxygenase in different varieties of Triticum aestivum L. under water stress. *Doklady Akademii Nauk Ukrainskoi SSR, Seriya B: Geologicheskie, Khimicheskie i Biologicheskie Nauki* **1989**, 65-8.

(236) Soto, M.; Larque-Saavedra, A. Abscisic acid accumulation in an edible drought resistant wild potato (Solanum cardiophyllum). *Phyton (Buenos Aires, Argentina)* **1987**, *47*, 69-71.

(237) Robertson, J. M.; Pharis, R. P.; Huang, Y. Y.; Reid, D. M.; Yeung, E. C. Drought-induced increases in abscisic acid levels in the root apex of sunflower. *Plant Phys.* **1985**, *79*, 1086-9.

(238) Bottini, R.; Racca, R. W.; Arguello, J. A.; Collino, D.; Tizio, R. Levels of growth inhibitors in soybean (Glycine max L. Merrill) cv. Lee, in response to drought, gibberellic acid and abscisic acid. *Phyton (Buenos Aires, Argentina)* **1981**, *41*, 97-102.

(239) Quarrie, S. A.; Henson, I. E. Abscisic acid accumulation in detached cereal leaves in response to water stress. II. Effects of leaf age and leaf position. *Zeitschrift fuer Pflanzenphysiologie* **1981**, *101*, 439-46.

(240) Zeevaart, J. A. D. Changes in the levels of abscisic acid and its metabolites in excised leaf blades of Xanthium strumarium during and after water stress. *Plant Phys.* **1980**, *66*, 672-8.

(241) Sivakumaran, S.; Horgan, R.; Heald, J.; Hall, M. A. Effect of water stress on metabolism of abscisic acid in Populus robusta x schnied and Euphorbia lathyrus L. *Plant Cell Env.* **1980**, *3*, 163-73.

(242) Kuhnle, J. A.; Moore, P. H.; Yauger, W. L.; Haddon, W. F. Drought-induced abscisic acid changes in three sugarcane cultivars. *Proceedings of the Plant Growth Regulator Working Group* **1979**, *6th*, 221-2.

(243) Liu, W. T.; Pool, R.; Wenkert, W.; Kriedemann, P. E. Changes in photosynthesis, stomatal resistance and abscisic acid of Vitis labruscana through drought and irrigation cycles. *American Journal of Enology and Viticulture* **1978**, *29*, 239-46.

(244) Hartung, W.; Kaiser, W. M.; Burschka, C. Release of abscisic acid from leaf strips under osmotic stress. *Zeitschrift fuer Pflanzenphysiologie* **1983**, *112*, 131-8.

(245) Raschke, K.; Hedrich, R. Simultaneous and independent effects of abscisic acid on stomata and the photosynthetic apparatus in whole leaves. *Planta* **1985**, *163*, 105.

(246) Liang, J.; Pang, J.; Chen, Y. Mechanism of osmotic stress-induced abscisic acid biosynthesis and its regulation in plant. *Zhiwu Shenglixue Tongxun* **2001**, *37*, 447-451.

(247) Liang, J.; Zhang, J.; Wong, M. H. Can stomatal closure caused by xylem ABA explain the inhibition of leaf photosynthesis under soil drying? *Photosynth. Res.* **1997**, *51*, 149.

(248) Daley, P. F.; Raschke, K.; Ball, J. T.; Berry, J. A. Topography of photosynthetic activity of leaves obtained from video images of chlorphyll fluorescence. *Plant Phys.* **1989**, *90*, 1233-8.

(249) Lauer, M. J.; Boyer, J. S. Internal carbon dioxide measured directly in leaves. Abscisic acid and low leaf water potential cause opposing effects. *Plant Phys.* **1992**, *98*, 1310-16.

(250) Zhang, J.; Gowing, D. J.; Davies, W. J. ABA as a root signal in root to shoot communication of soil drying. *Monograph - British Society for Plant Growth Regulation* **1990**, *21*, 163-74.

(251) Davies, W. J.; Atkinson, C. J.; Zhang, J. Perception of soil drying via the increased synthesis of abscisic acid in roots. *Monograph - British Society for Plant Growth Regulation* **1990**, *20*, 85-96.

(252) Davies, W. J.; Meinzer, F. C. Stomatal responses of plants in drying soil. *Biochemie und Physiologie der Pflanzen* **1990**, *186*, 357-66.

(253) Josefina Bota, H. M., Jaume Flexas, . Is photosynthesis limited by decreased Rubisco activity and RuBP content under progressive water stress? *New Phytol.* **2004**, *162*, 671-681.

(254) Liu, W.; Yuan, S.; Zhang, N.; Lei, T.; Duan, H.; Liang, H.; Lin, H. Effect of water stress on photosystem 2 in two wheat cultivars. *Biologia Plantarum* **2006**, *50*, 597-602.

(255) Thimmanaik, S.; Kumar, S. G.; Kumari, G. J.; Suryanarayana, N.; Sudhakar, C. Photosynthesis and the Enzymes of Photosynthetic Carbon Reduction Cycle in Mulberry During Water Stress and Recovery. *Photosynthetica* **2002**, *40*, 233-236.

(256) McCrea, K. E.; Herzog, H. In *Neuropeptide Y Protocols* **2000**, p 231.

(257) Qume, M. Overview of Ligand-Receptor Binding Techniques. *Meth. Mol. Biol.* **1998**; *106*, 3-23.

(258) Lazareno, S. Quantification of receptor interactions using binding methods. *J. Recep. Sig. Trans.* **2001**, *21,* 139-165.

(259) Bylund, D. B.; Murrin, L. C. Radioligand saturation binding experiments over large concentration ranges. *Life Sci.* **2000**, *67*, 2897.

(260) Waldo, G. L.; Harden, T. K. Agonist binding and Gq-stimulating activities of the purified human P2Y1 receptor. *Mol. Pharmacol.* **2004**, *65*, 426-36.

(261) Swillens, S. Interpretation of binding curves obtained with high receptor concentrations: practical aid for computer analysis. *Mol. Pharmacol.* **1995**, *47*, 1197-1203.

(262) Yajun Gao, Q. Z., Jianjun Guo, Jia Cheng, Brian E. Ellis, Jin-Gui Chen, . Genetic characterization reveals no role for the reported ABA receptor, GCR2, in ABA control of seed germination and early seedling development in Arabidopsis. *Plant J.* **2007**, *52*, 1001-1013.

(263) Johnston, C. A.; Temple, B. R.; Chen, J.-G.; Gao, Y.; Moriyama, E. N.; Jones, A. M.; Siderovski, D. P.; Willard, F. S. Comment on A G Protein Coupled Receptor Is a Plasma Membrane Receptor for the Plant Hormone Abscisic Acid. *Science* **2007**, *318*, 91

(264) Sang-Youl Park, Pauline Fung, Noriyuki Nishimura, Davin R. Jensen, Hiroaki Fujii, Yang Zhao, Shelley Lumba, Julia Santiago, Americo Rodrigues, Tsz-fung F. Chow, Simon E. Alfred, Dario Bonetta, Ruth Finkelstein, Nicholas J. Provart, Darrell Desveaux, Pedro L. Rodriguez, Peter McCourt, Jian-Kang Zhu, Julian I. Schroeder, Brian F. Volkman, and Sean R. Cutler. Science **2009** *324*, 1068-1071.

(265) Y. Ma, I. Szostkiewicz, A. Korte, D. Moes, Y Yang, A. Christmann, and E. Grill. *Science* **2009** *324* 1064-1068.